Model estimations of possible climate changes of surface solar radiation at regional scales over Southern Africa and the South West Indian Ocean

Chao Tang

École Doctorale « Sciences, Technologies et Santé » ED542
de
L'Université de La Réunion

THÈSE DE DOCTORAT

Pour obtenir le grade de docteur délivré par :

L'Université de La Réunion
Discipline : Physique Énergétique

Chao TANG

Model estimations of possible climate changes of surface solar radiation at regional scales over Southern Africa and the South West Indian Ocean

---

Dirigée par **Miloud BESSAFI** & **Béatrice MOREL**

Soutenue le 1er décembre 2017 devant le jury composé de :

Dr. Christopher LENNARD	University of Cape Town	rapporteur
Dr. Erika COPPOLA	International Centre for Theoretical Physics, Italy	rapporteur
Dr. Martin WILD	Swiss Federal Institute of Technology in Zurich	examinateur
Dr. Nathalie Philippon	Université Grenoble Alpes	examinatrice
Dr. Béatrice MOREL	Université de La Réunion	co-directrice
Pr Miloud BESSAFI	Université de La Réunion	directeur

Remerciements

« A PhD is not enough », which is a book (written by Peter J. Feibelman) that I had read in the beginning of my 4-year PhD study. At this time, facing the end of the PhD, I really feel this, as the name of his book, to survive in scientific career there are much more to understand and to explore after the PhD. The experiences and knowledge that I learned from the last 4 years are so unique and encourage me to continue my journey.

I'd like to firstly thank to the members of jury of my defense. Thanks to Prof. Martin Wild for being the president of my PhD jury. And Dr. Christopher LENNARD and Dr. Erika COPPOLA for being the reporters. Their reports are really constructive for the improvement of this thesis. Thanks to the two examiners. They are Dr. Nathalie Philippon and Prof. Mar-tin Wild.

Second, I give the great thanks to my supervisors, Prof. Miloud BESSAFI and Dr. Béatrice MOREL. Prof. BESSAFI gives great insights at some crucial points, making this PhD work in a sustainable direction. Dr. MOREL, she is the person really supports me a lot in the daily scientific activities. Thanks to the knowledge and discussions from her the work could be finished and be able to archive some impacting results.

Third, I will thanks to my dear colleges in the laboratory LE2P. Thanks to the director of our lab Prof. Jean-Pierre CHABRIAT, Mr. Patrick JEANTY, and Madam Kelly GRONDIN for their continuing and kind supports. Then many thanks to other students in my group, they're Peng LI, Qi LI, Pauline MIAHLE.

Forth, thanks to the friends and experts that I met oversea in Europe during the conferences and exchange. I thank to Prof. Stefan BOUHLER in University of Hamburg, and another Stefan in Max-Planck institute for the supervision and discussions. Also, many thanks to Benjamin POHL in University of Bourgogne, and Erika COPPOLA from ICTP (The Abdus Salam International Centre for Theoretical Physics), Babatunde ABIODUN from university of Cape Town, Roddy LOLLCHUND from University of Mauritius.

Finally, I'd like to thanks to my family. My parents in China, even they probably do not know what I am doing all day in front of the computer, I could feel them in the long distance and which warms me up in the hard time. My wife Shen JING, she is not only the partner in daily life and a good French teacher for me, who teach me to read and pronounce in French. All by archive is on her help, patient and encourage. Special thanks to my son, who was not yet born when I passed the defense, and he is 4 months already. He makes me much stronger in the last few months before the finial defense. And he will continue giving me more courage to face the difficulties in future research and to explore the unknowns in the wonderful universe.

Résumé

Les variations du rayonnement solaire en surface (SSR) peuvent avoir un impact significatif sur divers aspects du système climatique, et notamment sur le développement socio-économique d'un pays. Pour identifier les impacts possibles du changement climatique sur le rayonnement solaire en surface à l'échelle régionale (~ 50 km) en Afrique australe jusqu'à la fin du 21ème siècle, on a analysé les données mensuelles produites dans le cadre du projet CORDEX-Afrique sur la période 1979-2099. Ces données sont issues des sorties de 5 modèles régionaux de climat (RCM) forcés par 10 modèles globaux de climat (GCM) CMIP5, pour deux scénarios d'émissions, RCP4.5 et RCP8.5, en Afrique australe (SA) et sur une partie du SWIO (0-40°S; 0- 60°E). Pour contribuer au projet futur proposé qui vise à approfondir l'étude des changements de SSR à l'échelle locale (~ 1 km de résolution horizontale) à l'île de la réunion et à l'île de Maurice, situé dans le Sud-ouest de l'océan Indien (SWIO), près du bord d'Est du domaine CORDEX-Afrique, des simulations climatiques ont été réalisées sur trois fenêtres temporelles de 10 ans : a) le passé 1996-2005; et b) le futur 2046-2055 et 2090-2099, en utilisant la version 4 du RCM RegCM (RegCM4), forcé par: 1) les réanalyses climatiques ERA-Interim (ERAINT) du centre européen pour les prévisions météorologiques à moyen terme (ECMWF) pour simuler un passé récent seulement; et 2) deux GCMs (HadGEM2-ES et GFDL-ESM2M) de l'exercice CMIP5 de simulations du climat passé et futur pour le scénario d'émissions RCP8.5 à l'échelle régionale de 50km en Afrique australe et dans le sud-ouest de l'océan Indien (0-40°S; 0- 100°E). L'analyse de l'impact du changement climatique sur le SSR sur la base de ces simulations reste cependant limitée, à cause de leur couverture temporelle (3 périodes de 10 ans) et du nombre de modèles (2 GCMs, 1 RCM) et de scénarios (1 RCP) utilisés.

Il ressort de l'analyse des simulations de l'ensemble CORDEX-Afrique que : 1) sur la période passée récente, les GCMs forceurs surestiment généralement SSR d'environ 1 W/m^2 en été austral (DJF: Décembre-Janvier-Février), et de 7,5 W/m^2 en hiver austral (JJA : Juin-Juillet-Août), tandis que les RCMs, forcés par ces GCMs, sous-estiment SSR d'environ -32 W/m^2 et de -14 W/m^2 en été et en hiver, respectivement. 2) Les projections multi-modèles de changement de SSR simulées par les RCMs et leurs GCMs forceurs sont assez cohérentes: Les GCMs prévoient, en moyenne multi-modèles, une augmentation statistiquement significative de SSR d'environ 8 W/m^2 en 2099 selon le scénario RCP4.5 et de 12 W/m^2 en 2099 selon le scénario RCP8.5 sur le Centre de l'Afrique australe (SA-C), et une diminution de SSR, avec un degré de confiance élevé, d'environ -5 W/m^2 en 2099 selon le scénario RCP4.5 et de -10 W/m^2 en 2099 selon le scénario RCP8.5, pendant la saison DJF, en Afrique équatoriale (EA-E). Dans ces deux régions, les RCMs produisent, en moyenne multi-modèles, des tendances similaires (avec un degré de confiance élevé) à celles des GCMs, mais sur des zones d'extension spatiale plus faible que celle des GCMs. Cependant, pour la saison JJA, une augmentation de SSR, d'amplitude similaire dans les simulations GCMs et RCMs (~5 W/m^2 en 2099 selon le scénario RCP4.5 et 10 W/m^2 selon le scénario

RCP8.5), est attendue dans la région EA-E. 3) Une diminution significative de la nébulosité (environ -6% en 2099) est attendue sur le continent sud-africain pour les GCMs comme pour les RCMs. 4) Le scénario RCP8.5 produit des changements d'amplitude supérieure de 2.5W/m^2 pour les GCMs forceurs et de 5W/m^2 pour les RCMs en 2099 à celle pour le scénario RCP4.5. 5) Comme pour les sorties du modèle RegCM4, les structures des biais ou des changements de SSR issu des RCMs du programme CORDEX-Afrique sont globalement corrélées avec celles de couverture nuageuse totale des RCMs.

L'analyse des sorties du modèle RegCM4 indique que: 1) le modèle, forcé par les réanalyses ERAINT et les deux simulations CMIP5, simule assez bien la climatologie saisonnière pour l'actuel et le passé proche (température de l'air en surface, précipitations et SSR), mais présente un biais négatif sur la couverture nuageuse (environ -20% en pourcentage absolu). 2) La variabilité interne des moyennes annuelles de SSR simulées par RegCM4 (environ 0.2 W/m^2) est d'un ordre de grandeur inférieur au biais du modèle. 3) Le modèle simule des changements de SSR, pour le scénario RCP8.5, opposés à ceux des GCMs forceurs. 4) Le potentiel électrique, calculé à partir des simulations RegCM4 en utilisant une estimation du premier ordre, indique une variation inférieure à 2% par rapport au niveau actuel, à l'horizon 2099.

Mots-clefs: rayonnement solaire en surface, changements climatiques, CMIP5, CORDEX-Afrique, modèle climatique régional, modèle climatique global, RegCM, Afrique australe, SWIO

Abstract

Changes in Surface Solar Radiation (SSR) have the potential to significantly impact diverse aspects of the climate system, and notably the socio-economic development of any nation. Solar Energy, clean and renewable, promising to meet the increasing energy demand and to avoid the Greenhouse Gas (GHG) emission, is highly depending on the changes of SSR and other climate relevant variables (e.g. Surface Air Temperature). To identify the possible impacts of climate change on SSR at regional scales (~50 km) over Southern Africa (SA), an ensemble consisting of outputs from 20 regional climate downscaling realisations based on 5 RCMs that participated in the Coordinated Regional Downscaling Experiment (CORDEX) program (CORDEX-Africa) along with their 10 driving GCMs from CMIP5 covering southern Africa (0-40°S; 0- 60°E) during the period of 1979-2099 is analyzed under RCP4.5 and RCP8.5 up to 2099.

To contribute to the proposed future project that aiming to further investigate SSR changes at local scale (~ 1km horizontal resolution) in Reunion Island and Mauritius Island, located in the South West Indian Ocean (SWIO), near the broader of CORDEX-Africa domain, a slice downscaling experiment consisting of simulations covering three temporal windows: a) the present 1996-2005; b) the future 2046-2055 and 2090-2099 conducted with the Regional Climate Model (RCM) RegCM version 4, driven by the European Center for Medium-range Weather Forecasting (ECMWF) ERA-Interim reanalysis (ERAINT, only present) and 2 Global Climate Model (GCMs: HadGEM2-ES and GFDL-ESM2M) from the Coupled Model Intercomparison Project Phase 5 (CMIP5) under RCP8.5 scenario, are performed and evaluated at regional scale of 50km over SA-SWIO (0-40°S; 0- 100°E). This slice experiment is of limited temporal coverage, number of regional and driven global models and climate change forcings, which is mainly because of the limit of available computational resources at this time.

The ensemble study shows that: 1) GCMs ensemble mean overestimates SSR by about 1 W/m^2 in austral summer (December, January, and February, short as DJF) and 7.5 W/m^2 in austral winter (June, July and August, short as JJA), while RCMs ensemble mean shows underestimations of SSR by about -32 W/m^2 and -14 W/m^2 in summer and winter seasons respectively when driven by GCMs. 2) Multi-model mean projections of SSR change patterns simulated by the GCMs and their embedded RCMs are fairly consistent: GCMs project, in their multi-model means, a statistically significant increase of SSR of about 8 W/m^2 in RCP4.5 and 12 W/m^2 in RCP8.5 by 2099 over Centre Southern Africa (SA-C) and a highly confident decreasing SSR over Eastern Equatorial Africa (EA-E) of about -5 W/m^2 in RCP4.5 and -10 W/m^2 in RCP8.5 during the DJF season. RCMs simulate SSR change with statistical confidence over SA-C and EA-E area as well with a little spatial extension compared to GCMs. However, in the JJA season, an increase of SSR is found over EA-E of about 5 W/m^2 by 2099 under RCP4.5 and 10 W/m^2 under RCP8.5, of similar amplitudes in both the GCMs and RCMs simulations. 3) Significant cloudiness decrease (about -6 % to 2099) is found over continent of SA for GCMs and also shown in RCMs. 4) Larger SSR changes are found in the RCP8.5 scenario than in the RCP4.5 scenario in 2099, with about 2.5 W/m^2 enhanced changes in GCMs and about 5 W/m^2 in RCMs. 5) Either the biases or the chang-

es pattern of SSR are overall correlated with the patterns of total cloud cover from RCMs in CORDEX-Africa program (for RegCM4 as well).

The slice experiment indicates that 1) RegCM4 simulates present-day seasonal climatology, (surface air temperature, precipitation and SSR) quite well, but has a negative total cloud cover bias (about -20% in absolute percentage) when forced by the ERAINT and the two GCMs. 2) Internal variability of RegCM4-simulated annual means SSR (about 0.2 W/m^2) is of one order smaller than the model bias compared with reference data. 3) RegCM4 simulates SSR changes in opposite signs when driven by the different GCMs under RCP8.5 scenario. 4) Electricity potential calculated using first-order estimation based on the limited RegCM simulations indicates a change less then 2% to 2099 with respect on present level.

Keywords: surface solar radiation, climate change, CMIP5, regional climate model, CORDEX-Africa, RegCM, southern Africa, SWIO

Contents

List of Figures

List of tables

1 Introduction

OUTLINE:

1.1 Background

1.1.1 Increasing Energy Demand and Greenhouse Gas Emissions

Energy is the lifeblood of all societies, and is deeply implicated in each of the economic, social and environmental dimensions of human development (Dudley, 2004). Energy supply is undergoing a continuous and significant increase along with the long-term economic and population growth in human history. According to the U.S. Energy Information Administration's *International Energy Outlook 2016* (EIA, 2016), total energy demand will grow by 48% between 2012 and 2040.

Ever since the Industrial Revolution, the vast quantities of fossil fuels (oil, coal and natural gas) that have been used to power the economy have risen this type of primary energy sources to the dominant form of total energy supply. Nowadays, fossil fuels provide over 85% of the total energy supply, according to the estimation made by BP Statistical Review of World Energy (Dudley, 2016), and will remain the dominant form of total energy supply (up to 78%) in 2040 (EIA, 2016).

However, the global raise of fossil fuels usage, especially since 1900, has led to a rapid growth of carbon dioxide (CO_2) emissions. CO_2 is one of the major GHGs, which warm the Earth by absorbing energy and slowing the rate at which the energy escapes to space. Most of the observed increase in global average temperatures since the mid-20^{th} century is very likely due to the observed increase in anthropogenic GHG concentrations (IPCC, 2007a). This anthropogenic climate change is well established with a high confidence as well are the negative impacts on natural and socio-economic systems (R. H. Moss et al., 2010; Stern et al., 2006). These impacts include higher temperatures and heat waves that result in thousands of deaths from hyperthermia (Dhainaut, Claessens, Ginsburg, & Riou, 2003; Fouillet et al., 2006; Poumadere, Mays, Le Mer, & Blong, 2005), crop failures (Conseil, 2010; D'amato & Cecchi, 2008) that aggravate global hunger (Parry, Rosenzweig, & Livermore, 2005; Schmidhuber & Tubiello, 2007; Shearer, 2011), rising sea levels (Church & White, 2006; Hansen et al., 2005), erosion of shorelines, increased risk of floods (Nicholls, Hoozemans, & Marchand, 1999), droughts (Dai, 2013), and fires (Amiro, Stocks, Alexander, Flannigan, & Wotton, 2001; Flannigan, Stocks, Turetsky, & Wotton, 2009).

These negative externalities have been shown to be due to human activities with the confidence level of 95% (IPCC report 2013). Since primarily combustion of fossil fuels is the dominant cause of global warming from 1951 to 2010 (Flato et al., 2013), reducing consumption of fossil fuels in order to reduce CO_2 emissions has become a crucial countermeasure for global warming.

1.1.2 Renewable Energy

Clean and inexhaustible, renewable energy is the best way to meet our energy needs posed by increasing population, and to avoid GHG emissions and depletion of fossil energy resources (Branker, Pathak, & Pearce, 2011).

Renewable energy is generally defined as energy that is collected from resources which are naturally replenished on a human timescale, such as sunlight, wind, rain, tides, waves, and geothermal heat (Ellabban, Abu-Rub, & Blaabjerg, 2014). Renewable energy resources are environment-friendly, sustainable, and exist over wide geographical areas, in contrast to fossil fuels, which are not clean, concentrated in a limited number of countries and non-renewable. As the economic costs of Renewable Energy Technologies (RET) have decreased, they are now more competitive with traditional electricity sources in many regions and have increased rapidly (Kirkegaard, Hanemann, Weischer, & Miller, 2010; Martinot, 2005). Rapid deployment of renewable energy is resulting in significant energy security, improvement of environmental sustainability (Anita & Babypriya, 2009; Demirbas, 2005; Kishore, Prasad, & Karan, 2006), and social-economic benefits (Heidari & Pearce, 2016; IRENA, 2016). But perhaps one of RETs greatest benefits is the value they bring for mitigation of GHG emissions and the concomitant climate change (El-Fadel, Chedid, Zeinati, & Hmaidan, 2003; Granovskii, Dincer, & Rosen, 2007; Longo, Markandya, & Petrucci, 2008; R. Sims, 2004; Tsoutsos, Papadopoulou, Katsiri, & Papadopoulos, 2008). According to *BP Statistical Review of World Energy* (BP2016, Dudley 2016), renewables (wind, solar, etc.) accounted for 6.7% of global power generation in 2015.

The incentive to use 100% renewable energy for electricity, transport, or even total primary energy supply globally, has been motivated by global warming and other ecological as well as economic concerns.

At the national level, at least 30 nations around the world already have renewable energy contributing more than 20% of their energy supply. National renewable energy markets are projected to continue to grow strongly in the coming decade and beyond (Martinot, 2013). Some places and at least two countries, Iceland and Norway, generate all their electricity using renewable energy already, and many other countries have set the goal to reach 100% renewable energy in a near future.

In Southern Africa (SA) many nations suffer from unreliable power supply, and the economic cost of power outages is high: an estimated 5-7% of the gross domestic product (GDP) for Tanzania, South Africa and Malawi (Eberhard, Rosnes, Shkaratan, & Vennemo, 2011). Moreover, energy demand in this region is rising quickly as observed, with more than 12% per year in

Mozambique and more than 10% per year in Zimbabwe for example (Southern African Power Pool, 2012). On the other hand, Southern Africa has great domestic renewable energy potential, such as the solar resource, which could be used to provide much needed energy in an affordable and secure manner, and to contribute to universal access to modern energy while avoiding negative environmental impacts.

The South African government aims to reduce GHG emissions significantly, hoping to cut down on GHG emissions by 42% by 2025 compared to a business-as-usual scenario (RSA, 2010), and the Department of Energy in South Africa plans to achieve 30% clean energy by 2025 (Department of Energy, 2011). Namibia has developed scenarios for its renewable energy future, including a 70% Renewable Energy (RE) target by 2030 (Ministry of Mines and Energy of Namibia, 2016).

Over the South West Indian Ocean (SWIO), several geographically isolated islands which are located far from any continent, are suffering from the strong dependence on traditional energy (e.g., imported fossil fuels), which leads to electrical continuity risks in case of supply disruption, as well as from the high cost of power transport with associated increasing GHG emissions. Renewable energy technologies consequently appear to be the most attractive solution to move from a system based on fossil fuel to a 100% renewable energy-system for many islands in this situation. For example, the overseas French Region of La Réunion (or Reunion Island) is looking for energy autonomy by 2030, with a medium objective of generating more than 50% of their electricity from renewable energy sources (Mimura et al., 2007; Praene, David, Sinama, Morau, & Marc, 2012), with solar energy being a very promising one. The Island of Mauritius is seeking to achieve about 35% self-sufficiency in terms of electricity supply through the use of renewable sources of energy by 2025 (Mimura et al., 2007; Ministry of Renewable Energy of Mauritius, 2009).

1.1.3 Solar Energy

Solar energy reaches the Earth's surface either as direct beam from the Sun or in diffuse form after scattering in the atmosphere. The sum of the direct and diffuse radiation incident on the surface is known as global radiation (mostly among experimentalists), or surface solar radiation (SSR) and surface downward solar radiation (RSDS, among modellers), sometimes also as surface insolation or solar/shortwave irradiance (Wild, 2009).

Readily available at the surface all over the world, solar energy is the most promising source of renewable energy. Direct use of solar resource through photovoltaic (PV) is considered as a clean, sustainable, renewable energy conversion technology that can help meet the energy demands of the world's growing population, whilst reducing the adverse anthropogenic impacts of fossil fuel use (IEA, 2008; Pearce, 2002; R. E. Sims, Rogner, & Gregory, 2003). Over the last ten years, an exponential increase of PV installations has been observed worldwide. Solar power generation grew by 32.6% in last decade (up to 2015), due to both technological innovations and various government incentives (Jogleka & Graber-Lopez, 2008; Junfeng et al., 2009; Kirkegaard et al., 2010; Price & Margolis, 2010; Primer, 2009) reaching around 227 GWe (gigawatt electrical) at the end of 2015 (world energy resource 2016). An estimation by Greentech Media (GTM) marks that the total capacity of solar energy will probably reaching the same level as nuclear energy in the end of 2017 and will continuously increase to 871 GW in 2020, which is the twice of current nuclear energy capacity (Attia, Heggarty, & Parikh, 2017).

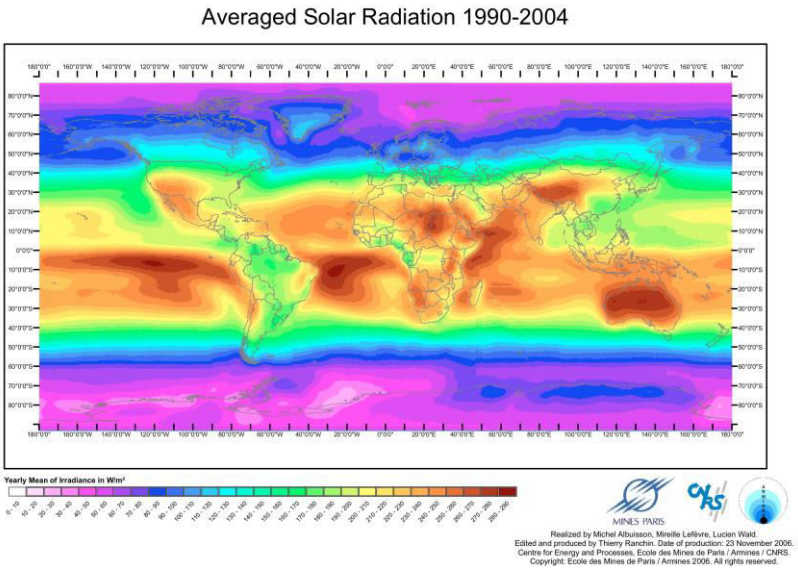

Fig. 1-1 Annual mean surface solar irradiance (in units of W/m^2) as observed by satellite during the time 1990 - 2004. This fiture is taken from Ecole des Mines de Paris, Armines 2006.

Regionally, in the SA-SWIO, the average amount of solar radiation incident on the Earth's surface around 250 W/m^2, makes it one of the first regions in the world in regard to the available solar resource, along with the southwestern U.S.A, Australia and Indonesia, central Asia and many areas of Africa (mainly deserts).

Because of its location in the centre of the SWIO, Reunion Island has abundant energy resource. To meet the electricity autonomy target, PV farms connected to the grid will have to be largely developed. At the end of 2010 in Reunion, PV systems represented approximately a power of 80 MWp (Mega Watt peak) for an electricity production of 60 GWh (Gigawatt hours) (FJ., 2010). Over the last 5 years, an exponential increase of the PV installations has been observed. The first PV systems set up in Reunion were stand-alone systems. Today, the economy of the island is focused on the PV farms connected to the grid. In 2009, with a ratio of 52 Wp (Watt peak) of PV per inhabitant, Reunion was the third best-equipped territory after Spain and Germany (OER, 2010).

Energy yields of PV systems first of all depend on the available amount of solar radiation reaching the Earth's surface. In addition, changes in ambient temperatures have to be taken into account, since increasing ambient temperatures decreases PV power output. There are also other meteorological factors that influence energy yields of PV systems, such as the wind, the snow or the deposition of dust on the PV panels. They have relatively smaller impact on PV system (see e.g., (Huld, Šúri, & Dunlop, 2008; Reich et al., 2012; Thevenard & Pelland, 2013) for more details on energy yields of PV systems). Changes in surface temperature are a widely acknowledged aspect of climate change, while changes in SSR have been discussed to a much lesser degree.

1.1.4 Surface Solar Radiation Variability

SSR shows variations at various scales in both time and space (Perez & Hoff, 2013). In general, the value of SSR in a location depends on the position of the sun, the clearness of the sky, land use and vegetation of the surface, which are continuously changing in different time scales. As an example, changes of SSR in a location can be of natural origin, such as those induced by changing atmospheric cloud condition on time scales of minutes, Sun-Earth geometric-resulting diurnal and seasonal variation, a major volcanic eruption on time scales of a few years (McCormick, Thomason, & Trepte, 1995; Robock, 2000). On the other hand, there is growing evidence that human interference with climate leads to alteration of solar radiation in polluted atmospheres (Wild, 2009).

SSR in southern Africa varies significantly across regions of different climate types and at seasonal time scales. The Inter Tropical Convergence Zone (ITCZ) oscillates north and south as the solar declination changes with season. During the austral summer (DJF), ITCZ reaching its southernmost position (with precipitation maxima in southern tropical Africa and Madagascar), together with the moisture coming with the easterly flow from the Indian Ocean (to Eastern Africa), brings strong precipitation and associated enhanced cloudiness over Central and South equatorial Africa, which leads to a reduction of solar radiation reaching the Earth's surface. At higher latitudes, SSR increases toward the southwest of the SA continent (hereafter SA-WS), reaching its peak value areas west of over the Kalahari, which is related to the seasonal changing solar zenith angle toward the position of the sun in this season, and a dryer atmosphere with less cloudiness resulting from large-scale atmospheric subsidence associated with the poleward limb of the Hadley cell (Salby, 1996; Schneider, Bischoff, & Haug, 2014).

In the JJA season, in spite of the fact that the centre of the rain belt shifts to its most northerly position (in the northern hemisphere) with the ITCZ, its southern extension still remains in the southern hemispheric part of the tropical Atlantic Ocean, with reflective clouds. SSR is reduced by these clouds in the area, thus shows relatively lower values than its southern neighbour, the centre of southern Africa (here after SA-C). In the south of ~5°S, precipitation in JJA decreases to its lowest value, with ~ < 1mm/day. Cloudiness is much less compared with the equatorial area and with DJF, and together with the decreasing clear-sky SSR, leading to a generally meridional SSR gradient decreasing poleward over the African continent and the ocean. However, in Madagascar cloud cover fraction has a geographic variation, with a much higher value on the mountainous eastern coast than on the western part of the island.

The time-and space-dependent global solar radiation at the location of interest is the most critical input parameter employed in the design and prediction of the performance of a solar energy device (Davy & Troccoli, 2012; Hussain, Rahman, & Rahman, 1999; Journée & Bertrand, 2010; Monforti et al., 2014). In this context, a comprehensive assessment of SSR is required, not only

the mean characteristics of the solar resource at any location but also its temporal repartition. In particular, the impacts of long-term variability and possible climate change of the solar resource on system performance need to be addressed when considering the life expectancy of solar energy systems from 20-25 years up to 40 years for PV panels (Jordan & Kurtz, 2013; Skoczek, Sample, & Dunlop, 2009).

Decadal variability of SSR

There is growing evidence from long-term observational radiation records, that surface solar radiation undergoes substantial large-scale decadal variations in SSR, which should be considered in solar resource assessments (Müller, Wild, Driesse, & Behrens, 2014; Wild, 2012; Wild, Folini, Henschel, Fischer, & Müller, 2015). As an example, one of the longest records of SSR, available from Potsdam (Germany) since 1937, is illustrated in **Fig. 1-2** (taken from Wild 2016).

The various studies analysing long-term records of surface radiation measurements suggest a widespread decrease in surface solar radiation between the 1950s and 1980s (''global dimming''), with a partial recovery more recently at many locations (''brightening''). There are also some indications for an ''early brightening'' in the first part of the 20th century (Ohmura, 2009; Wild, 2009). These variations are in line with independent long-term observations of sunshine duration, diurnal temperature range, pan evaporation, and, more recently, satellite-derived estimates, which add credibility to the existence of these changes and their larger-scale significance (Wild, 2005; Wild, 2009; Wild, 2012, 2016). Note that "global" thereby originally referred to "global radiation", rather than to a global scale dimension of the phenomenon, and the term "brightening" was thereby coined to emphasize that the decline in SSR and associated global dimming no longer continued after the 1980s (Wild, 2005).

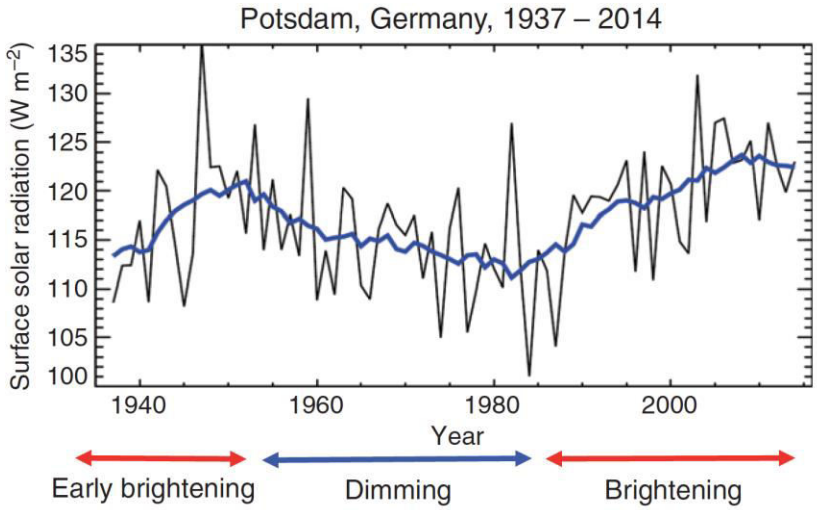

Fig. 1-2 Annual mean surface solar radiation (in W/m^2) as observed at Potsdam, Germany, from 1937 to 2014. Five year moving Annual mean surface solar radiation (in Wm−2) as observed at Potsdam, Germany, from 1937 to 2014. Five year moving average is in blue. Distinct phases of inclines (1930s–1940s, 'early brightening'), declines (1950s–1980s, 'dimming'), and renewed inclines (since 1980s, 'brightening') can be seen. In addition, a stabilization since around 2010 can be noted. Figure from Wild 2016.

Although data sparsity and heterogeneity make it really challenging to study SSR decadal variation in a global perspective (**Fig. 1-3**), evidence for dimming/brightening has been documented widespread, based on data from direct SSR measurements, satellite-derived fluxes and relevant meteorological quantities used as proxies for SSR changes. The first evidence is pointed by studies based on sites in Europe (Ohmura et al., 1998), the Baltic (Russak 1990), the South Pole (Dutton et al. 1991), as well as in different regions globally (Stanhill and Moreshet 1992), Germany (Liepert et al. 1994), and the former Soviet Union (Abakumova et al. 1996). Benefiting from the fact that high-quality data with known accuracy are becoming increasingly available, decadal variations of SSR are further examined regionally and with a global perspective. In addition, satellite-derived fluxes and relevant meteorological quantities (as proxies for SSR changes) are used to detect SSR decadal variation. By now, a comprehensive literature exists that confirms declines of SSR over a period of roughly 1960–1990 in different parts of the world, summarized by (Wild, 2016) and references therein. The brightening of SSR is also observed worldwide. However, the picture is somewhat less globally coherent, with trend reversals and increases at widespread locations, but also some regions with continued decrease (e.g., India: (Soni, Pandithurai, & Pai, 2012)). SSR evolution beyond the year 2000 is of more concern to the solar energy community, because of its significant increase in this period. SSR variation show mixed tendencies after 2000 worldwide (Wild, 2016). Overall, the direct observations suggest that brightening is less distinct after 2000 than in the 1990s.

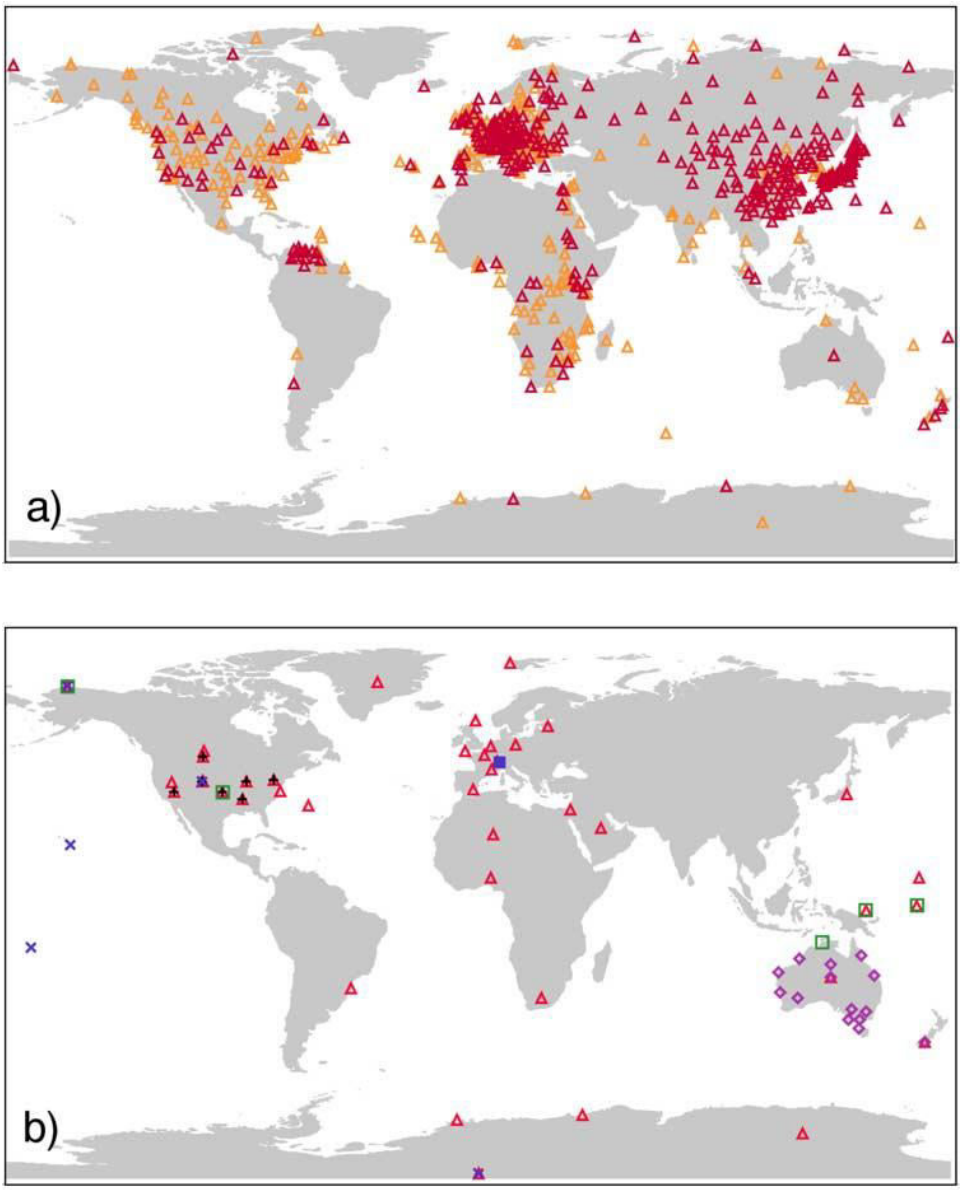

Fig. 1-3 Global distribution of surface radiation networks: (a) historic GEBA/WRDC stations with more than 10 years (orange triangles) and 20 years of measurement records (red triangles), many of them going back to the 1960s, (b) modern high-accuracy stations with multiyear records: BSRN (38 sites worldwide, red triangles), ARM (5 sites worldwide, green squares), NOAA/SURFRAD (7 sites in the United States, black plus signs), NOAA/ESRL (5 sites worldwide, blue crosses), Australian Network (14 sites in Australia, purple diamonds), and the Alpine Surface Radiation Budget network (ASRB) (7 sites in the Swiss Alps, filled blue square).

To sum up, literature estimates for the overall SSR decline during dimming range from 3 to 9 W m^{-2}, and from 1 to 4 W m^{-2} for the partial recovery during subsequent brightening (Stanhill and Moreshet 1992; Liepert et al. 1994; Abakumova et al. 1996; Gilgen et al. 1998; Stanhill and Cohen 2001; Alpert et al. 2005; Kvalevag and Myhre 2007; Kim and Ramanathan 2008; Wild 2009). Note that observed brightening has generally not fully compensated for prior dimming, so that

insolation levels at the turn of the millennium were typically still below those in the 1950s (Wild, 2016). SSR evolution beyond 2000 shows mix trends over the world.

The region of SA-SWIO, and especially the ocean areas representing the SWIO, is insufficiently covered by direct surface radiation stations (see **Fig. 1-3**). The SSR variability over SA-SWIO is not yet well documented. Using data from four sites in Central Africa, two in Zaire and two in Zimbabwe, Ohmura (2009) found a decrease of 32 W/m^2 over 52 years 1954 to 2005. Power and Mills (2005) analyzed data from eight sites in South Africa and two sites in Namibia covering roughly the 1960 to 1990 period. They found decreasing SSR at eight of these sites (six statistically significant) and no station with a statistically significant increase, and determined a mean decrease of 2.2% per decade (5.4 W/m^2/decade). Wild (2005) found a decrease of SSR during 1965 – 2000 using data from 3 sites in Zimbabwe. Gilgen, Roesch, Wild, and Ohmura (2009) made use of the numerous records collected in Global Energy Balance Archive (Wild, Ohmura, et al. 2017), and sampled them onto a global 2.5° x 2.5° grid. They found that SSR decreased significantly in large regions of Africa at 2% per decade on average from the late 1950s up to 1990. In another study with a global perspective, Liepert (2002) used 252 long-term records from GEBA/WRDC (with several sites located in the southern Africa) as well as 43 time series contained in the United States National Solar Radiation Database. They estimated a decline of SSR at these worldwide distributed sites of 7 W/m^2, or 4%, on average over the period 1961 – 1990. However, as our knowledge, no detailed assessment has been conducted for the SWIO.

Many works study SSR decadal changes simulated by climate models, including global and regional models (although relatively rare). Global Climate Models (GCMs) are the most powerful tools currently available to investigate the effect of anthropogenic activities on the climate system, and to project the future evolution of Earth's climate. A large number of studies have investigated the ability of the GCMs to reproduce the decadal changes in standard observations like temperature or precipitation. Fewer studies have focused on the ability of the models to simulate the variations in SSR. Overall, the available studies suggest that GCMs simulate smaller decadal changes in SSR than what has been inferred from surface observations during the 20th century (Allen, Norris, & Wild, 2013; Wild, 2009; Wild & Schmucki, 2011). The origins of the discrepancies between simulated and observed decadal changes in SSR are still not clear and require further research.

Causes of the Variations

It is well established that the origins of these SSR variations cannot be changes in the output of the sun itself, because these are at least an order of magnitude smaller (Willson & Mordvinov, 2003) and uncorrelated, but rather be variations in the transparency of the atmosphere for solar radiation. Particularly, clouds and aerosols are the major contributors to the SSR variations.

Changes in cloud amount and cloud optical properties can substantially alter SSR. Aerosols can also attenuate SSR, by scattering and absorbing solar radiation (direct effect), or indirectly by cloud mediated effects, through their ability to act as Cloud Condensation Nuclei (CCNs), thereby increasing cloud reflectivity and lifetime (first and second indirect effects; e.g., (Lohmann & Feichter, 2004; VCPJ Ramanathan, Crutzen, Kiehl, & Rosenfeld, 2001). Both direct and indirect aerosol effects act toward reducing SSR with increasing aerosol levels. The relative importance of clouds and aerosols, as well as their interactions for the explanation of the observed SSR variations have been widely disputed, but this issue is far from being settled. The relative importance of aerosols, clouds, and aerosol-cloud interactions may differ depending on the region and pollution level. Anthropogenic air pollution has led to substantial changes in atmospheric aerosol levels over past decades (Stern et al., 2006; Streets et al., 2009; Wang, Dickinson, & Liang, 2009). The anthropogenic air pollution strongly increased from the 1950s to the 1980s and declined thereafter in the Northern Hemisphere, while pollution levels on the Southern Hemisphere were an order of magnitude lower and steadily increased with no trend reversal (Stern et al., 2006; Wild, 2012) indicative probably a dominate role of cloud as SSR factor in the Southern Hemisphere.

Impacts of long-term variations of SSR

SSR plays a prominent role in the climate system as it states a major energy exchange at the interface between the atmospheric component, land, biosphere, cryosphere and ocean components. Variations in SSR have, therefore, the potential to significantly impact diverse aspects of the climate system.

First, SSR changes may have impacts on surface temperature and global warming, since SSR governs evolution of temperature to a considerable degree at the Earth's surface. Studies on both observations or climate models pointed out that the dimming/brightening of SSR has a suppression/contribution to the global warming as reviewed by Wild (2009) and references therein. That indicates the crucial role that decadal SSR variations may play in modulating global warming.

Second, radiative energy available at the Earth's surface is the principal driver of the hydrological cycle (VCPJ Ramanathan et al., 2001). Surface net radiation (the sum of the solar and thermal energy exchanges at the Earth's surface), governs the intensity of the global hydrological cycle through altering the energy available for evaporation (Ohmura & Wild, 2002). There are studies reporting that correlation between changes of surface net radiation and hydrological cycle, in "early brightening" (Wild, 2008; Wild, 2009), dimming (Liepert, Feichter, Lohmann, & Roeckner, 2004; Peterson, 1995; Wild, Ohmura, Gilgen, & Rosenfeld, 2004), and brightening periods (IPCC, 2007a; Wild, 2009; Wild, Grieser, & Schär, 2008). Impacts of SSR variation on other aspects of hydrological cycle are also found, for example, the long-term soil moisture changes (Robock, Mu, Vinnikov, Trofimova, & Adamenko, 2005), droughts and famines (Rotstayn & Lohmann, 2002) and monsoon systems (Menon, Hansen, Nazarenko, & Luo, 2002;

V Ramanathan et al., 2005). Overall, this implies that decadal variations in SSR, combined with increasing downwelling thermal radiation, indeed had a discernible impact on the variations of the hydrological cycle over the 20th century.

1.1.5 Previous Works on Future Long-term Changes in Solar Surface Radiation

Estimating potential future changes in surface solar radiation, has to rely on projections from comprehensive numerical models of the climate system. These models have become the primary tools for the development of climate change scenarios for the 21st century, such as those released in the latest (fifth) assessment report of the Intergovernmental Panel on Climate Change (IPCC, 2013).

However, despite the importance and growing interest of SSR for energy applications and for climate modelling, only few studies have investigated directly the future projections of SSR. A limited number of studies describe the scenarios of SSR changes based on global climate model (GCM) simulations mainly in relation to future solar energy applications (Crook, Jones, Forster, & Crook, 2011; Gaetani et al., 2014; Remund & Müller, 2010; Wild, Folini, Hakuba, et al., 2015).

Future projection SSR over SA-SWIO could be seen in several global studies based on GCMs. In the work of Wild, Folini, Henschel, et al. (2015) decadal changes in all- and clear-sky surface solar radiation, cloud amount and surface temperature as projected up to 2050 under the Representative Concentration Pathway, RCP8.5 forcing scenarios of 39 GCMs used in the framework of the latest (5th) IPCC assessment report, have been analysed. Globally robust and statistically significant trends of temperature are observed. Small and generally positive impacts of climate change on the mean of SSR has been found in southern Africa over land (except South Africa), even with a low level of consistency of model projections and statistically significance (Wild, Folini, Henschel, et al., 2015). They further pointed that the signs of cloud and all-sky radiation changes, which are more difficult to predict for the models, are still fairly consistent in large parts of the globe. This suggests that projections of all-sky radiation changes on these timescales are not purely random, but provide an overall reasonably consistent response pattern to the imposed forcing under the RCP8.5 scenario. Gaetani et al. (2015) found an increase of less than 5% in SSR up to 2030 over Africa under the IPCC SRES B2 scenario. A general concern regarding GCM outputs, in particular with any plausible future of renewable resource availability they may project, are the inherent uncertainties of climate modelling. The fact that only few studies have looked at future changes in solar resource, is likely due to the uncertainties in GCM cloud cover estimations (Fant, Schlosser, & Strzepek, 2015). Studies of SSR projections based on regional climate models (RCM) were conducted in recent years (Alexandri et al., 2015; Bartók et al., 2016; Fant et al., 2015; Finger, Heinrich, Gobiet, & Bauder, 2012; Gunderson, Goyette, Gago-Silva, Quiquerez, & Lehmann, 2015; Jerez et al., 2015; Panagea, Tsanis, Koutroulis, & Grillakis, 2014; Pasicko, Branković, & Šimić, 2012). While local most studies are focusing on Europe.

Research in SA is particularly rare, although this area is one of the most vulnerable regions to weather and climate variability (IPCC, 2007b). To estimate the risk of climate-change on wind and solar resource potential in Southern Africa, Fant et al. (2015) combined the risk-based cli-

mate projections from the Integrated Global Systems Model (IGSM), which considers emissions and global climate sensitivity uncertainty, with more regionally detailed climate information from 8 GCMs available from the Coupled Model Intercomparison Project phase 3 (CMIP-3) and concluded that the long-term mean wind and solar resource potential will, most likely, remain unchanged by 2050.

To summarize, SSR long-term changes is not well documented over SA and there's no public research works on SSR future projection over the particular area of SWIO by now. And the few previous works focusing on SA is conducted based on limited number of models, and relative short projection time (to 2050) and using only single climate change scenarios, thus lacking the analysis of climate change sensitivity to the anthropogenic GHG emissions.

1.2 Scopes and Objectives

The characterization of variability in SSR at the location of interest is the most critical input parameter employed in the design and prediction of the performance of a solar energy device. In this study, possible impact of climate change on SSR will be simulated and evaluated at regional scales by downscaling projections from CMIP5 models over SA-SWIO, where solar PV system is a promising alternative to meet our increasing energy demand, and potentially mitigating energy-related GHG emission.

As discussed above (**section 1.1.5**), SSR long-term changes is by now not well documented over SA and especially the particular area of SWIO. And the few previous works focusing on SA is conducted based on limited number of models (only GCMs), and relative short projection time (to 2050) and using only single climate change scenarios, thus lacking the analysis of climate change sensitivity to the anthropogenic GHG emissions.

The aim of this study is to provide a comprehensive picture of the effects of climate change on SSR projections in SA-SWIO. For this purpose, we use ensembles from the most up-to-date of regional climate models from AFRICA-CORDEX and their associated driving global models from CMIP5 under the RCP4.5 and RCP8.5 scenarios.

Besides providing the information of solar energy industry over the SA-SWIO, this study will also promisingly i) provide a comprehensive examination of long-term SSR changes in the SA-SWIO, which will fill the gaps of current knowledge in this area, ii) give an example of assessment of solar resources using projections from state-of-art CMIP5 models and dynamical downscaling technique conducted by RCMs, iii) draw attention from downscaling community on the concern of model performance in downscaling long-term SSR, and iv) address the important role that long-term SSR changes may play in modulating future climate and climate change.

1.3 Outline of the thesis

This thesis is organized as follow: methods and reference data are described in Chapter 2, along with the reference data used in this study; Chapter 3 illustrates SSR long-term changes simulated by a regional climate model, namely RegCM4 over SA-SWIO. Then an SSR projection ensembles including simulations from 5 RCMs that participated to the CORDEX-Africa experiment and their driven 10 GCMs are examined in Chapter 4. Finally, conclusions and discussions are given in Chapter 5.

2 Methods and Reference Data

OUTLINE:

Present-day and future projections of SSR are simulated by Global Climate Models (GCMs) with a horizontal resolution of about a few hundreds of kilometres. To get SSR at regional scales (~ 50 km), dynamical downscaling conducted by Regional Climate Models (RCMs) is used in this study (**Section 2.1**). RCMs are constructed for limited areas with a considerably higher resolution than the GCMs to describe regional-scale climate variability and change. The study towards a comprehensive knowledge of SSR changes in context of climate change is thus conducted, using outputs from CORDEX-Africa program (Filippo Giorgi, Jones, & Asrar, 2009). Continuous outputs from 5 RCMs participated into CORDEX-Africa program driven by 10 GCMs are analysed over southern Africa (SA) domain under RCP4.5 and RCP8.5 based on the experience of modeling African climate in the climate modeling community (**section 2.2)**. The references data used for model evaluation are listed in **section 2.4**.

In the context of energy autonomy target in near future of Reunion island and Mauritius island, a future downscaling project has been proposed to further investigate the impact of changes of SSR on the solar power system at local scale (~ 1km horizontal resolution). To contribute to the proposed downscaling project at local scale in Reunion Island and Mauritius Island, located in the South West Indian Ocean (SWIO), near the broader of CORDEX-Africa domain, a particular RCM, namely RegCM version 4 (hereafter referred to as RegCM4 or simply RegCM) is used to downscale the GCMs outputs over Southern Africa and South West Indian Ocean (SA-SWIO) at a 50-km resolution up to the end of the 21st century (**Section 2.2**) as the first step of downscaling towards 1 km resolution. This particular model has been chosen because of the experience of climate modeling research using RegCM (Li, 2015; Li, Morel, Bessafi, Solmon, & Chiacchio, 2013) and easy access to technical support from the International Centre for Theoretical Physics (ICTP), where the RegCM4 model has been developed and maintained. Considering the requirements of long-term temporal coverage for climate change analysis and available computing power to run RegCM over a large domain such as SA-SWIO, thus limiting the length of the simulations, a slice experiment has been designed covering three temporal windows: a) the present 1996-2005; b) the future 2046-2055 and 2090-2099, in line with the methodology of, e.g., Crook et al. (2011) and Gula and Peltier (2012). Firstly, to better understand the model (RegCM4) performance in this particular region (SA-SWIO) with little experience, an ensemble of RegCM4 simulations forced by ERA-Interim reanalyses (ERAINT hereafter) with various model physical setups are conducted as a "sensitivity study". Optimal parameter settings for the model physics are estimated to define to have the acceptable small bias of interesting variables, including SSR, Surface Air Temperature (TAS), Total Precipitation (PR), and Total Cloud Fraction (CLT) (**Section 2.3.2**). Internal variability gives rise to large uncertainty in projections of future climate. An experiment consisting of 20 ensembles of RegCM runs driven by ERA-Interim is taken to understand the behaviour of the model in response to the internal variability (**Section 2.3.3).**

The conducted slice simulation was taken mainly because of the limit of available computational resources for a requirement of long-term climate change impact study. Although there are several previous works using 10-year windows to estimate long-term climatology, e.g. Crook et al. (2011)

and Gula and Peltier (2012), continuous simulations are the first choice because of better temporal coverage to capture inter-decadal variations (Wild, 2009; Wild, 2016). For solar energy application study, covering the near-term future is necessary when considering the life time of solar power equipment of 20-30 years. In this study, only two GCMs are downscaled to regional scale in a single RCP8.5 scenario. Understanding the role that boundary condition plays in the downscaling process is a major concern for the climate community. However, to isolate the impact of forcing data, a range of different boundary conditions has to be applied to particular RCMs, or one single forcing to drive several RCMs. In addition, at least another climate change scenario is needed to estimate the sensitivity to different forcings.

2.1 SSR climatology over SA-SWIO and Dynamical Downscaling

2.1.1 Dynamical downscaling

Due to the complex nature of these SSR related processes, especially those associated with cloud, no theoretical calculation of SSR is entirely accurate. Nevertheless, numerical models (e.g. General Circulation Models or GCMs) can reasonably simulate all the factors influencing SSR, by taking all of the necessary processes into account, working as a physical model of the whole climate system. GCMs, representing physical processes in the atmosphere, ocean and land surface, are the most advanced tools currently available for simulating the response of the global climate system to increasing GHG concentrations.

While the GCMs are most reliable at the continental scale, they cannot account for the fine-scale heterogeneity of climate variability and possible change due to their coarse resolution. Numerous landscape features such as mountains, water bodies, infrastructures, land-cover characteristics, and components of the climate system such as convective clouds and coastal breezes, have scales that are much finer than those resolved explicitly by GCMs (100–500 km). Such heterogeneities are important for decision makers who require information on potential impacts on crop production, hydrology, species distribution, solar energy prediction, etc. at local (1-5 km) or regional scales (10-50 km). Downscaling is the term to describe the various methods used to translate different sources (e.g., climate projections from coarse resolution GCMs or reanalysis) to finer resolutions deemed more helpful for assessing impacts. It is used as an attempt to increase the understanding of climate change influences at the regional scale.

Downscaling approaches are generally categorized as statistical, using empirical relationships, and dynamical, using regional climate models. Statistical downscaling is likely to be preferred where estimates of specific variables, especially at point locations, are sought for input to sector models (e.g., hydrologic models) or for decision making. However, statistical modelling could mask a true understanding of regional climate dynamics and estimates may also be overconfident (Brown, Greene, Block, & Giannini, 2008). Dynamical downscaling is useful for incorporating topographic features, such as strong orography, and land use and vegetation. It is recommended where those features play a significant role in the regional climate. However, computational time and the uncertainties that accompany complex models have to be considered.

Because the main objective of this study is to archive regional estimation of SSR, which varies from hourly to decadal time scales over a region characterised by complex surface (as shown in **Fig. 2-1**), dynamical downscaling conducted by regional climate models is used in the following to produce geographically and physically consistent results.

Dynamical downscaling method have improved and have been widely applied over various regions over the world (Dickinson et al., 1989; Giorgi and Bates, 1989; Kida et al., 1991; Juang and Kanamitsu, 1994; Bosilovich and Sun, 1999; Leung and Ghan, 1999; Laprise et al., 2000; Liang et al., 2001; Xue et al., 2001; Castro et al., 2005). There is high confidence that downscaling adds value both in regions with highly variable topography and for various small-scale phenomena (Feser, Rockel, von Storch, Winterfeldt, & Zahn, 2011).

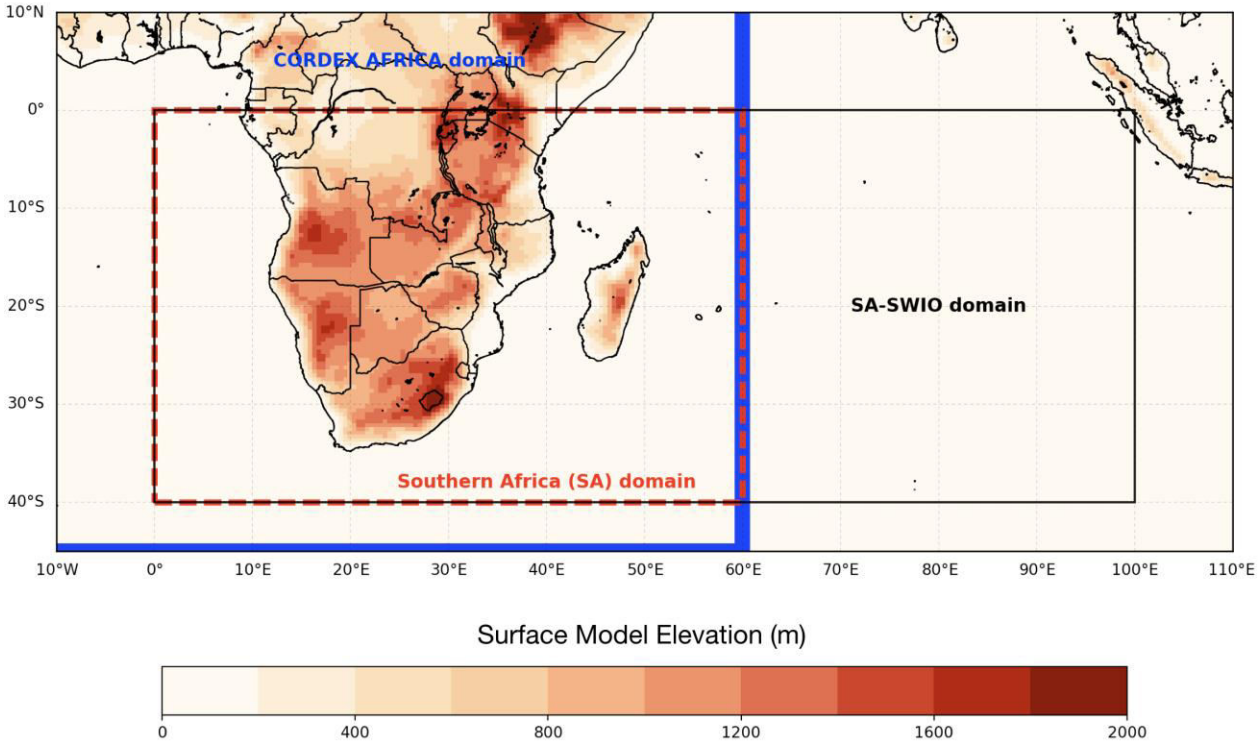

Fig. 2-1 Surface Model Elevation (m) of Southern Africa (SA, in read dash box) and Southern Africa & South West Indian Ocean (SA-SWIO, in black solid box) in 50 km horizontal resolution. The blue lines on the maps indicate the eastern and southern borders of CORDEX-AFRICA domain. For the CORDEX-AFRICA domain and SA-SWIO domains (covered by RegCM4 simulation), buffer zones outside their boundaries has been removed. SA domain is the area that CORDEX-AFRICA simulations ensembles are collected and analyzed in present study (see **Fig. 4-6** and Chapter 4).

The derivation of fine-scale climate information by dynamical downscaling is based on the assumption that the local climate is conditioned by interactions between large-scale atmospheric characteristics (circulation, temperature, moisture, etc.) and local features (water bodies, mountain ranges, land surface properties, etc.). It is possible to model these interactions and establish relationships between present-day local climate and atmospheric conditions through the downscaling process (e.g., **Morel et al. 2014**, **Pohl et al. 2016**). It is important to understand that the downscaling process adds information to the coarse GCM output so that information is more realistic at a finer scale, capturing sub-grid scale contrasts and inhomogeneities.

Employing dynamical downscaling via RCMs and highlighting their performance in regional climate research. The Coordinated Regional Downscaling Experiment (CORDEX; e.g. **Giorgi et al. 2009**; **Farneti 2017**, http://www.cordex.org) program, established by the World Climate Research Program (WCRP), for example, was a direct response to the need of downscaled products in climate modelling (Jones, Giorgi, & Asrar, 2011). CORDEX studies have demonstrated that added value arises from higher resolution of stationary features like local orography, land-sea contrast, and small-scale atmospheric features such as convective cells, which are not well represented in global climate models.

Practically, the dynamical downscaling method employs a continuous integration of a RCM where GCM data are used to provide initial conditions, lateral boundary conditions (LBCs) and SSTs. One shortcoming of this nesting approach is that the regional models necessarily inherit biases from the global models used to provide boundary conditions. Furthermore, the ability to systematically evaluate regional climate models is still challenging. Thus, the selection of driving GCMs and careful evaluation of RCMs' outputs are playing a particular important role in regional downscaling studies. Dependences on Initial and Boundary Condition (ICBC) from GCMs are also investigated in this study (e.g. RegCM4 simulations in Chapter 3 and CORDEX simulations in Chapter 4), and widely compared with many previous studies highlighting the impact of GCMs (via ICBC) on dynamical downscaling. Due to the inherent uncertainty of the climate system and the inevitable existence of model errors, multi-model ensembling is the recommended approach for characterizing expected climate changes.

2.2 Long-term dynamical downscaling within CORDEX-Africa program

In this study, the outputs of downscaling experiments (**Table 2-1**) embedded into the Coordinated Regional Climate Downscaling Experiment (CORDEX, Giorgi et al. 2009) has been collected. The outputs of their 10 driving GCMs are also considered, to analyse the impact of GCMs (via ICBC) on dynamical downscaling. To quantify the sensitivity of climate change to the anthropogenic Green House Gas (GHG) emission, simulations' results under RCP4.5 and RCP8.5 scenarios (R. H. Moss et al., 2010; Van Vuuren et al., 2011) are considered.

RCM Name (version)	Institution (abbreviation)	Exp. NO.	Forcing GCM
RCA4 (v1)	Swedish Meteorological and Hydrological Institute, Rossby Centre (SMHI)	1	CanESM2
		2	CNRM-CM5
		3	CSIRO-Mk3-6-0
		4	EC-EARTH
		5	IPSL-CM5A-MR
		6	MIROC5
		7	HadGEM2-ES
		8	MPI-ESM-LR
		9	NorESM1-M
		10	GFDL-ESM2M
CCLM4-8-17 (v1)	Climate Limited-area Modelling Community (CLM-Community, CLMcom)	11	CNRM-CM5
		12	EC-EARTH
		13	HadGEM2-ES
		14	MPI-ESM-LR
HIRHAM5 (v2)	Danish Meteorological Institute (DMI)	15	EC-EARTH
		16	NorESM1-M
RACMO22T (v1)	Royal Netherlands Meteorological Institute (KNMI)	17	EC-EARTH
		18	HadGEM2-ES
REMO (v1)	Helmholtz-Zentrum Geesthacht, Climate Service Center, Max Planck Institute for Meteorology (MPI-CSC)	19	EC-EARTH
		20	IPSL-CM5A-LR
		21	MPI-ESM-LR

Table 2-1. 20 regional climate model simulations considered in this study and their forcing GCMs.

CORDEX AFRICA (**Fig. 2-1**) program provides regional climate projections for the African domain at a grid spacing of about 50 km (0.44 resolution). The selection of GCMs is based on their use in the CORDEX Africa downscaling experiment. It is limited because only a few GCMs are currently downscaled to a high resolution of 0.44° over the Africa domain. The monthly RSDS, total cloud cover fraction (CLT, units in %, as absolute percentage and not relative value, if not indicated otherwise) are used in this study. **Table 2-1** contains 5 regional climate models considered in the study, where the driving GCMs realizations are also listed.

RCM Name	Institution	Reference	Exp. NO	Forcing model	Radiative forcing
RCA4	Swedish Meteorological and Hydrological Institute, Rossby Centre (SMHI)	Samuelsson et al. (2011)	1	CanESM2	RCP4.5, RCP8.5
			2	CNRM-CM5	RCP4.5, RCP8.5
			3	CSIRO-Mk3-6-0	RCP4.5, RCP8.5
			4	EC-EARTH	RCP2.6, RCP4.5, RCP8.5
			5	IPSL-CM5A-MR	RCP4.5, RCP8.5
			6	MIROC5	RCP4.5, RCP8.5
			7	HadGEM2-ES	RCP2.6, RCP4.5, RCP8.5
			8	MPI-ESM-LR	RCP2.6, RCP4.5, RCP8.5
			9	NorESM1-M	RCP4.5, RCP8.5
			10	GFDL-ESM2M	RCP4.5, RCP8.5
CCLM4-8-17	Climate Limited-area Modelling Community (CLM-Community, CLMcom)	(Panitz, Berg, Schädler, & Fosser, 2012; Panitz, Dosio, Büchner, Lüthi, & Keuler, 2014; Rockel, Will, & Hense, 2008)	11	CNRM-CM5	RCP4.5, RCP8.5
			12	EC-EARTH	RCP4.5, RCP8.5
			13	HadGEM2-ES	RCP4.5, RCP8.5
			14	MPI-ESM-LR	RCP4.5, RCP8.5
HIRHAM5	Danish Meteorological Institute (DMI)	Christensen OB (2006)	15	EC-EARTH	RCP4.5, RCP8.5
			16	NorESM1-M	RCP4.5, RCP8.5
RACMO22T	Royal Netherlands Meteorological Institute (KNMI)	Van Meijgaard et al. (2008)	17	EC-EARTH	RCP2.6, RCP4.5, RCP8.5
			18	HadGEM2-ES	RCP2.6, RCP4.5, RCP8.5
REMO2009	Helmholtz-Zentrum Geesthacht, Climate Service Center, Max Planck Institute for Meteorology (MPI-CSC)	(Fotso-Nguemo et al., 2017); (Jacob et al., 2012)	19	EC-EARTH	RCP2.6, RCP4.5, RCP8.5
			20	MPI-ESM-LR	RCP2.6, RCP4.5, RCP8.5

Table 2-2 List of the Regional Climate Models used in this study. All the 20 experiments are available under RCP4.5 and RCP8.5 but only 6 under RCP2.6 are used mainly because of data availability.

2.2.1 Separate sources of uncertainty of climate projections

Different sources of uncertainty in SSR projection is to be separated into three different type: Scenario uncertainty, Internal Variability (nature variability) and Model uncertainty (GCM and RCM). To qualify their relative contribution to the total uncertainty, and because of the data availability, the analysis is taken with data from two different groups: Group I consists only 7 experiments, while they are available under all the 3 RCP scenarios (RCP2.6, RCP4.5, RCP8.5) as listed in **Table 2-2**; and Group II consists all the 20 RCM experiments, but under only two RCP scenarios (RCP4.5 and RCP8.5). Obviously, the scenario uncertainty becomes smaller in Group

II when only 2 scenarios are considered (**Table 2-3**). On the other hand, model uncertainty may increase when more models are included.

GCMs	RCA4	RACMO22T	REMO2009
EC-EARTH	YES	YES	YES
HadGEM2-ES	YES	YES	
MPI-ESM-LR	YES		YES

Table 2-3 7 GCM-RCM combinations that are available from CORDEX-Africa dataset under RCP2.6, RCP4.5 and RCP8.5 scenarios defined as Group II.

The method is similar to that of Hawkins and Sutton (2009) and Hawkins and Sutton (2011), where they separated uncertainty of global mean surface temperature predictions from 15 different GCMs under three different emission scenarios into 3 parts: (1) internal variability of the climate system, that is, the natural fluctuations that arise in the absence of any radiative forcing of the planet; (2) model uncertainty in response to the same radiative forcing, different models simulate somewhat different changes in climate; and (3) scenario uncertainty, i.e. the uncertainty in future radiative forcing. Here we analysis projections from RCMs and further separate model uncertainty into two components that introduced by GCMs, as lateral boundary conditions of downscaling simulations and RCMs as the regional response to the same lateral boundary condition.

The method used for separating the three components of uncertainty is as follows: Each individual prediction of spatial averaged (over southern Africa) annual SSR was fit, using ordinary least squares, with a fourth-order polynomial over the years 1970-2099. The raw predictions for each model m, scenario s and year t can be written as

$$Prediction_{m,s,t} = Fit_{m,s,t} + Ref_{m,s} + Residual_{m,s,t}$$

where the smooth fit is represented by $Fit_{m,s,t}$; the reference is the mean value of 1970-1999, denoted by $Ref_{m,s}$; and the residual is $Residual_{,s,t}$.

- Then, the Internal Variability (IV) for each model was defined as the variance of the residuals from the fits, estimated independently of scenario and time. The multimodel mean of these variances is taken to be the internal variability component,

$$IV = \frac{1}{N_m}\sum_{m} var_{s,t}\,(Residual_{s,t})$$

  where $var_{s,t}$ denotes the variance across scenarios and time and IV is assumed to be constant in time.

- The Model uncertainty is separated into two parts; GCM uncertainty and RCM uncertainty. First, for the GCM uncertainty: 1) the multi-RCM mean of Residuals driven by a given GCM is calculated, 2) then GCM-introduced uncertainty in each scenario is the variance of all these multi-RCM means under that scenario; 3) finally, the multi-scenario mean is taken as an estimation of the GCM uncertainty.

$$G(t) = \frac{1}{N_s}\left[\sum_s var_{gcm}\left(\frac{1}{N_{rcm}}\sum_{rcm} Residual_{gcm}\right)\right]$$

- Then the RCM uncertainty, which is similar to that of the GCMs: 1) the mean of Residuals conducted by a given RCM but forced by different GCMs is calculated, 2) then the RCM-introduced uncertainty in each scenario is the variance of all these multi-GCM means under that scenario; 3) finally, the multi-scenario mean is taken as an estimation of the RCM uncertainty.

$$R(t) = \frac{1}{N_s}\left[\sum_s var_{rcm}\left(\frac{1}{N_{gcm}}\sum_{gcm} Residual_{rcm}\right)\right]$$

- Finally, the Scenario uncertainty is simply the variance of the weighted multimodel means for the three scenarios:

$$S(t) = var_s\left(\frac{1}{N_m}\sum_m Residual_s\right)$$

In this method all simulations are treated equally, no weighting has been introduced in the estimation even though it would be possible to be done by examining their ability to simulate the changes in the past as done in Hawkins and Sutton (2009).

These four uncertainty components are assumed to be well separated by this method and being independent from each other. Thus, the Total uncertainty T(t) is estimated as the sum of these four:

$$T(t) = IV + G(t) + R(t) + S(t)$$

and the Mean change of all the predictions M(t), is

$$M(t) = \frac{1}{N_{s,m}}\sum_{s,m} Fit_{s,m}$$

Then the Fractional uncertainty F (t) (90% confidence level) can be estimated by

$$F(t) = \frac{1.65\sqrt{T(t)}}{M(t)}$$

2.3 Long-term simulation with RegCM4

The overall objective of this work is to identify the possible impacts of climate change on the solar resources, over Southern Africa and the South West Indian Ocean (SA-SWIO) up to the end of the 21st century at regional scales (~50 km). In the context of energy autonomy target in near future of Reunion island and Mauritius island, a future downscaling project has been proposed to further investigate the impact of changes of SSR on the solar power system at local scale (~ 1km horizontal resolution). To contribute to the proposed downscaling project at local scale in Reunion Island and Mauritius Island, located in the South West Indian Ocean (SWIO), near the broader of CORDEX-Africa domain, projections from 2 Coupled Model Intercomparison Project Phase 5 (CMIP5) GCMs under one Representative Concentration Pathway (RCP) scenario, namely RCP8.5 are dynamically downscaled to regional scales by the regional climate model RegCM4 in three temporal windows: a) the present 1996-2005; b) the future 2046-2055 and 2090-2099, in line with the methodology of, e.g., Crook et al. (2011) and Gula and Peltier (2012). As discussed above this RegCM4 downscaling experiment is limited because of computational resources and can be regarded as the first step downscaling towards to the 1 km resolution local scale target of the proposed future project.

CMIP5 experiment

CMIP5 is a set of coordinated climate model experiments, to be known as phase five of the Coupled Model Intercomparison Project. The purpose of these experiments is to address outstanding scientific questions that arose as part of the Intergovernmental Panel on Climate Change (IPCC) fourth Assessment Report (AR4) assessment process, to improve understanding of climate, and to provide estimates of future climate change that will be useful to those considering its possible consequences. CMIP5 is meant to provide a framework for coordinated climate change experiments and thus includes simulations for assessment in the AR5 as well as others that extend beyond the AR5 (Taylor, Stouffer, & Meehl, 2012), see also https://www.wcrp-climate.org/wgcm-cmip/wgcm-cmip5).

RCPs' scenarios

The RCPs' scenarios are four GHG concentration trajectories adopted by the IPCC for its fifth Assessment Report (AR5) in 2014. It supersedes the Special Report on Emissions Scenarios (SRES) projections published in 2000. The pathways are used for climate modeling and research. They describe four possible climate futures, all of which are considered possible depending on how much GHG are emitted in the years to come. The four RCPs, RCP2.6, RCP4.5, RCP6.0, and RCP8.5 are named after a possible range of radiative forcing values in the year 2100 relative to pre-industrial values (+2.6, +4.5, +6.0, and +8.5 W/m^2, respectively). The RCPs are consistent

with a wide range of possible changes in future anthropogenic (i.e., human) introduced GHG emissions. RCP 2.6 assumes that global annual GHG emissions (measured in CO2-equivalents) peak between 2010-2020, with emissions declining substantially thereafter. Emissions in RCP 4.5 peak around 2040, then decline. In RCP 6.0, emissions peak around 2080, then decline. In RCP 8.5, emissions continue to rise throughout the 21st century. The four RCPs are consistent with certain socio-economic assumptions but are to be substituted with the Shared Socio-economic Pathways which are anticipated to provide flexible descriptions of possible futures within each RCP (Moss et al. 2010; Meinshausen et al. 2011).

2.3.1 Regional Climate Model: RegCM4

The Regional Climate Model system RegCM, originally developed at the National Center for Atmospheric Research (NCAR), is maintained by the Earth System Physics (ESP) section of the International Centre for Theoretical Physics (ICTP). Specifically, RegCM4 is a substantially improved version of the model compared to its predecessor RegCM3 (Pal et al., 2007) with regard to software code and physics (e.g., radiative transfer, planetary boundary layer, convection schemes over land and ocean, land types and surface processes, ocean–air exchanges). Details on the historical evolution of RegCM from the late 1980s until today and a full description of RegCM4's basic features are given in F. Giorgi et al. (2012).The latest version of the model, RegCM4, is now fully supported by the ESP, while previous versions are no longer available. This version includes major upgrades in the structure of the code and its pre- and post- processors, along with the inclusion of some new physics parameterizations. The model is flexible, portable and easy to use.

RegCM can be applied for a wide range of studies, from process studies, such as convection land surface (Halder, Dirmeyer, & Saha, 2015), radiation transfer (Alexandri et al., 2015; Li, Morel, Solmon, Chiacchio, & Bessafi, 2014), micro physics (Nogherotto, Tompkins, Giuliani, Coppola, & Giorgi, 2016), cloud (O'Brien, Chuang, Sloan, Faloona, & Rossiter, 2012) and aerosol (Solmon, Giorgi, & Liousse, 2006) to paleoclimate and future climate simulation as summarised by F. Giorgi et al. (2012). RegCM has been applied for many regions of the world such as tropical band (Coppola, Giorgi, Mariotti, & Bi, 2012). Over Europe, the ability of RegCM4 to simulate surface solar radiation patterns is assessed by Alexandri et al. (2015). Evaluation against satellite-based observations from the Satellite Application Facility on Climate Monitoring (CM SAF), shows that the model simulates adequately the SSR patterns over the region within a bias of about 3.3 %. And Total Cloud Fraction (CLT) is reported as one of the major determinants of these RegCM4–CM SAF SSR deviations on a monthly basis (Alexandri et al., 2015). For the most relevant researches over SA-SWIO: M. B. Sylla et al. (2010) assess performance of RegCM (version 3) in simulating general climate over SA and with particular focus on precipitation (M. Sylla, Giorgi, Coppola, & Mariotti, 2013) and on West Africa Monsoon (M. Sylla, Diallo, & Pal, 2013).

Kgatuke, Landman, Beraki, and Mbedzi (2008) examine the internal variability of the RegCM3 over South Africa. Davis, Bowden, Semazzi, Xie, and Onol (2009) apply RegCM over Eastern Africa and a Tropical Indian Ocean Domain.

This particular model is taken in present study mainly because of the experience of climate modeling research using RegCM (Li, 2015; Li et al., 2014) and easy access to technical support from ICTP on the basis of scientific cooperation.

RegCM4 is a hydrostatic, compressible, sigma-p vertical coordinate model run on an Arakawa B-grid in which wind and thermodynamical variables are horizontally staggered. A time-splitting explicit integration scheme is used in which the 2 fastest gravity modes are first separated from the model solution and then integrated with smaller time steps. This allows the use of a longer time step for the rest of the model. Essentially, the model dynamics are the same as that of the hydrostatic version of MM5 (Grell et al. 1994), and since this has not changed in RegCM4, it is not further discussed here (see Giorgi et al. 1993a and Grell et al. 1994 for more details).

RegCM version 4 with hydrostatic core (or RegCM4; **Giorgi et al., 2012**) was used in this study. The model has a wide choice of physical parameterizations for processes. The model physical parameterizations used in this work are listed below (**Table 2-4**).

Model aspects	options	Sensitivity study	Ensemble runs	Long-term runs
Dynamics	• Hydrostatic (Giorgi et al. 1993a)	YES	YES	YES
Radiative transfer	• Modified CCM3 (Kiehl et al. 1996)	YES	YES	YES
	• RRTM (Mlawer et al. 1997)	YES		
PBL	• Modified Holtslag (Holtslag et al. 1990)	YES	YES	YES
	• UW-PBL (Bretherton et al. 2004)	YES		
Cumulus convection over land	• Grell (Grell 1993)	YES	YES	YES
	• MIT (Emanuel & Zivkovic-Rothman 1999)	YES		
	• Tiedtke (Tiedtke 1989)	YES		
Cumulus convection over ocean	• Grell (Grell 1993)	YES		
	• MIT (Emanuel & Zivkovic-Rothman 1999)	YES	YES	YES
	• Tiedtke (Tiedtke 1989)	YES		
Resolved scale precipitation	• SUBEX (Pal et al. 2000)	YES	YES	YES
	• New Micro Physics scheme (Nogherotto et al. 2016)	YES		
Land surface	• BATS (Dickinson et al. 1993)	YES		
	• Community Land Model (CLM4.5; Oleson et al. 2008)		YES	YES
Ocean fluxes	• Zeng (Zeng et al. 1998)	YES	YES	YES

Table 2-4. Physical options of RegCM4 used in this study, for: 1) the sensitivity tests (3nd column), 2) the ensemble simulations (4th column) and 3) the long-term simulations (5th column).

Radiative transfer

Radiative transfer calculations in RegCM4 are performed based on two radiative transfer schemes: The default modified Community Climate Model (CCM3; Kiehl et al. 1996, Giorgi et al. 2012), and the newly implemented Rapid Radiative Transfer Model (RRTM; Mlawer et al. 1997). CCM3 scheme includes calculations for the short-wave and infrared parts of the spectrum, including both atmospheric gases and aerosols. The scheme includes contributions from all main GHG, i.e. H_2O, CO_2, O_3, CH_4, N_2O, and CFCs, and solar radiative processes are treated using a delta-Eddington formulation (Briegleb 1992). Scattering and absorption of solar radiation by aerosols are also included based on the aerosol optical properties (absorption coefficient and single scattering albedo). Concerning cloud radiation calculations, the solar spectrum optical properties are based on the cloud liquid water amount prognostically calculated by the model, cloud fractional cover, which is calculated diagnostically as a function of relative humidity, and effective cloud droplet radius, which is parameterized as a function of temperature and land sea mask for liquid water and as a function of height for ice phase. In addition, the scheme diagnostically calculates a fraction of cloud ice as a function of temperature. In the infrared spectrum, the cloud emissivity is calculated as a function of cloud liquid/ice water path and cloud infrared absorption cross sections depending on effective radiation for the liquid and ice phases.

The main features of RRTM are described in Clough et al. (2005). RRTM utilizes the k-correlated method to calculate shortwave (SW) fluxes, longwave (LW) fluxes and heating rates efficiently and accurately. The absorption coefficients used to build the relevant k-distributions are obtained from the Line-By-Line Radiative Transfer Model (LBLRTM; Clough et al. 1981), which includes the MT_CKD water vapor continuum model (Mlawer et al. 2003), and the HITRAN line parameter database. RRTM is divided into sixteen contiguous bands in the LW (hereafter referred to as RRTM-LW) from 10 to 3250 cm–1, and fourteen bands in the SW (hereafter referred to as RRTM-SW; Mlawer et al. 1998) from 820 to 50000 cm–1. Spectral bands were chosen based on the major absorption features of the active gaseous species. Modeled absorbers in RRTM-LW include water vapor, carbon dioxide, ozone, nitrous oxide, methane, oxygen, nitrogen, and the common halocarbons. Modeled sources of extinction in RRTM-SW include water vapor, carbon dioxide, ozone, methane, oxygen, aerosols, and Rayleigh scattering. In addition to clear sky radiative transfer, parameterizations of the radiative effects of water clouds (Hu & Stamnes 1993) and ice clouds (Fu et al. 1998) are available in RRTM. RRTMG further includes the Monte-Carlo Independant Column Approximation (McICA) capability to represent sub-grid cloud variability with random, maximum-random and maximum options for cloud overlap (Barker et al. 2003; Pincus et al. 2003).

A preliminary comparison of the seasonal radiation budget at the surface and top-of-atmosphere during austral summer and winter from RegCM4 using CCM and RegCM4 using RRTM shows good qualitative agreement over South West Indian Ocean (SWIO), though RegCM4-CCM tends to overestimate the radiative fluxes when compared to RegCM4-RRTM. in the work of Li et al. (2013).

Planetary boundary layer

In RegCM4, the planetary boundary layer (PBL) scheme, are of Holtslag et al (1990) and the University of Washington PBL (Grenier & Bretherton 2001, Bretherton et al. 2004) In the Holtslag scheme, a PBL height is first diagnostically calculated based on an iteration procedure employing a bulk critical Richardson number formulation. Then a non-local vertical profile of eddy diffusivity for heat, moisture, and momentum is specified from the surface to the PBL height, and a counter gradient transport term is added for temperature and moisture. The eddy diffusivity depends on the friction velocity, height, Monin-Obhukov length, and PBL height.

Cumulus convection

Convective precipitation in RegCM4 is computed using one of the four following schemes: (1) Modified-Kuo scheme (Anthes 1977); (2) Grell scheme (Grell 1993); (3) MIT-Emanuel scheme (Emanuel 1991; Emanuel & Zivkovic-Rothman 1999); and (4) Tiedtke scheme (Tiedtke 1989). In addition, the Grell parameterization is implemented using one of two following closure assumptions: (1) the Arakawa and Schubert closure (AS74, Grell et al 1994); (2) the Fritsch and Chappell (1980) closure (FC80). And the new version of RegCM4 has the capability of running different convection schemes over land and ocean, which is referred as mixed convection schemes. A series of preliminary test experiments showed that different schemes have different performance over different regions, particularly over land and ocean areas (Giorgi & Shields 1999; Martínez-Castro et al. 2006; Sylla et al. 2012).

In present study, sensitivity tests over the SA-SWIO domain are performed with all above available cumulus convection schemes (see section 2.3.2).

Land surface processes

The Biosphere-Atmosphere Transfer Scheme (BATS) of Dickinson et al. (1993) has been used in the RegCM since the earliest versions. It includes a 1-layer vegetation module, a 1-layer snow module, a force-restore model for soil temperatures, a 3-layer soil scheme, and a simple surface runoff parameterization. This land surface scheme includes 20 surface types and 12 soil color and soil texture types. In addition, a sub-grid land surface configuration can be used by which each

model grid point is divided into a regular sub-grid, and land surface processes are calculated at each sub-grid point taking into account the local land-use and topography (Giorgi et al. 2003). The latter scheme was shown to be especially useful in improving the simulation of the surface hydrologic cycle in mountainous areas (Giorgi et al. 2003). There are two major augmentations for land surface processes in RegCM4. First is, 2 new land use types were added to BATS to represent urban and suburban environments. Urban development not only modifies the surface albedo and alters the surface energy balance, but also creates impervious surfaces with large effects on runoff and evapotranspiration. These effects can be described by modifying relevant properties of the land surface types in the BATS package.

Ocean flux parameterization

Zeng et al. (1998) ocean flux scheme has been used in RegCM4 for our simulations. Pal et al. (2007) implemented the scheme of Zeng et al. (1998), which is based on a Monin-Obhukov turbulence representation for improving the excessive evaporation over warm tropical oceans found in the BATS option. Sea surface temperatures (SST) are prescribed every 6h from temporally interpolated weekly or monthly SST products by default in RegCM. These products, which are produced from satellite retrievals and in situ measurements, are representative of the mean temperature in the top few meters of the ocean. However, the actual SST can differ significantly from this mean temperature due to the cool-skin and warm-layer effects described by Fairall et al. (1996). To improve the calculation of diurnal fluxes over the ocean, the prognostic SST scheme described by Zeng & Beljaars (2005) was implemented in RegCM4. The scheme is based on a 2-layer, 1-dimensional heat transfer model, with the top layer representing the upper few millimeters of the ocean which is cooled by net longwave radiation loss and surface fluxes. The bottom layer is 3 m thick, is warmed by solar radiation, and exchanges heat with the top layer. This diurnal SST scheme appears to provide significant, although not major, effects on the model climatology mostly over tropical oceans, for example the Indian Ocean, and now it is used as default in RegCM4.

Large-scale precipitation scheme

Subgrid Explicit Moisture Scheme (SUBEX, Pal et al. 2000) is used to handle nonconvective clouds and precipitation resolved by the model. SUBEX accounts for the subgrid variability in clouds by linking the average grid cell relative humidity to the cloud fraction and cloud water following the work of Sumdqvist et al. (1989). It first calculates fractional cloud cover at a given grid point based on the local relative humidity. Then, in the cloudy fraction it uses a Kessler-type bulk formulation in which cloud water is turned into precipitation via an autoconversion and an accretion term. Below-cloud evaporation of falling raindrops is also accounted for based on the

local relative humidity and an evaporation rate coefficient. Key sensitivity parameters in this scheme are the in-cloud liquid water threshold for the activation of the autoconversion term (Oth) and the rate of sub-cloud evaporation (Cevap). Greater values of Qth and Cevap lead to decreased precipitation amounts.

2.3.2 Sensitivity study

To better understand the model (RegCM4) performance in this particular region (SA-SWIO) with little experience, an ensemble of RegCM4 simulations forced by ERA-Interim reanalyses (ERAINT hereafter) with various model physical setups are conducted as a "sensitivity study". Optimal parameter settings for the model physics are estimated to define to have the acceptable small bias of interesting variables, including SSR, TAS, PR, and Total Cloud Fraction (CLT).

A series of simulations was conducted covering 2001-2005, taking advantage that many modern observations becomes available and easily accessed during this period. Several physical parameterizations are considered in this sensitivity test, including the most relevant processes of SSR, including radiation transfer scheme, the PBL, convection, precipitation, land surface and ocean fluxes.

All these simulations are conducted over the SA-SWIO domain (see Fig. 2-1) driven by ERA-Interim reanalysis, covering 2001 to 2005. Observations are easily accessed during this period. The seasonal climatology is analysed for: Surface Downward Solar Radiation (RSDS, same as SSR), Surface Air Temperature (TAS), total precipitation (PR), and Total Cloud Fraction (CLT). The physics settings of all the simulations are listed in Table 2-5. Note that, at the time when this sensitivity is conducted, the particular version of ReGMC4 suffers from a crash when using Micro and UW PBL scheme together, thus outputs are not obtained from these simulations.

NO.	Radiation transfer		Cumulus Convection (land_ocean)					Resolved scale precipitation		PBL		Land surface
	RRTM	CCM	G_E	E_E	G_G	E_G	T_T	SUBEX	Micro	Holtslag	UW	BATS
1	YES		YES					YES		YES		YES
2	YES		YES					YES			YES	YES
3	YES		YES						YES	YES		YES
~~4~~	~~YES~~	-	~~YES~~	-	-	-	-	-	~~YES~~	-	~~YES~~	~~YES~~
5	YES			YES				YES		YES		YES
6	YES			YES				YES			YES	YES
7	YES			YES					YES	YES		YES
~~8~~	~~YES~~	-	-	~~YES~~	-	-	-	-	~~YES~~	-	~~YES~~	~~YES~~
9	YES				YES			YES		YES		YES
10	YES				YES			YES			YES	YES
11	YES				YES				YES	YES		YES
~~12~~	~~YES~~	-	-	-	~~YES~~	-	-	-	~~YES~~	-	~~YES~~	~~YES~~
13	YES					YES		YES		YES		YES

14	YES					YES		YES			YES	YES
15	YES					YES			YES	YES		YES
~~16~~	~~YES~~	-	-	-	-	~~YES~~	-	-	~~YES~~	-	~~YES~~	~~YES~~
17	YES						YES	YES		YES		YES
18	YES						YES	YES			YES	YES
19	YES						YES		YES	YES		YES
~~20~~	~~YES~~	-	-	-	-	-	~~YES~~	-	~~YES~~	-	~~YES~~	~~YES~~
21		YES	YES					YES		YES		YES
22		YES	YES					YES			YES	YES
23		YES	YES						YES	YES		YES
~~24~~	-	~~YES~~	~~YES~~	-	-	-	-	-	~~YES~~	-	~~YES~~	~~YES~~
25		YES		YES				YES		YES		YES
26		YES		YES				YES			YES	YES
27		YES		YES					YES	YES		YES
~~28~~	-	~~YES~~	-	~~YES~~	-	-	-	-	~~YES~~	-	~~YES~~	~~YES~~
29		YES			YES			YES		YES		YES
30		YES			YES			YES			YES	YES
31		YES			YES				YES	YES		YES
~~32~~	-	~~YES~~	-	-	~~YES~~	-	-	-	~~YES~~	-	~~YES~~	~~YES~~
33		YES				YES		YES		YES		YES
34		YES				YES		YES			YES	YES
35		YES				YES			YES	YES		YES
~~36~~	-	~~YES~~	-	-	-	~~YES~~	-	-	~~YES~~	-	~~YES~~	~~YES~~
37		YES					YES	YES		YES		YES
38		YES					YES	YES			YES	YES
39		YES					YES		YES	YES		YES
~~40~~	-	~~YES~~	-	-	-	-	~~YES~~	-	~~YES~~	-	~~YES~~	~~YES~~

Table 2-5 Physical options for the sensitivity study conducted with RegCM4. The line under strikethrough indicates the simulations with Micro physics as resolved precipitation scheme together with UW as PBL schemes suffer a crash at the time of running this particular version of RegCM, and thus no date is obtained.

2.3.3 Ensemble runs with RegCM4

Model response to the internal climate variability could be regarded as a background noise of the climate change signal. Before downscaling the outputs from GCMs using RegCM4, an experiment consisting of 20 ensembles of RegCM runs driven by ERA-Interim were taken to understand its internal variability.

The ensemble simulations cover the period from 1997 to 1998, when a strong El Nino (Boulard, Pohl, Crétat, Vigaud, & Pham-Xuan, 2013; Wolter & Timlin, 1998) taken place. The ensemble simulations are starting from initial times: 1st of Nov in 1996 for the first simulation and one day after for each of the rest 19 runs, following the methodology of Pohl et al. (2016). The physical configuration of ReCM4 in this ensemble simulation is shown in Table 2-4.

2.3.4 Driving GCMs selection for the long-term simulations

Selection of GCMs that "do better" over a research domain, is difficult and probably not warranted, given the general parity in model skill and the difficulty in identifying which models are more skilful (Brown et al., 2008). Ensemble means or medians offer the highest level of projection accuracy. However, because of the limitation of computational resources, a limited while state-of-art selection of driven GCMs were carried out for this specific downscaling experiment using RegCM4. This method is based on several widely used criteria in the impact study community. There are at least four criteria for selection of which GCMs output to use for an impact study: vintage, resolution, validity and representativeness of results.

1.1 Vintage. In general, recent model simulations are likely (though by no means certain) to be more reliable than those of an earlier vintage. They are based on recent knowledge, incorporate more processes and feedbacks and are usually of a higher spatial resolution than earlier models.

1.2 Resolution. As climate models have evolved and computing power has increased, there has been a tendency towards increased resolution. Some of the early GCMs operated on a horizontal resolution of some 1000 km with between 2 and 10 levels in the vertical. More recent models are run at nearer 250 km spatial resolution with perhaps 20 vertical levels. However, although higher resolution models contain more spatial detail this does not necessarily guarantee a superior model performance.

1.3 Validity. A more persuasive criterion for model selection is to adopt the GCMs that simulate the present-day climate most faithfully, on the premise (but not sufficient to guarantee) that these GCMs would also yield the most reliable representation of future climate. The approach involves comparing GCM simulations that represent present-day conditions with the observed climate.

1.4 Representativeness. Results from more than one GCM are to be applied in an impact assessment (and given the known uncertainties of GCMs), another criterion for selection is to examine the representativeness of the results. Where several GCMs are to be selected, it might be prudent to choose models that show a range of changes in a key variable in the study region (for example, models showing little change in precipitation, models showing

an increase and models showing a decrease). The selections may not necessarily be the best validated models (see above), although some combination of models satisfying both criteria could be agreed upon.

Surface Temperature (variable name: TAS) is of particular concern in climate change projection. The uncertainty of surface temperature projections depends on GCM's ability to simulate climate and to predict the response of climate forcing and represents our best understanding of the climate system. The GCMs have been chosen so that they could capture the TAS dispersion of all the GCMs, which are potentially having good representativeness of the known uncertainties of GCM ensemble (Figure 2.1)

By applying these selection criteria to GCMs from CMIP5 (Taylor et al. 2012), Hadley Global Environment Model 2 - Earth System, short as HadGEM2-ES (Collins et al., 2008) and the Geophysical Fluid Dynamics Laboratory Earth System Model, short as GFDL-ESM2M (Dunne et al., 2012) are selected as the driving models of RegCM4. The 2 GCMs downscaling simulation is taken mainly because of the limit of available computational resources.

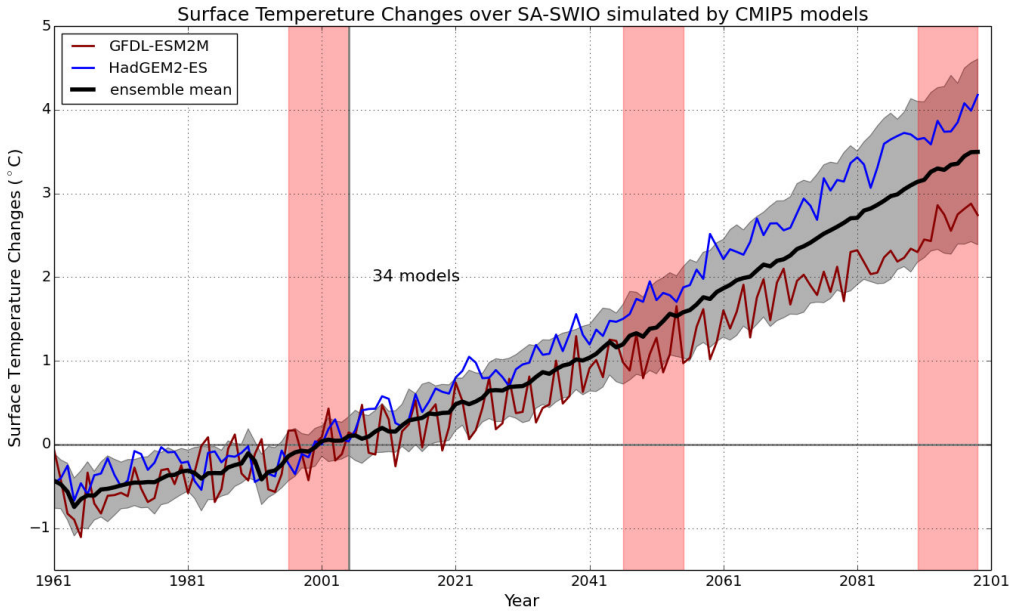

Fig. 2-2 Temperature changes projections by CMIP5 models over the SA-SWIO. Three simulation windows are shown in red background.

2.4 Reference data

The accuracy of the reference data is among the most important concerns in model evaluation. In this section, the references data used in present study are described, including the references for the RegCM4 simulation (**section 2.4.2**) and for the ensemble analysis (**section 2.4.1**).

2.4.1 References for the ensemble analysis

2.4.1.1 Surface Solar Radiation

Surface measurements are the most optimal references for climate model evaluation. In this study, the monthly data of ground-based SSR are coming from the Global Energy Balance Archive (GEBA: (Gilgen, Wild, & Ohmura, 1998; Ohmura, Gilgen, & Wild, 1989; Wild, Folini, & Henschel, 2017) – see also: http://www.geba.ethz.ch). Data selection for the present study was based on: 1) the quality control procedures adopted within GEBA and that helped removing data with the probability of being erroneous and 2) the temporal coverage of the RCMs' simulations for the historical period simulations (e.g., REMO2009 simulations all start on the 1st of February 1989). The spatial distribution of the 33 selected GEBA stations selected for the period 1990-2005 is presented in **Fig. 2-3**, along with the number of monthly records at each station. SSR ground-based data suffer from a highly irregular station distribution within the African landscape even taking the most profound observational network, such as GEBA considered here. Thus, additional references from satellite-based retrievals and reanalyses are also used.

The second edition of the Surface Solar Radiation Data Set - Heliosat Edition 2 (SARAH-2: (Pfeifroth et al., 2017) – see also https://wui.cmsaf.eu) is a satellite-based climate data record derived from satellite-observations of the visible channels of the MVIRI and the SEVIRI instruments onboard the geostationary Meteosat satellites. The data are available from 1983 to 2015 and cover the region ±65° longitude and ±65° latitude. Monthly SSR fields covering the SA domain (with a small uncovered area located around 40°S, 60°E) with a spatial resolution of 0.05° x 0.05° are used in this study.

The NASA/GEWEX Surface Radiation Budget (SRB: (S. Gupta, Stackhouse Jr, Cox, Mikovitz, & Zhang, 2006) – see also https://eosweb.larc.nasa.gov/project/srb/srb_table) Release-3.0 dataset contains global 3-hourly, daily, monthly/3-hourly, and monthly averages of surface and top-of atmosphere (TOA) longwave and shortwave radiative parameters on a 1°x1° grid. Monthly SSR from 1990 to 2005 are considered.

ERA-Interim (hereafter refered to as ERAINT) is a global re-analysis data product of the European Centre for Medium-Range Weather Forecasts (ECMWF), with a horizontal spectral resolution of T255 (about 80km at the equator), covering the period from 1979 onwards, and that continues to be extended forward in near-real time. Radiation is calculated based on the Rapid Radiation Transfer Model (RRTM, (Mlawer, Taubman, Brown, Iacono, & Clough, 1997)). ERA-Interim monthly mean SSR and CLT for the time period 1990-2005 were used for the evaluation of the RCM simulations and for the identification of the sources of errors.

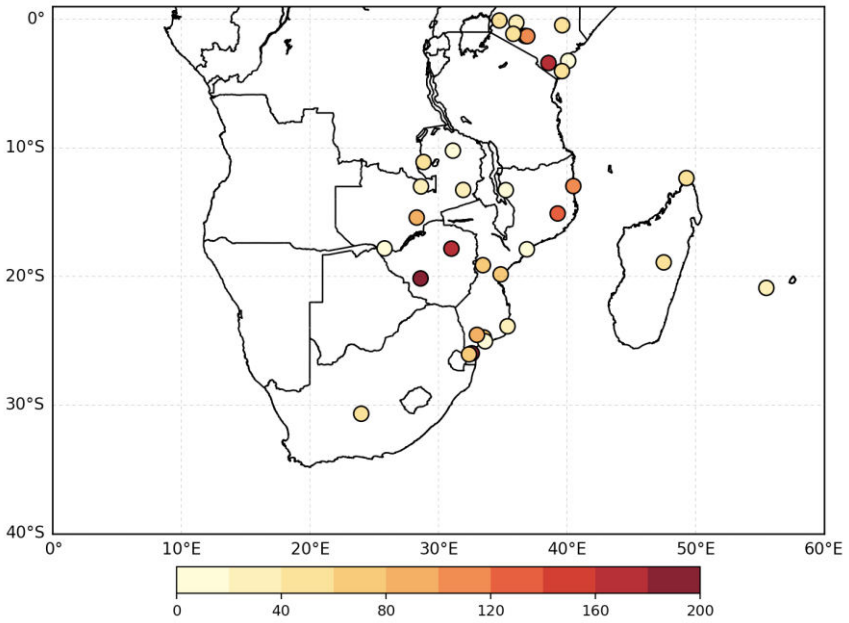

Fig. 2-3 The 33 GEBA stations over Southern Africa collected during the period 1990-2005, with numbers of monthly SSR records indicated by the respective colour at each station.

2.4.1.2 Cloudiness

Additionally, to analyse cloud-radiation interactions, monthly total cloud cover fraction (CLT) are collected from CM SAF CLARA-A2 and ISCCP the satellite-derived products, and from ERA-Interim and NCEP-CSFR the reanalyses.

The CM SAF CLoud, Albedo and surface Radiation dataset from AVHRR Edition 2, denoted as CLARA-A2 (Karlsson et al., 2017) https://wui.cmsaf.eu/), is a global cloud product that has been compiled in the CM SAF project for the time period 1982-2015. The monthly-mean CLT from 1990 to 2005 was taken, along with other cloud datasets discussed above, to evaluate the models' cloud cover fraction. Validation studies of CLARA-A2 based on CALIPSO-CALIOP observations show that for clouds having a vertically integrated cloud optical thickness greater than 0.15 the overall global bias is -3.2 %. The largest underestimation (10-25 %) occurs over the Polar

regions during the Polar winter season whereas some overestimation (up to 10 %) can be found over some oceanic regions (mainly in the Tropics). These results agree very well with corresponding validation studies based on surface stations (Synoptic weather observations from surface stations, SYNOP) showing a global bias of -3.1 % (Karlsson et al., 2017).

The GCM simulator-oriented ISCCP cloud product (hereafter refered to as ISCCP) (Rossow & Schiffer, 1999), for the period 1990 to 2005, is used to evaluate the GCMs and RCMs' results. This monthly, 2.5 deg. resolution product is derived from the ISCCP D1 data (http://isccp.giss.nasa.gov). As mentioned above, monthly CLT from ERA-Interim and NCEP-CSFR reanalyses for the time period 1990 to 2005 are also used. Characteristics of all the reference datasets used in this study are listed in **Table 2-6.**

Name	Type	Variable	Time period	Time res.	Spatial res. (deg.)	reference
GEBA	ground	ssr	1990-2005	monthly	station	Gilgen et al. 1998; Ohmura et al. 1989; Wild et al. 2017
SARAH-2	satellite	ssr	1990-2005	monthly	0.05	Pfeifroth 2017
SRB v3.0	satellite	ssr	1990-2005	monthly	1.0	Gupta et al. 2006
CLARA-2	satellite	clt	1990-2005	monthly	0.25	Karlsson et al. 2017
ISCCP	satellite	clt	1990-2005	monthly	2.5	Rossow & Schiffer 1999
ERA_Interim	reanalysis	ssr, clt	1990-2005	monthly	0.75	Simmons et al. 2007; Dee et al. 2011
NCEP-CFSR	reanalysis	ssr, clt	1990-2005	monthly	0.3	Saha et al. 2010

Table 2-6 Reference datasets used in this study for the evaluation of the model results. Note that ssr and clt stand for Surface Downward Solar Radiation and Total Cloud Fraction, respectively.

SARAH-2

The Satellite Application Facility on Climate Monitoring (CM SAF) is a ground segment of the European Organization for the Exploitation of Meteorological Satellites (EUMETSAT). The monthly satellite retrievals of RSDS covering 1983 to 2005 are used in this study. First, the SARAH-2 monthly RSDS has been validated over southern Africa against ground-based SSR observations from GEBA (see Chapter 3), which indicates an overall Mean Bias of ~ 9 W/m^2 over SA domain. Then, SARAH-2 monthly data has been used to validate models' outputs.

CLARA-A2

The CM SAF CLoud, Albedo and surface Radiation dataset from AVHRR Edition 2, denoted as CLARA-A2, (Karlsson et al., 2017), is a global cloud product that have been compiled in the CM SAF project in the time period 1982-2015. The monthly mean CLT from 1983 to 2005 was taken, along with other datasets, to evaluate the models' cloud cover fraction. Validation studies of CLARA-A2 based on CALIPSO-CALIOP observations show that for clouds having a vertically integrated cloud optical thickness greater than 0.15 the overall global bias is -3.2 %. The largest underestimation (10-25 %) occurs over the Polar regions during the Polar winter season whereas some overestimation (up to 10 %) can be found over some oceanic regions (mainly in the Tropics). These results agree very well with corresponding validation studies based on surface stations (Synoptical weather observations from surface stations, SYNOP) showing a global bias of -3.1 % (Karlsson et al., 2017).

ERA_Interim

ERA-Interim is a global re-analysis data product of the European Centre for Medium-Range Weather Forecasts (ECMWF), with a horizontal spectral resolution of T255 (about 80 km at the equator), which is available since 1979. The ERA-Interim project was conducted in part to prepare for a new atmospheric reanalysis to replace ERA-40. The data assimilation method used to produce ERA-Interim is based on an updated version of the ECMWF forecasting model [version cycle 31r1 (Cy31r2)]. Besides the increased resolution compared to ERA-40, ERA-Interim includes a four-dimensional variational analysis (4D-Var). The 4D-Var is a temporal extension of the 3D-Var (Saha et al., 2010). The cost function was used to minimize the difference between the model and the observations with a 12 h assimilation window. Radiation is calculated based on the Rapid Radiation Transfer Model (RRTM, (Mlawer et al., 1997)).

To valid RegCM4, monthly Surface Temperature (TAS) and precipitation (PR) are used during 1996-2005. For the evaluation of the CORDEX/CMIP5 simulations, ERA-Interim monthly mean RSDS and CLT, for the time period 1979 to 2005 were used. Although ERA-Interim assimilates numerous measured parameters, it is still a modeling product. Basis is the ECMWF Integrated

Forecast System (IFS) (http://www.ecmwf.int/research/ifsdocs/). For instance, the IFS model used for aerosol optical depth the Tegen climatology (Tegen et al., 1997), which is based on aerosol transport modeling, and a (Tiedtke, 1989) based convection parameterization.

GEWEX/SRB

The GEWEX/SRB project provides a satellite-based dataset of 3-hourly short- and long-wave radiation components at the surface, and the Top-of-the-Atmosphere on a 1 ° global grid (S. Gupta et al., 2006). The release 3.0 of the dataset for short-wave fluxes was used. The surface radiation fluxes were evaluated in a variety of studies with data of the BSRN or the GEBA projects, which provided good agreement with monthly data, i.e., within 5–20W/m^2 for short-wave fluxes (S. K. Gupta et al., 1999; Y. Zhang, Rossow, & Stackhouse, 2007). The SRB algorithms use cloud parameters derived from the DX data of the International Satellite Cloud Climatology Project (ISCCP) (Rossow & Schiffer, 1999) and temperature and moisture profiles taken from the 4-D data assimilation product provided by the Data Assimilation Office at NASA GSFC, and produced with the Goddard Earth Observing System model version 4 (GEOS-4).

ISCCP

The GCM simulator-oriented ISCCP cloud product (refer to as ISCCP) (Rossow & Schiffer, 1999), covering 1984 to 2005 at monthly scale is used to evaluate the GCMs and RCMs' results. This 2.5 deg. resolution product is derived from the ISCCP D1 data (http://isccp.giss.nasa.gov) which are quasi-instantaneous spatial averages of pixel-level retrievals over equal-area grid cells.

CFSR

The NCEP Climate Forecast System Reanalysis (Saha et al., 2010) is the newest reanalysis dataset from NCEP, which was initially provided over the 31-year period from 1979 to 2009, and has been currently extended to March 2011. The atmospheric model used is the Global Forecast System at a horizontal resolution of T382 Gaussian grids with 64 vertical layers. Shortwave radiation is parameterized according to the NASA approach (Chou, Suarez, Ho, Yan, & Lee, 1998; Hou, Moorthi, & Campana, 2002). Monthly RSDS and CLT from 1983 to 2005 are used in this study.

CRU TS3.23

Climatic Research Unit Time-Series Version 3.23 of High Resolution Gridded Data (Harris, Jones, Osborn, & Lister, 2014). CRU TS3.23 is from monthly observations at meteorological

stations across the world's land areas. Station anomalies (from 1961 to 1990 means) were interpolated into 0.5° latitude/longitude grid cells covering the global land surface (excluding Antarctica), and combined with an existing climatology to obtain absolute monthly values. The dataset includes six mostly independent climate variables (mean temperature, diurnal temperature range, precipitation, wet-day frequency, vapour pressure and cloud cover). In this study, monthly TAS and PR are used to validate RegCM4 over SA-SWIO.

GPCP

The Global Precipitation Climatology Project (GPCP) Version-2 Monthly Precipitation Analysis (Adler et al., 2003). This globally complete, monthly analysis of surface precipitation at 2.5° latitude/longitude resolution is available from January 1979 to the present. It is a merged analysis that incorporates precipitation estimates from low-orbit satellite microwave data, geosynchronous-orbit satellite infrared data, and surface rain gauge observations. Monthly PR in the period of 1996-2005 is used in the validation of RegCM4.

2.4.2 References for the RegCM4 simulation

The monthly SSR records are taken from satellite and reanalysis for the RegCM4 simulations (see
Table 2-7). To evaluate the cloudiness, total cloud cover fraction from both satellite (CM SAF CLARA-2 and ISCCP) and reanalysis (ERA_Interim and NCEP-CSFR) are used. Characteristics of these references datasets are listed in **Table 2-6**. Additionally, Surface Air Temperature (TAS) and Precipitation (PR) are also two key variables to validate RegCM4, where reference data from Climatic Research Unit Time-Series (CRU, Harris et al. 2014) and the Global Precipitation Climatology Project (GPCP, Harris et al. 2014) are taken.

Name	Type	Variable	Time period	Time res.	Spatial res. (deg.)	reference
CRU	ground OBS	tas	1996-2005	monthly	0.5	Harris et al. 2014
GPCP	ground OBS	pr	1996-2005	monthly	2.5	Adler et al. 2003
CLARA-2	Satellite	ssr, clt	1996-2005	monthly	0.05	Karlsson et al. 2017

Table 2-7. Reference datasets used in this study for evaluation of RegCM4 simulations. Note that ssr and clt stand for Surface downward Solar Radiation and Total Cloud Fraction, respectively, the corresponding variable names in these datasets may be different.

3 Numerical simulation of Surface Solar Radiation: CORDEX-AFRICA & CMIP5

OUTLINE:

* This Chapter was to be published on "Climate Dynamics" as two papers:

1) Tang, C., Morel, B., Wild, M., Pohl, B., Abiodun, B., & Bessafi, M. (2018). Numerical simulation of surface solar radiation over Southern Africa. Part 1: Evaluation of regional and global climate models. *Climate Dynamics*. doi:10.1007/s00382-018-4143-1

2) Tang, C., Morel, B., Wild, M., Pohl, B., Abiodun, B., Bessafi, M., & Lennard, C. (2018). Numerical simulation of surface solar radiation over Southern Africa. Part 2: Projections of regional and global climate models. *Climate Dynamics*.

The study is to have a comprehensive knowledge of SSR changes in the context of climate change. However, the slice experiment conducted by RegCM4 discussed in Chapter 3 is of limited number of driving Global Climate Models (GCMs), number of climate forcings (only RCP8.5) and temporal coverage since the lack of computational resources. Thus, the slice experiment has then been extended, using outputs from CORDEX-Africa. Over 100-year continuous outputs from 5 RCMs driven by 20 GCMs over southern Africa (SA) under RCP4.5 and RCP8.5 were analysed. Evaluation based on various references from satellite retrievals, reanalysis and ground-based measurement of this large ensemble is performed (**section 3.1**), and then the future projections are assessed in **section 3.2**.

3.1 Evaluation of GCMs and RCMs outputs against observations

3.1.1 Evaluation against ground-based measurements

In this section, SSR from GCMs and RCMs are firstly compared to ground-based measurements (GEBA), which cover only the eastern part of SA, including Madagascar and Reunion islands. To examine the performance of models over the western part of the domain, the model results are then validated against the gridded products from satellite retrievals and reanalysis, which are compared with GEBA as well.

Table 3-1 summarizes the statistical measures for the evaluation results of the monthly SSR results from the ERA-Interim reanalysis data, GCMs and RCMs (as driven by ERA-Interim and GCMs). According to Table 4, ERAINT overestimates monthly SSR in the eastern part of southern Africa (SA-E), including Madagascar and Reunion, with a mean bias of 6.56 W/m^2. A positive discrepancy was also found for the entire African domain when compared with surface measurements in the period of 2001-2009 collected from 20 observational stations within the Baseline Surface Radiation Network (BSRN) and GEBA networks (X. Zhang et al., 2016). Most GCMs (6 out of 10) overestimate monthly SSR in this area with mean biases of seasonal climatology up to ~45 W/m^2 (IPSL-CM5A-MR), while the other 4 GCMs show negative biases in the range between -18.00 and -3.13 W/m^2. However, in the case of the RCMs, the vast majority of the simulations (21 out of 25) underestimate SSR compared with GEBA data in the range between -43.99 and -0.51 W/m^2, with the positive biases from the other 4 RCM simulations in a relatively small range from 0.51 to 7.21 W/m^2. The RCM biases for the evaluation runs driven by ERA-Interim are generally small compared with the runs driven by the GCMs, expect for RCM RACMO22T whose evaluation run bias (7.21 W/m^2) is larger than the GCM forcing run bias (up to 1.61 W/m^2).

When driven by different GCMs, the RCMs simulate SSR biases with overall the same signs, such as in the case of CCLM4, RCA4 (with the exception of the CNRM-CM5 run), HIRHAM5 and REMO2009. RACMO22T has a positive bias of 7.21 W/m^2 when driven by ERAINT, but biases of -1.60 W/m^2 and 1.61 W/m^2 when driven by EC-EARTH and HadGEM2-ES, respectively. However, RACMO22T (as HIRHAM5 and REMO2009) is only driven by 2 GCM runs, and thus has less statistical confidence. It could be argued that the radiation processes in the RCMs are likely to be mainly controlled by internal processes of the RCM and little influenced by the boundary forcing applied, which is in line with the finding of (Bartók et al., 2016) for Europe.

Evaluation with GEBA	Forcing Data		CCLM4		RCA4		HIRHAM5		RACMO22T		REMO2009	
	MBE	RMSE	MBE	RMSE	MBE	RMSE	MBE	RMSE	MBE	RMSE	MBE	RMSE
ERA-Interim	6.56	33.92	-29.12	55.17	0.51	39.43	-0.51	35.48	7.21	37.36	-0.73	40.22
CNRM-CM5	3.70	40.18	-41.00	62.89	3.16	43.00						
CSIRO-Mk3-6-0	18.05	42.25			-2.94	42.27						
CanESM2	10.18	46.14			-0.72	43.69						
EC-EARTH	-3.13	38.65	-43.99	67.53	-3.09	42.30	-10.61	40.84	-1.60	39.05	-8.67	42.71
GFDL-ESM2M	-4.86	46.10			-6.43	41.21						
HadGEM2-ES	18.84	42.61	-30.79	57.04	-3.85	40.80			1.61	38.70		
IPSL-CM5A-MR	44.74	58.86			-6.35	44.64						
MIROC5	-3.62	38.64			-5.33	43.90						
MPI-ESM-LR	4.71	40.29	-38.69	61.76	-4.97	42.75					-8.12	42.52
NorESM1-M	-18.00	49.38			-3.67	43.75	-3.02	62.66				

Table 3-1 Mean bias error (MBE) and Root Mean Square Error (RMSE) of monthly SSR between GEBA and ERA-Interim and CMIP5 GCMs (columns 1 and 2) and CORDEX-African RCMs (as driven by ERA-Interim and the GCMs; columns 3 to 12). Statistics are calculated using 2065 monthly surface records at the selected 33 GEBA stations covering the eastern part of SA (SA-E), Madagascar and Reunion from 1990 to 2005. Unit is W/m^2.

3.1.2 Evaluation against gridded products

The accuracy of the representation of SSR strongly depends on the capability of the models to simulate the major climatic characteristics of different regions, especially the cloudiness on a seasonal scale. We first evaluate the spread among the different reference datasets over SA to get an estimate of the accuracy and consistency of the available gridded reference datasets for model evaluation, which is of crucial importance over the regions where ground-based measurements are lacking (e.g. in the western part of SA). Statistics are calculated as an average of all of the 2065 monthly records over 33 stations. For the gridded products, nearest points are taken. Results of the evaluation of the monthly SSR from satellite and reanalysis data sets is listed in **Table 3-2** as averages over the 33 GEBA stations. It is obvious that the gridded products show an overall discrepancy of about 10 W/m^2 with all products showing overall positive biases.

Data	MBE	RMSE	Sigma
SARAH-2	9.83	27.60	0.90
SRB	0.64	30.78	0.81
ERAINT	6.56	33.92	0.93
NCEP-CFSR	0.45	35.09	1.04

Table 3-2 Evaluation of monthly SSR from references datasets using 2065 monthly means of surface measurements recorded at 33 GEBA stations during 1990-2005 over Southern Africa. For more information on this evaluation, please see **Fig. 2-3**.

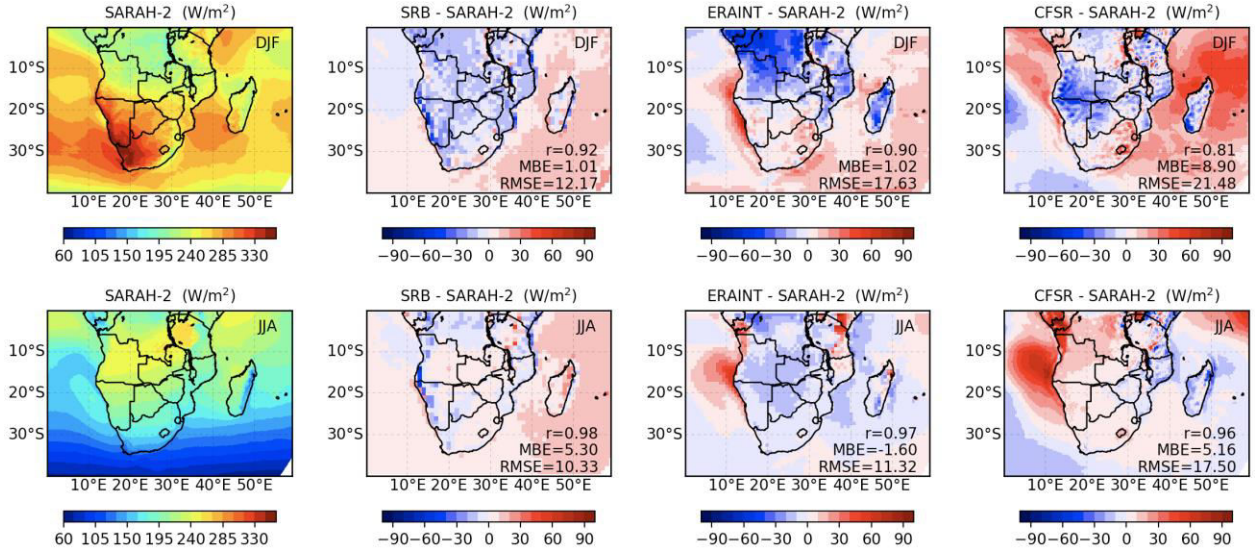

Fig. 3-1 Mean seasonal surface solar radiation in DJF (top row) and JJA (bottom row) of SARAH-2 (1st column), and its differences with other datasets, namely SRB (2nd column), ERAINT (3rd column), and CFSR (4th column). Note that these observational date sets are covering the same period from 1990 to 2005. The White area in the bottom right is out of SARAH-2 coverage. Spatial correlation (r), Mean Bias Error (MBE) and Root Mean Square Error (RMSE) are indicated in the corresponding plots.

All gridded products agree quite well in the large-scale SSR patterns (Figures not shown), but as depicted in **Fig. 3-1**, significant deviations occur locally with regard to the magnitude and spatial extent of the mean SSR.

Validation of gridded products with ground-based measurement from GEBA indicates an uncertainty generally less than 10 W/m^2. However, this validation using GEBA observations suffers from the spatial inhomogeneity and temporal incompleteness (no station selected in the west of the southern African continent), thus the uncertainty of gridded datasets is still difficult to estimate. (Posselt, Mueller, Stöckli, & Trentmann, 2012) compared GEWEX/SRB and ERA-Interim with ground-based measurements from the BSRN (Baseline Surface Radiation Network), and they found that ERAINT and SRB showed similar results compared to two available BSRN stations in Africa (only one in southern Africa, South Africa), with an absolute bias below 13

W/m2. It was also found that the accuracy of these references is generally increasing with the latitude, with mean absolute bias from 30 W/m^2 near the equator to about 10 W/m^2 at about 30° S (**Fig. 3-2**).

The satellite dataset GEWEX/SRB matches quite well with SARAH-2 in terms of the seasonal mean pattern, with differences mostly < 20 W/m^2 over the entire domain in both DJF and JJA. However, the reanalysis datasets have large differences in some sub-regions. Over tropical SA, ERAINT provides less SSR up to -50 W/m^2 (-30 W/m^2) compared with SARAH-2 in DJF (JJA), which is associated with less or more clouds (**Fig. 3-3**). Over the oceans, SARAH-2 shows much larger local differences in SSR with respect to the reanalyses: CFSR has much higher values up to 80 W/m^2 during JJA over tropical Atlantic Ocean and 50 W/m^2 during DJF over SWIO. ERAINT and CFSR show higher values of about 40 W/m^2 along the western coast of the Africa continent in both seasons, which is likely due to the underestimation of the stratiform boundary layer clouds in this area.

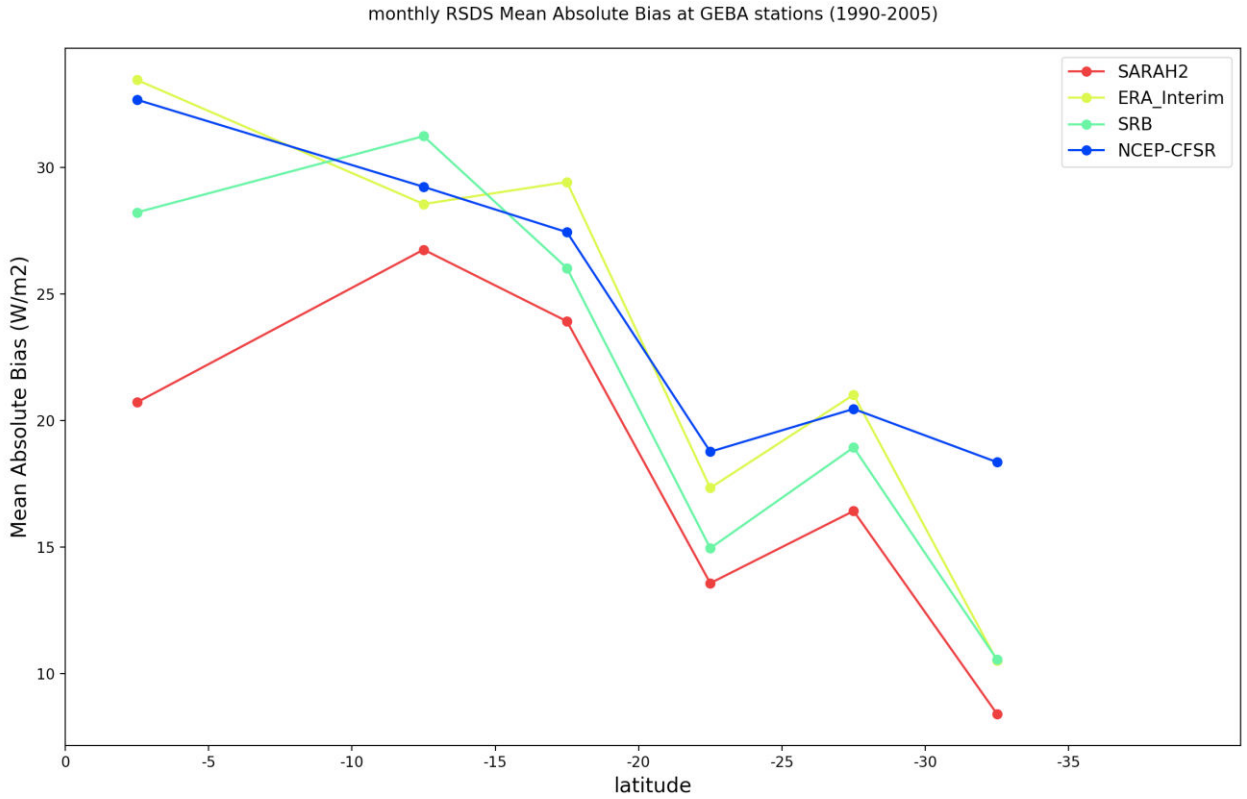

Fig. 3-2 Latitudinal variation of the monthly SSR Mean Absolute Bias (MAB) from SARAH-2 (red), ERAINT (yellow), SRB (green) and CFSR (blue) at the GEBA stations (**Fig. 2-3**) during 1990-2005. Each MAB is an averaged value from all the stations located in a 5-degree interval.

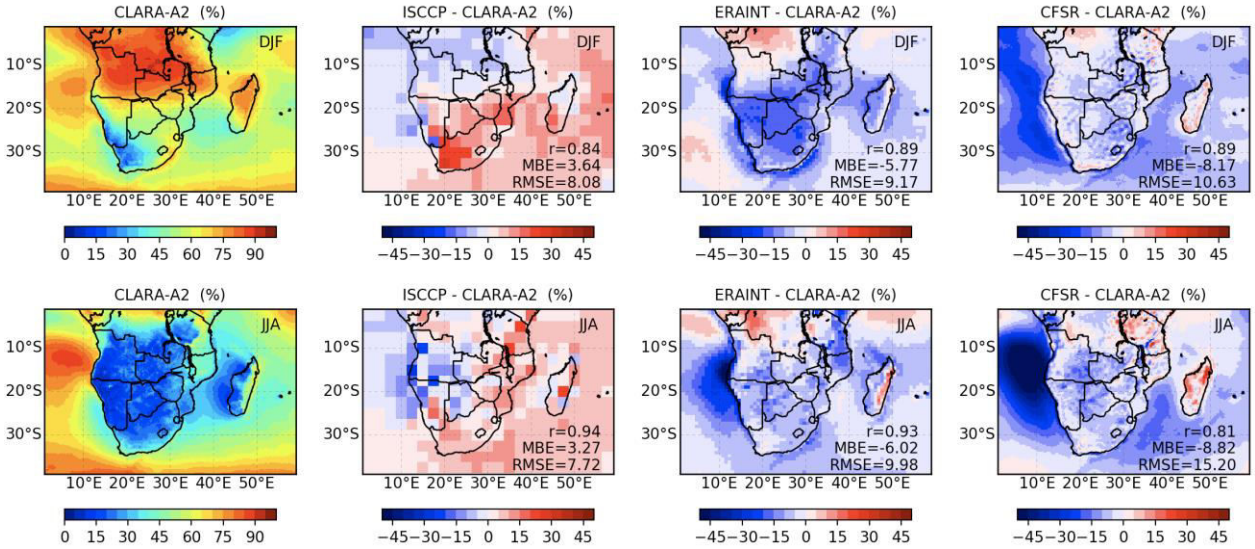

Fig. 3-3 Mean seasonal cloud cover fraction in DJF (top row) and JJA (bottom row) of CLARA-A2 (1st column), and its differences with other datasets, namely ISCCP (2nd column), ERAINT (3rd column), and CFSR (4th column). Note that these observational date sets are over the same period from 1990 to 2005. Spatial correlation (r), Mean Bias Error (MBE) and Root Mean Square Error (RMSE) are indicated in the corresponding plots.

3.1.2.1 SSR seasonal mean: DJF

As shown in **Fig. 3-5**, seasonal-mean SSR for austral summer (DJF) exhibits strong local variations among the different GCMs (in a range of up to ±80 W/m^2). This inter-model dispersion is also depicted by the statistical measures: the spatial correlation ranges from 0.65 (CNRM…) to 0.86 (Had…), and the Mean Bias Error (MBE) from -10.48 to 26.34 W/m^2. IPSL-CM5A-MR has relatively uniform positive SSR bias over the whole domain with MBE of 26.34 W/m^2, while the other GCMs produce different signs of biases over different sub-regions of the domain, leading to a small MBE in the range ±10 W/m^2 when averaged of the entire domain. Multi-model mean bias of SSR simulated by GCMs is 1.1 W/m^2 in DJF, with strong lower bias (~ 50 W/m^2) over the sub-tropical land and higher bias (~ 50 W/m^2) over the sub-tropical ocean (**Fig. 3-4**).

RCMs evaluation simulations (i.e., driven by ERAINT) show much larger (negative) SSR MBE (varying between -59.86 to -2.06 W/m^2) than the forcing ERAINT (1.02 W/m^2). CCLM4 and REMO2009 show overall negative biases, with MBE of about -60 W/m^2 and -27 W/m^2, respectively (similar bias pattern also shown when driven by different GCMs). Opposite signs of SSR bias with respect to the forcing ERAINT could be found in some sub-regions: Tropical Africa continent for RCA4; southern of SA for CCLM4, RACMO22T and REMO2009; subtropical oceans for CCLM4, RCA4 and REMO2009; Madagascar for HIRHAM5 and RACMO22T. It is obvious that RCMs are likely to produce their own SSR patterns and seem insensitive to the forcing ERAINT. The RCM+ERAINT multi-model SSR bias is about -24 W/m^2 in DJF.

For RCM GCM-forcing runs, the patterns of SSR remain similar when forcing by several GCMs with very different SSR biases. For example, CCLM4 simulations driven by 4 GCMs (CNRM-CM5, EC-EARTH, HadGEM2-ES and NorESM1-M) show similar overall negative SSR biases of about -60 W/m^2 across the entire domain, though the driving GCMs have opposite biases in some sub-regions (e.g. CNRM-CM5 show strong positive bias of about 50 W/m^2 in the centre of southern Africa, while EC-EARTH has a bias of about -50 W/m^2). This RCM dominating SSR pattern is also evident in the case of other RCMs, especially for RCA4 simulations with 10 different driven GCMs (**Fig. 3-5**). Again, the radiation processes in the RCM are mainly controlled by internal processes of the RCM and little influenced by the boundary forcing applied. The GCM biases aren't likely to transfer to the downscaled results through the boundaries. For example, the five RCM simulations forced by EC-EARTH show very different patterns of SSR bias among each other as well as with the forcing EC-EARTH. However, for each RCM, the SSR bias patterns are similar to the results of the evaluation run. Thus, the RCMs multi-model mean SSR bias is likely due to the regional model itself instead of the biases from their forcing GCMs. The multi-model mean SSR biases of RCMs forced by GCMs are about -32 W/m^2 in summer, which is dominated by the 4 CCLM4 simulations (biases of -76 W/m^2) and the 10 RCA4 simulations with biases of up to about -30 W/m^2 in DJF. Because of these large biases for particular models, RCMs' ensemble has larger SSR uncertainty compared with their driving GCMs' ensemble. For

a particular RCM, the dispersion of the simulations driven by different GCMs is thus likely due to the bias induced by the RCM, not the dispersion of forcing GCMs.

It is evident in DJF that SSR bias simulated by ERAINT is negatively correlated with the bias of CLT as shown in **Fig. 3-6** except for Madagascar where the biases are both negative. This anti-correlation between SSR and CLT bias is physical reasonable mainly because of the reflection effect of clouds. Correlation of SSR/CLT biases is also found for the majority of GCMs (CanESM2, EC-EARTH, GFDL-ESM2M, HadGEM2-ES, IPSL-CM5A-MR, MPI-ESM-LR, NorESM1-M), and also for the regional simulations conducted by CCLM, RCA4 and HIRHAM5. The high dependence of SSR biases on CLT and surface albedo uncertainties was reported by several previous studies (e.g., Pessacg et al. (2014) and García-Díez, Fernández, and Vautard (2015)). However, for REMO2009 forced by ERAINT and EC-EARTH and MPI-ESM-LR GCMs, SSR has a negative bias as well as CLT over the continental part of SA.

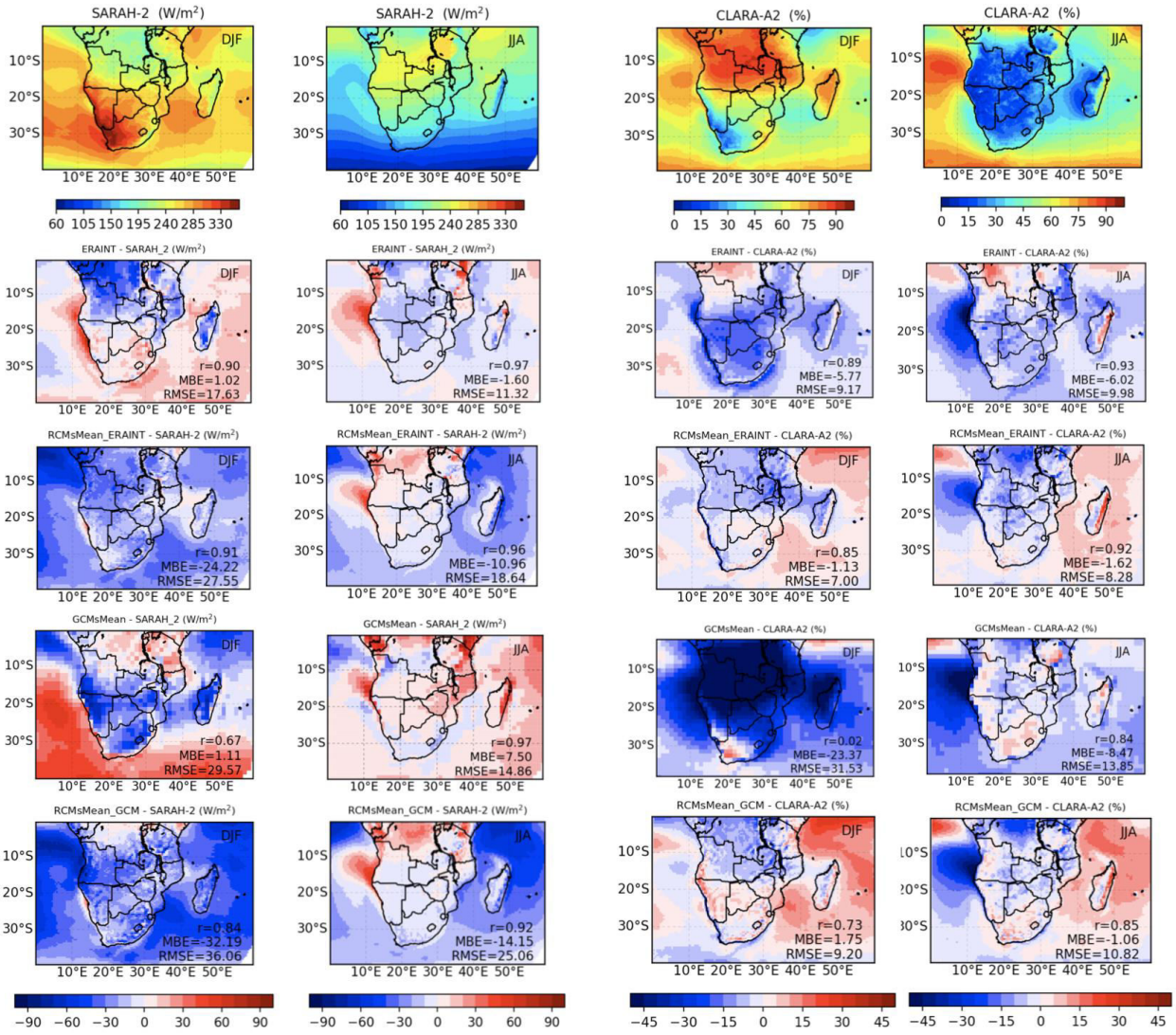

Fig. 3-4 Seasonal mean SSR and CLT difference between ERA-Interim (ERAINT), GCM ensemble mean, RCM ensemble mean (driven by ERAINT and GCMs) and satellite retrievals in the period of 1996-2005.

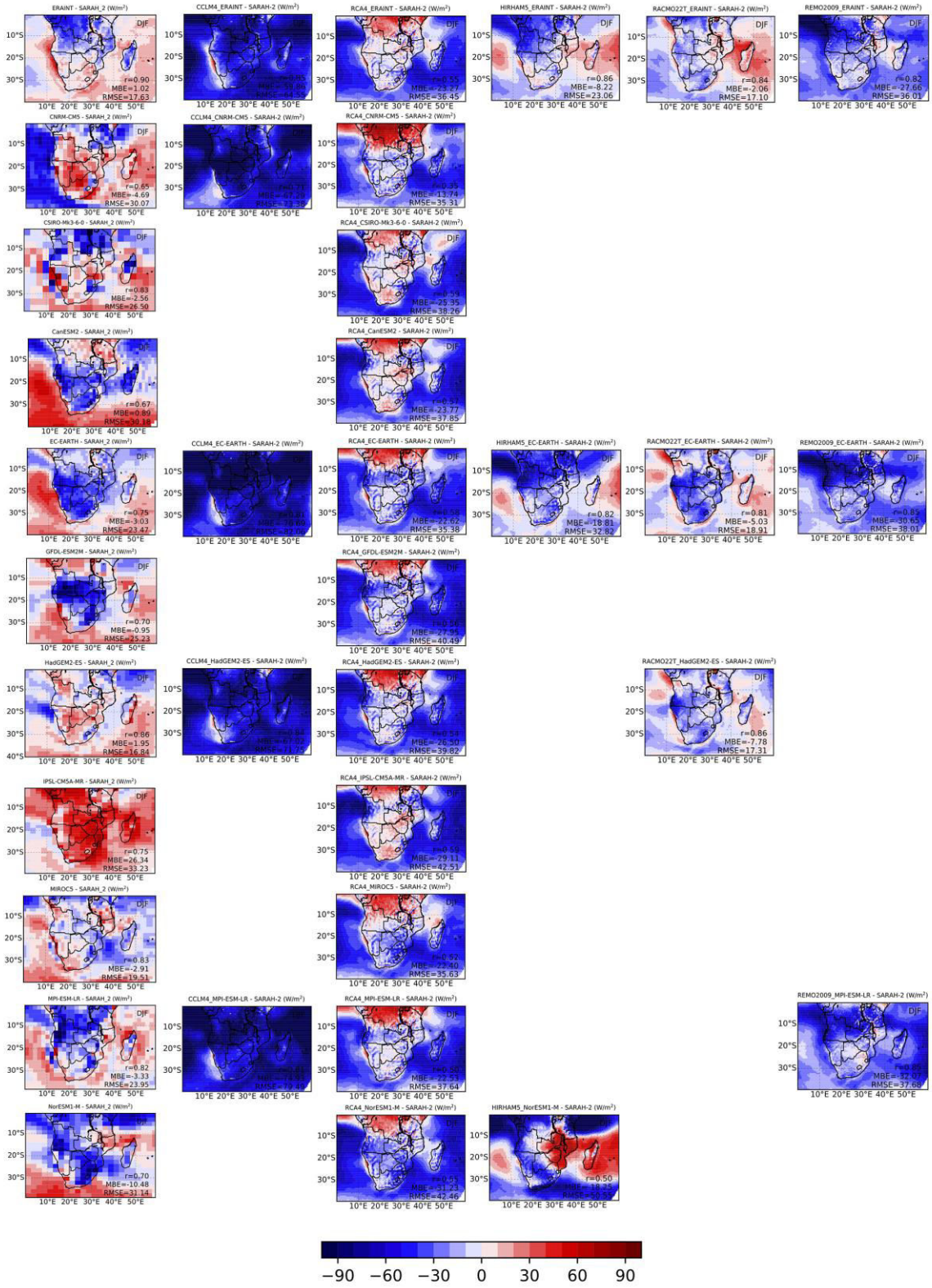

Fig. 3-5 Austral summer (DJF) mean bias of surface downward solar radiation (SSR) during 1990 - 2005, compared to SARAH-2 (used as reference) for ERA-Interim (ERAINT), the GCMs and the RCMs driven by ERA-Interim and the GCMs. For the comparison, SARAH-2 data were remapped to the models' resolution. Spatial correlation (r),

Mean Bias Error (MBE) and Root Mean Square Error (RMSE) are indicated in the corresponding plots. Resolution and reference of each model are listed in **Table 2-2**.

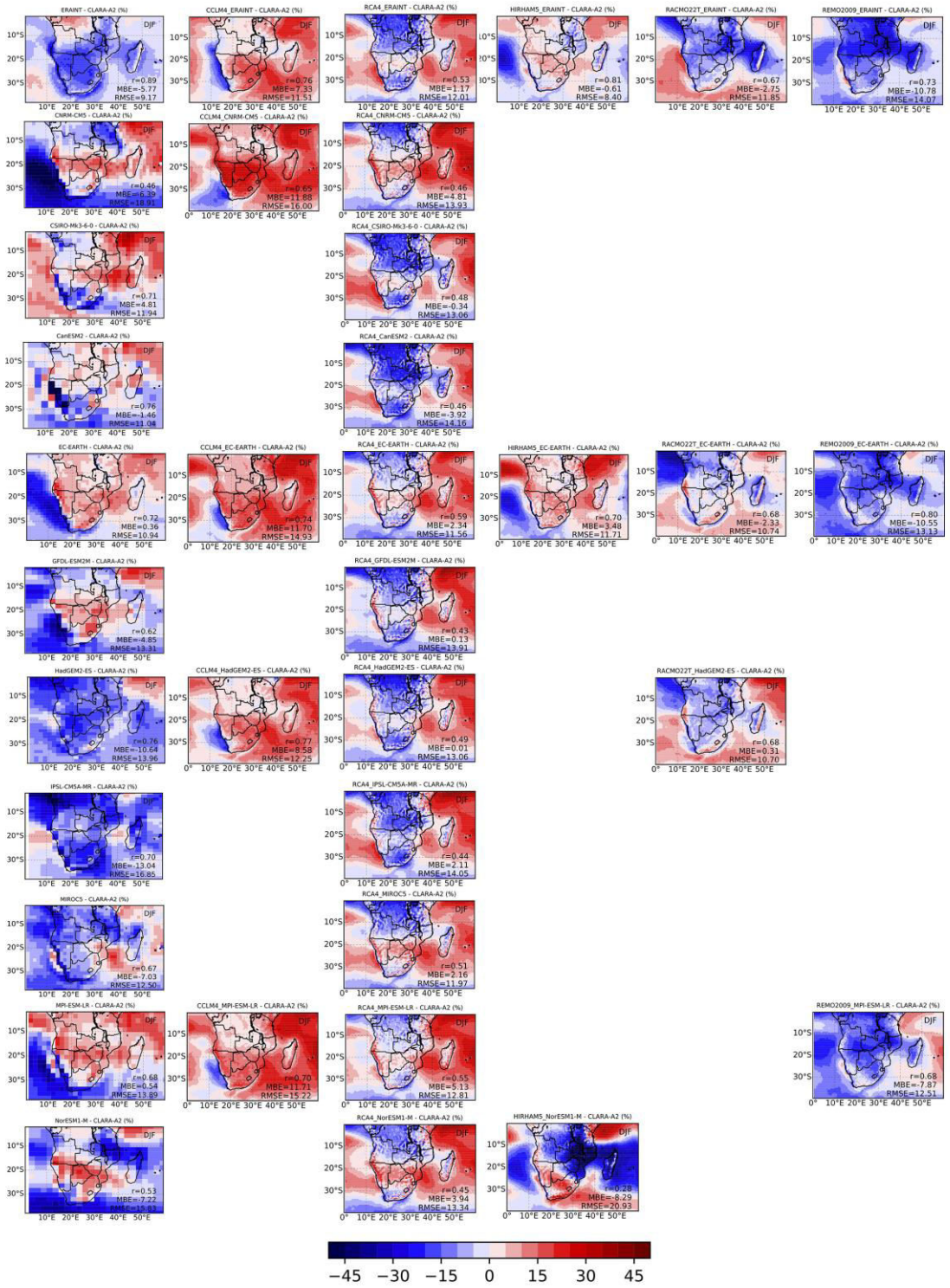

Fig. 3-6 The same as **Fig. 4**, but for CLT. The statistics were calculated using CLARA-A2.

3.1.2.2 SSR seasonal mean: JJA

As shown in **Fig. 3-7**, GCM models have a SSR bias in austral winter (JJA) varying in the range of about ±60 W/m^2. Multi-model mean bias of SSR simulated by GCMs is 7.5 W/m^2 in JJA. RCMs evaluation simulations (as driven by ERAINT) show an overall much larger SSR MBE (varying between -24.93 to -2.27 W/m^2) than the forcing ERAINT (1.60 W/m^2). The RCM+ERAINT multi-model SSR bias is about -10 W/m^2 in JJA, dominating by the strong negative bias of CCLM4 and RCA4 runs. For the RCMs' runs forced by the GCMs, the patterns of SSR remain similar when forcing by several GCMs with very different SSR bias. There again, the impact of GCM biases in JJA is not obvious as in DJF. SSR and CLT biases are overall negatively correlated in JJA for individual model.

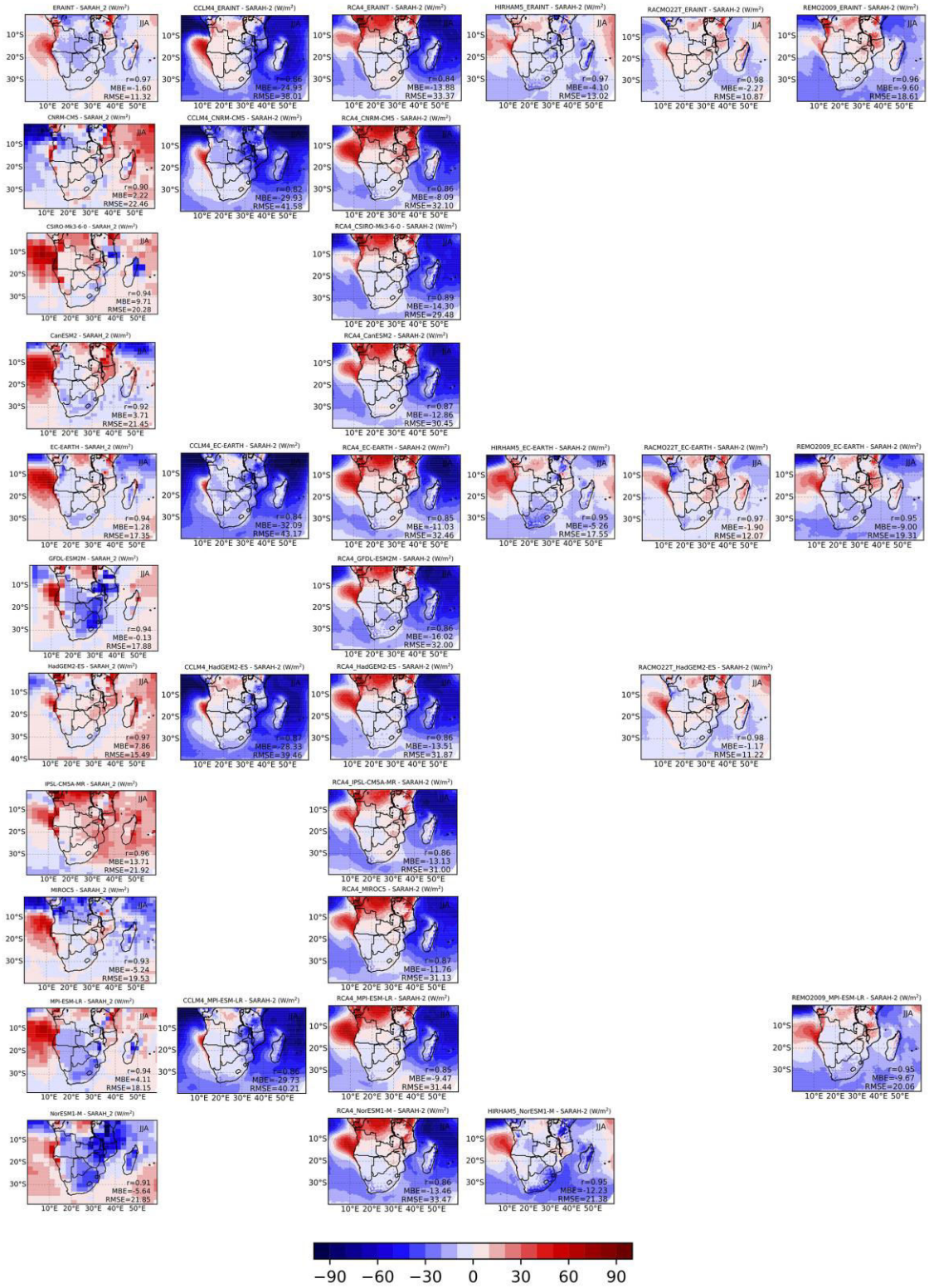

Fig. 3-7 Same as **Fig. 3-5**, but for JJA.

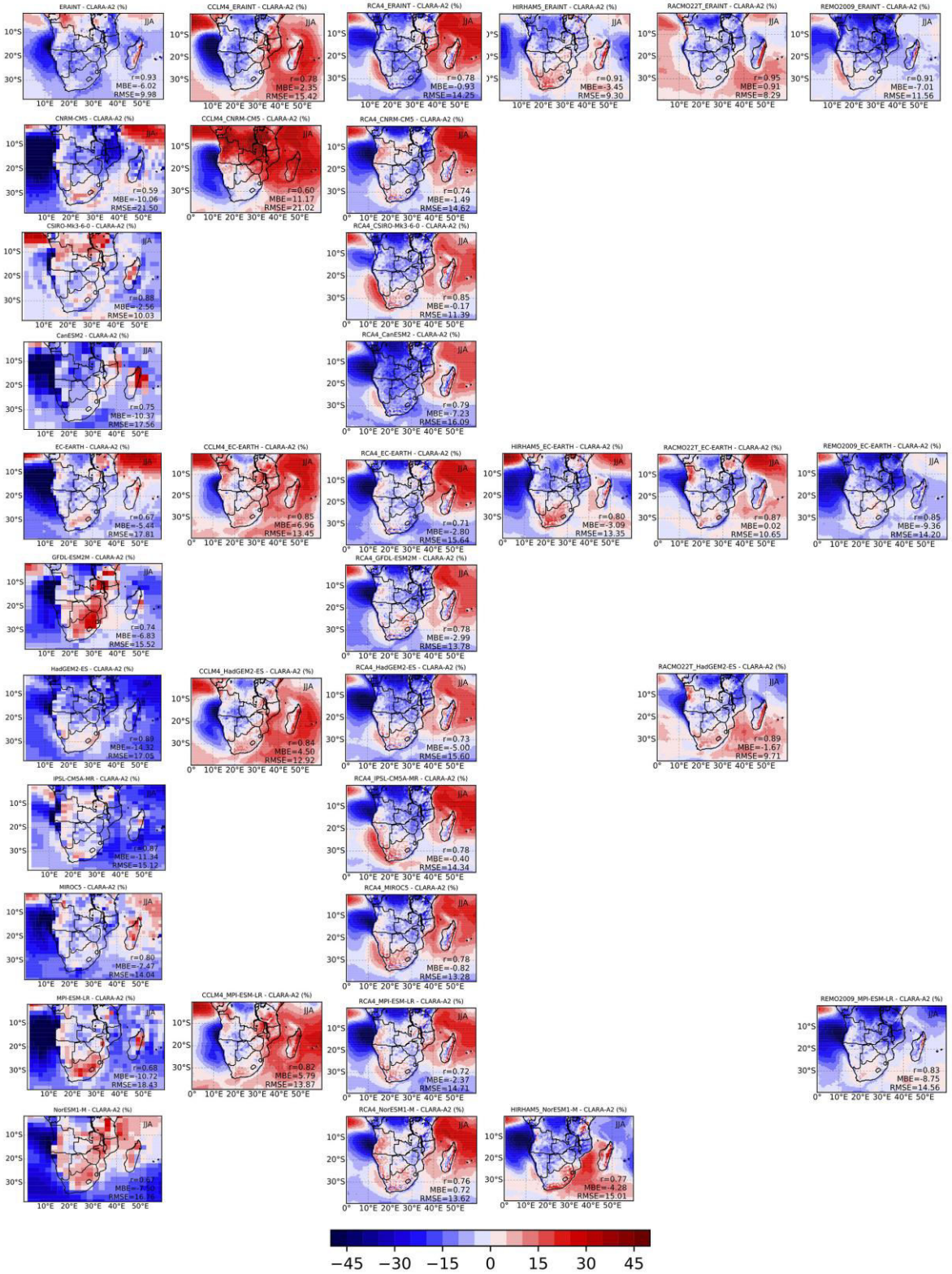

Fig. 3-8 Same as **Fig. 3-6**, but for JJA.

3.2 Climate changes projections

3.2.1 Seasonal mean projected changes in SSR

In this section future projections of SSR based on regional and global climate model simulations are assessed.

Multi-model seasonal mean SSR differences against historical runs (period DJF 1970–1999) for the period 2036-2065 and 2070-2099 (hereafter refered to as mid/end changes) simulated by the GCMs/RCMs in RCP4.5/RCP8.5 are shown in **Fig. 3-9** for DJF and **Fig. 3-10** for JJA. Only significant differences at the 95% level are represented. The lower panels in **Fig. 3-9/Fig. 3-10** show the number (expressed in percentage) of models (out of 10 GCMs and 20 RCMs) that are in agreement (in terms of changes of the same sign and with the same statistical significance level) with respect to their projected changes in the above panels.

In general, multi-model mean changes in the SSR patterns are overall quite similar in the RCMs and GCMs. Both global and regional climate models project a statistically significant increase of SSR in the DJF season over the centre of the SA continent (SA-C) in a range of 5 – 15 W/m^2 depending on the period (mid or end of the 21th century), models (global or regional) and the RCP scenario. At the same time, an SSR decrease with high confidence is also obvious over Equatorial East Africa (EA-E), where a tendency towards more humid conditions was found as a robust feature of climate change of Africa based on GCMs simulations (Pohl, Macron, & Monerie, 2017). The two multi-model averaged trends in each corresponding area show a high consensus between models, and the percentage of climate models in agreement with the mean evolution is high (typically 80-100%). The end-changes are generally larger than the mid-changes for GCM/RCM in both RCP scenario (e.g. over SA-C and EA-E). The RCM projections usually show spatial extensions of the significant changes compared with GCMs. Compared with RCP4.5 the projections under RCP8.5 don't have obvious enhanced changes in the mid-changes for both GCM and RCM simulations, which is reasonable because of the little difference between the two forcings by 2050. As expected in 2100, the end-changes in RCP8.5 show larger changes than that in RCP4.5, with about 2.5 W/m^2 enhanced changes in GCMs and about 5 W/m^2 enhanced in RCMs. The RCMs seems more sensitive to the RCP forcings.

Particularly, for DJF the GCMs in theirmultimodel mean project a mid-change over SA-C of +5 W/m^2 in both RCP4.5 and RCP8.5, as well as an end-change of +10 W/m^2 in RCP4.5 and +12.5 W/m^2 in RCP8.5. The RCMs project in their multimodel mean a mid-change over SA-C of about +5 W/m^2 in RCP4.5 and RCP8.5, as well as an end-change of +10 W/m^2 in RCP4.5 and +15 W/m^2 in RCP8.5. Over EA-E, the GCMs project a mid-change of -5 W/m^2 in RCP4.5 and RCP8.5, as well as an end-change of -10 W/m^2 in RCP4.5 and about -12.5 W/m^2 in RCP8.5. The

RCMs project a mid-change of about -10 W/m^2 in RCP4.5 and RCP8.5, as well as an end-change of -10 W/m^2 in RCP4.5 and -15 W/m^2 in RCP8.5

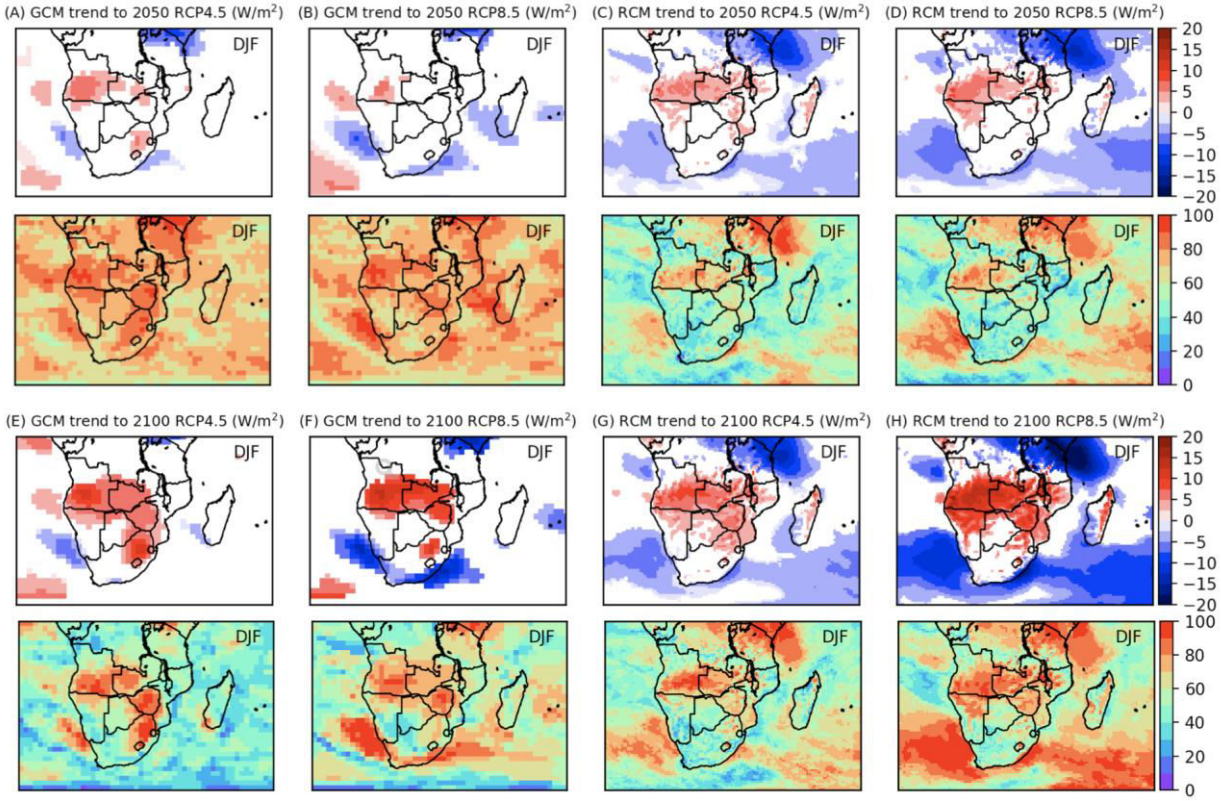

Fig. 3-9 Multi-model seasonal mean SSR differences (W/m^2) against historical runs (period DJF 1970–1999) for the mid of 21st century (DJF 2036-2065, **A**-**D**), simulated by GCMs in RCP4.5 (**A**) and RCP8.5 (**B**), and by RCMs in RCP4.5 (**C**) and RCP8.5 (**D**). (**E**–**H**) as (**A**–**D**) but for the end of 21st century (DJF 2070-2099). Only significant differences at the 95% level are represented. Lower panels show the number (shown in percentage) of models (out of 10 for GCM and 20 for RCM) that are in agreement (changes of the same sign, with the same statistical significance level) with the above panels. GCM outputs are remapped to the horizontal resolution of 1.12*1.12 degree, corresponding to the grid of EC-EARTH.

In the JJA season for the mid/end of 21st century (**Fig. 3-10**), the GCMs project increases in SSR over EA-E (mainly in Tanzania) and South Africa. Larger increases over these regions are projected in RCP8.5 than RCP4.5 and with larger spatial extension in the RCMs than in the GCMs. These multi-model average changes are coming with a low percentage of models that agree (typically 50-80% over the statistical confident area) compared with that in DJF (typically 80-100%, see **Fig. 3-9**). The RCMs project a decrease of over the Sub-Tropical Atlantic Ocean (not obvious in the GCM projections) of about -5 W/m^2 as mid-change in RCP4.5 and RCP8.5; of -7.5 W/m^2 in RCP4.5 and -10W/m^2 in RCP8.5 as end-changes.

Particularly, for JJA the GCMs project a mid-change over EA-E (mainly Tanzania) of +5 W/m^2 in RCP4.5 and RCP8.5 (the latter over a smaller area), and an end-change of +5 W/m^2 in RCP4.5 and +10 W/m^2 in RCP8.5. Again, the RCMs seem more sensitive than the GCMs in this area.

The RCMs project a mid-change over EA-E of about +5 W/m^2 in RCP4.5 and RCP8.5, and an end-change of +5 W/m^2 in RCP4.5 and +10 W/m^2 in RCP8.5. Over South Africa, the GCMs project a mid-change of + 2.5 W/m^2 in RCP4.5 and + 5 W/m^2 in RCP8.5 and an end-change of +5 W/m^2 in RCP4.5 and in RCP8.5. RCMs project a mid-change of less than +2.5 W/m^2 in RCP4.5 and RCP8.5, and an end-change of less than +2.5 W/m^2 in RCP4.5 and +5 W/m^2 in RCP8.5.

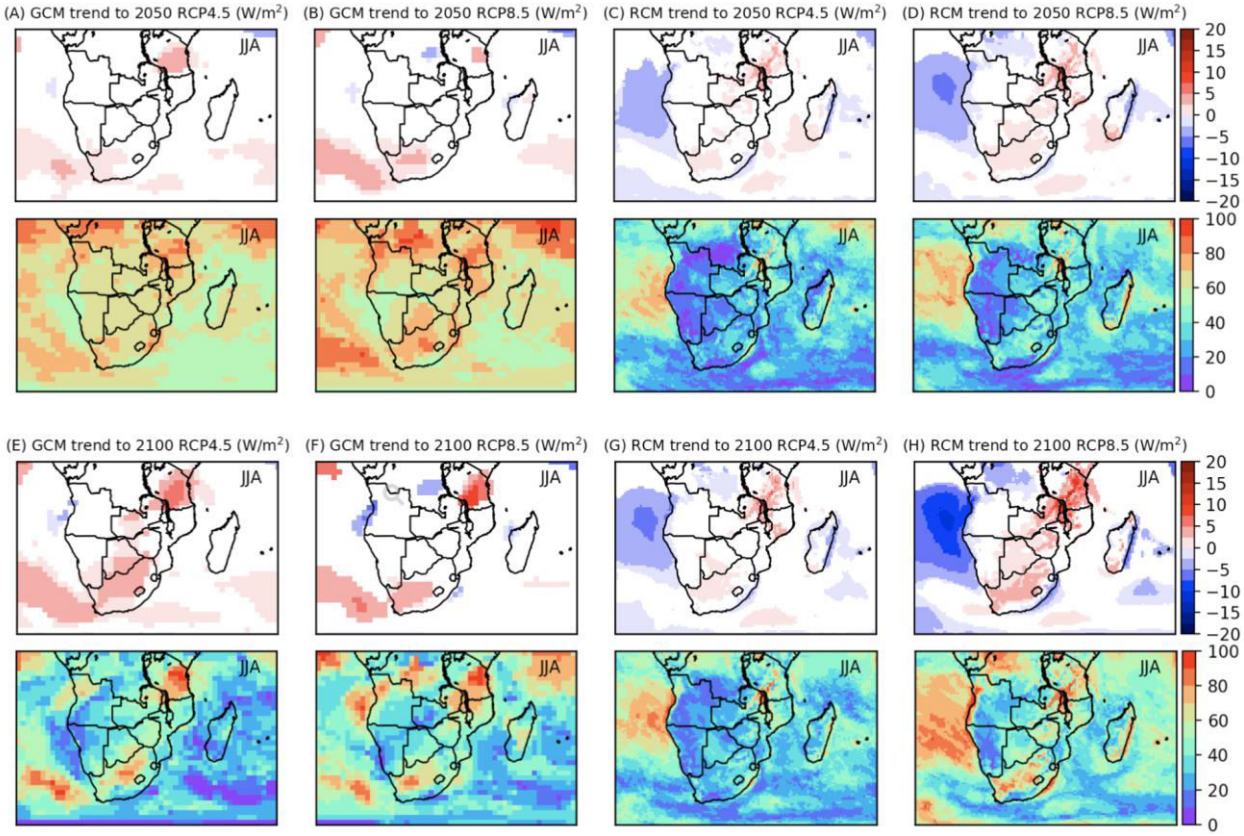

Fig. 3-10 Same as **Fig. 3-9**, but for JJA.

3.2.2 Seasonal mean projected changes in CLT

Multi-model seasonal mean CLT changes are shown in **Fig. 3-11** and **Fig. 3-12** for DJF and JJA, respectively. It is evident that the RCMs simulate CLT changes over land of the same signs with their forcing GCMs in both seasons, which is not the case in Europe (Bartók et al., 2016).

In DJF, decreases of CLT are generally projected over land by the climate models, with a mid-change about -2% for GCMs and RCMs in both scenarios and end-change about -4/-6 % in RCP4.5/RCP8.5 for both global and regional models. The model consensus over the areas of significant changes is generally between 70-80 % for the GCMs (end-change under RCP4.5 in a lower value of about 40%), and 40-70% for RCMs, with expectation of end-change under RCP8.5 with a value of 60-100%). CLT changes in RCP8.5 are larger by about 2% (absolute value) than in RCP4.5 for the end-change simulated by the GCMs and the RCMs. The difference of CLT changes in 2050 is not obvious. The RCM-projected CLT increase over the sub-tropical ocean (absent in thr GCMs) is consistent with the decreasing trend in SSR.

In JJA, similar to DJF, climate models project decreases of CLT over the SA continent, in a range of -2% to -6%, depending on the period considered, the model, and the RCP scenarios. Increases in 2050 and 2100 are shown over the Sub-Tropical Atlantic Ocean in the RCM projections in line with the projected decreasing SSR in the same area.

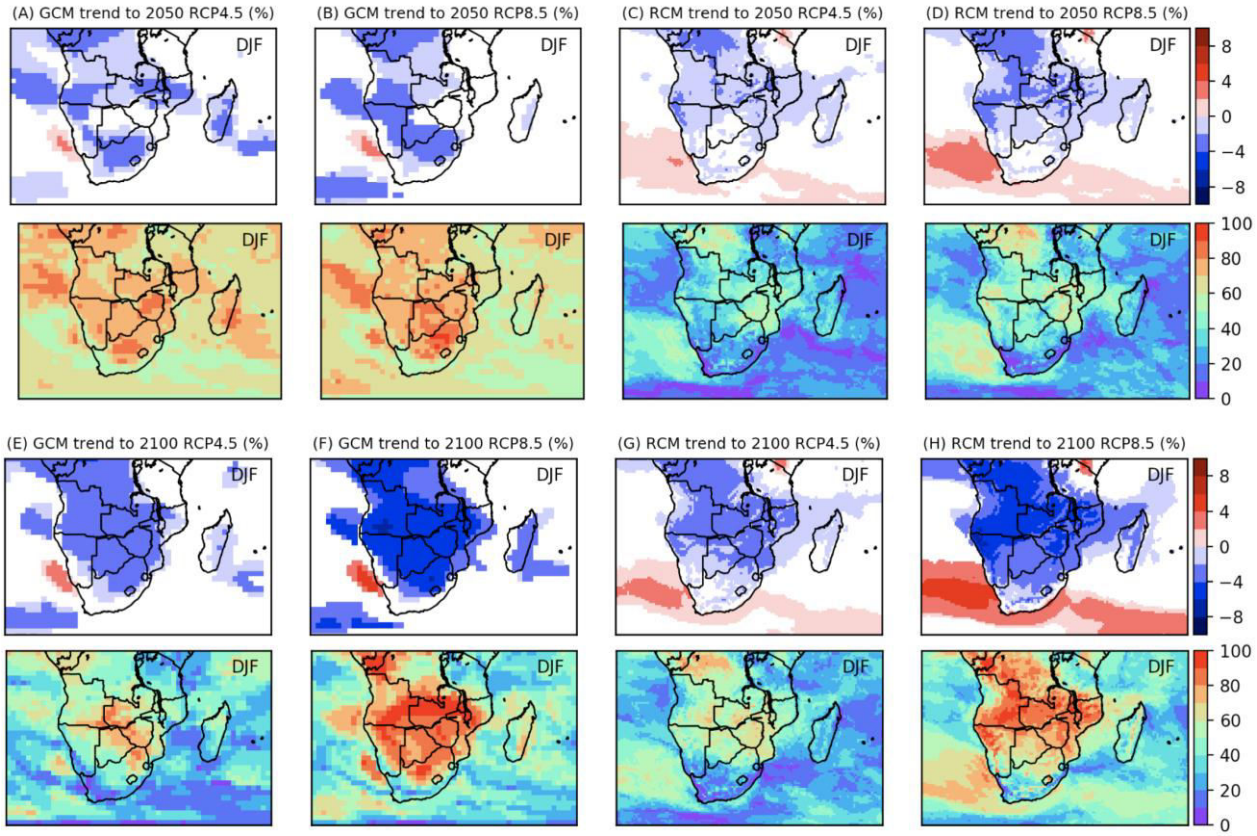

Fig. 3-11 Same as **Fig. 3-9** but for CLT.

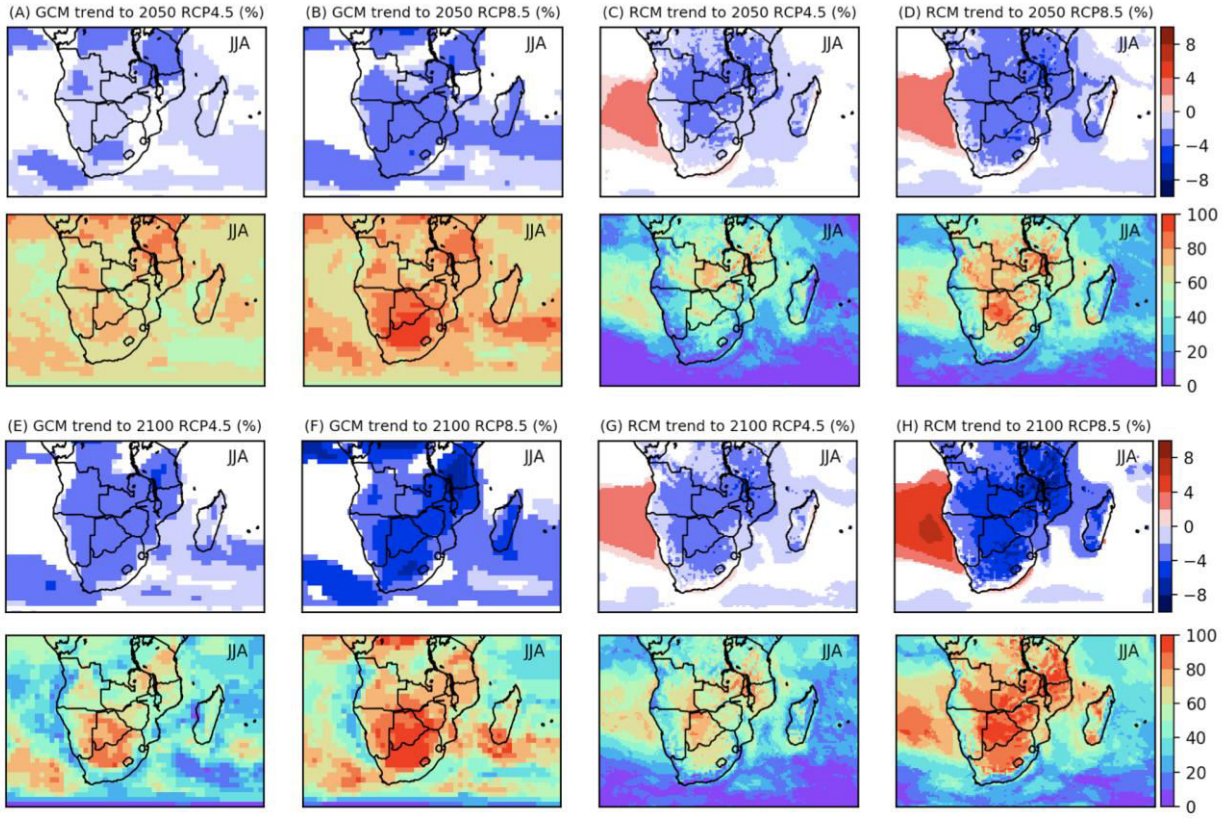

Fig. 3-12 Same as **Fig. 3-9**, but for CLT in JJA.

Multimodel mean projections of SSR (as well as CLT) change patterns by the GCMs and their embedded RCMs are fairly consistent, which is in contrast to the results shown over Europe in (Bartók et al., 2016). However, when looking at individual simulations, the projected changes of SSR between RCMs and their driving GCMs are not so similar. (Bartók et al., 2016) demonstrated that both the pattern of SSR changes and the mean change over the EURO-CORDEX domain are very similar in all 10 realizations of RCA4 despite much stronger differences in SSR in their 10 driving GCM experiments. They further argued that the SSR changes in the RCMs are mainly controlled by internal processes of the RCM and little influenced by the boundary forcing applied. Benefiting from the fact that the regional RCA4 was driven by 10 different GCMs, we have a chance to examine the impact of the driving GCMs on the resulting SSR projections now for the region of SA. **Fig. 3-13** shows the end-change of SSR simulated by the RCA4 regional model at 0.44° resolution (1st and 3rd rows) with 10 different driving GCMs (2nd and 4th rows) as boundary forcing.

While the GCMs show strong intermodel differences in the projected SSR changes, the embedded RCA4 model (as well as the case of CCLM4 model) shows very similar patterns over land despite being driven by different GCMs, with decreasing SSR over Tropical Africa, and increases to the south of 10°S (except for RCA4 forced by IPSL-CM5A-MR over Madagascar). Regionally,

over tropical Africa the GCMs project opposite change signals, with 6 GCMs showing an increase up to 10 % while 4 GCMs projected a decrease. In spite of the difference between the GCM projections, the RCM, RCA4 here, projects the very similar decreases in these 10 realizations. The RCMs may generate opposite SSR changes with respect to their driving GCMs. Over the Atlantic Ocean, 7 GCMs predict an increase of SSR while all RCM experiments with RCA4 give decreasing signals.

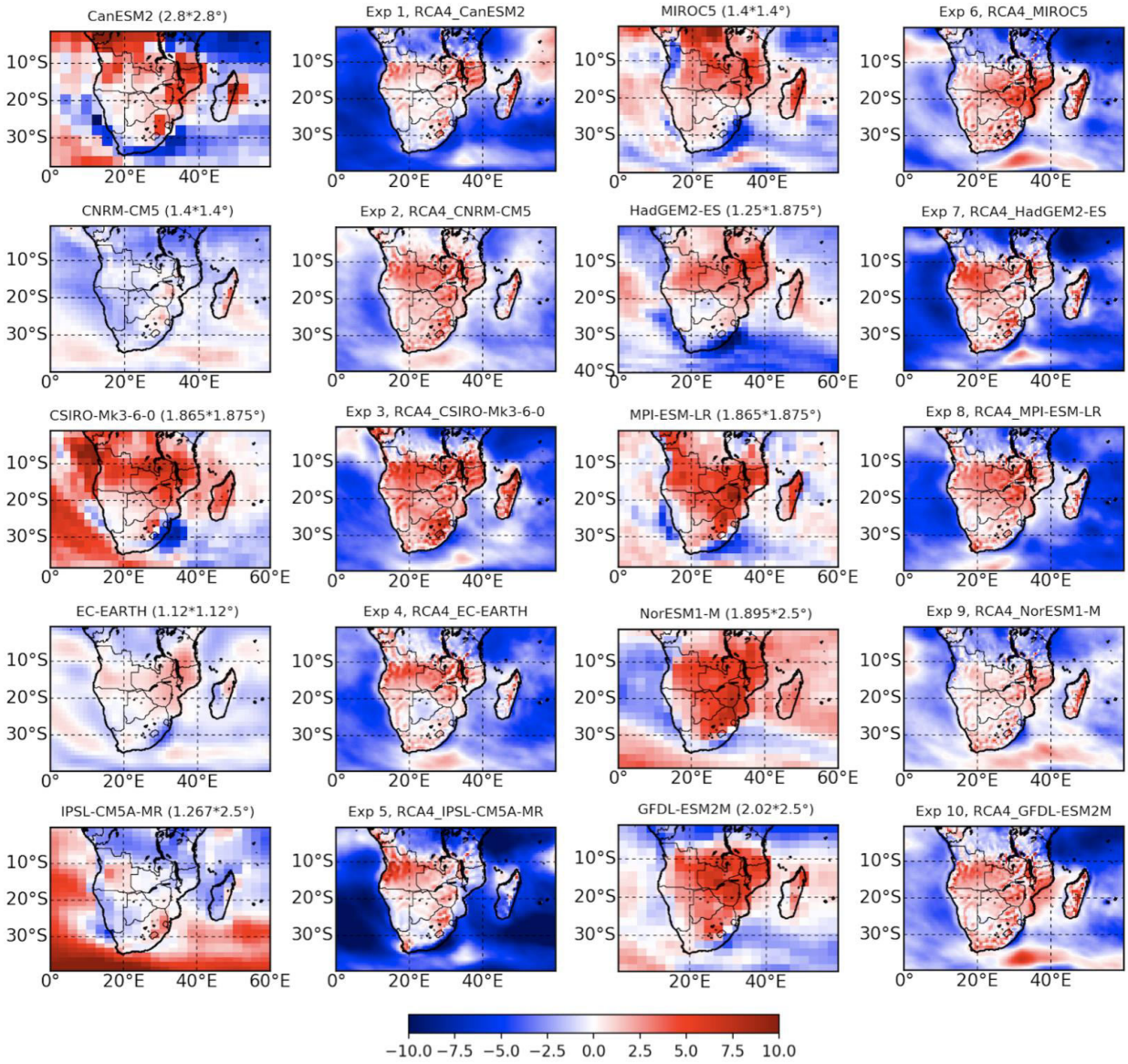

Fig. 3-13 Projected mean changes of SSR (2070-2099) from GCMs (1st and 3rd rows) and RCA4 (2nd and 4th rows) expressed in % with respect with the mean value of the reference period 1970-1999.

It is thus noteworthy that, as found by (Bartók et al., 2016) over the EURO-CORDEX domain, the patterns of SSR changes seem to be very similar in all realizations of RCA4 (the same applies for other RCMs but not shown), despite much stronger differences both in SSR magnitudes and patterns in the driving GCM ensemble. It was also shown in Paper 1, that the SSR biases are quite similar when a single RCM is forced by GCMs with very different bias patterns. Obviously, the SSR changes in the RCMs are mainly controlled by internal processes of the RCM and little influenced by the boundary forcings applied.

3.2.3 Time-dependent seasonal changes in SSR from GCMs and RCMs

In this section, seasonal time-series of SSR based on regional and global climate model simulations under the RCP8.5 scenario are assessed. Results in RCP4.5 are not shown for simplicity, while the sensitivity of SSR changes to the RCP scenario could be estimated based on the comparison of seasonal climatologies as discussed in section 3.2.1. To better understand the seasonal time-series, the whole SA domain has been divided into 7 sub-regions based on the level of mean SSR over 1983-2005 (**Fig. 3-14**). The seasonal SSR anomalies simulated by 20 RCM simulations and their 10 driven GCMs are shown in **Fig. 3-15** and **Fig. 3-16** for DJF and JJA, respectively. Thirty-year running mean time series of the SSR anomalies from the global CMIP5 (black) and the regional CORDEX (blue) models have been determined for each region. Anomalies are computed with respect to the mean values over the reference period 1970–1999 and are expressed in percentage (%). Solid lines depict the multi-model mean values, with shadows showing the ensemble spread. Vertical red bars depict 0 ± the multi-model mean value of the standard deviation of the seasonal series of SSR anomalies in the reference period, as representative of the "background noise" of the climate change signal. If the multi-model mean change exceeds such a quantity, it signifies an obvious change signal and could be easily detected.

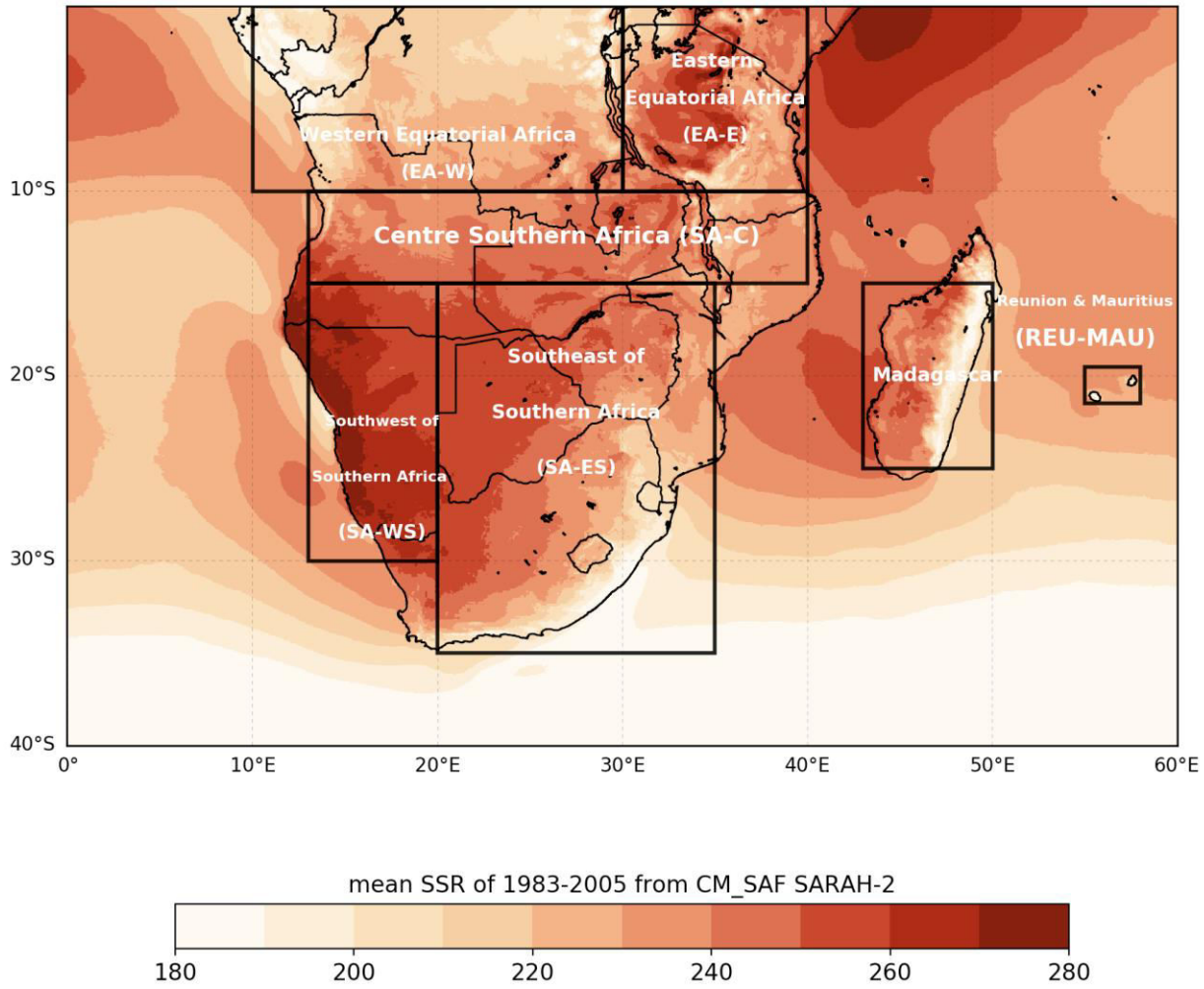

Fig. 3-14 Mean SSR of 1983-2005 from CM_SAF SARAH-2 project over Southern Africa. Unit is W/m^2. Sub-regions are defined by the level of SSR.

RCM-simulated SSR anomalies are generally following that of the forcing GCMs in terms of the signs, except the DJF anomalies in EA-W. The RCM results show comparable intermodal dispersion as the GCMs, when considering several RCMs and their forcing GCMs. The multi-model averaged seasonal SSR anomalies are smaller than the inter-annual standard variations depicted by the red bars in the plot over all the 7 sub-regions.

However, regional climate simulations are usually having the possible biases, coming from the regional model as well as from the forcing GCMs through boundary conditions. Efforts have been made to separate the impacts of RCM- and GCM-introduced- biases on the downscaling results in **section 3.1** by analyzing not only the GCM ensemble and the GCM-forced RCM ensemble, but also by comparing SSR patterns from a single RCM with its several driving GCMs or from a single GCM and several forced RCMs. It was argued in Paper 1, that the downscaled SSR bias is RCM dependent and is little influenced by the forcing GCMs.

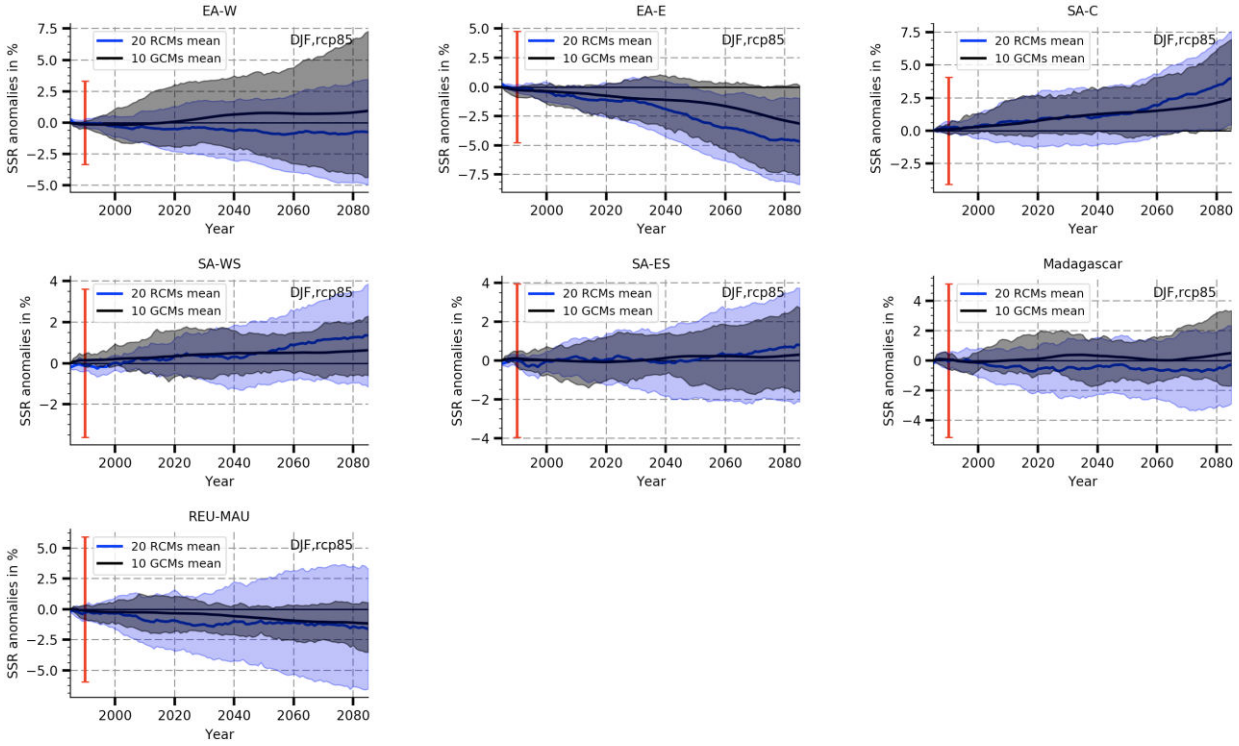

Fig. 3-15 Seasonal time-series of SSR anomalies along the 21st century under RCP8.5 for DJF. Thirty-year running mean time series of the SSR anomalies from CMIP5 (black) and the CORDEX (blue) models in each region as specified in Supplementary Figure 1. Anomalies are computed with respect to the mean values in the reference period 1970–1999 and expressed in %. Solid lines depict the multi-model mean values, with shadows showing the ensemble spread. Vertical red bars depict 0 ± the multi-model mean value of the standard deviation of the annual series of SSR anomalies in the reference period, as representative of the "background noise" of the climate change signal.

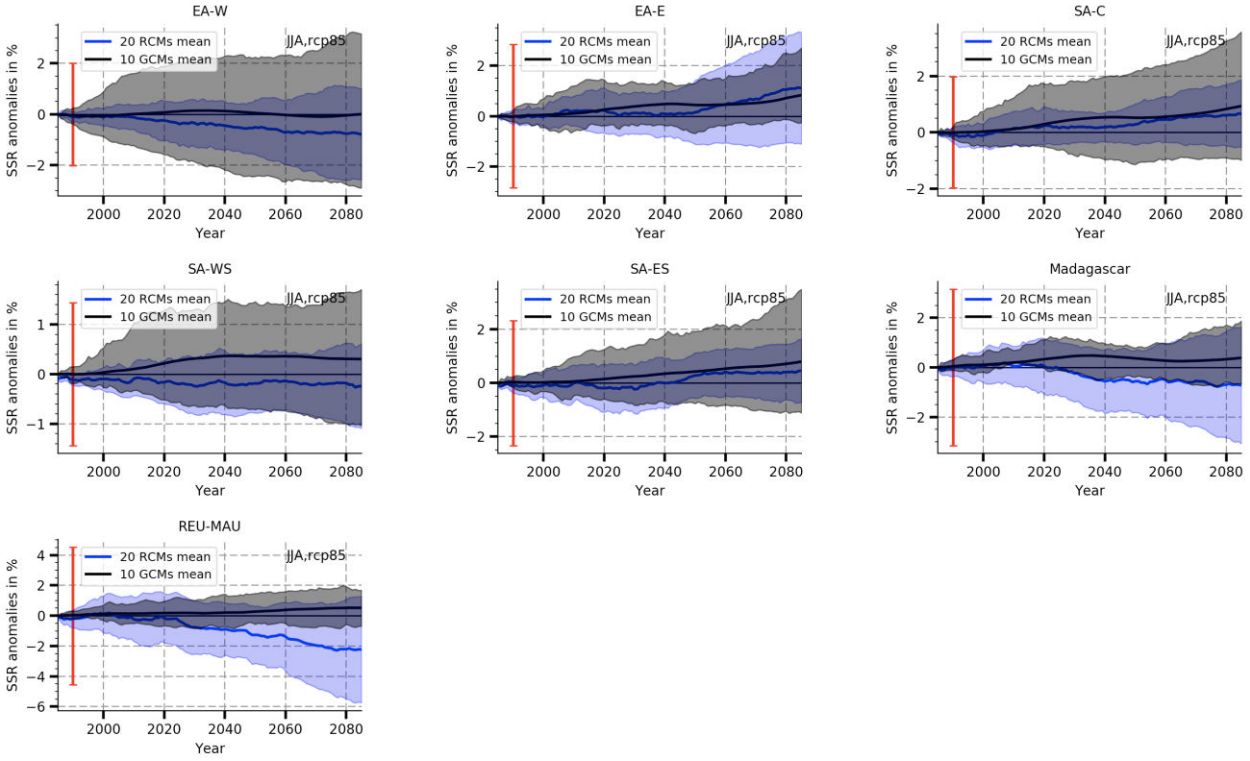

Fig. 3-16 Same as **Fig. 3-15**, but for JJA.

Seasonal series of SSR anomalies during the 21st century under RCP8.5 simulated by RCA4 and its 10 driving GCMs (**Table 2-2**) are shown in Fig. 3-17 and Fig. 3-18 for the DJF and JJA season, respectively. In both seasons, the RCA4 seasonal means show a smaller intermodel spread than their 10 forcing GCMs in the areas of EA-W, EA-E, SA-ES and SA-WS. In contrast, for SA-C, where the GCMs have consistent SSR change projections with high consensus between models, the spread of the RCM projections remains similar to those of the forcing GCMs. It is worth to note that only the SSR changes in DJF averaged over the 10 RCA4 ensemble in EA-W and EA-E, by the end of 21st century, have an amplitude larger than the background noise depicted by the red bars. The RCMs may have their own evolutions even of opposite signs of the SSR changes in some areas.

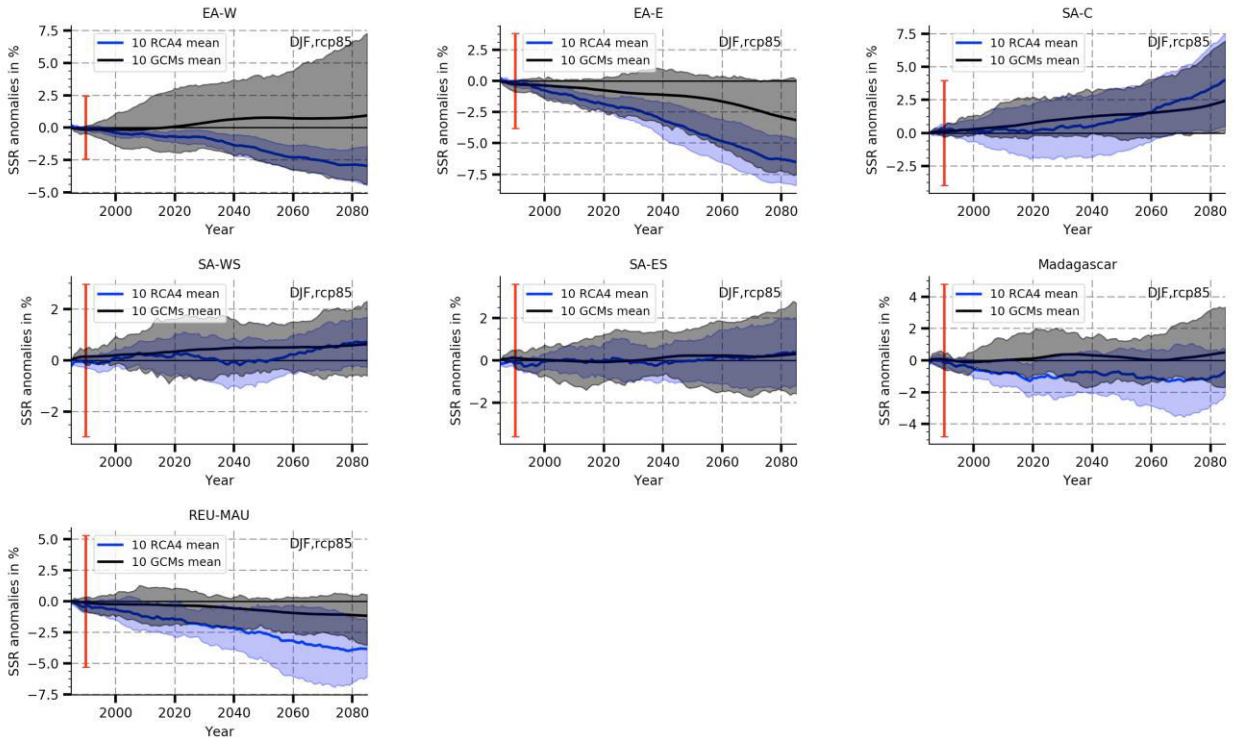

Fig. 3-17 Seasonal (DJF) time-series of SSR anomalies during the 21st century under RCP8.5 simulated by RCA4 and its 10 driving GCMs (**Table 2-1**). Thirty-year running mean time series of the SSR anomalies from the CMIP5 GCM (black) and the CORDEX RCM (blue) models in each region. Anomalies are computed with respect to the mean values in the reference period 1970–1999 and expressed in %. Solid lines depict the multi-model mean values, with shadows showing the ensemble spread. Vertical red bars depict 0 ± the multi-model mean value of the standard deviation of the seasonal series of SSR anomalies in the reference period, as representative of the "background noise" of climate change signal.

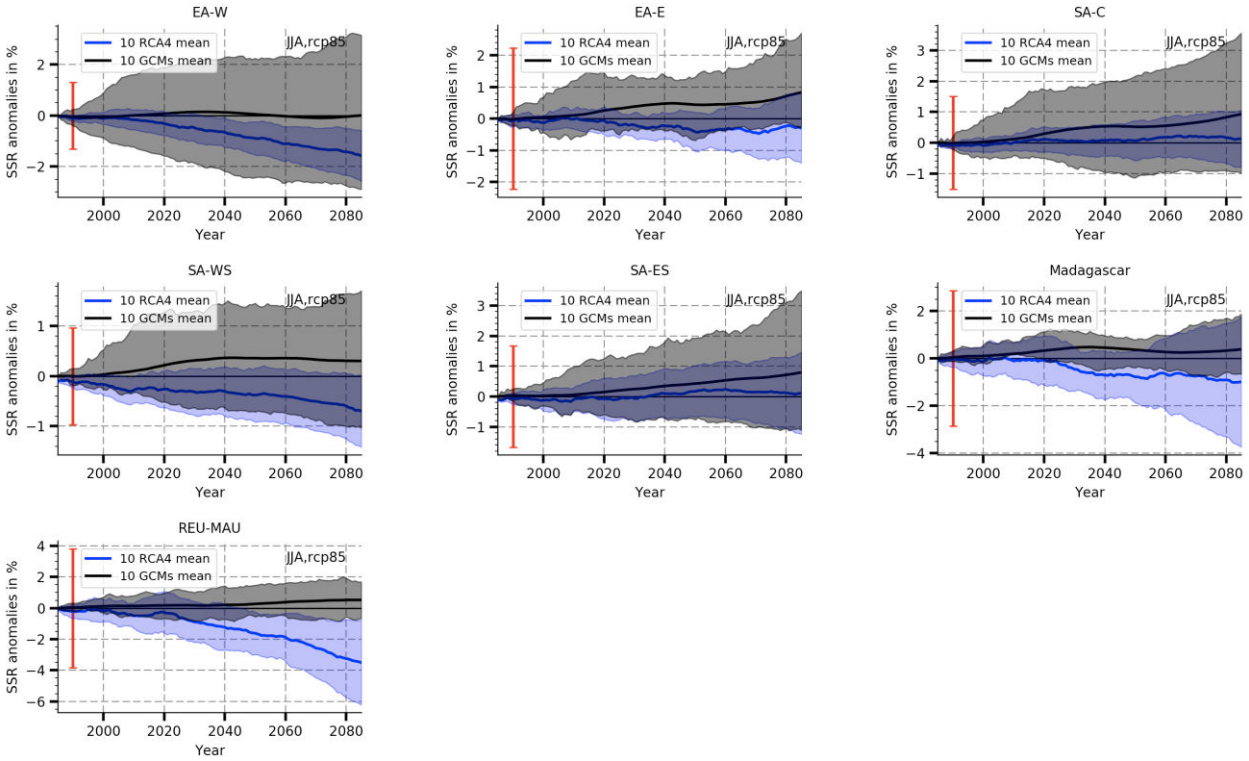

Fig. 3-18 Same as **Fig. 3-17** but for JJA.

On the other hand, considering one specific GCM and its forced 5 RCMs in **Fig. 3-19** and **Fig. 3-20**, where EC-EARTH projected seasonal SSR anomalies are shown, together with the results from its forced 5 RCMs. Since the RCMs are likely to produce SSR change patterns depending on only the regional model and without obvious impact from their driving GCMs, the RCM ensemble shows large SSR differences between each other despite driven by the same GCMs.

For the land area, both the amplitude and spread of DJF and JJA anomalies simulated by the RCMs in **Fig. 3-15** and **Fig. 3-16** may be explained by **Fig. 3-19** and **Fig. 3-20**, where projection of multi-RCM (driven by a single GCM, namely EC-EARTH) show quite similar SSR changes and spread. Thus, the GCMs have little impact on the downscaled projections.

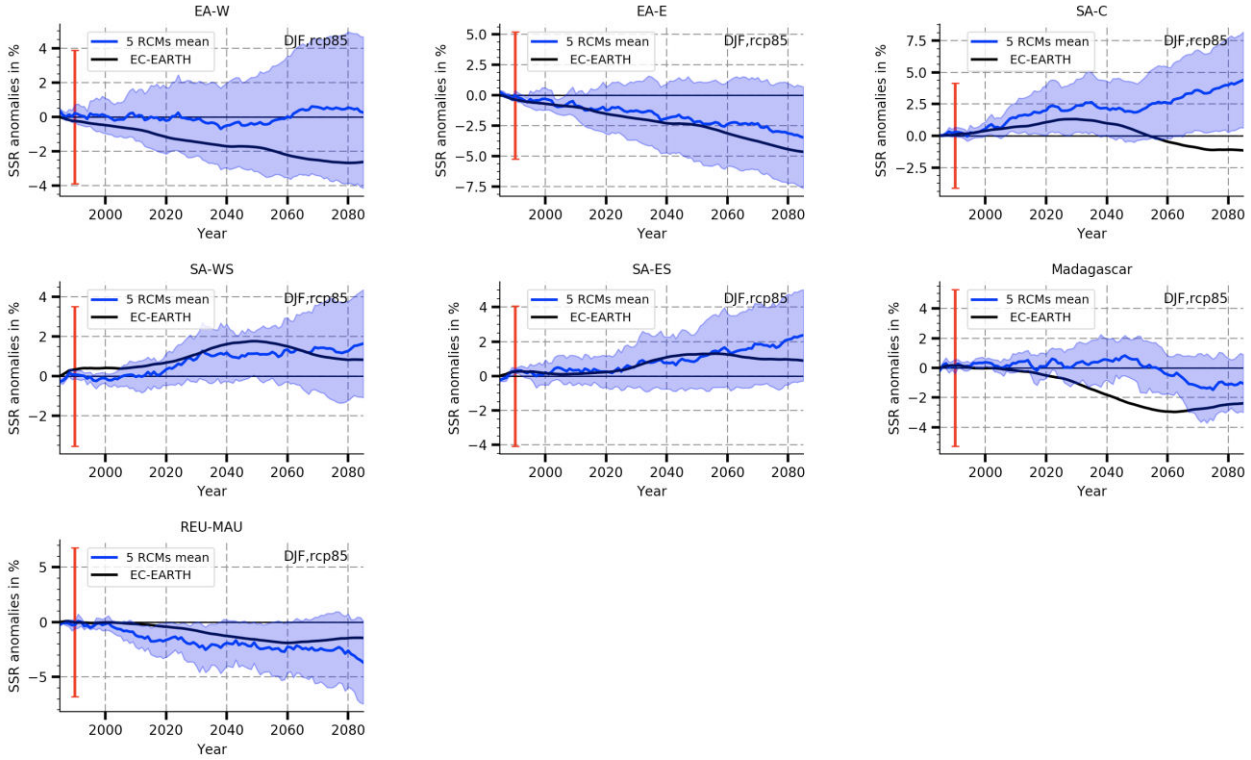

Fig. 3-19 Same as **Fig. 3-17**, but for EC-EARTH and its 5 forced RCMs (see **Table 2-1**).

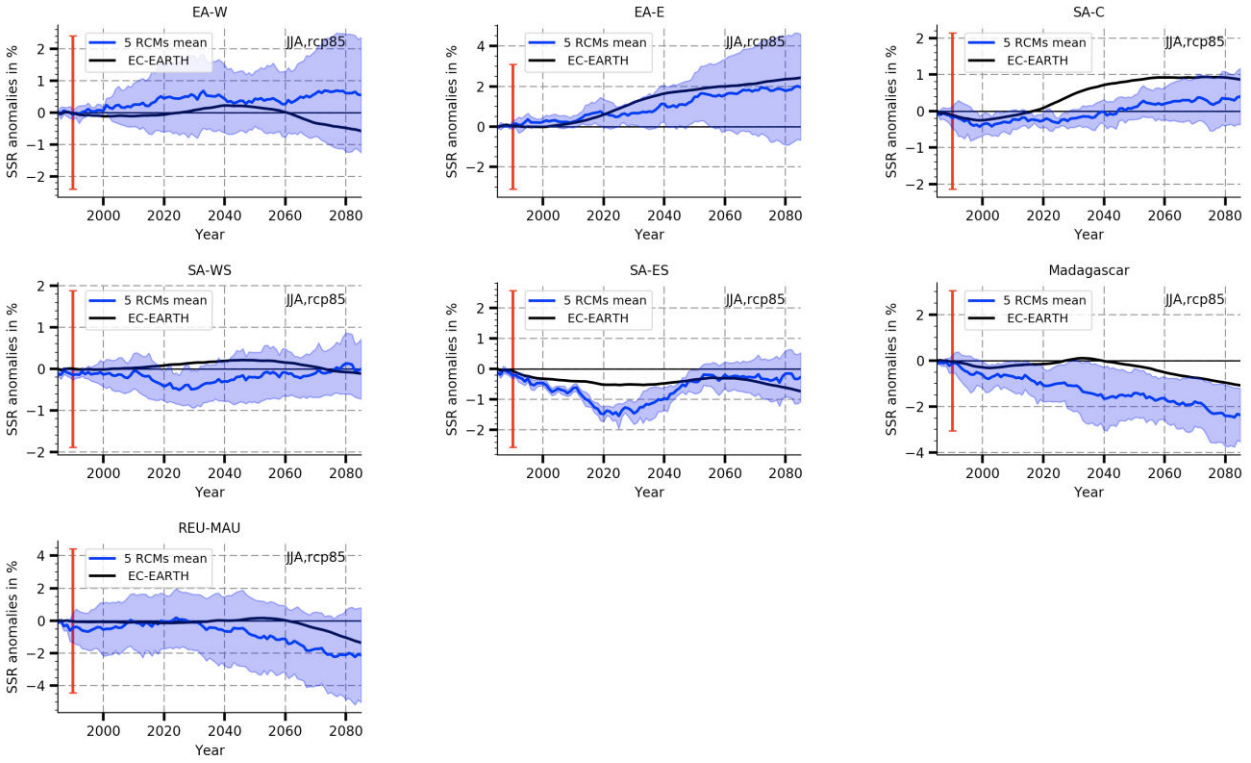

Fig. 3-20 Same as Fig. **3-19**, but for JJA.

3.2.4 Time-dependent seasonal changes in CLT from GCMs and RCMs

Model simulated seasonal CLT time-series are shown in **Fig. 3-21** and **Fig. 3-22** for DJF and JJA, respectively. It is evident that the RCMs simulate a CLT trend which is fairly consistent with their driving GCMs in the multimodel mean, which is in contrast with the findings in Europe (Bartók et al., 2016). The model-simulated CLT will decrease until 2100 in both global and regional model results, except in DJF over EA-E, with a constant flat anomaly. In the case of RCA4 driven by 10 GCMs as shown in **Fig. 3-23** and **Fig. 3-24**, the RCM ensemble shows a smaller spread than the forcing GCMs in many sub-regions for both seasons.

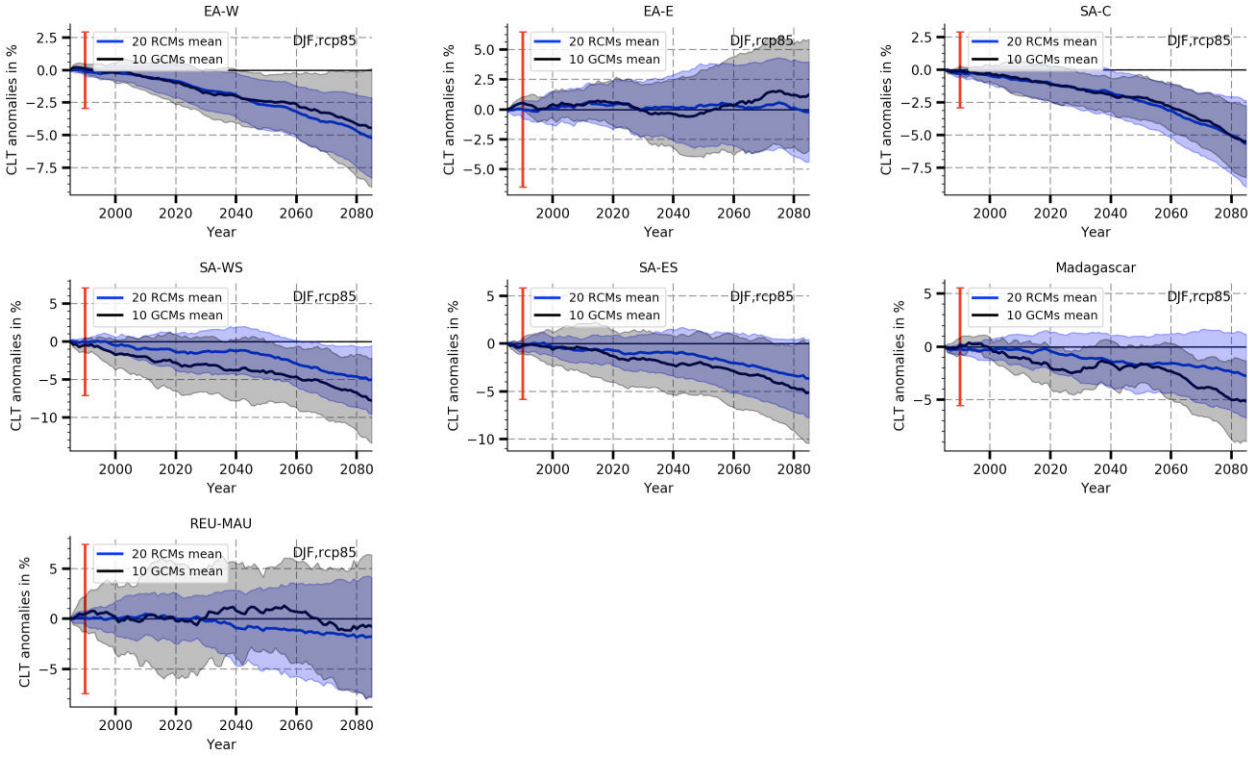

Fig. 3-21 Same as Fig. 3-15, but for CLT.

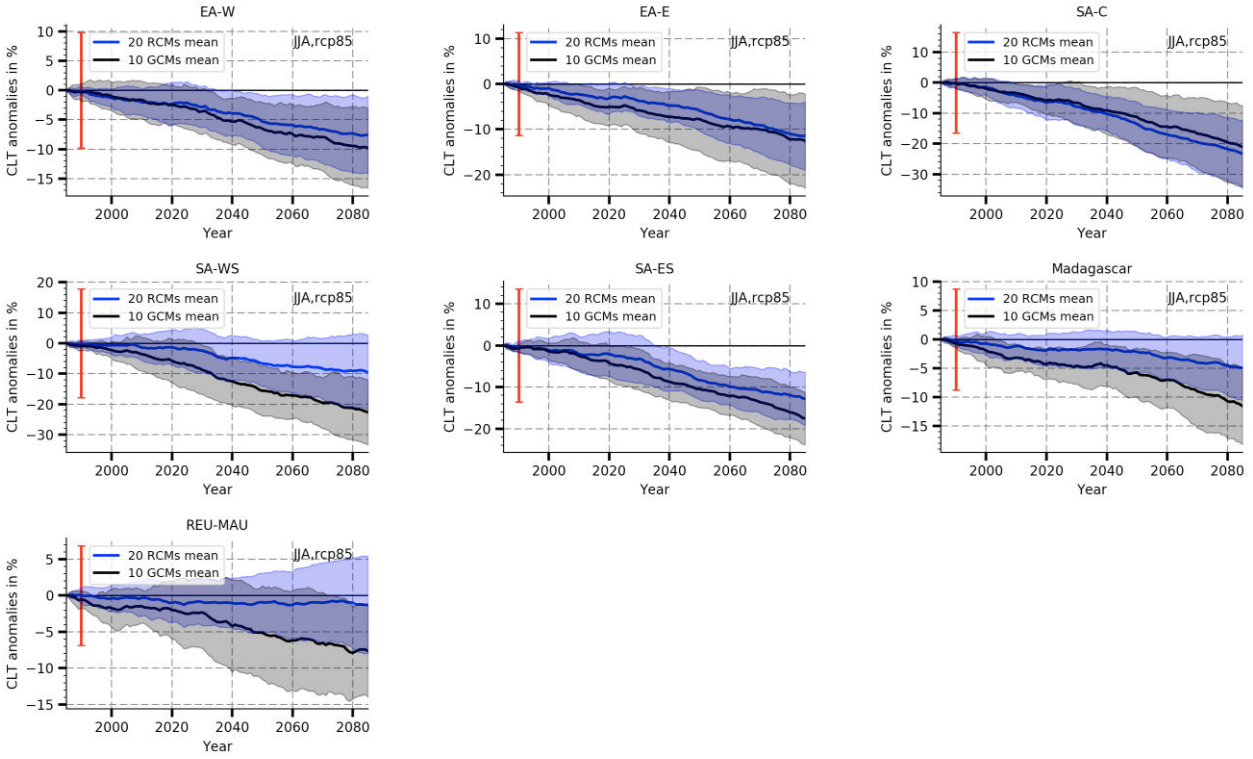

Fig. 3-22 Same as **Fig. 3-15**, but for CLT in JJA.

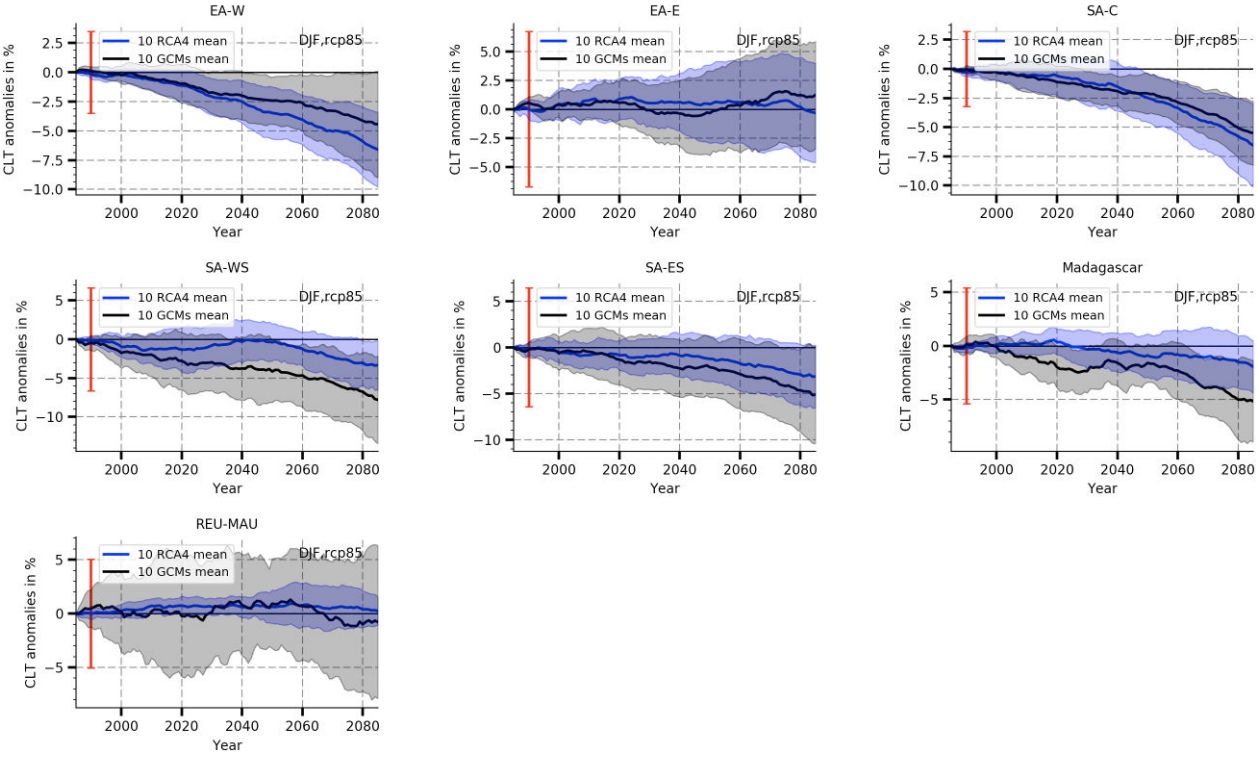

Fig. 3-23 Same as **Fig. 3-17**, but for CLT.

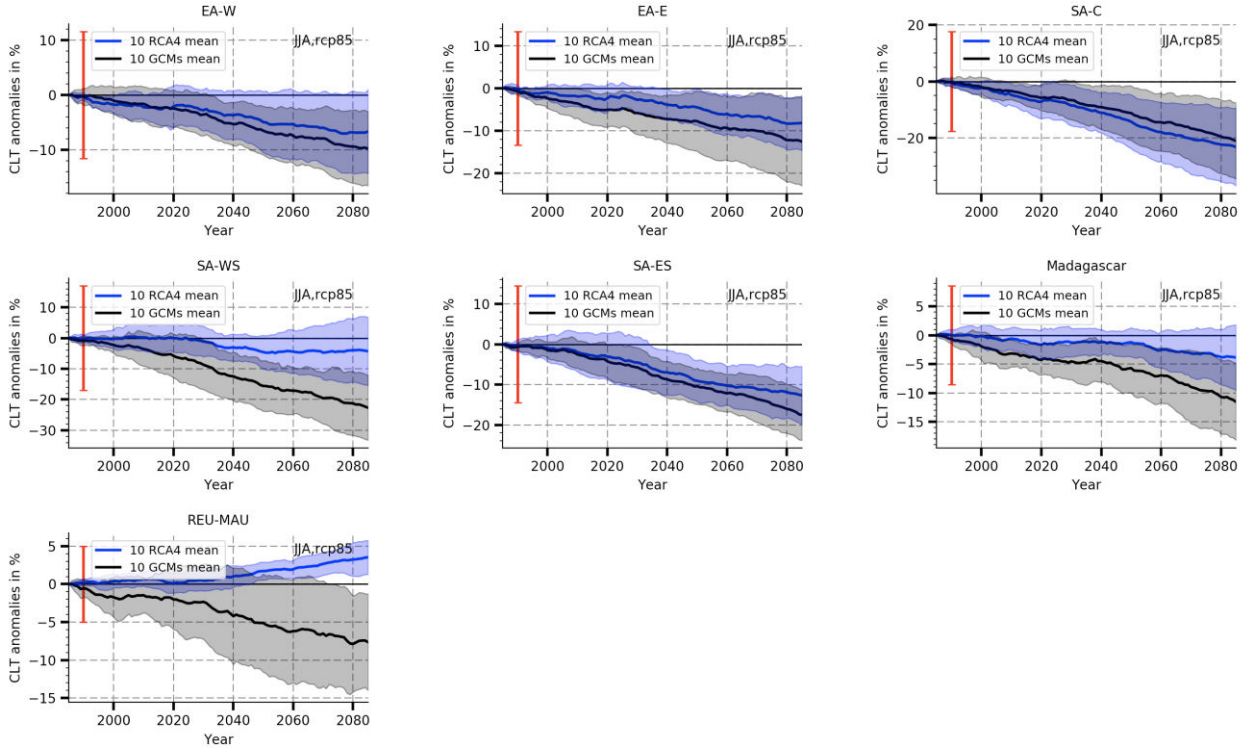

Fig. 3-24 Same as **Fig. 3-18** but for CLT.

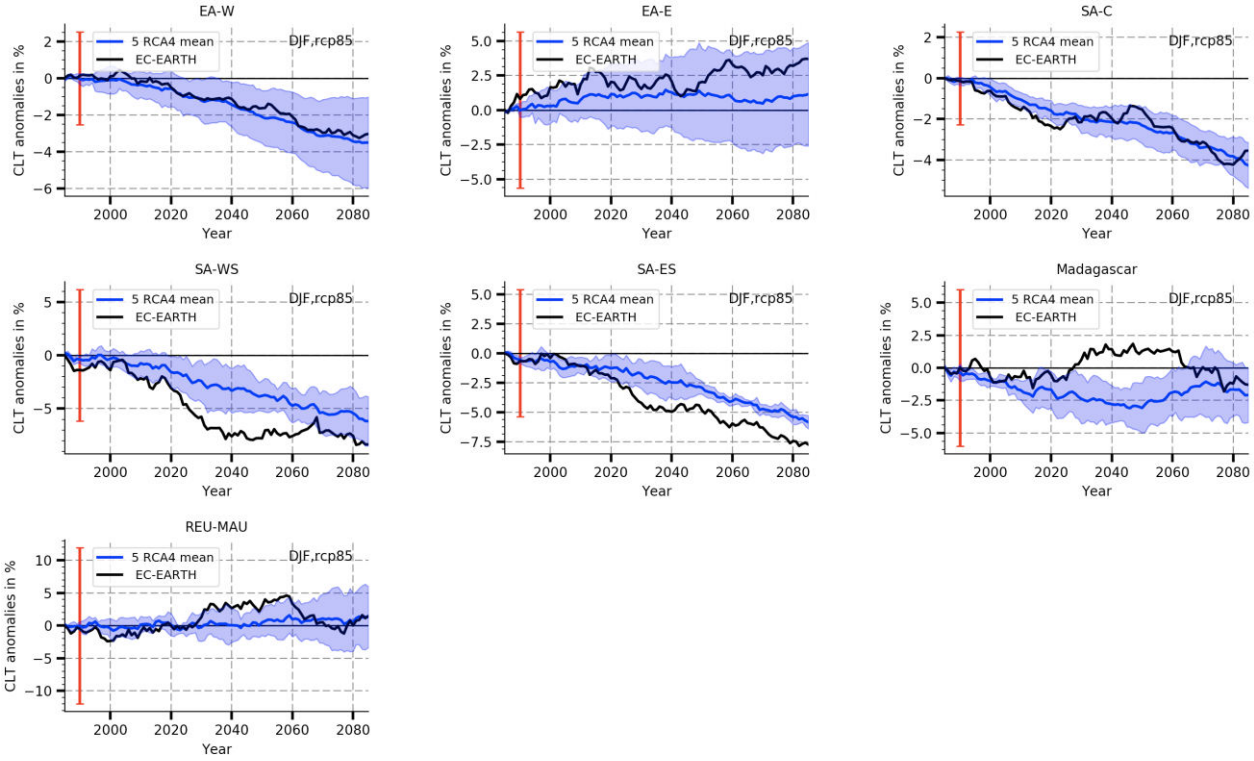

Fig. 3-25 Same as **Fig. 3-19**, but for CLT.

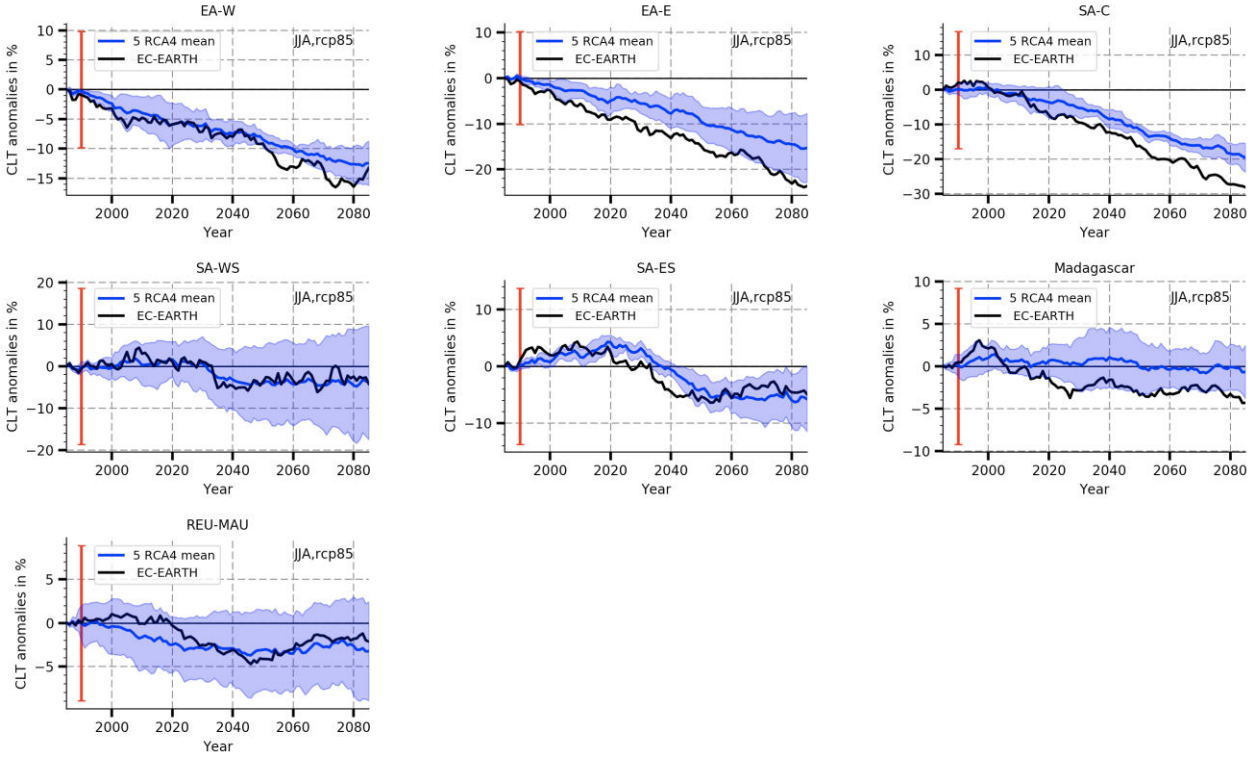

Fig. 3-26 Same as **Fig. 3-19**, but for CLT in JJA.

3.2.5 Uncertainty in SSR projections

In this section, different sources of uncertainty in the process of downscaling climate projections have been separated and further investigated with their relative contribution to the total uncertainty. The same analysis is taken parallelly with data from two different groups: Group I consists 7 experiments under 3 RCP scenarios (RCP2.6, RCP4.5 and RCP8.5); and Group II includes 20 experiments but under 2 RCP scenarios (RCP4.5 and RCP8.5). Please note that the uncertainty estimated from these limited datasets is unlikely to represent the full range of possibilities, as model uncertainty may be underestimated in Group I, and scenario uncertainty maybe underestimated in Group II.

Projections of SSR anomalies (DJF) from two data groups are shown in **Fig. 3-27**.The multi-model mean change is about -5 W/m^2 at 2100 in Group I. The same value in Group II is much smaller, of about -2 W/m^2, when removing RCP2.6 and including more models.

The total variance for the SSR projections from 2006 to the end of the 21st century is shown in the mid row of **Fig. 3-27**. Four uncertainty components are separated and demonstrated differently to show their relative importance to the total uncertainty. The internal variability estimated from Group I and II are similar, of about 8-10 in the unit of $(W/m^2)^2$. However, the scenario uncertainty and model uncertainty are quite different in terms of their absolute values and relative ratio to internal variability in these two data groups. For Group I, 1) the scenario uncertainty increases markedly after about 2040, and become comparable with model uncertainty (GCM + RCM uncertainty) around 2070, then reaching its top around 2090 of about 5 $(W/m^2)^2$, still smaller than internal variability, and decrease after that to 2100; 2) model continuously increase from 2040 to 2100, with the largest value about 5 $(W/m^2)^2$, where RCM uncertainty is similar to that of GCM; 3) total uncertainty is dominated by internal variability in the early projections until about 2070, and then become comparable to the sum of other components in the late century. On the other hand, for Group II, 1) scenario uncertainty remains almost unchanged with a very small value less than 1 $(W/m^2)^2$ through all the century; 2) model uncertainty grow dramatically during the entire century (2006 to 2100) from 1 to 12/27 $(W/m^2)^2$, for GCM/RCM; 3) model uncertainty dominates the total uncertainty after 2050, and RCM uncertainty becomes to the largest components after 2070.

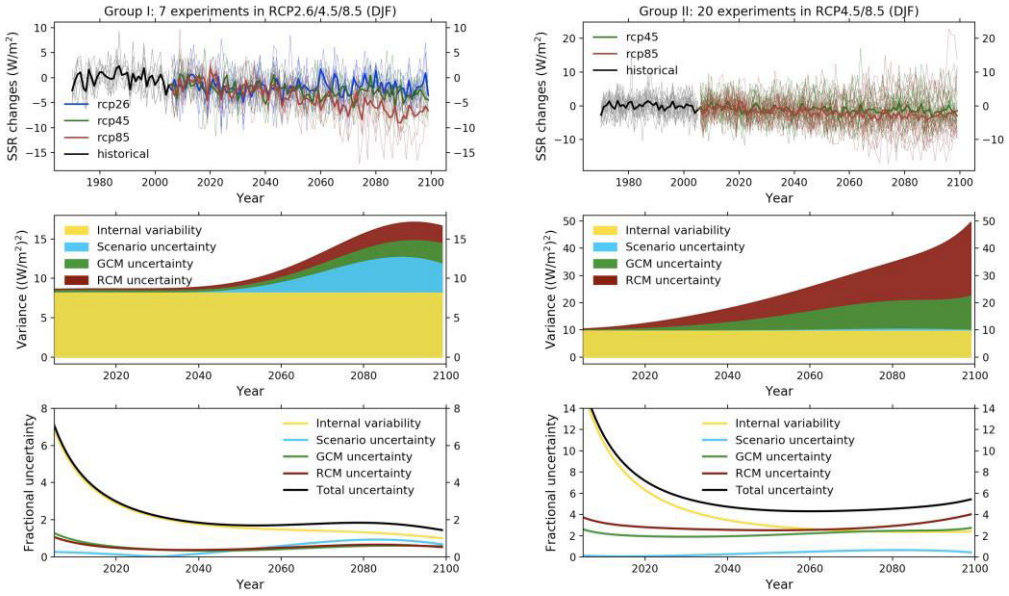

Fig. 3-27 Projections of annual mean SSR anomalies with respect to the reference period calculated as the mean value of the period from 1970 to 1999 using outputs of simulations listed in **Table 2-3** under RCP2.6, RCP4.5 and RCP8.5.

The 3rd row of **Fig. 3-27** shows the contributions of different uncertainty components to fractional uncertainty (to the SSR change in 90% confidence level) as a function of prediction lead-time. The fraction of total uncertainty falls very rapidly before 2050 with lead-time for Group I and II as the signal of climate change strengthens; and then increases slowly because of the increase of model/scenario uncertainty in the case of Group I or of model uncertainty in the case of Group II. Regardless of the data used, the total fractional uncertainty exhibits a minimum at a lead-time of around 2050, with value much large than 1, denoting the total uncertainty is much smaller than SSR change signal throughout the 21st century.

In JJA season (Fig. 3-28), the relative roles of different uncertainty components are similar to that in DJF. The fractional uncertainty is larger because of the lower SSR change projected in JJA.

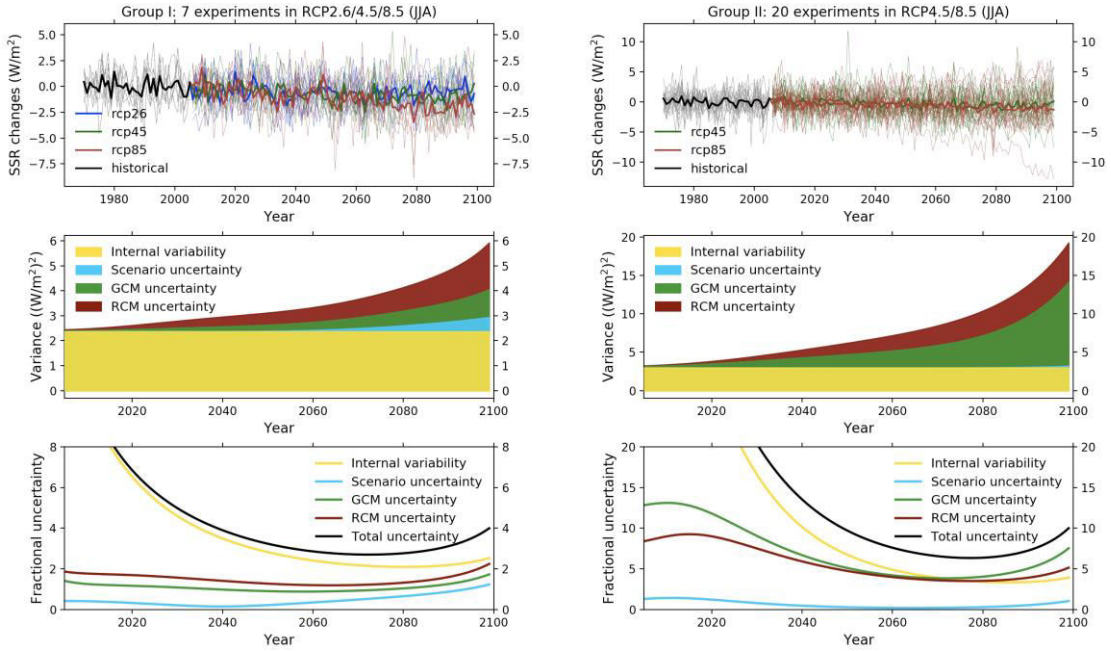

Fig. 3-28 The same as **Fig. 3-27** but for JJA.

3.3 Summary and conclusions of Chapter 3

In this chapter, outputs from CORDEX-Africa Over 100-year continuous outputs from 5 RCMs driven by 20 GCMs over southern Africa (SA) under RCP4.5 and RCP8.5 were analysed. Evaluation based on various references of this large ensemble has pointed out that: References from satellites retrievals and reanalyses compared well with ground-based measurements from GEBA, essentially located in the eastern part of SA, Madagascar and Reunion Island. An overall overestimation of about 10 W/m^2 was found.

GCMs generally overestimate SSR by about 1 W/m^2 (compensation of opposite biases over sub-regions of the domain) in austral summer and 7.5 W/m^2 in austral winter. RCMs ensemble mean shows underestimations of SSR in both seasons when driven by GCMs. This multi-model lower bias is dominated by the 4 simulations of CCLM4 and 10 of RCA4 models, where the negative biases are of up to -76 W/m^2 in summer and -32 W/m^2 in winter. RCMs ensemble has larger SSR uncertainty, because of large biases of particular RCM models (e.g. CCLM4 an RCA4) and not the internal variability as discussed above, compared with their driven GCMs ensemble.

For individual RCM model, the SSR fields seem rather insensitive to the different forcings including ERA-Interim and GCMs. Simulated SSR change patterns are overall consistent with that in CLT as the finding from RegCM4 simulations.

GCMs project, in their multimodel means, a statistically significant increase of SSR over Centre Southern Africa (SA-C) and a highly confident decreasing SSR over Eastern Equatorial Africa (EA-E) during the DJF season. RCMs simulate SSR with statistical confidence over the similar area with a little spatial extension compared with GCMs, but the changes are in higher amplitude.

Significant cloudiness decrease was found over continent of SA for GCMs and consistently shown in RCMs. As expected in 2100, the larger SSR changes are found in the RCP8.5 than in the RCP4.5 scenario, with about 2.5 W/m^2 enhanced changes in GCMs and about 5 W/m^2 in RCMs.

RCMs do not reduce obviously the uncertainty of SSR projections from their driving GCMs. The ratio of uncertainty over SSR changes is above 1 all the time along the 21st century. Internal variability gives the most importance contribution to the total uncertainty in the first few decade and then decrease as the signal of climate change strengthens over time. GCM/RCM and scenario uncertainties grow along time until they reach the same level of Internal variability at 2100.

Total uncertainty of dynamical downscaling projection conducted by RCMs is dominated by the Internal Variability of climate system before 2050, and after that the scenario uncertainty and

model uncertainty increase significantly and become comparable with or larger then that Internal Variability after about 2070.

* This Chapter was to be published on "Climate Dynamics" as two papers:

1) Tang, C., Morel, B., Wild, M., Pohl, B., Abiodun, B., & Bessafi, M. (2018). Numerical simulation of surface solar radiation over Southern Africa. Part 1: Evaluation of regional and global climate models. *Climate Dynamics*. doi:10.1007/s00382-018-4143-1

2) Tang, C., Morel, B., Wild, M., Pohl, B., Abiodun, B., Bessafi, M., & Lennard, C. (2018). Numerical simulation of surface solar radiation over Southern Africa. Part 2: Projections of regional and global climate models. *Climate Dynamics*.

4 Numerical simulation of Surface Solar Radiation: RegCM4

OUTLINE:

Following the strategy defined in Chapter 2, long-term downscaling simulations conducted with the Regional Climate Model (RCM) RegCM version 4 (RegCM4 or simply RegCM hereafter) under the most pessimistic scenario, namely RCP8.5 (R. Moss et al., 2008; R. H. Moss et al., 2010), are produced and examined in this Chapter, in order to identify the possible impacts of climate change on Solar Surface Radiation (SSR) at regional scales (~50 km) over Southern Africa and the South West Indian Ocean (SA-SWIO) up to the end of the 21st century. Considering the requirements of long-term temporal coverage for climate change analysis (reference?) and available computing power to run RegCM over a large domain such as SA, thus limiting the length of the simulations, a slice experiment has been designed covering three temporal windows: a) the present 1996-2005; b) the future 2046-2055 and 2090-2099, in line with the methodology of, e.g., Crook et al. (2011) and Gula and Peltier (2012).

Firstly, to better understand the model (RegCM4) performance in this particular region (SA-SWIO) with little experience, an ensemble of RegCM4 simulations forced by ERA-Interim reanalyses (ERAINT hereafter) with various model physical setups are conducted as a "sensitivity study". RCMs are very sensitive to the physical parameterizations that are chosen (Christensen et al., 2004). Optimal parameter settings for the model physics are estimated to archive (define?) the acceptable small bias of interesting variables, including Surface Downward Solar Radiation (RSDS same as SSR), Surface Air Temperature (TAS), total precipitation (PR), and Total Cloud Fraction (CLT). The results of sensitivity study are shown in Section **4.1.** Model validation is a crucial step to understand future projections. Reproduced climatic variables are carefully validated against references from satellite retrievals and reanalyses in Section **4.2.** Internal variability gives rise to large uncertainty in projections of future climate. Before analysing the downscaled future projections from GCMs using RegCM4, an experiment consisting of 20 ensembles of RegCM runs driven by ERA-Interim is taken to understand the behaviour of the model in response to the internal variability in Section **4.3**. Future projections and estimated electric energy potential are investigated in Section **4.4**. A brief summary is given at the end of the chapter.

4.1 Sensitivity study of RegCM4

As mentioned in the introduction of this Chapter and in **Chapter 2**, a sensitivity study to different physics parameterizations: radiative transfer, convection, planetary boundary layer (PBL) and land surface, is first conducted with RegCM4. A series of 40 simulations, which are summarized in Table 3.1, was thus performed. All these simulations are driven by ERA-Interim reanalysis, covering 2001 to 2005. Observations are easily accessed during this period. The seasonal climatology is analysed for variables: Surface Downward Solar Radiation (RSDS, same as SSR), Surface Air Temperature (TAS), total precipitation (PR), and Total Cloud Fraction (CLT). The physics settings of all the simulations are listed in Table 2-5 in section 2.3.2 of Chapter 2.

Summer mean of Surface Air Temperature (TAS), Precipitation (PR), Surface Downward Solar Radiation (RSDS same as Surface Solar Radiation short as SSR) and Total Cloud Cover (CLT) during 2001-2005 are shown in **Fig. 4-1** along with the statistics in **Fig. 4-2**.

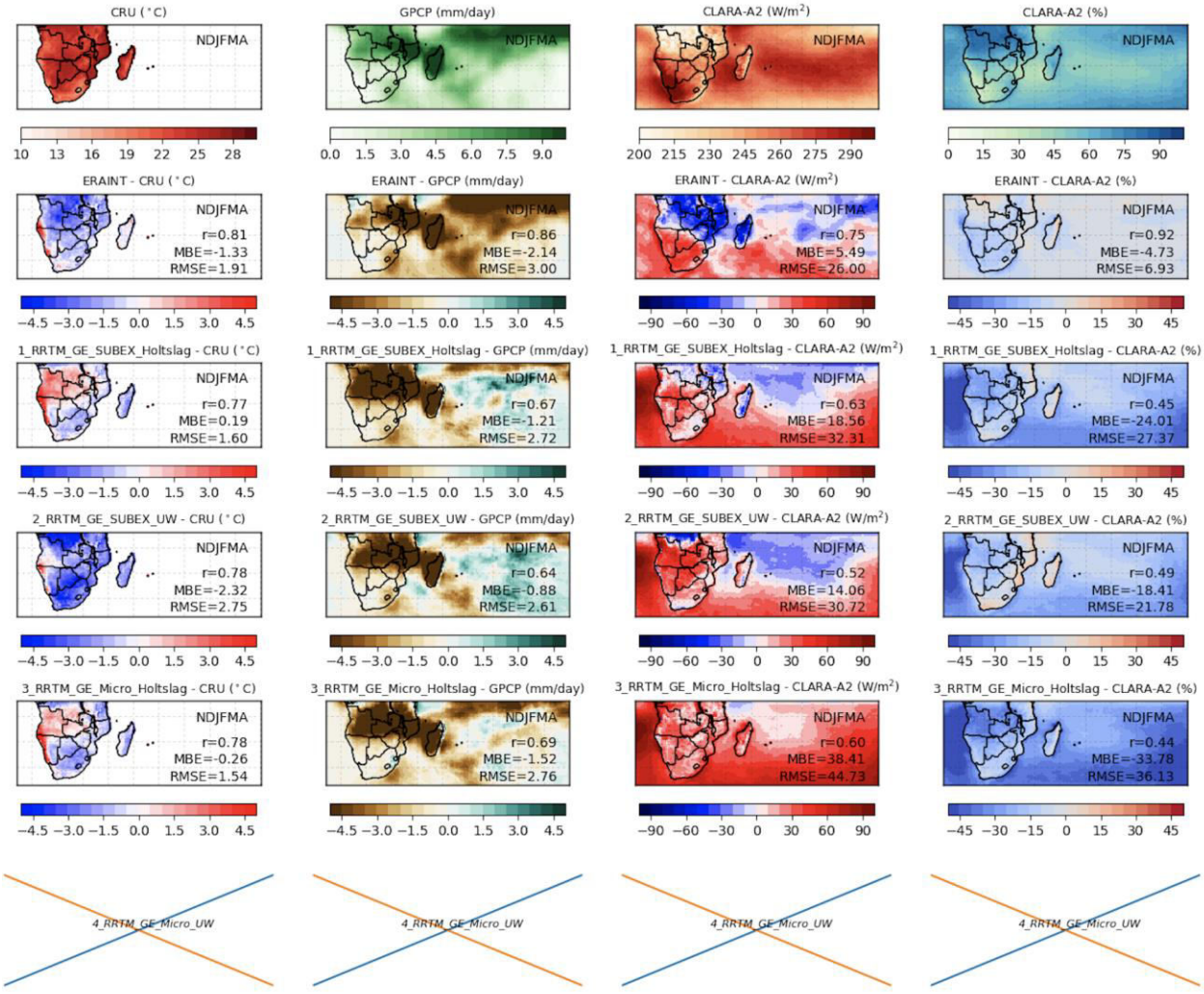

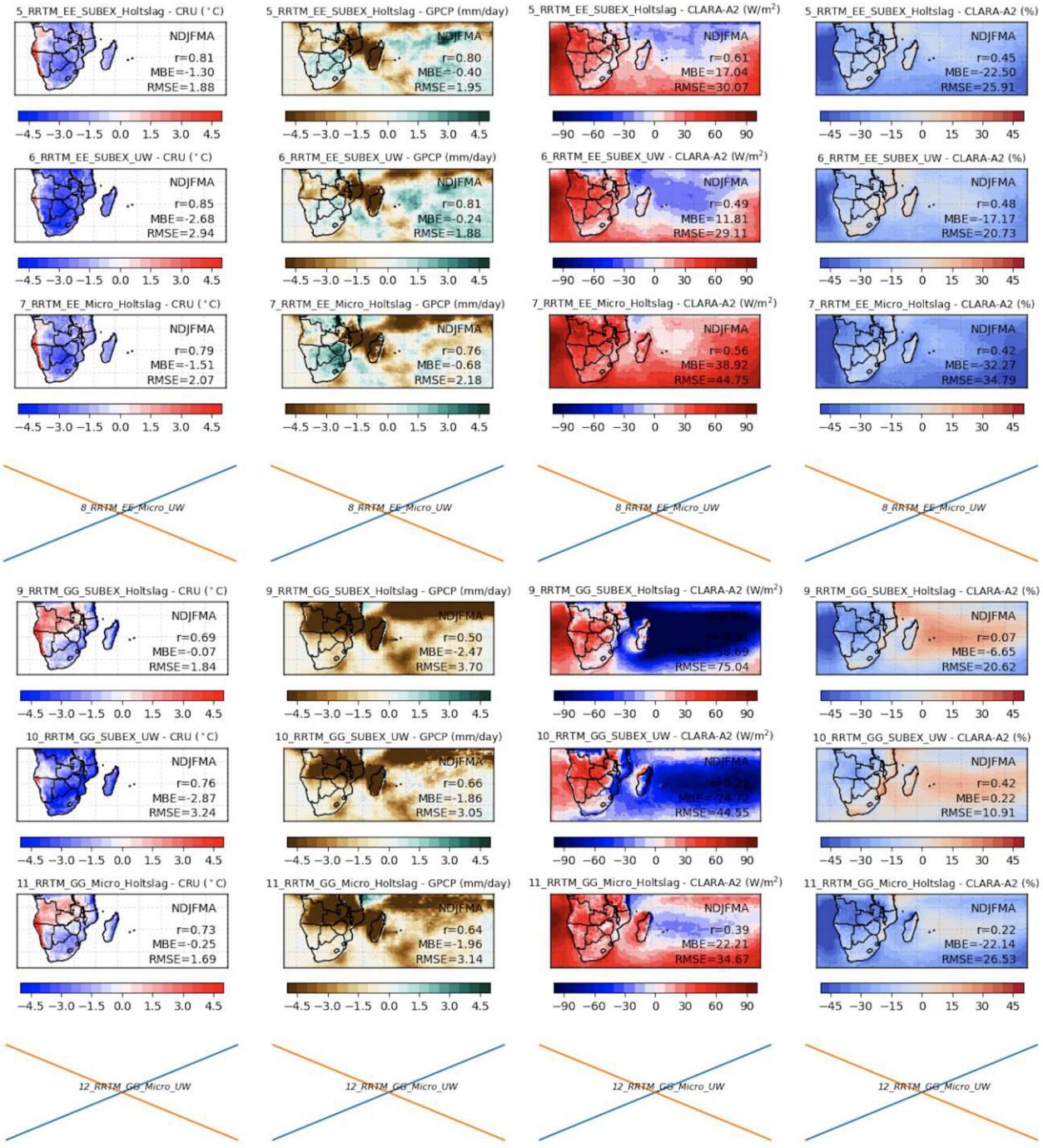
5_RRTM_EE_SUBEX_Holtslag - CRU (°C)
NDJFMA
r=0.81
MBE=-1.30
RMSE=1.88
−4.5 −3.0 −1.5 0.0 1.5 3.0 4.5
5_RRTM_EE_SUBEX_Holtslag - GPCP (mm/day)
NDJFMA
r=0.80
MBE=-0.40
RMSE=1.95
−4.5 −3.0 −1.5 0.0 1.5 3.0 4.5
5_RRTM_EE_SUBEX_Holtslag - CLARA-A2 (W/m²)
NDJFMA
r=0.61
MBE=17.04
RMSE=30.07
−90 −60 −30 0 30 60 90
5_RRTM_EE_SUBEX_Holtslag - CLARA-A2 (%)
NDJFMA
r=0.45
MBE=-22.50
RMSE=25.91
−45 −30 −15 0 15 30 45
6_RRTM_EE_SUBEX_UW - CRU (°C)
NDJFMA
r=0.85
MBE=-2.68
RMSE=2.94
−4.5 −3.0 −1.5 0.0 1.5 3.0 4.5
6_RRTM_EE_SUBEX_UW - GPCP (mm/day)
NDJFMA
r=0.81
MBE=-0.24
RMSE=1.88
−4.5 −3.0 −1.5 0.0 1.5 3.0 4.5
6_RRTM_EE_SUBEX_UW - CLARA-A2 (W/m²)
NDJFMA
r=0.49
MBE=11.81
RMSE=29.11
−90 −60 −30 0 30 60 90
6_RRTM_EE_SUBEX_UW - CLARA-A2 (%)
NDJFMA
r=0.48
MBE=-17.17
RMSE=20.73
−45 −30 −15 0 15 30 45
7_RRTM_EE_Micro_Holtslag - CRU (°C)
NDJFMA
r=0.79
MBE=-1.51
RMSE=2.07
−4.5 −3.0 −1.5 0.0 1.5 3.0 4.5
7_RRTM_EE_Micro_Holtslag - GPCP (mm/day)
NDJFMA
r=0.76
MBE=-0.68
RMSE=2.18
−4.5 −3.0 −1.5 0.0 1.5 3.0 4.5
7_RRTM_EE_Micro_Holtslag - CLARA-A2 (W/m²)
NDJFMA
r=0.56
MBE=38.92
RMSE=44.75
−90 −60 −30 0 30 60 90
7_RRTM_EE_Micro_Holtslag - CLARA-A2 (%)
NDJFMA
r=0.42
MBE=-32.27
RMSE=34.79
−45 −30 −15 0 15 30 45
8_RRTM_EE_Micro_UW
8_RRTM_EE_Micro_UW
8_RRTM_EE_Micro_UW
8_RRTM_EE_Micro_UW
9_RRTM_GG_SUBEX_Holtslag - CRU (°C)
NDJFMA
r=0.69
MBE=-0.07
RMSE=1.84
−4.5 −3.0 −1.5 0.0 1.5 3.0 4.5
9_RRTM_GG_SUBEX_Holtslag - GPCP (mm/day)
NDJFMA
r=0.50
MBE=-2.47
RMSE=3.70
−4.5 −3.0 −1.5 0.0 1.5 3.0 4.5
9_RRTM_GG_SUBEX_Holtslag - CLARA-A2 (W/m²)
RMSE=75.04
−90 −60 −30 0 30 60 90
9_RRTM_GG_SUBEX_Holtslag - CLARA-A2 (%)
NDJFMA
r=0.07
MBE=-6.65
RMSE=20.62
−45 −30 −15 0 15 30 45
10_RRTM_GG_SUBEX_UW - CRU (°C)
NDJFMA
r=0.76
MBE=-2.87
RMSE=3.24
−4.5 −3.0 −1.5 0.0 1.5 3.0 4.5
10_RRTM_GG_SUBEX_UW - GPCP (mm/day)
NDJFMA
r=0.66
MBE=-1.86
RMSE=3.05
−4.5 −3.0 −1.5 0.0 1.5 3.0 4.5
10_RRTM_GG_SUBEX_UW - CLARA-A2 (W/m²)
RMSE=44.55
−90 −60 −30 0 30 60 90
10_RRTM_GG_SUBEX_UW - CLARA-A2 (%)
NDJFMA
r=0.42
MBE=0.22
RMSE=10.91
−45 −30 −15 0 15 30 45
11_RRTM_GG_Micro_Holtslag - CRU (°C)
NDJFMA
r=0.73
MBE=-0.25
RMSE=1.69
−4.5 −3.0 −1.5 0.0 1.5 3.0 4.5
11_RRTM_GG_Micro_Holtslag - GPCP (mm/day)
NDJFMA
r=0.64
MBE=-1.96
RMSE=3.14
−4.5 −3.0 −1.5 0.0 1.5 3.0 4.5
11_RRTM_GG_Micro_Holtslag - CLARA-A2 (W/m²)
NDJFMA
r=0.39
MBE=22.21
RMSE=34.67
−90 −60 −30 0 30 60 90
11_RRTM_GG_Micro_Holtslag - CLARA-A2 (%)
NDJFMA
r=0.22
MBE=-22.14
RMSE=26.53
−45 −30 −15 0 15 30 45
12_RRTM_GG_Micro_UW
12_RRTM_GG_Micro_UW
12_RRTM_GG_Micro_UW
12_RRTM_GG_Micro_UW

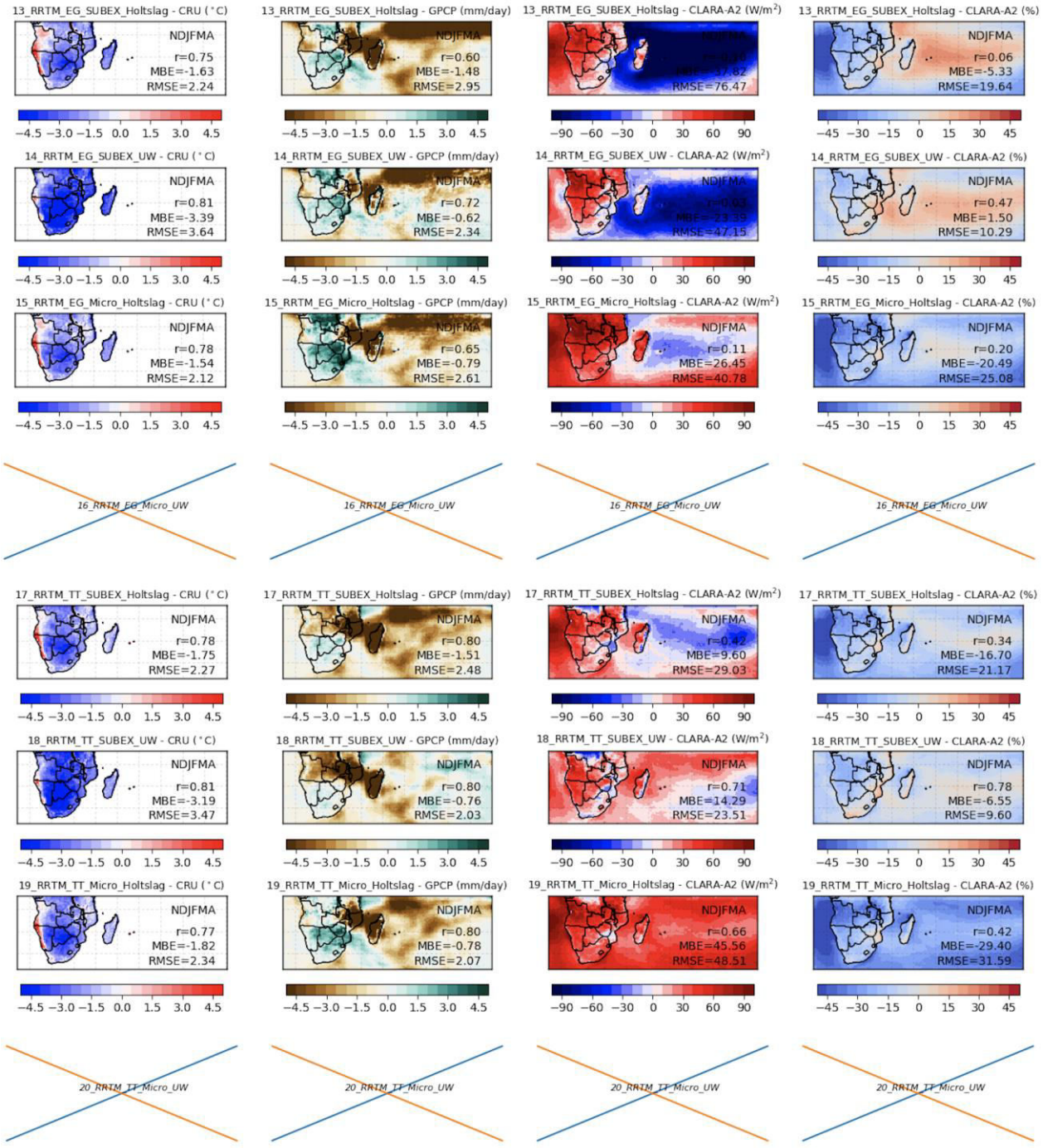
13_RRTM_EG_SUBEX_Holtslag - CRU (°C)
NDJFMA
r=0.75
MBE=-1.63
RMSE=2.24
13_RRTM_EG_SUBEX_Holtslag - GPCP (mm/day)
NDJFMA
r=0.60
MBE=-1.48
RMSE=2.95
13_RRTM_EG_SUBEX_Holtslag - CLARA-A2 (W/m²)
RMSE=76.47
13_RRTM_EG_SUBEX_Holtslag - CLARA-A2 (%)
NDJFMA
r=0.06
MBE=-5.33
RMSE=19.64
14_RRTM_EG_SUBEX_UW - CRU (°C)
NDJFMA
r=0.81
MBE=-3.39
RMSE=3.64
14_RRTM_EG_SUBEX_UW - GPCP (mm/day)
NDJFMA
r=0.72
MBE=-0.62
RMSE=2.34
14_RRTM_EG_SUBEX_UW - CLARA-A2 (W/m²)
RMSE=47.15
14_RRTM_EG_SUBEX_UW - CLARA-A2 (%)
NDJFMA
r=0.47
MBE=1.50
RMSE=10.29
15_RRTM_EG_Micro_Holtslag - CRU (°C)
NDJFMA
r=0.78
MBE=-1.54
RMSE=2.12
15_RRTM_EG_Micro_Holtslag - GPCP (mm/day)
NDJFMA
r=0.65
MBE=-0.79
RMSE=2.61
15_RRTM_EG_Micro_Holtslag - CLARA-A2 (W/m²)
NDJFMA
r=0.11
MBE=26.45
RMSE=40.78
15_RRTM_EG_Micro_Holtslag - CLARA-A2 (%)
NDJFMA
r=0.20
MBE=-20.49
RMSE=25.08
16_RRTM_EG_Micro_UW
16_RRTM_EG_Micro_UW
16_RRTM_EG_Micro_UW
16_RRTM_EG_Micro_UW
17_RRTM_TT_SUBEX_Holtslag - CRU (°C)
NDJFMA
r=0.78
MBE=-1.75
RMSE=2.27
17_RRTM_TT_SUBEX_Holtslag - GPCP (mm/day)
NDJFMA
r=0.80
MBE=-1.51
RMSE=2.48
17_RRTM_TT_SUBEX_Holtslag - CLARA-A2 (W/m²)
NDJFMA
r=0.42
MBE=9.60
RMSE=29.03
17_RRTM_TT_SUBEX_Holtslag - CLARA-A2 (%)
NDJFMA
r=0.34
MBE=-16.70
RMSE=21.17
18_RRTM_TT_SUBEX_UW - CRU (°C)
NDJFMA
r=0.81
MBE=-3.19
RMSE=3.47
18_RRTM_TT_SUBEX_UW - GPCP (mm/day)
NDJFMA
r=0.80
MBE=-0.76
RMSE=2.03
18_RRTM_TT_SUBEX_UW - CLARA-A2 (W/m²)
NDJFMA
r=0.71
MBE=14.29
RMSE=23.51
18_RRTM_TT_SUBEX_UW - CLARA-A2 (%)
NDJFMA
r=0.78
MBE=-6.55
RMSE=9.60
19_RRTM_TT_Micro_Holtslag - CRU (°C)
NDJFMA
r=0.77
MBE=-1.82
RMSE=2.34
19_RRTM_TT_Micro_Holtslag - GPCP (mm/day)
NDJFMA
r=0.80
MBE=-0.78
RMSE=2.07
19_RRTM_TT_Micro_Holtslag - CLARA-A2 (W/m²)
NDJFMA
r=0.66
MBE=45.56
RMSE=48.51
19_RRTM_TT_Micro_Holtslag - CLARA-A2 (%)
NDJFMA
r=0.42
MBE=-29.40
RMSE=31.59
20_RRTM_TT_Micro_UW
20_RRTM_TT_Micro_UW
20_RRTM_TT_Micro_UW
20_RRTM_TT_Micro_UW

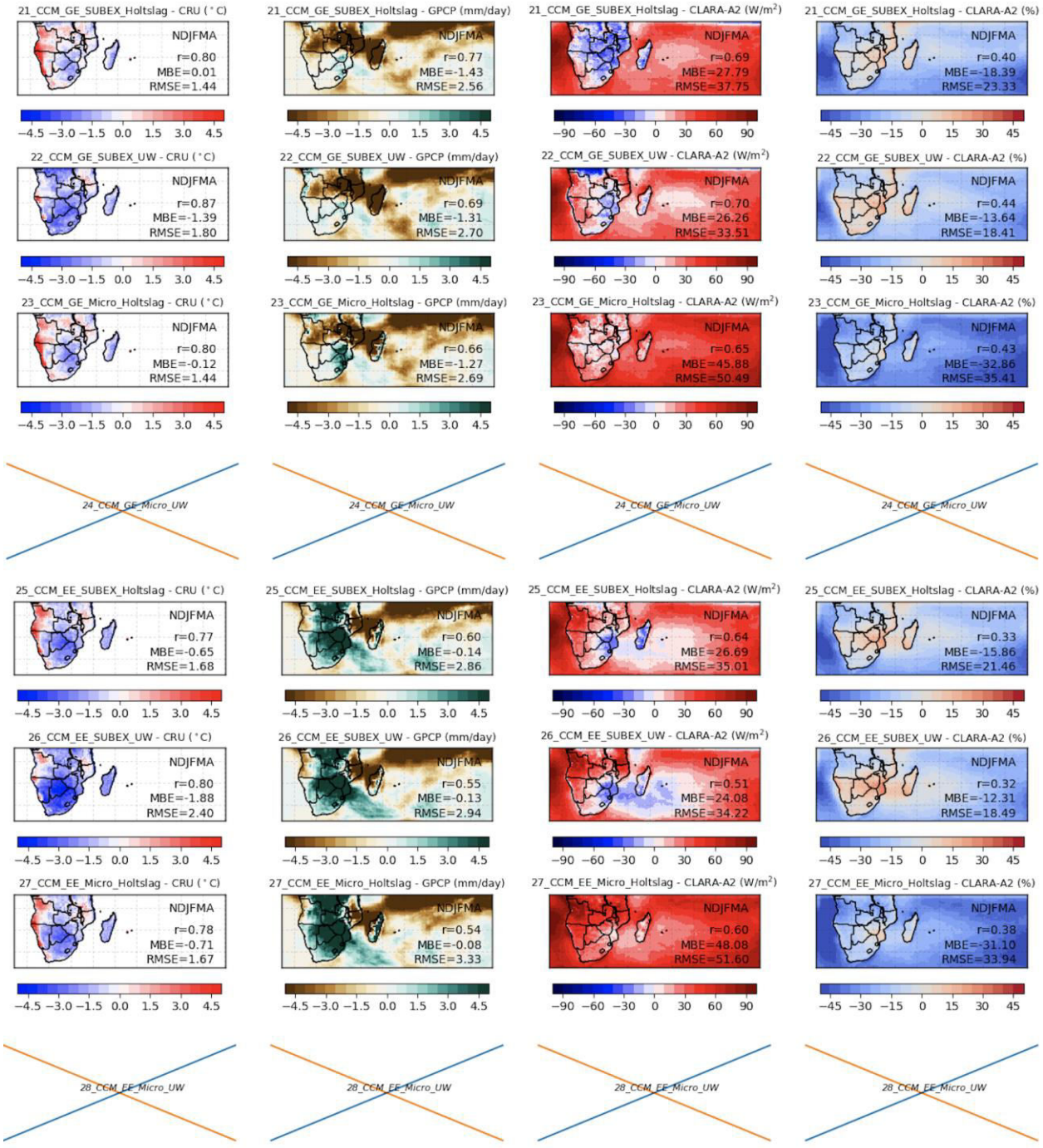
21_CCM_GE_SUBEX_Holtslag - CRU (°C)
NDJFMA
r=0.80
MBE=0.01
RMSE=1.44
21_CCM_GE_SUBEX_Holtslag - GPCP (mm/day)
NDJFMA
r=0.77
MBE=-1.43
RMSE=2.56
21_CCM_GE_SUBEX_Holtslag - CLARA-A2 (W/m²)
NDJFMA
r=0.69
MBE=27.79
RMSE=37.75
21_CCM_GE_SUBEX_Holtslag - CLARA-A2 (%)
NDJFMA
r=0.40
MBE=-18.39
RMSE=23.33
22_CCM_GE_SUBEX_UW - CRU (°C)
NDJFMA
r=0.87
MBE=-1.39
RMSE=1.80
22_CCM_GE_SUBEX_UW - GPCP (mm/day)
NDJFMA
r=0.69
MBE=-1.31
RMSE=2.70
22_CCM_GE_SUBEX_UW - CLARA-A2 (W/m²)
NDJFMA
r=0.70
MBE=26.26
RMSE=33.51
22_CCM_GE_SUBEX_UW - CLARA-A2 (%)
NDJFMA
r=0.44
MBE=-13.64
RMSE=18.41
23_CCM_GE_Micro_Holtslag - CRU (°C)
NDJFMA
r=0.80
MBE=-0.12
RMSE=1.44
23_CCM_GE_Micro_Holtslag - GPCP (mm/day)
NDJFMA
r=0.66
MBE=-1.27
RMSE=2.69
23_CCM_GE_Micro_Holtslag - CLARA-A2 (W/m²)
NDJFMA
r=0.65
MBE=45.88
RMSE=50.49
23_CCM_GE_Micro_Holtslag - CLARA-A2 (%)
NDJFMA
r=0.43
MBE=-32.86
RMSE=35.41
24_CCM_GE_Micro_UW
24_CCM_GE_Micro_UW
24_CCM_GE_Micro_UW
24_CCM_GE_Micro_UW
25_CCM_EE_SUBEX_Holtslag - CRU (°C)
NDJFMA
r=0.77
MBE=-0.65
RMSE=1.68
25_CCM_EE_SUBEX_Holtslag - GPCP (mm/day)
NDJFMA
r=0.60
MBE=-0.14
RMSE=2.86
25_CCM_EE_SUBEX_Holtslag - CLARA-A2 (W/m²)
NDJFMA
r=0.64
MBE=26.69
RMSE=35.01
25_CCM_EE_SUBEX_Holtslag - CLARA-A2 (%)
NDJFMA
r=0.33
MBE=-15.86
RMSE=21.46
26_CCM_EE_SUBEX_UW - CRU (°C)
NDJFMA
r=0.80
MBE=-1.88
RMSE=2.40
26_CCM_EE_SUBEX_UW - GPCP (mm/day)
NDJFMA
r=0.55
MBE=-0.13
RMSE=2.94
26_CCM_EE_SUBEX_UW - CLARA-A2 (W/m²)
NDJFMA
r=0.51
MBE=24.08
RMSE=34.22
26_CCM_EE_SUBEX_UW - CLARA-A2 (%)
NDJFMA
r=0.32
MBE=-12.31
RMSE=18.49
27_CCM_EE_Micro_Holtslag - CRU (°C)
NDJFMA
r=0.78
MBE=-0.71
RMSE=1.67
27_CCM_EE_Micro_Holtslag - GPCP (mm/day)
NDJFMA
r=0.54
MBE=-0.08
RMSE=3.33
27_CCM_EE_Micro_Holtslag - CLARA-A2 (W/m²)
NDJFMA
r=0.60
MBE=48.08
RMSE=51.60
27_CCM_EE_Micro_Holtslag - CLARA-A2 (%)
NDJFMA
r=0.38
MBE=-31.10
RMSE=33.94
28_CCM_EE_Micro_UW
28_CCM_EE_Micro_UW
28_CCM_EE_Micro_UW
28_CCM_EE_Micro_UW

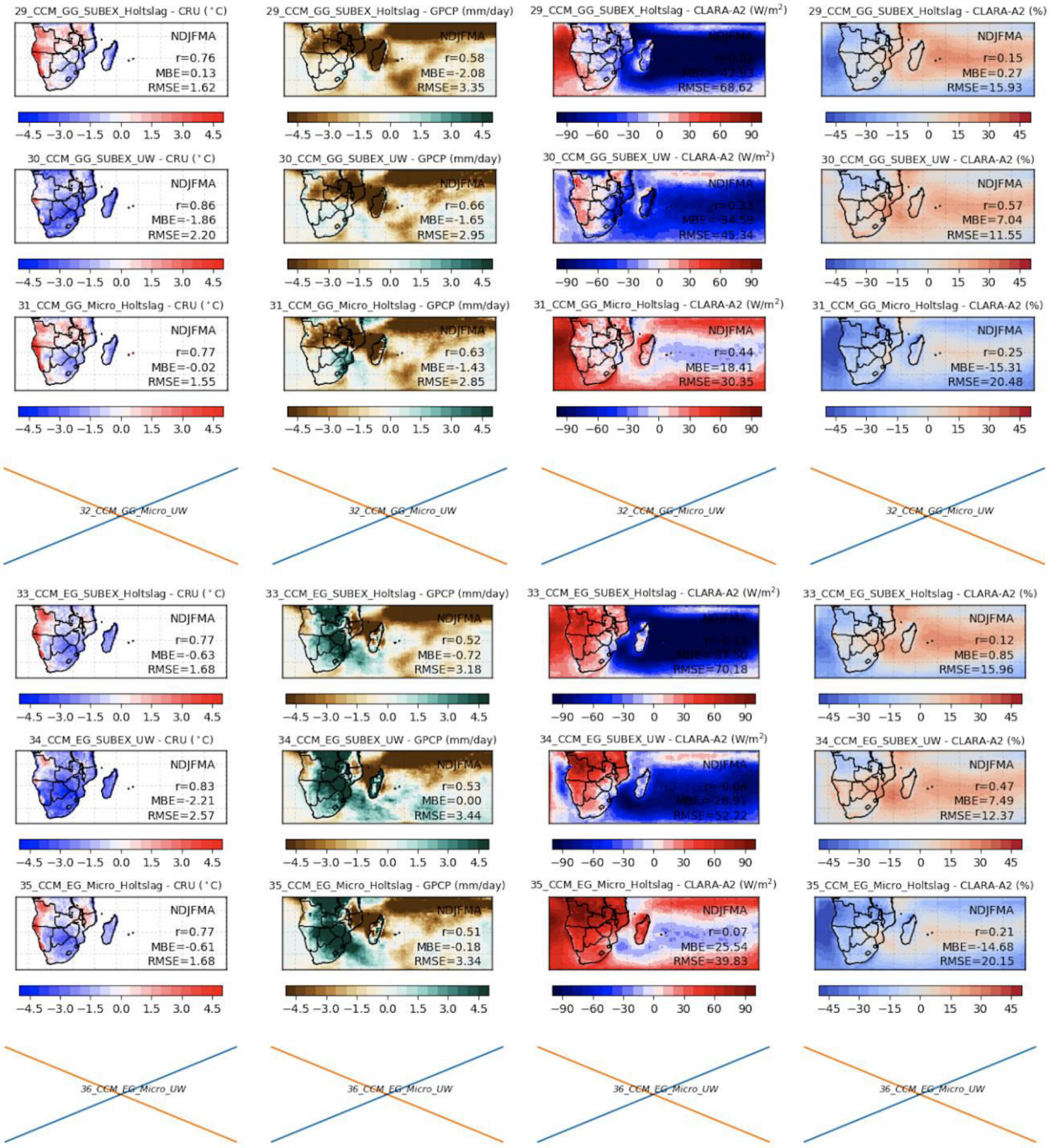
29_CCM_GG_SUBEX_Holtslag - CRU (°C)
NDJFMA
r=0.76
MBE=0.13
RMSE=1.62
29_CCM_GG_SUBEX_Holtslag - GPCP (mm/day)
NDJFMA
r=0.58
MBE=-2.08
RMSE=3.35
29_CCM_GG_SUBEX_Holtslag - CLARA-A2 (W/m²)
RMSE=68.62
29_CCM_GG_SUBEX_Holtslag - CLARA-A2 (%)
NDJFMA
r=0.15
MBE=0.27
RMSE=15.93
30_CCM_GG_SUBEX_UW - CRU (°C)
NDJFMA
r=0.86
MBE=-1.86
RMSE=2.20
30_CCM_GG_SUBEX_UW - GPCP (mm/day)
NDJFMA
r=0.66
MBE=-1.65
RMSE=2.95
30_CCM_GG_SUBEX_UW - CLARA-A2 (W/m²)
RMSE=45.34
30_CCM_GG_SUBEX_UW - CLARA-A2 (%)
NDJFMA
r=0.57
MBE=7.04
RMSE=11.55
31_CCM_GG_Micro_Holtslag - CRU (°C)
NDJFMA
r=0.77
MBE=-0.02
RMSE=1.55
31_CCM_GG_Micro_Holtslag - GPCP (mm/day)
NDJFMA
r=0.63
MBE=-1.43
RMSE=2.85
31_CCM_GG_Micro_Holtslag - CLARA-A2 (W/m²)
NDJFMA
r=0.44
MBE=18.41
RMSE=30.35
31_CCM_GG_Micro_Holtslag - CLARA-A2 (%)
NDJFMA
r=0.25
MBE=-15.31
RMSE=20.48
32_CCM_GG_Micro_UW
32_CCM_GG_Micro_UW
32_CCM_GG_Micro_UW
32_CCM_GG_Micro_UW
33_CCM_EG_SUBEX_Holtslag - CRU (°C)
NDJFMA
r=0.77
MBE=-0.63
RMSE=1.68
33_CCM_EG_SUBEX_Holtslag - GPCP (mm/day)
NDJFMA
r=0.52
MBE=-0.72
RMSE=3.18
33_CCM_EG_SUBEX_Holtslag - CLARA-A2 (W/m²)
RMSE=70.18
33_CCM_EG_SUBEX_Holtslag - CLARA-A2 (%)
NDJFMA
r=0.12
MBE=0.85
RMSE=15.96
34_CCM_EG_SUBEX_UW - CRU (°C)
NDJFMA
r=0.83
MBE=-2.21
RMSE=2.57
34_CCM_EG_SUBEX_UW - GPCP (mm/day)
NDJFMA
r=0.53
MBE=0.00
RMSE=3.44
34_CCM_EG_SUBEX_UW - CLARA-A2 (W/m²)
RMSE=52.22
34_CCM_EG_SUBEX_UW - CLARA-A2 (%)
NDJFMA
r=0.47
MBE=7.49
RMSE=12.37
35_CCM_EG_Micro_Holtslag - CRU (°C)
NDJFMA
r=0.77
MBE=-0.61
RMSE=1.68
35_CCM_EG_Micro_Holtslag - GPCP (mm/day)
NDJFMA
r=0.51
MBE=-0.18
RMSE=3.34
35_CCM_EG_Micro_Holtslag - CLARA-A2 (W/m²)
NDJFMA
r=0.07
MBE=25.54
RMSE=39.83
35_CCM_EG_Micro_Holtslag - CLARA-A2 (%)
NDJFMA
r=0.21
MBE=-14.68
RMSE=20.15
36_CCM_EG_Micro_UW
36_CCM_EG_Micro_UW
36_CCM_EG_Micro_UW
36_CCM_EG_Micro_UW

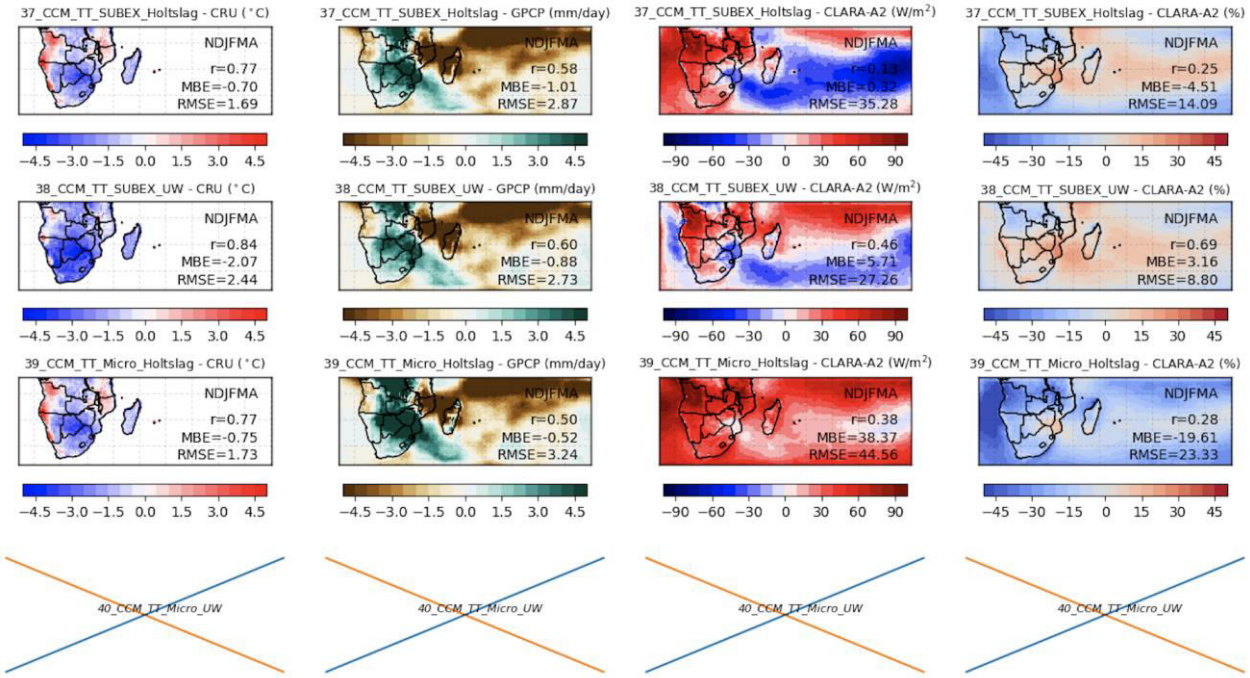

Fig. 4-1 Seasonal (NDJFMA) mean of TAS (1st column), PR (2nd column), SSR (3rd column), and CLT (4th column) from observations (top row) and the differences with ERA-Interim reanalyses (2nd row), and RegCM4 forced by ERA-Interim with different physical options (indicated in the title of each subplot, see section 2.3.2. from 3th to the last row). All the simulations use A buffer zone of 4 degrees has been removed.

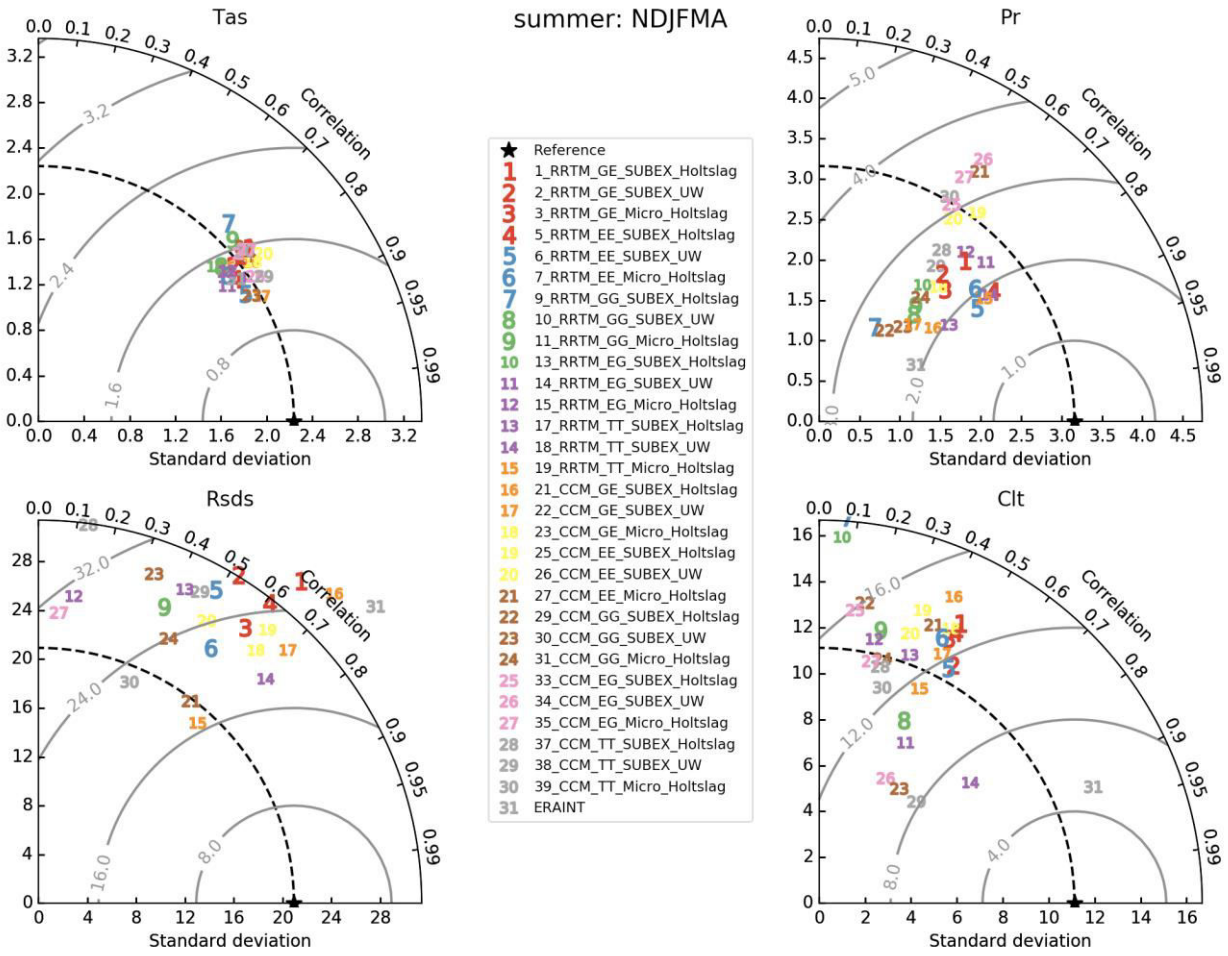

Fig. 4-2 Seasonal (austral summer) Standard Deviation (STD) and Spatial Correlation (COR) over SA-SWIO during 2001-2005 from each number of the sensitivity study, their driven ERA-Interim (ERAINT) and reference data (see **section 2.4.2**).

4.1.1 Radiation transfer: RRTM vs CCM (summer)

In general, RegCM4_RRTM simulate larger negative CLT bias than RegCM4_CCM (except when working with Grell schemes over ocean, SUBEX and UW schemes) in **Fig. 4-1**. This larger CLT bias simulated by RegCM4_RRTM compared with RegCM4_CCM is associated with an overall larger SSR spatial mean bias, which is reasonable as cloudiness can be considered as the main local modulator of SSR. Several regional climate model studies also highlight the dominating effect of cloud cover on the SSR levels or the net surface shortwave radiation (Chiacchio, Solmon, Giorgi, Stackhouse, & Wild, 2015; García-Díez et al., 2015; Jaeger et al., 2008; S Kothe & Ahrens, 2010; Steffen Kothe, Dobler, Beck, & Ahrens, 2011; Markovic et al., 2008; Zubler et al., 2011). These two radiation transfer schemes are also compared in the work of Li et al. (2014). A underestimation of CLT by 24.3% was found over Europe, with a overestimation of SSR by up to 3.3 % when using CCM scheme compared with Satellite Application Facility on Climate Monitoring (CM SAF) (Alexandri et al., 2015).

4.1.2 Cumulus Convection: Grell vs Emanuel vs Tiedtke (summer)

Emanuel scheme is found having a tend to produce excessive precipitation (F. Giorgi et al., 2012), which is also shown in present study as shown in **Fig. 4-1**,. Especially when working with CCM the wet bias is of about 4 mm/day compared with reference data, much larger then working with RRTM (about 2 mm/day).

Conversely, Grell scheme is likely to be much drier (about -5 mm/day over tropical ocean, also see F. Giorgi et al. (2012) and Adeniyi (2014)) and much cloudy (about 20 % and thus a strong negative SSR bias of about -80 W/m^2) over ocean compared with references. These preliminary tests suggested that a mixed convection approach by which, for example, the Emanuel scheme is used over oceans and the Grell scheme over land, might be the most suitable option to domain consisting both land and ocean, like SA-SWIO.

Tiedtke scheme trends to have too much SSR when working with Micro as resolved scale precipitation scheme.

4.1.3 PBL: Holtslag vs UW (summer)

As shown in **Fig. 4-1**, Holtslag trends to smaller TAS cold bias over tropical Africa land area compared with UW. When working with Emanuel scheme over the ocean, Holtslag has smaller negative SSR bias over Tropical Indian ocean than UW with Emanuel over ocean. Guttler et al. (2014) found that the UW scheme, in a 10-year experiments over the European domain, shows a substantial cooling. It reduces winter warm bias over the north-eastern Europe by 2 °C and reduces summer warm bias over central Europe by 3 °C compared with the default Holtslag in RegCM4.2. RegCM- UW was found to appropriate for stratocumulus investigations at scales ranging from hourly to decadal (O'Brien et al., 2012).

4.1.4 Resolved scale precipitation: SUBEX vs Micro (summer)

Compared to the pre-existing SUBEX scheme, the newly implemented Micro-physics scheme allows a proper treatment of mixed-phase clouds and a more physically realistic representation of cloud microphysics and precipitation (Nogherotto et al., 2016). In present sensitivity test, RegCM with Micro physics scheme trends to simulate stronger low CLT bias and larger higher SSR bias over western Equatorial Africa.

To sum up the sensitivity test, RegCM4 performs quite differently with various physics options over the SA-SWIO. Taylor plots of the statistics, Standard Deviation (STD) and Spatial Correlation (COR) are summarized in **Fig. 4-2** and **Fig. 4-3** for summer and winter respectively. Model performance in summer seasons has been examined (quite similar results are shown in winter as **Fig. 4-3** and **Fig. 4-4**, and a physics options within RegCM4 for the SA-SWIO domain is proposed: CCM as radiation transfer scheme, Grell over land & Emanuel over Ocean, SUBEX as the resolved precipitation, and Holtslag as the PBL schemes. this physics setup is used to estimate the internal variability of RegCM (**section 2.3.3**) then applied to the long-term simulation (**section 2.2**).

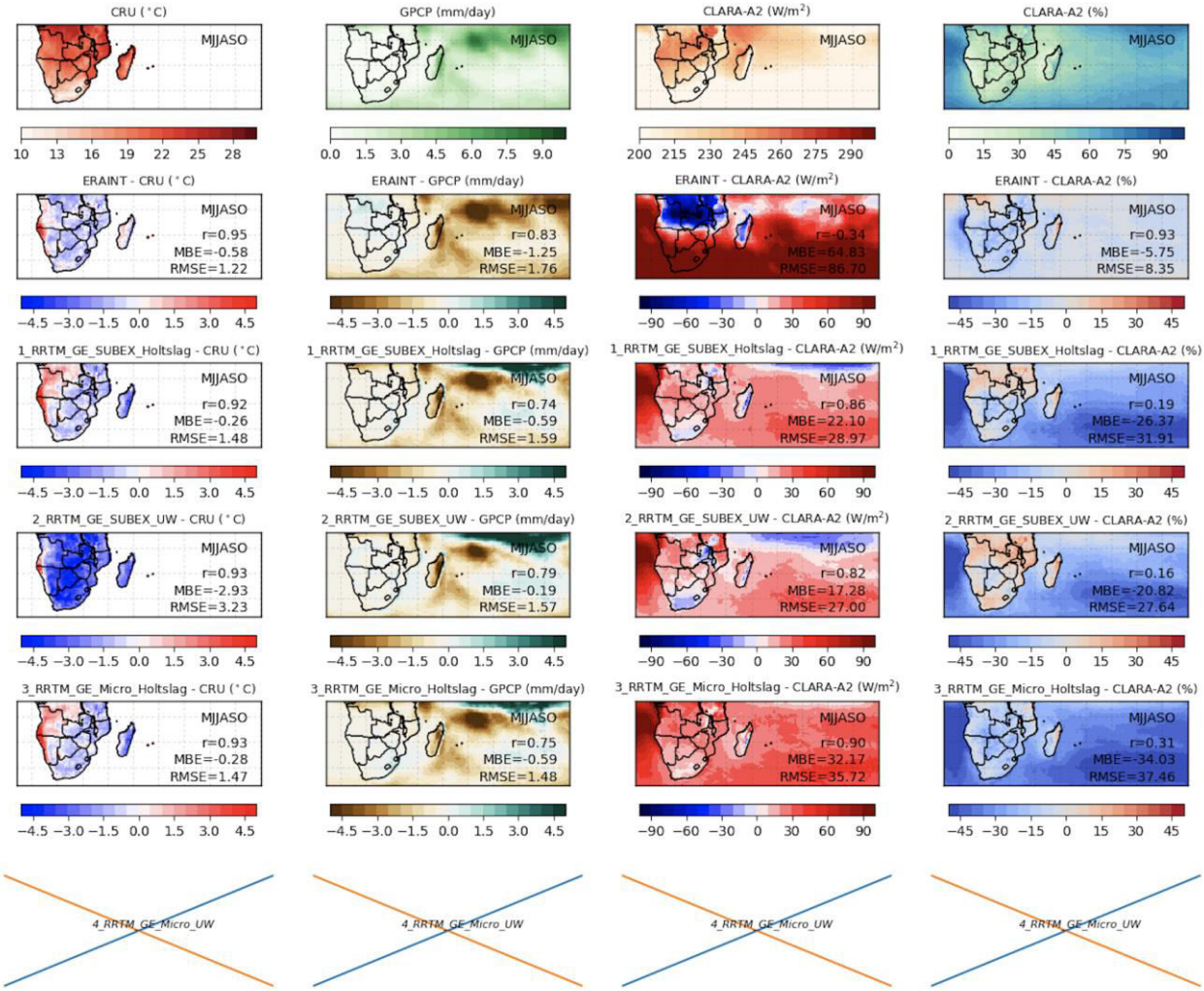
CRU (°C)
GPCP (mm/day)
CLARA-A2 (W/m²)
CLARA-A2 (%)
MJJASO
10 13 16 19 22 25 28
0.0 1.5 3.0 4.5 6.0 7.5 9.0
200 215 230 245 260 275 290
0 15 30 45 60 75 90
ERAINT - CRU (°C)
ERAINT - GPCP (mm/day)
ERAINT - CLARA-A2 (W/m²)
ERAINT - CLARA-A2 (%)
r=0.95 MBE=-0.58 RMSE=1.22
r=0.83 MBE=-1.25 RMSE=1.76
r=-0.34 MBE=64.83 RMSE=86.70
r=0.93 MBE=-5.75 RMSE=8.35
−4.5 −3.0 −1.5 0.0 1.5 3.0 4.5
−90 −60 −30 0 30 60 90
−45 −30 −15 0 15 30 45
1_RRTM_GE_SUBEX_Holtslag - CRU (°C)
1_RRTM_GE_SUBEX_Holtslag - GPCP (mm/day)
1_RRTM_GE_SUBEX_Holtslag - CLARA-A2 (W/m²)
1_RRTM_GE_SUBEX_Holtslag - CLARA-A2 (%)
r=0.92 MBE=-0.26 RMSE=1.48
r=0.74 MBE=-0.59 RMSE=1.59
r=0.86 MBE=22.10 RMSE=28.97
r=0.19 MBE=-26.37 RMSE=31.91
2_RRTM_GE_SUBEX_UW - CRU (°C)
2_RRTM_GE_SUBEX_UW - GPCP (mm/day)
2_RRTM_GE_SUBEX_UW - CLARA-A2 (W/m²)
2_RRTM_GE_SUBEX_UW - CLARA-A2 (%)
r=0.93 MBE=-2.93 RMSE=3.23
r=0.79 MBE=-0.19 RMSE=1.57
r=0.82 MBE=17.28 RMSE=27.00
r=0.16 MBE=-20.82 RMSE=27.64
3_RRTM_GE_Micro_Holtslag - CRU (°C)
3_RRTM_GE_Micro_Holtslag - GPCP (mm/day)
3_RRTM_GE_Micro_Holtslag - CLARA-A2 (W/m²)
3_RRTM_GE_Micro_Holtslag - CLARA-A2 (%)
r=0.93 MBE=-0.28 RMSE=1.47
r=0.75 MBE=-0.59 RMSE=1.48
r=0.90 MBE=32.17 RMSE=35.72
r=0.31 MBE=-34.03 RMSE=37.46
4_RRTM_GE_Micro_UW
4_RRTM_GE_Micro_UW
4_RRTM_GE_Micro_UW
4_RRTM_GE_Micro_UW

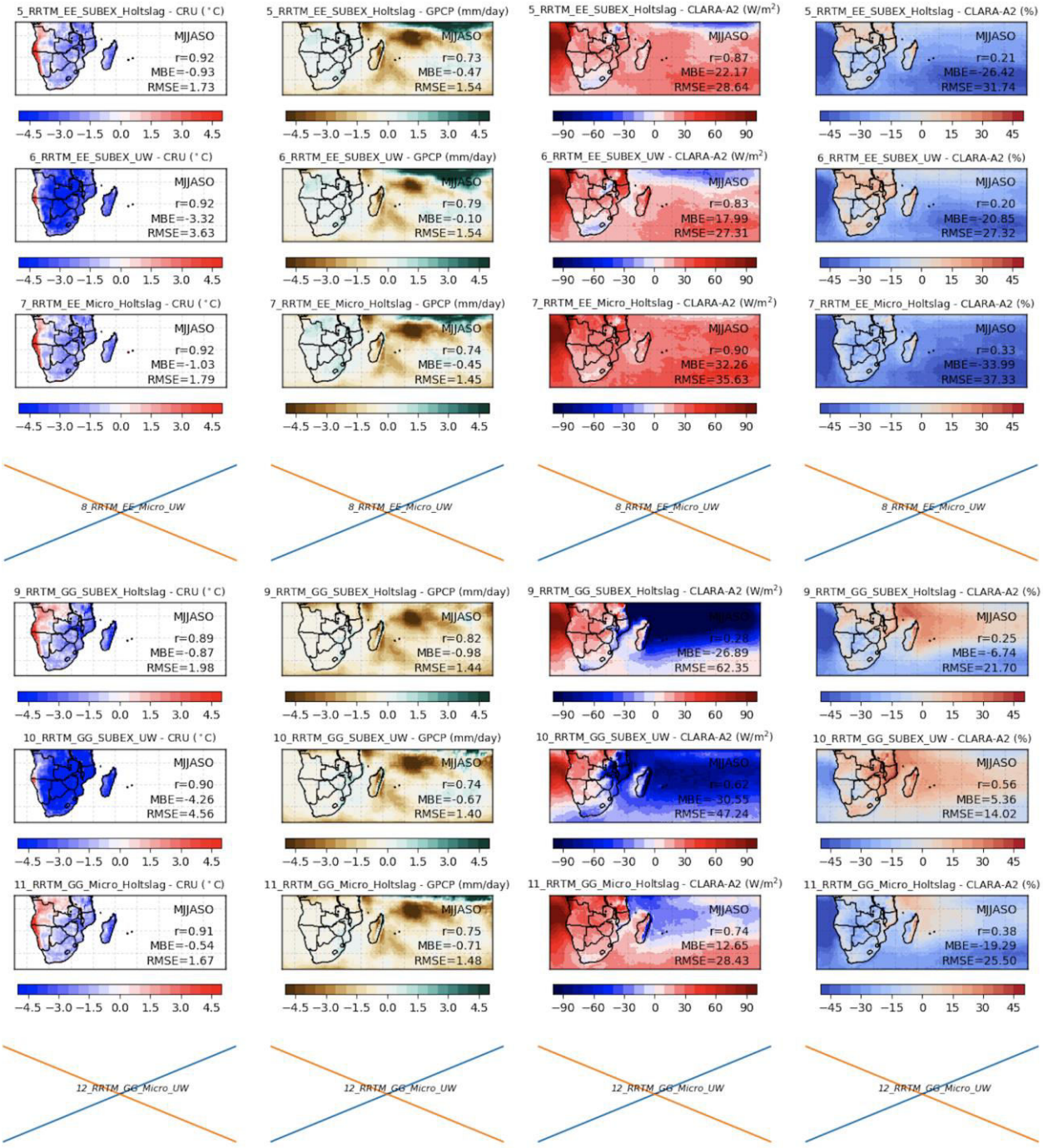
5_RRTM_EE_SUBEX_Holtslag - CRU (°C)
MJJASO
r=0.92
MBE=-0.93
RMSE=1.73
−4.5 −3.0 −1.5 0.0 1.5 3.0 4.5
5_RRTM_EE_SUBEX_Holtslag - GPCP (mm/day)
MJJASO
r=0.73
MBE=-0.47
RMSE=1.54
−4.5 −3.0 −1.5 0.0 1.5 3.0 4.5
5_RRTM_EE_SUBEX_Holtslag - CLARA-A2 (W/m²)
MJJASO
r=0.87
MBE=22.17
RMSE=28.64
−90 −60 −30 0 30 60 90
5_RRTM_EE_SUBEX_Holtslag - CLARA-A2 (%)
MJJASO
r=0.21
MBE=-26.42
RMSE=31.74
−45 −30 −15 0 15 30 45
6_RRTM_EE_SUBEX_UW - CRU (°C)
MJJASO
r=0.92
MBE=-3.32
RMSE=3.63
−4.5 −3.0 −1.5 0.0 1.5 3.0 4.5
6_RRTM_EE_SUBEX_UW - GPCP (mm/day)
MJJASO
r=0.79
MBE=-0.10
RMSE=1.54
−4.5 −3.0 −1.5 0.0 1.5 3.0 4.5
6_RRTM_EE_SUBEX_UW - CLARA-A2 (W/m²)
MJJASO
r=0.83
MBE=17.99
RMSE=27.31
−90 −60 −30 0 30 60 90
6_RRTM_EE_SUBEX_UW - CLARA-A2 (%)
MJJASO
r=0.20
MBE=-20.85
RMSE=27.32
−45 −30 −15 0 15 30 45
7_RRTM_EE_Micro_Holtslag - CRU (°C)
MJJASO
r=0.92
MBE=-1.03
RMSE=1.79
−4.5 −3.0 −1.5 0.0 1.5 3.0 4.5
7_RRTM_EE_Micro_Holtslag - GPCP (mm/day)
MJJASO
r=0.74
MBE=-0.45
RMSE=1.45
−4.5 −3.0 −1.5 0.0 1.5 3.0 4.5
7_RRTM_EE_Micro_Holtslag - CLARA-A2 (W/m²)
MJJASO
r=0.90
MBE=32.26
RMSE=35.63
−90 −60 −30 0 30 60 90
7_RRTM_EE_Micro_Holtslag - CLARA-A2 (%)
MJJASO
r=0.33
MBE=-33.99
RMSE=37.33
−45 −30 −15 0 15 30 45
8_RRTM_EE_Micro_UW
8_RRTM_EE_Micro_UW
8_RRTM_EE_Micro_UW
8_RRTM_EE_Micro_UW
9_RRTM_GG_SUBEX_Holtslag - CRU (°C)
MJJASO
r=0.89
MBE=-0.87
RMSE=1.98
−4.5 −3.0 −1.5 0.0 1.5 3.0 4.5
9_RRTM_GG_SUBEX_Holtslag - GPCP (mm/day)
MJJASO
r=0.82
MBE=-0.98
RMSE=1.44
−4.5 −3.0 −1.5 0.0 1.5 3.0 4.5
9_RRTM_GG_SUBEX_Holtslag - CLARA-A2 (W/m²)
MJJASO
r=0.28
MBE=-26.89
RMSE=62.35
−90 −60 −30 0 30 60 90
9_RRTM_GG_SUBEX_Holtslag - CLARA-A2 (%)
MJJASO
r=0.25
MBE=-6.74
RMSE=21.70
−45 −30 −15 0 15 30 45
10_RRTM_GG_SUBEX_UW - CRU (°C)
MJJASO
r=0.90
MBE=-4.26
RMSE=4.56
−4.5 −3.0 −1.5 0.0 1.5 3.0 4.5
10_RRTM_GG_SUBEX_UW - GPCP (mm/day)
MJJASO
r=0.74
MBE=-0.67
RMSE=1.40
−4.5 −3.0 −1.5 0.0 1.5 3.0 4.5
10_RRTM_GG_SUBEX_UW - CLARA-A2 (W/m²)
MJJASO
r=0.62
MBE=-30.55
RMSE=47.24
−90 −60 −30 0 30 60 90
10_RRTM_GG_SUBEX_UW - CLARA-A2 (%)
MJJASO
r=0.56
MBE=5.36
RMSE=14.02
−45 −30 −15 0 15 30 45
11_RRTM_GG_Micro_Holtslag - CRU (°C)
MJJASO
r=0.91
MBE=-0.54
RMSE=1.67
−4.5 −3.0 −1.5 0.0 1.5 3.0 4.5
11_RRTM_GG_Micro_Holtslag - GPCP (mm/day)
MJJASO
r=0.75
MBE=-0.71
RMSE=1.48
−4.5 −3.0 −1.5 0.0 1.5 3.0 4.5
11_RRTM_GG_Micro_Holtslag - CLARA-A2 (W/m²)
MJJASO
r=0.74
MBE=12.65
RMSE=28.43
−90 −60 −30 0 30 60 90
11_RRTM_GG_Micro_Holtslag - CLARA-A2 (%)
MJJASO
r=0.38
MBE=-19.29
RMSE=25.50
−45 −30 −15 0 15 30 45
12_RRTM_GG_Micro_UW
12_RRTM_GG_Micro_UW
12_RRTM_GG_Micro_UW
12_RRTM_GG_Micro_UW

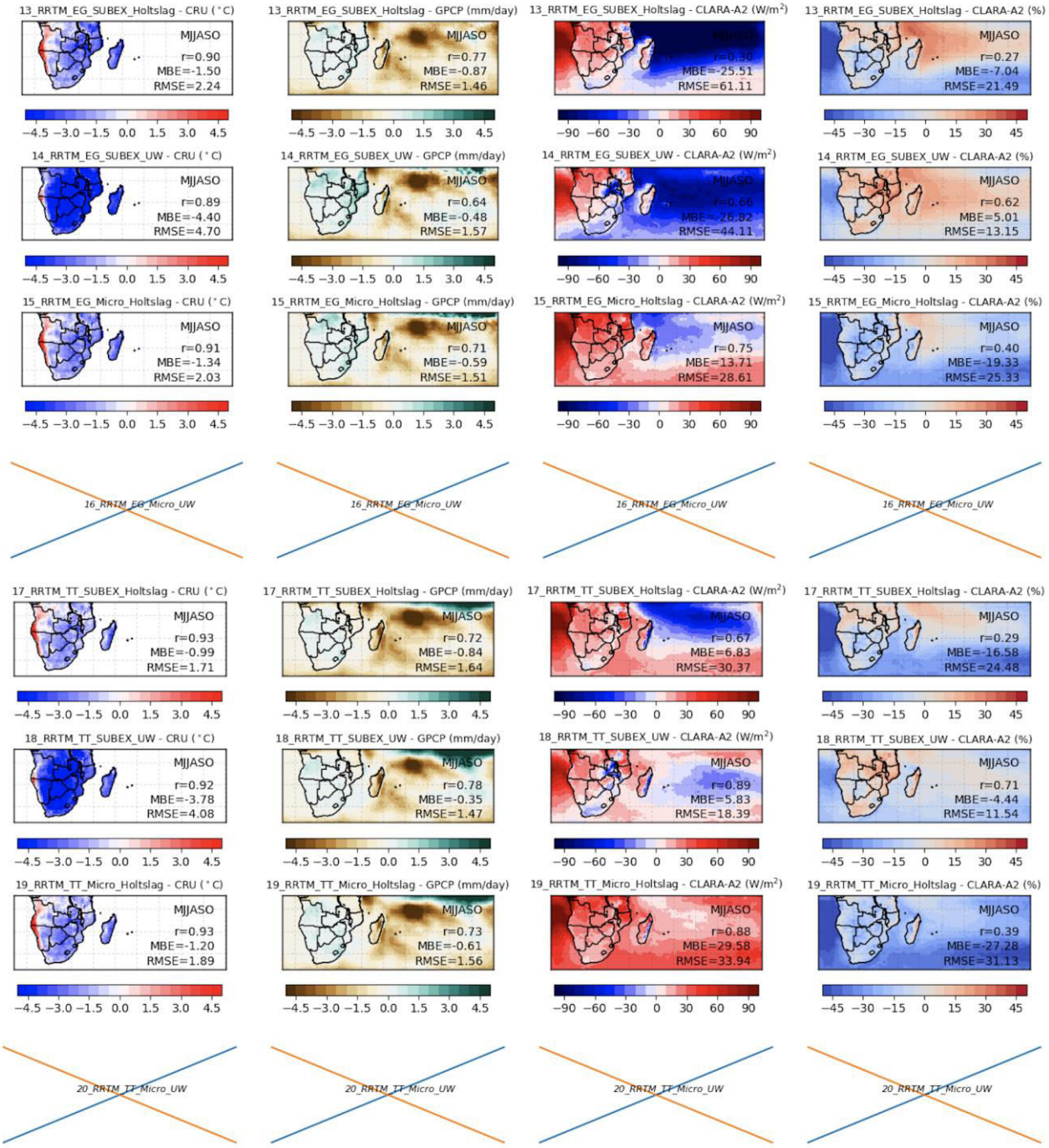
13_RRTM_EG_SUBEX_Holtslag - CRU (°C)
MJJASO
r=0.90
MBE=-1.50
RMSE=2.24
−4.5 −3.0 −1.5 0.0 1.5 3.0 4.5
13_RRTM_EG_SUBEX_Holtslag - GPCP (mm/day)
MJJASO
r=0.77
MBE=-0.87
RMSE=1.46
−4.5 −3.0 −1.5 0.0 1.5 3.0 4.5
13_RRTM_EG_SUBEX_Holtslag - CLARA-A2 (W/m²)
MJJASO
r=0.30
MBE=-25.51
RMSE=61.11
−90 −60 −30 0 30 60 90
13_RRTM_EG_SUBEX_Holtslag - CLARA-A2 (%)
MJJASO
r=0.27
MBE=-7.04
RMSE=21.49
−45 −30 −15 0 15 30 45
14_RRTM_EG_SUBEX_UW - CRU (°C)
MJJASO
r=0.89
MBE=-4.40
RMSE=4.70
−4.5 −3.0 −1.5 0.0 1.5 3.0 4.5
14_RRTM_EG_SUBEX_UW - GPCP (mm/day)
MJJASO
r=0.64
MBE=-0.48
RMSE=1.57
−4.5 −3.0 −1.5 0.0 1.5 3.0 4.5
14_RRTM_EG_SUBEX_UW - CLARA-A2 (W/m²)
MJJASO
r=0.66
MBE=-26.82
RMSE=44.11
−90 −60 −30 0 30 60 90
14_RRTM_EG_SUBEX_UW - CLARA-A2 (%)
MJJASO
r=0.62
MBE=5.01
RMSE=13.15
−45 −30 −15 0 15 30 45
15_RRTM_EG_Micro_Holtslag - CRU (°C)
MJJASO
r=0.91
MBE=-1.34
RMSE=2.03
−4.5 −3.0 −1.5 0.0 1.5 3.0 4.5
15_RRTM_EG_Micro_Holtslag - GPCP (mm/day)
MJJASO
r=0.71
MBE=-0.59
RMSE=1.51
−4.5 −3.0 −1.5 0.0 1.5 3.0 4.5
15_RRTM_EG_Micro_Holtslag - CLARA-A2 (W/m²)
MJJASO
r=0.75
MBE=13.71
RMSE=28.61
−90 −60 −30 0 30 60 90
15_RRTM_EG_Micro_Holtslag - CLARA-A2 (%)
MJJASO
r=0.40
MBE=-19.33
RMSE=25.33
−45 −30 −15 0 15 30 45
16_RRTM_EG_Micro_UW
16_RRTM_EG_Micro_UW
16_RRTM_EG_Micro_UW
16_RRTM_EG_Micro_UW
17_RRTM_TT_SUBEX_Holtslag - CRU (°C)
MJJASO
r=0.93
MBE=-0.99
RMSE=1.71
−4.5 −3.0 −1.5 0.0 1.5 3.0 4.5
17_RRTM_TT_SUBEX_Holtslag - GPCP (mm/day)
MJJASO
r=0.72
MBE=-0.84
RMSE=1.64
−4.5 −3.0 −1.5 0.0 1.5 3.0 4.5
17_RRTM_TT_SUBEX_Holtslag - CLARA-A2 (W/m²)
MJJASO
r=0.67
MBE=6.83
RMSE=30.37
−90 −60 −30 0 30 60 90
17_RRTM_TT_SUBEX_Holtslag - CLARA-A2 (%)
MJJASO
r=0.29
MBE=-16.58
RMSE=24.48
−45 −30 −15 0 15 30 45
18_RRTM_TT_SUBEX_UW - CRU (°C)
MJJASO
r=0.92
MBE=-3.78
RMSE=4.08
−4.5 −3.0 −1.5 0.0 1.5 3.0 4.5
18_RRTM_TT_SUBEX_UW - GPCP (mm/day)
MJJASO
r=0.78
MBE=-0.35
RMSE=1.47
−4.5 −3.0 −1.5 0.0 1.5 3.0 4.5
18_RRTM_TT_SUBEX_UW - CLARA-A2 (W/m²)
MJJASO
r=0.89
MBE=5.83
RMSE=18.39
−90 −60 −30 0 30 60 90
18_RRTM_TT_SUBEX_UW - CLARA-A2 (%)
MJJASO
r=0.71
MBE=-4.44
RMSE=11.54
−45 −30 −15 0 15 30 45
19_RRTM_TT_Micro_Holtslag - CRU (°C)
MJJASO
r=0.93
MBE=-1.20
RMSE=1.89
−4.5 −3.0 −1.5 0.0 1.5 3.0 4.5
19_RRTM_TT_Micro_Holtslag - GPCP (mm/day)
MJJASO
r=0.73
MBE=-0.61
RMSE=1.56
−4.5 −3.0 −1.5 0.0 1.5 3.0 4.5
19_RRTM_TT_Micro_Holtslag - CLARA-A2 (W/m²)
MJJASO
r=0.88
MBE=29.58
RMSE=33.94
−90 −60 −30 0 30 60 90
19_RRTM_TT_Micro_Holtslag - CLARA-A2 (%)
MJJASO
r=0.39
MBE=-27.28
RMSE=31.13
−45 −30 −15 0 15 30 45
20_RRTM_TT_Micro_UW
20_RRTM_TT_Micro_UW
20_RRTM_TT_Micro_UW
20_RRTM_TT_Micro_UW

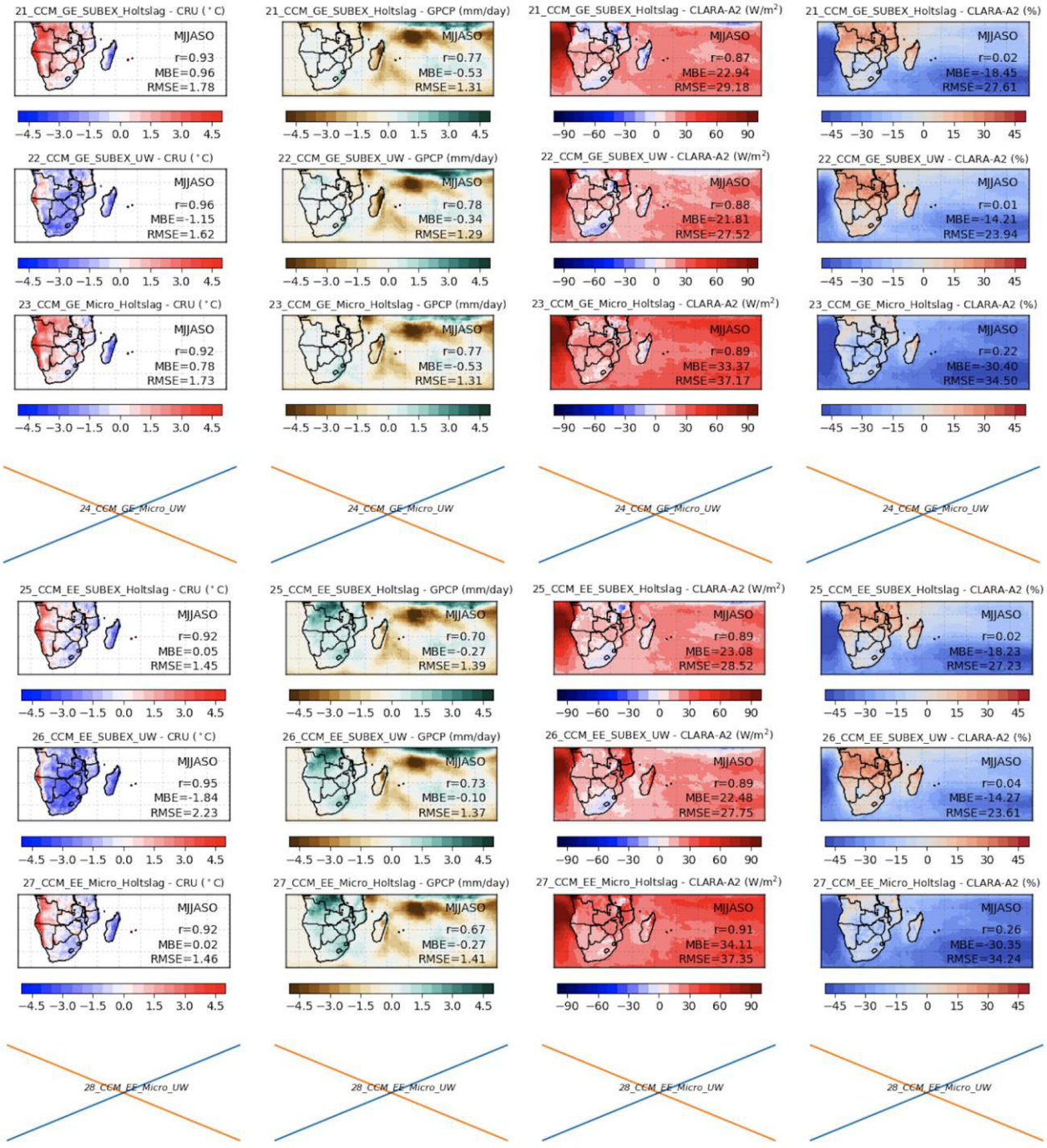
21_CCM_GE_SUBEX_Holtslag - CRU (°C)
MJJASO
r=0.93
MBE=0.96
RMSE=1.78
−4.5 −3.0 −1.5 0.0 1.5 3.0 4.5
21_CCM_GE_SUBEX_Holtslag - GPCP (mm/day)
MJJASO
r=0.77
MBE=-0.53
RMSE=1.31
−4.5 −3.0 −1.5 0.0 1.5 3.0 4.5
21_CCM_GE_SUBEX_Holtslag - CLARA-A2 (W/m²)
MJJASO
r=0.87
MBE=-22.94
RMSE=29.18
−90 −60 −30 0 30 60 90
21_CCM_GE_SUBEX_Holtslag - CLARA-A2 (%)
MJJASO
r=0.02
MBE=-18.45
RMSE=27.61
−45 −30 −15 0 15 30 45
22_CCM_GE_SUBEX_UW - CRU (°C)
MJJASO
r=0.96
MBE=-1.15
RMSE=1.62
−4.5 −3.0 −1.5 0.0 1.5 3.0 4.5
22_CCM_GE_SUBEX_UW - GPCP (mm/day)
MJJASO
r=0.78
MBE=-0.34
RMSE=1.29
−4.5 −3.0 −1.5 0.0 1.5 3.0 4.5
22_CCM_GE_SUBEX_UW - CLARA-A2 (W/m²)
MJJASO
r=0.88
MBE=21.81
RMSE=27.52
−90 −60 −30 0 30 60 90
22_CCM_GE_SUBEX_UW - CLARA-A2 (%)
MJJASO
r=0.01
MBE=-14.21
RMSE=23.94
−45 −30 −15 0 15 30 45
23_CCM_GE_Micro_Holtslag - CRU (°C)
MJJASO
r=0.92
MBE=0.78
RMSE=1.73
−4.5 −3.0 −1.5 0.0 1.5 3.0 4.5
23_CCM_GE_Micro_Holtslag - GPCP (mm/day)
MJJASO
r=0.77
MBE=-0.53
RMSE=1.31
−4.5 −3.0 −1.5 0.0 1.5 3.0 4.5
23_CCM_GE_Micro_Holtslag - CLARA-A2 (W/m²)
MJJASO
r=0.89
MBE=33.37
RMSE=37.17
−90 −60 −30 0 30 60 90
23_CCM_GE_Micro_Holtslag - CLARA-A2 (%)
MJJASO
r=0.22
MBE=-30.40
RMSE=34.50
−45 −30 −15 0 15 30 45
24_CCM_GE_Micro_UW
24_CCM_GE_Micro_UW
24_CCM_GE_Micro_UW
24_CCM_GE_Micro_UW
25_CCM_EE_SUBEX_Holtslag - CRU (°C)
MJJASO
r=0.92
MBE=0.05
RMSE=1.45
−4.5 −3.0 −1.5 0.0 1.5 3.0 4.5
25_CCM_EE_SUBEX_Holtslag - GPCP (mm/day)
MJJASO
r=0.70
MBE=-0.27
RMSE=1.39
−4.5 −3.0 −1.5 0.0 1.5 3.0 4.5
25_CCM_EE_SUBEX_Holtslag - CLARA-A2 (W/m²)
MJJASO
r=0.89
MBE=23.08
RMSE=28.52
−90 −60 −30 0 30 60 90
25_CCM_EE_SUBEX_Holtslag - CLARA-A2 (%)
MJJASO
r=0.02
MBE=-18.23
RMSE=27.23
−45 −30 −15 0 15 30 45
26_CCM_EE_SUBEX_UW - CRU (°C)
MJJASO
r=0.95
MBE=-1.84
RMSE=2.23
−4.5 −3.0 −1.5 0.0 1.5 3.0 4.5
26_CCM_EE_SUBEX_UW - GPCP (mm/day)
MJJASO
r=0.73
MBE=-0.10
RMSE=1.37
−4.5 −3.0 −1.5 0.0 1.5 3.0 4.5
26_CCM_EE_SUBEX_UW - CLARA-A2 (W/m²)
MJJASO
r=0.89
MBE=22.48
RMSE=27.75
−90 −60 −30 0 30 60 90
26_CCM_EE_SUBEX_UW - CLARA-A2 (%)
MJJASO
r=0.04
MBE=-14.27
RMSE=23.61
−45 −30 −15 0 15 30 45
27_CCM_EE_Micro_Holtslag - CRU (°C)
MJJASO
r=0.92
MBE=0.02
RMSE=1.46
−4.5 −3.0 −1.5 0.0 1.5 3.0 4.5
27_CCM_EE_Micro_Holtslag - GPCP (mm/day)
MJJASO
r=0.67
MBE=-0.27
RMSE=1.41
−4.5 −3.0 −1.5 0.0 1.5 3.0 4.5
27_CCM_EE_Micro_Holtslag - CLARA-A2 (W/m²)
MJJASO
r=0.91
MBE=34.11
RMSE=37.35
−90 −60 −30 0 30 60 90
27_CCM_EE_Micro_Holtslag - CLARA-A2 (%)
MJJASO
r=0.26
MBE=-30.35
RMSE=34.24
−45 −30 −15 0 15 30 45
28_CCM_EE_Micro_UW
28_CCM_EE_Micro_UW
28_CCM_EE_Micro_UW
28_CCM_EE_Micro_UW

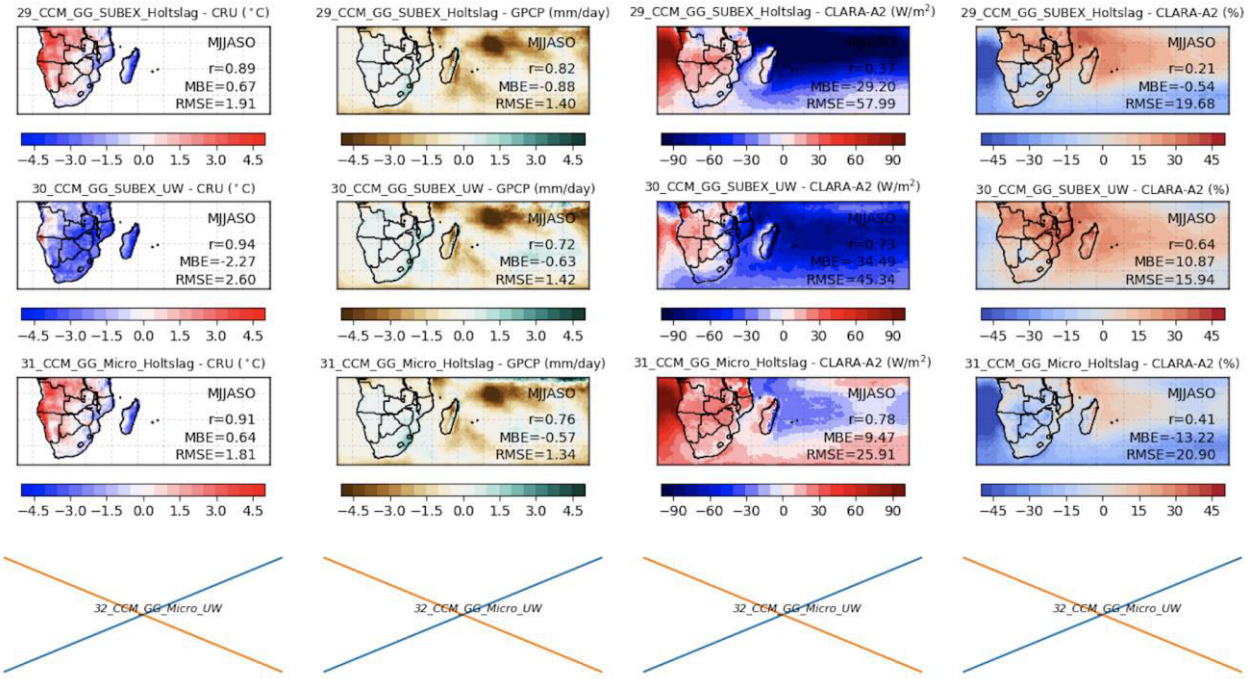
29_CCM_GG_SUBEX_Holtslag - CRU (°C)
MJJASO
r=0.89
MBE=0.67
RMSE=1.91
−4.5 −3.0 −1.5 0.0 1.5 3.0 4.5
29_CCM_GG_SUBEX_Holtslag - GPCP (mm/day)
MJJASO
r=0.82
MBE=-0.88
RMSE=1.40
−4.5 −3.0 −1.5 0.0 1.5 3.0 4.5
29_CCM_GG_SUBEX_Holtslag - CLARA-A2 (W/m2)
MJJASO
r=0.37
MBE=-29.20
RMSE=57.99
−90 −60 −30 0 30 60 90
29_CCM_GG_SUBEX_Holtslag - CLARA-A2 (%)
MJJASO
r=0.21
MBE=-0.54
RMSE=19.68
−45 −30 −15 0 15 30 45
30_CCM_GG_SUBEX_UW - CRU (°C)
MJJASO
r=0.94
MBE=-2.27
RMSE=2.60
−4.5 −3.0 −1.5 0.0 1.5 3.0 4.5
30_CCM_GG_SUBEX_UW - GPCP (mm/day)
MJJASO
r=0.72
MBE=-0.63
RMSE=1.42
−4.5 −3.0 −1.5 0.0 1.5 3.0 4.5
30_CCM_GG_SUBEX_UW - CLARA-A2 (W/m2)
MJJASO
r=0.73
MBE=-34.49
RMSE=45.34
−90 −60 −30 0 30 60 90
30_CCM_GG_SUBEX_UW - CLARA-A2 (%)
MJJASO
r=0.64
MBE=10.87
RMSE=15.94
−45 −30 −15 0 15 30 45
31_CCM_GG_Micro_Holtslag - CRU (°C)
MJJASO
r=0.91
MBE=0.64
RMSE=1.81
−4.5 −3.0 −1.5 0.0 1.5 3.0 4.5
31_CCM_GG_Micro_Holtslag - GPCP (mm/day)
MJJASO
r=0.76
MBE=-0.57
RMSE=1.34
−4.5 −3.0 −1.5 0.0 1.5 3.0 4.5
31_CCM_GG_Micro_Holtslag - CLARA-A2 (W/m2)
MJJASO
r=0.78
MBE=9.47
RMSE=25.91
−90 −60 −30 0 30 60 90
31_CCM_GG_Micro_Holtslag - CLARA-A2 (%)
MJJASO
r=0.41
MBE=-13.22
RMSE=20.90
−45 −30 −15 0 15 30 45
32_CCM_GG_Micro_UW
32_CCM_GG_Micro_UW
32_CCM_GG_Micro_UW
32_CCM_GG_Micro_UW

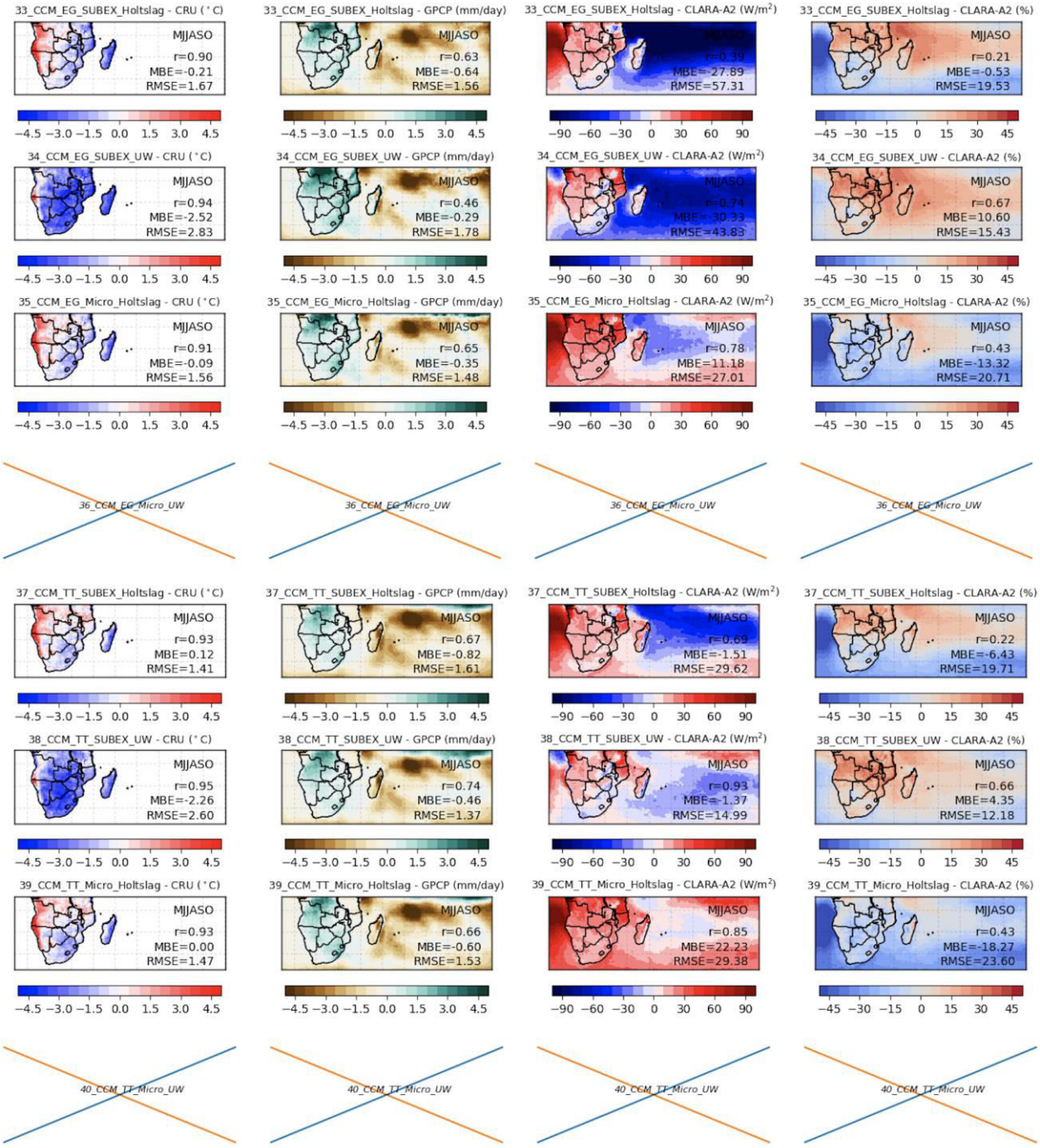

Fig. 4-3 Same as **Fig. 4-1**, but for winter.

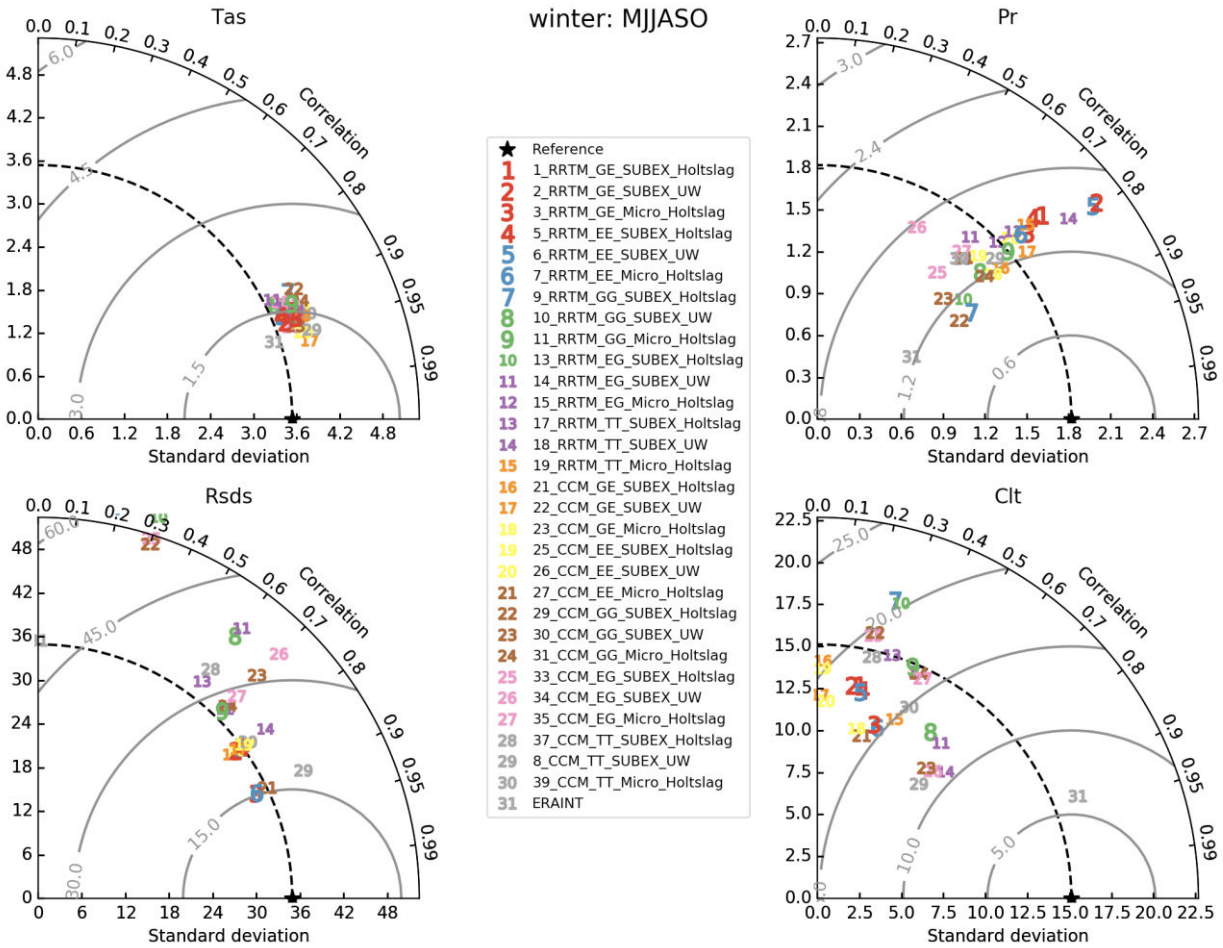

Fig. 4-4 Same as **Fig. 4-2**, but during austral winter.

4.2 Validation of RegCM4 simulations for present-day conditions

In order to interpret future climate projections, an evaluation of the ability of RegCM4 to accurately simulate SSR is a crucial first step. In this section, we first validate model reproduced climatic variables (TAS, PR, SSR and CLT) during the past window, 1996-2005. 10-year seasonal climatology of TAS, PR, SSR, and CLT are compared with observations (see **section 2.4.2**) at seasonal scales in **Fig. 4-5** and **Fig. 4-6** for austral summer and winter, respectively.

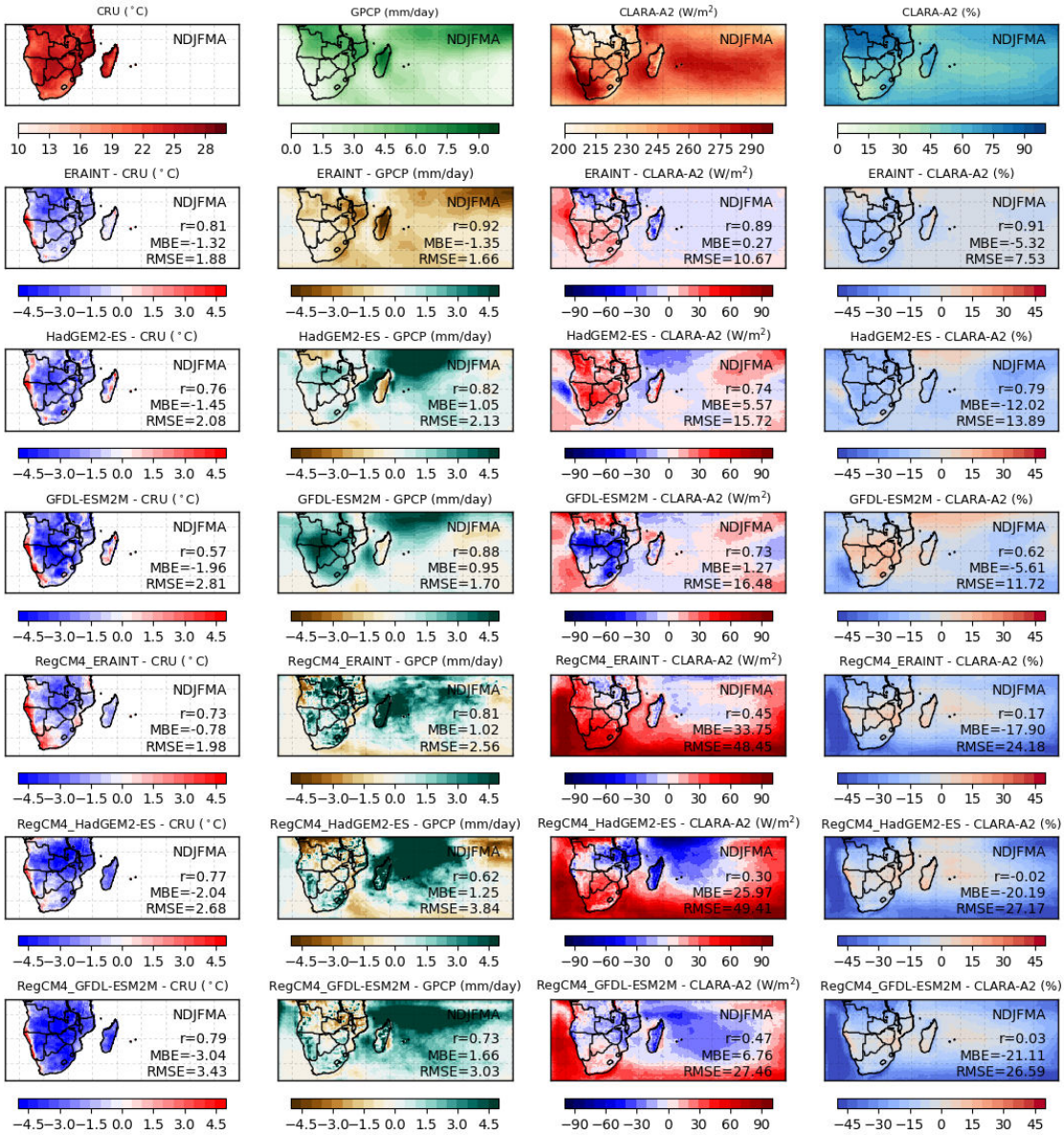

Fig. 4-5 Seasonal (NDJFMA) mean of TAS (1st column), PR (2nd column), SSR (3rd column), and CLT (4th column) from observations (top row) and the differences with ERA-Interim reanalyses (2nd row), GCMs (3rd and 4th rows) and RegCM4 forced by ERA-Interim and GCMs (5th, 6th, and last row). A buffer zone of 4 degrees has been removed.

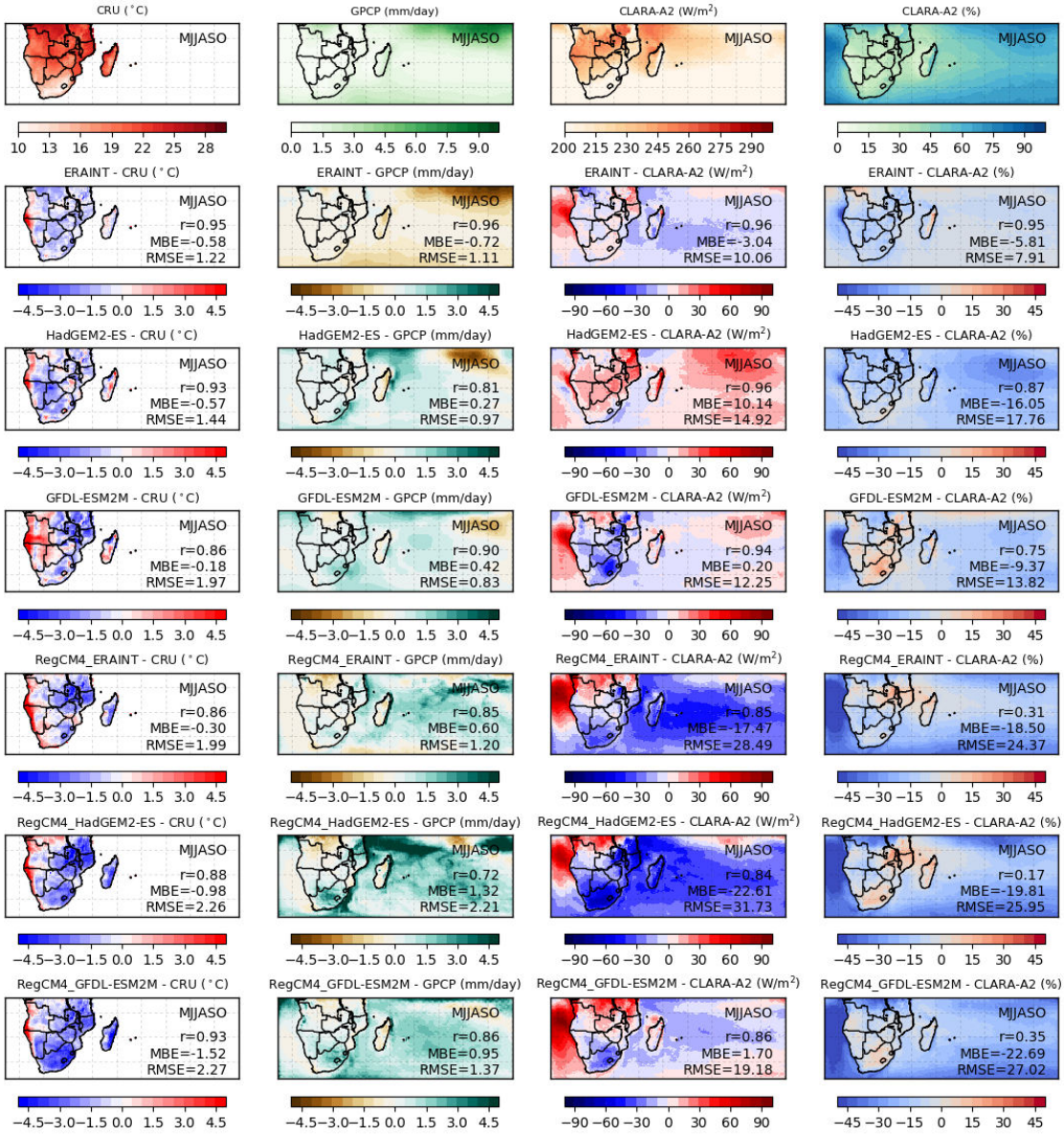

Fig. 4-6 Same as **Fig. 4-5** but for austral winter (MJJASO).

When nesting a Regional Climate Model (RCM) into outputs of a course resolution Global Circulation Model (GCM), the downscaled result is likely to suffer from two types of biases: the bias raised from the regional processes in the RCM, and the bias injected from the GCMs through initial and boundary conditions. To separate those two types of biases is of important concern for the downscaling community. In this study, RegCM4 was driven by both "perfect" boundary con-

ditions as provided by ERAINT reanalyses and the GCMs, from which the RegCM4 bias could be potentially isolated, and thus the impact of GCMs as well.

4.2.1 Austral summer: NDJFMA

GCMs, namely HadGEM2-ES and GFDL-ESM2M, produce overall similar patterns of bias in TAS and SSR with ERAINT, but a much stronger positive PR bias along the ITCZ and a much better reproduced CLT pattern. It is evident that the pattern of CLT bias is consistently correlated with that of SSR bias. For HadGEM2-ES, a positive SSR bias over the African continent is to be associated with a negative CLT bias there. Over the western tropical Indian Ocean, HadGEM2-ES simulates lower SSR biases? and reasonable higher CLT biases. On the other hand, GFDL-ESM2M simulates a higher SSR bias and a lower CLT bias over the tropical continent (as for GFDL), and less SSR with more CLT over the subtropical African continent (in contrast to GFDL).

RegCM4, when driven by ERAINT, simulates the same signs of bias in TAS, SSR, and CLT than ERAINT, but produces much more PR along the ICTZ leading to a positive MBE of 1.02 mm/day compared to GPCP. TAS MBE is reduced, from -1.32 to -0.78 °C, with respect to ERAINT, RegCM4 notably performing better than ERAINT over the central part of the continent. The large negative CLT bias remains similar with ERAINT, while much stronger positive bias of SSR is to be found over the subtropical areas.

RegCM4, when driven by both GCMs, produces a reduced warmer TAS bias along the western coast but an enhanced colder TAS bias over the rest of African continent. The GCMs' wet bias over the subtropical continent is reduced when downscaled by RegCM4, but at the same time their drier bias over the tropical continent and wetter bias over the Indian Ocean are enhanced by RegCM4. RegCM4 produces SSR in very similar ways when driven by different forcing boundaries (ERAINT and GCMs). HadGEM2-ES forced simulation results in SSR bias pattern similar to that for ERAINT forced simulation, with a strong positive bias over the subtropical ocean. The pattern of SSR bias produced by RegCM4 driven by GFDL-ESM2M is similar to the previous, though the amplitude of the bias is much smaller. CLT doesn't change much, with still large negative biases when ERAINT and the two GCMs are downscaled by RegCM4. In contrast to ERAINT, it seems to me that the CLT bias pattern for the GCMs and RegCM4 forced by the GCMs are different. The RCM seems to produce his own CLT independently of the boundary.

4.2.2 Austral winter: MJJASO

In austral winter (**Fig. 4-6**), ERAINT simulates reduced cold/dry bias with MBE of about -0.6°C/-0.7 mm per day in comparison to summer (about -1.3°C/-1.4 mm per day). Less SSR (that is reduced bias = EAINT producing less SSR than observations? Or lower SSR bias than for summer?) is found over the subtropical Indian Ocean and the tropical African continent. As in summer, lower CLT bias is evident with a MEB of about -50% in absolute percentage. RegCM4, when driven by ERAINT, simulates reduced TAS MEB (-0.3°C) with respect to ERAINT (-0.6°C). Wet bias appears over the Indian Ocean in contrast with the forcing ERAINT. SSR bias has similar pattern with ERAINT over ocean, but quite different over land.

GCMs, namely HadGEM2-ES and GFDL-ESM2M, simulate TAS and PR with smaller MBE than ERAINT. HadGEM2-ES (GFDL-ESM2M) has a positive (negative) SSR bias over the African continent. As in austral summer these patterns are correlated with the negative/positive CLT biases in the same region. RegCM4, when driven by GCMs, produces negative (cold) TAS bias over Madagascar in contrast to the GCMs themselves. As for summer, the GCMs' wet bias over the Indian ocean in winter is enhanced and extended when downscaled by RegCM4. RegCM4 produces SSR in very similar ways when driven by different forcing boundaries (ERAINT and GCMs) but with different amplitudes as for RegCM-GFDL over the Indian ocean where the negative SSR bias is reduced in comparison to that for RegCM-ERAINT and RegCM-HadGEM. CLT are quite similar between simulations with different forcing data, still remaining large lower bias when downscaled by RegCM4.

In a word, RegCM4 is not likely to have influences from the forcing GCMs in simulating SSR. It could be argued that SSR and CLT are not the variables that have been directly inputted to RegCM4 as boundary conditions and thus have little (reduced?) constraints on RegCM4 downscaled results, which gives more freedom to RegCM4 to develop its own patterns of SSR and CLT.

4.3 Ensembles study:

Model response to the internal climate variability can be regarded as a background noise of the climate change signal as it gives rise to large uncertainty in projections of future climate (Filippo Giorgi & Mearns, 2002; Kay et al., 2015). The uncertainty in future climate due to internal climate variability can be estimated from large ensembles of climate change simulations in which the experiment setup is the same from one ensemble member to the next but for small perturbations in the initial atmospheric state. However, this long-term large ensemble is computational expensive and out of reach of current research condition. Thus, to estimate the internal variability of RegCM4 and to understand projection spread, an ensemble experiment including 20 members of the model driven by EARINT are made in the past 1997-1998, when strong ENSO event occurred as ENSO is the most important mode of (internal) variability globally (Wolter & Timlin, 1998).

An ensemble consisting of 20 RegCM4 realizations is generated by applying boundary conditions from ERAINT reanalyses. These simulations are conducted with exactly the same design as for the long-term simulation, including the same SA-SWIO domain, resolution of 50 km, and the same physical parameterizations (see section 2.3.3), but different starting times, 1st of Nov in 1996 in the first simulation and one day after for each of the rest 19 runs, following the methodology of Pohl et al. (2016).

Standard deviation (STD) of the 20-member ensemble of simulated annual mean TAS, PR, SSR and CLT is shown in **Fig. 4-7** as an indicator of internal variability of RegCM4. Ensemble simulations simulate TAS with very small dispersion with STD less than 0.05°C over the ocean area and of about 0.2°C over land. Dispersion is found mainly over the subtropical African continent. Unlike TAS, ensemble simulated STD of SSR and CLT expend over the whole research domain. PR suffers from stronger internal variability over mainly almost the whole research domain with a mean STD of about 0.9 mm/day. SSR and CLT have a mean STD of about 0.19 W/m^2 and 0.27%, respectively. It is worth to point out that the inter-model dispersion of annual means (or spatial means, **Fig. 4-12**) are of an order smaller than the model biases as shown in section **4.2**.

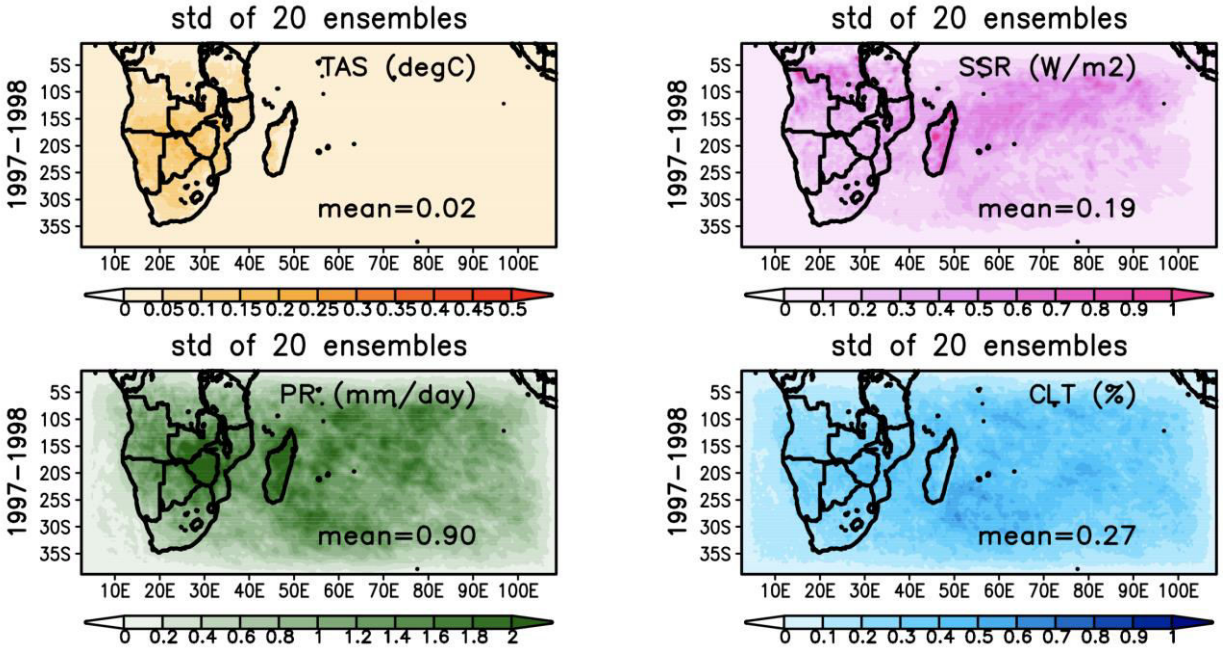

Fig. 4-7 Standard deviation (STD) of the 20-member ensemble in annual mean TAS, PR, SSR and CLT during 1997-1998.

Inter-model dispersion is more obvious at the seasonal scale. Strong ensemble STDs of TAS, PR, SSR and CLT mainly happen in the warm season, with values up to about 0.8°C, 5 mm/day, 10 W/m^2 and 5%, respectively**Fig. 4-8**, **Fig. 4-9**, **Fig. 4-10**, **Fig. 4-11**), of the same order of magnitude than the summer bias (**Fig. 4-5**). In the cold months, dispersions are of one order of magnitude smaller than the winter biases (**Fig. 4-6**) as well.

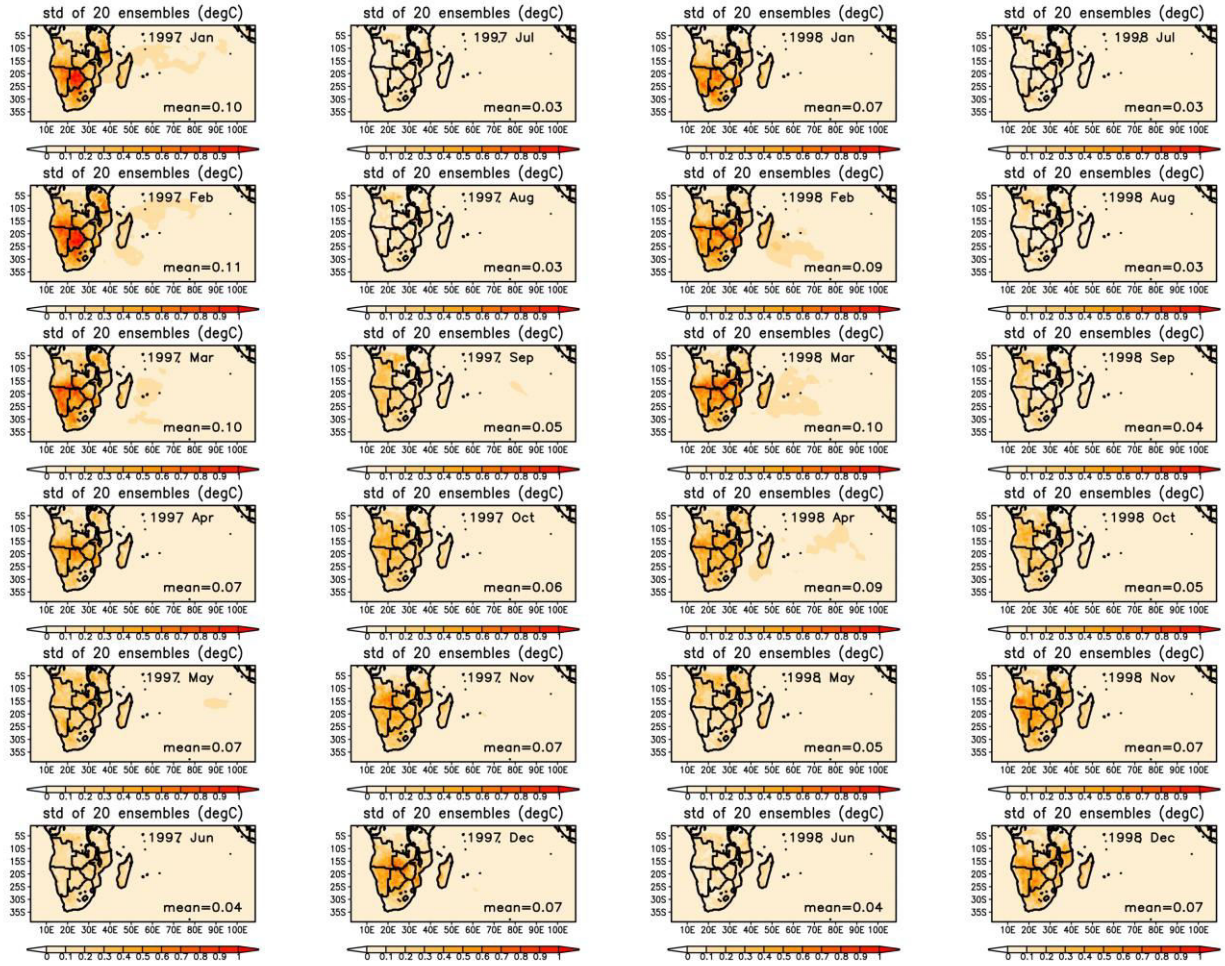

Fig. 4-8 TAS standard deviation of the 20-member ensemble for each month between January 1997 and December 1998.

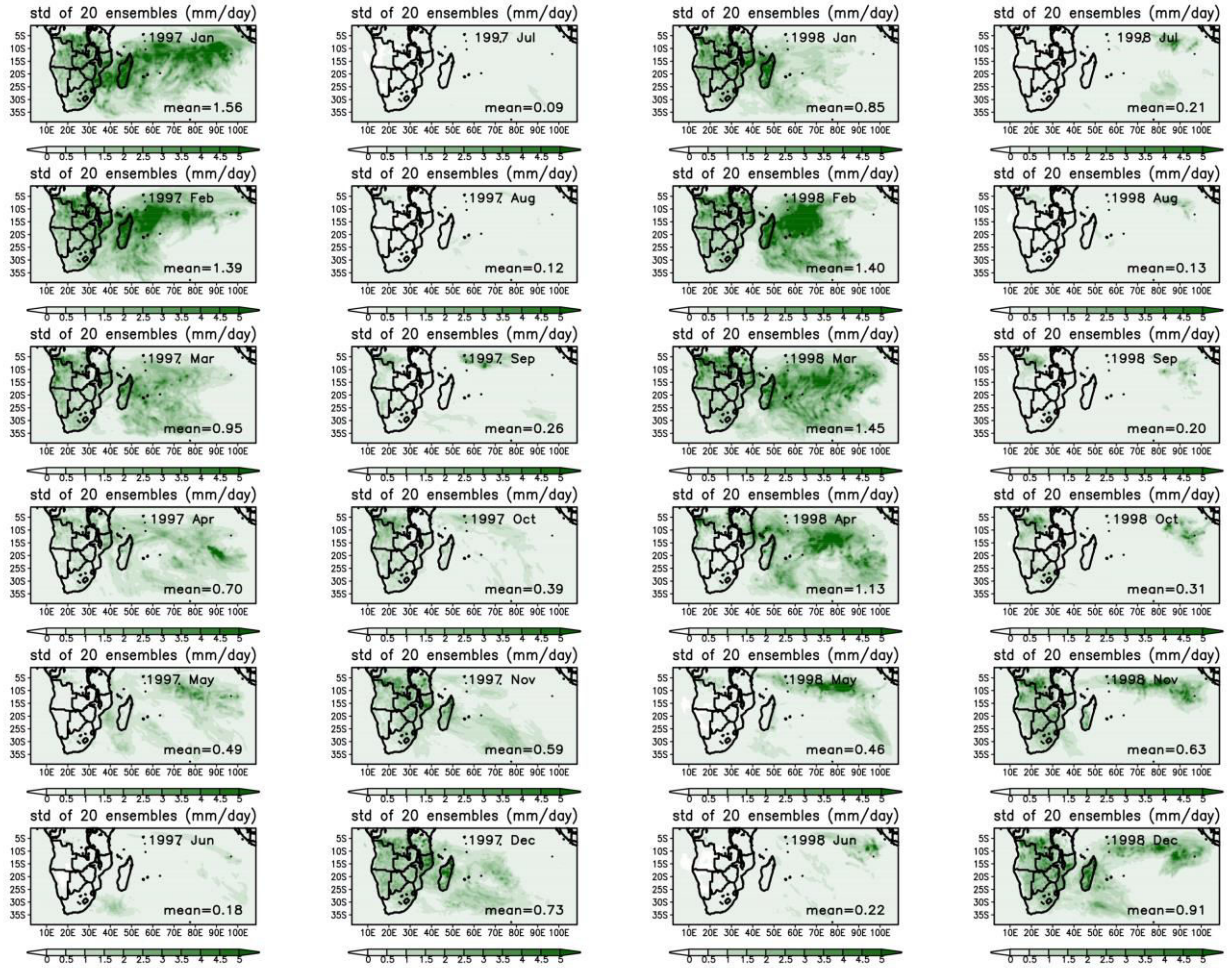

Fig. 4-9 Same as **Fig. 4-8**, but for precipitation (PR).

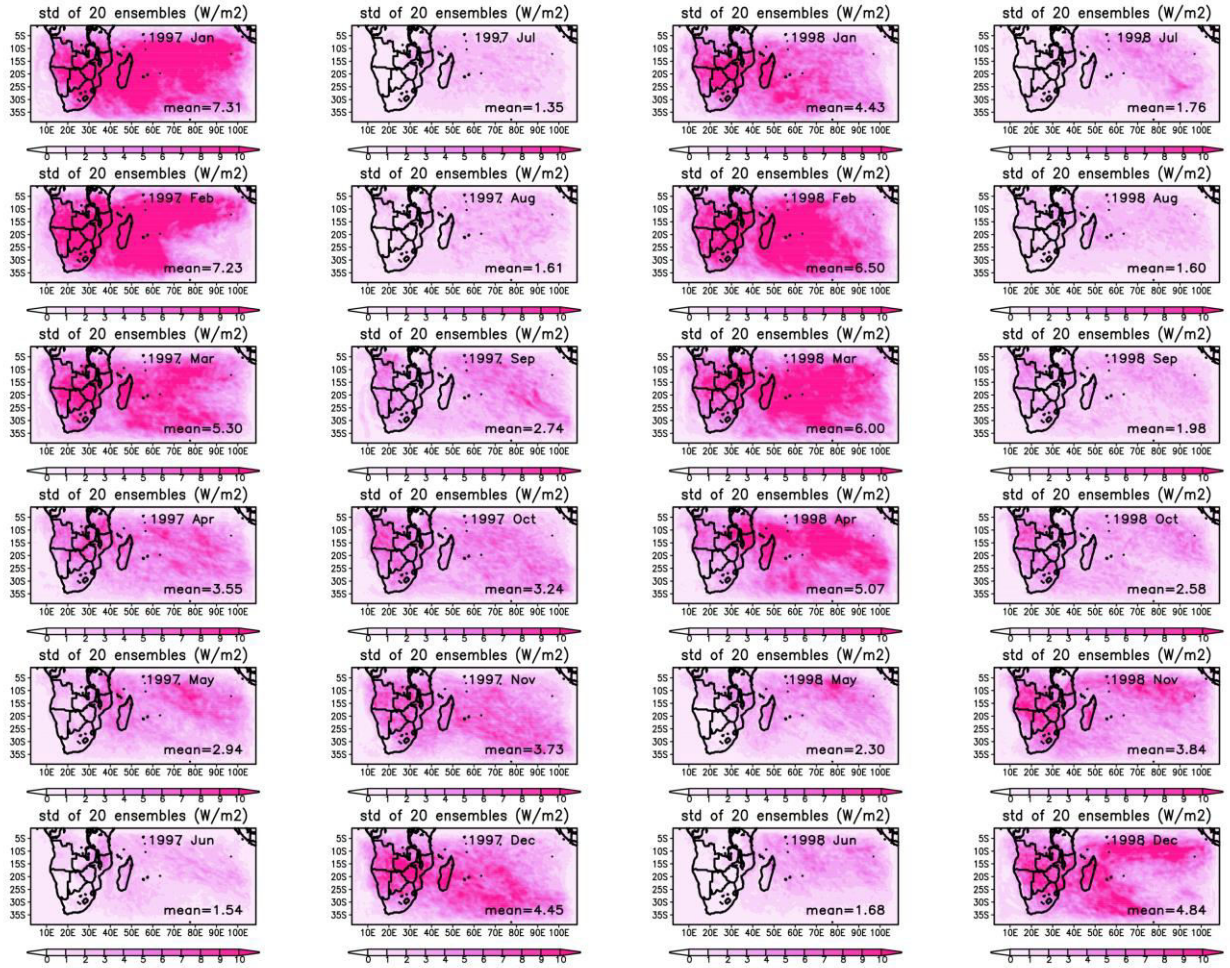

Fig. 4-10 Same as **Fig. 4-8**, but for SSR.

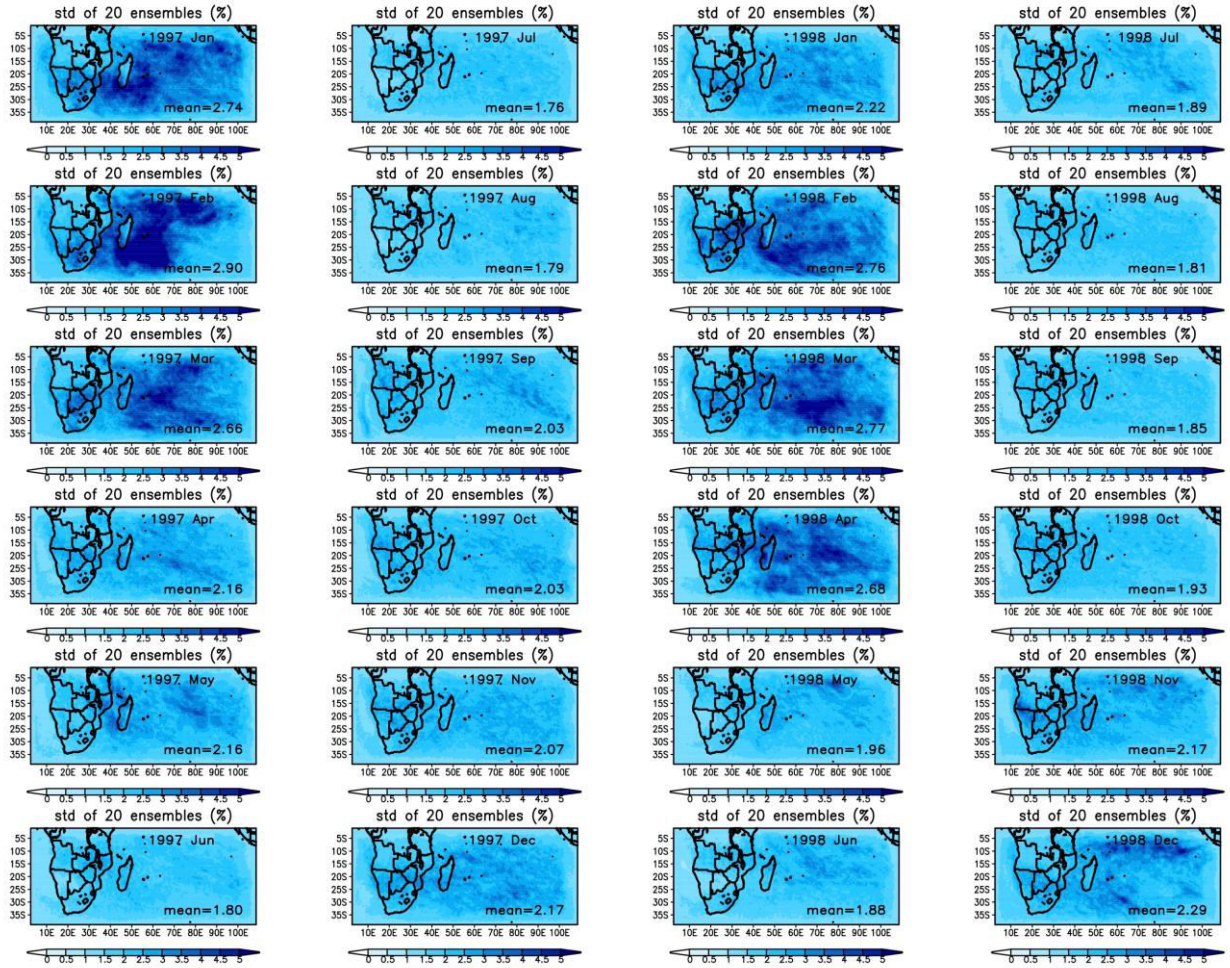

Fig. 4-11 Same as **Fig. 4-8**, but for CLT.

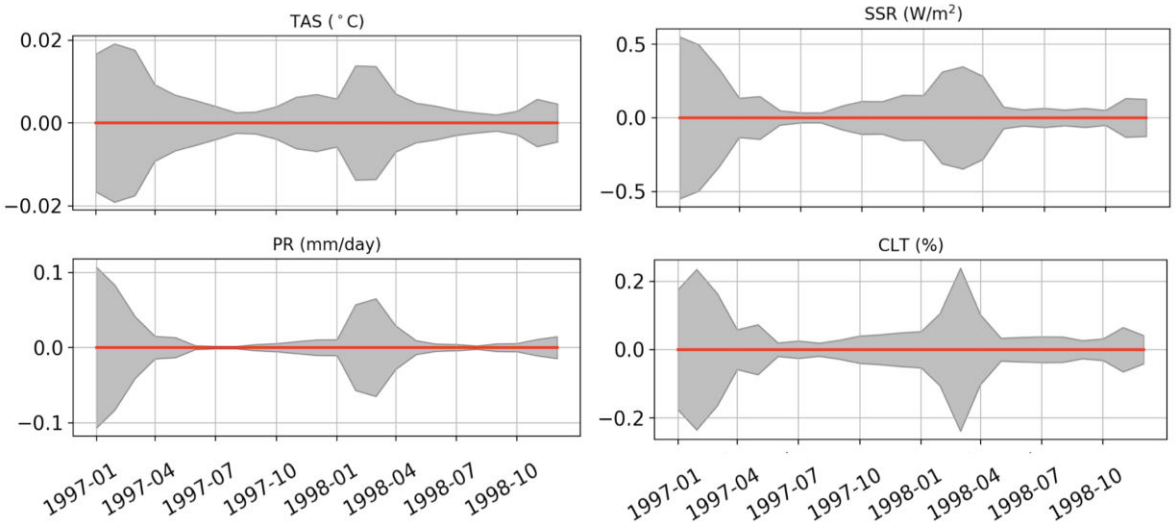

Fig. 4-12 Ensemble STD of TAS, PR, SSR and CLT spatial means during 1997-1998.

To summarize, internal variability of simulated annual means (and winter means) is of one order of magnitude smaller than the model bias. Thus, the possible dispersion of future projection is expected to be dominated by the model bias, and little imprinted by internal variability. However, in the case of simulated summer means, internal variability could play similar role as summer bias in contributing to the future projection dispersions.

4.4 Future projections of RegCM4 simulations

Projected future changes of TAS and SSR from RegCM4 are investigated (two variables directly related to solar electricity generation) in this section along with outputs from the driving GCMs, namely HadGEM2-ES and GFDL-ESM2M. Then electric potential (EP) is estimated according to the projections.

4.4.1 Surface temperature changes

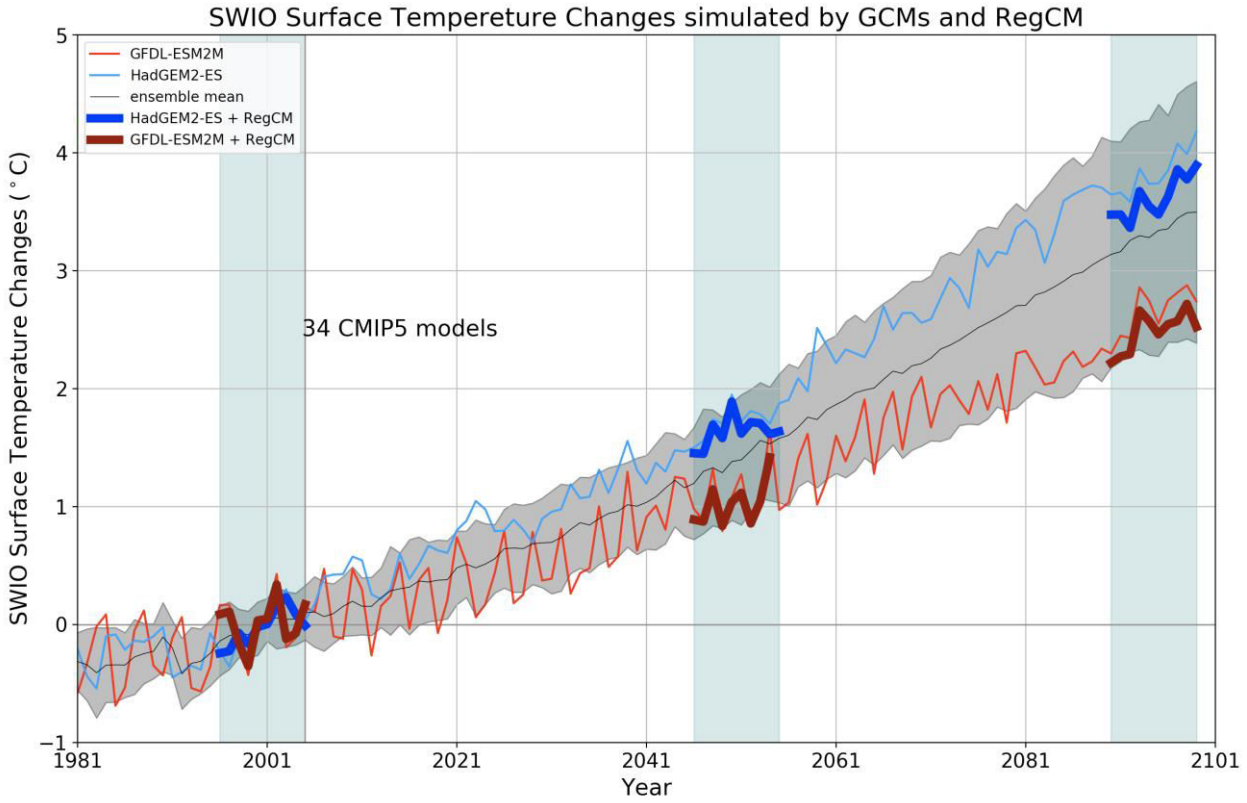

Fig. 4-13 Model simulated annual series of surface temperature (TAS) changes over the SA-SWIO. The mean values of 1996-2005 in each GCM and RegCM4 configuration are used as reference. Changes of surface temperature simulated by RegCM4 are in the three coloured simulation windows. Grey background indicates the 5-95% range of CMIP5 GCMs' dispersion, more information see section **2.3.4**.

Both of these two downscaling experiments show increasing surface temperature projections, with annual variations following the projections of their driving models. A trend to 2050 of about 1°C and to 2100 of about 3°C are projected. RegCM4 anticipates less temperature changes compared with their two driven GCMs, and the difference increases with time. The difference between RegCM4 outputs and the driving models (about 0.1°C) is larger than the model's internal variability (**Fig. 4-12**), and thus could be related to the model bias. Spatial patterns of trends to 2050/2100 are shown in **Fig. 4-14**.

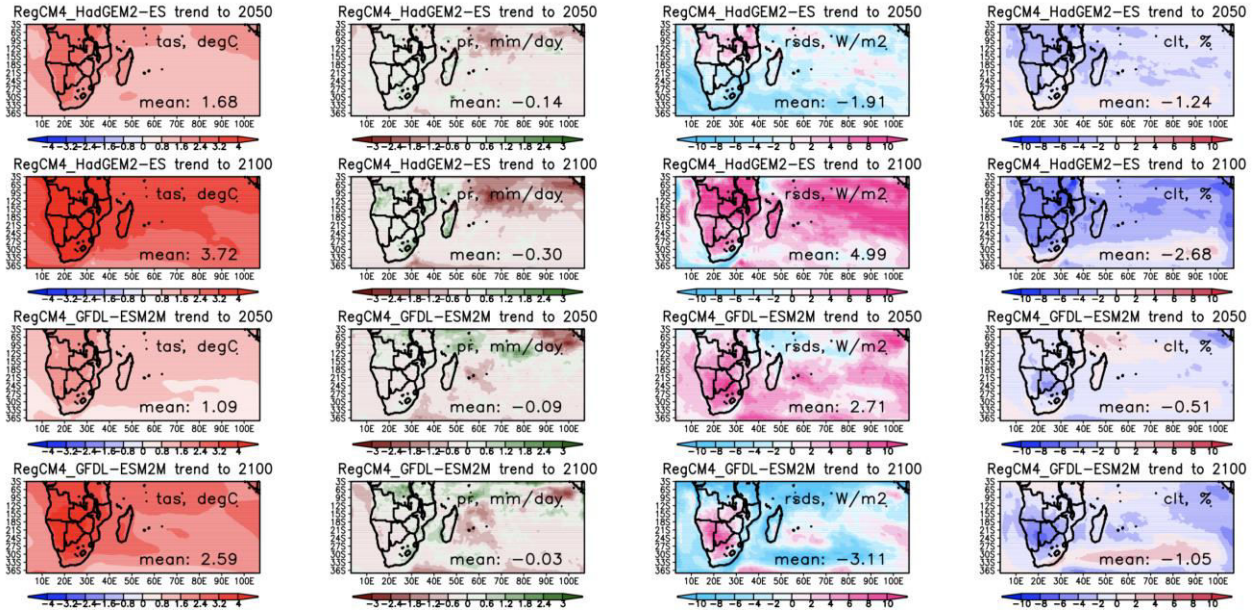

Fig. 4-14 Changes to 2050/2100 simulated by RegCM4 driven by HadGEM2-ES and GFLD-ESM2M in TAS, PR, SSR and CLT.

4.4.2 SSR changes

RegCM4 projections of SSR changes show higher variation then the driving GCMs and the CMIP5 ensemble (**Fig. 4-15**). The mean value of SSR changes is about ±2/±3 W/m^2 by 2050/2100, depending on the driving GCM. This is one order of magnitude larger than the magnitude of the model's internal variability (**Fig. 4-12**) but of the same order of magnitude than the model bias.

The signs of SSR changes are highly dependent on the driving GCM. HadGEM2-ES/GFDL-ESM2M forced RegCM4 simulation projects a mean decrease/increase of SSR to 2050, and a mean increase/decrease trend to 2100. It is evident from **Fig. 4-14** that the pattern of SSR changes is related to that of CLT.

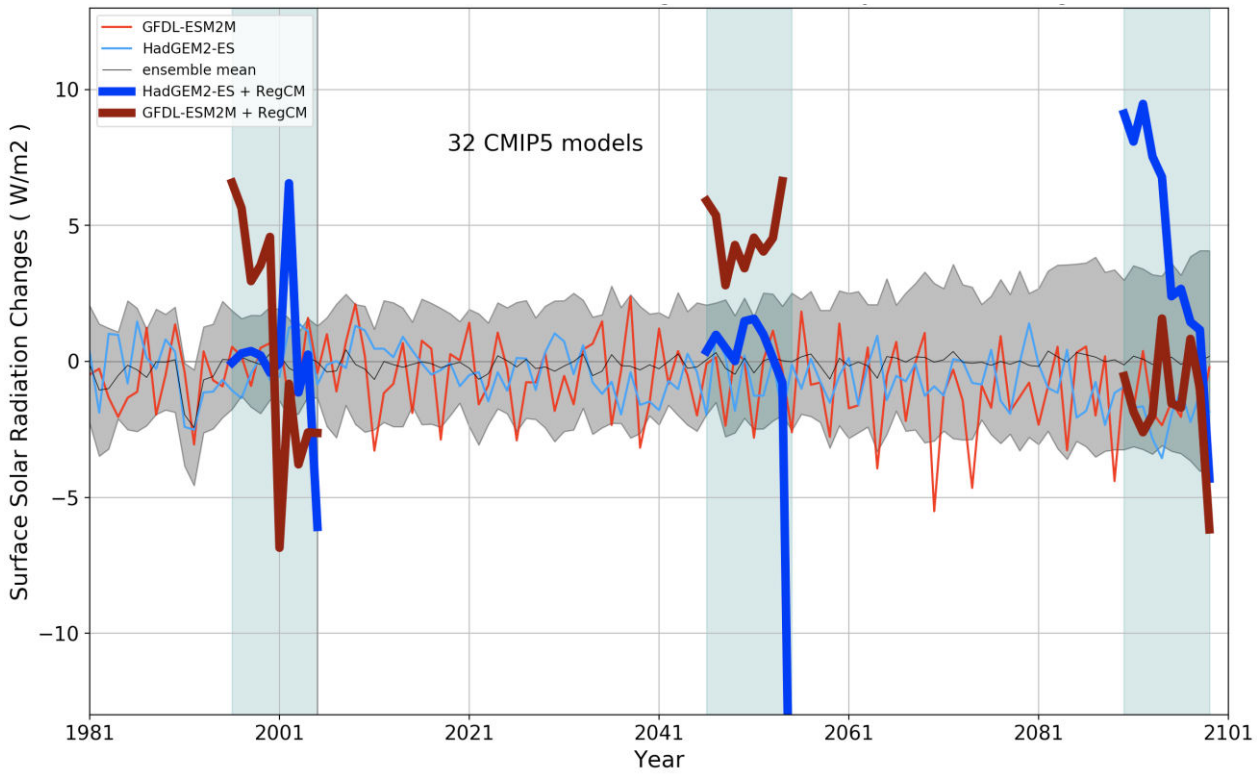

Fig. 4-15 Same as **Fig. 4-13**, but for SSR.

4.4.3 Electricity potential changes

Projections of Electricity Potential (EP) changes downscaled from these two driving GCMs is calculated using the same first-order estimation from Wild, Folini, Henschel, et al. (2015)**,** where EP increases with SSR and decreases with TAS (**Fig. 4-16**). RegCM4 simulations show different trends to 2050/2100 depending on the driving GCMs. In general, climate change has little impact on EP, with mean changes less than 2%.

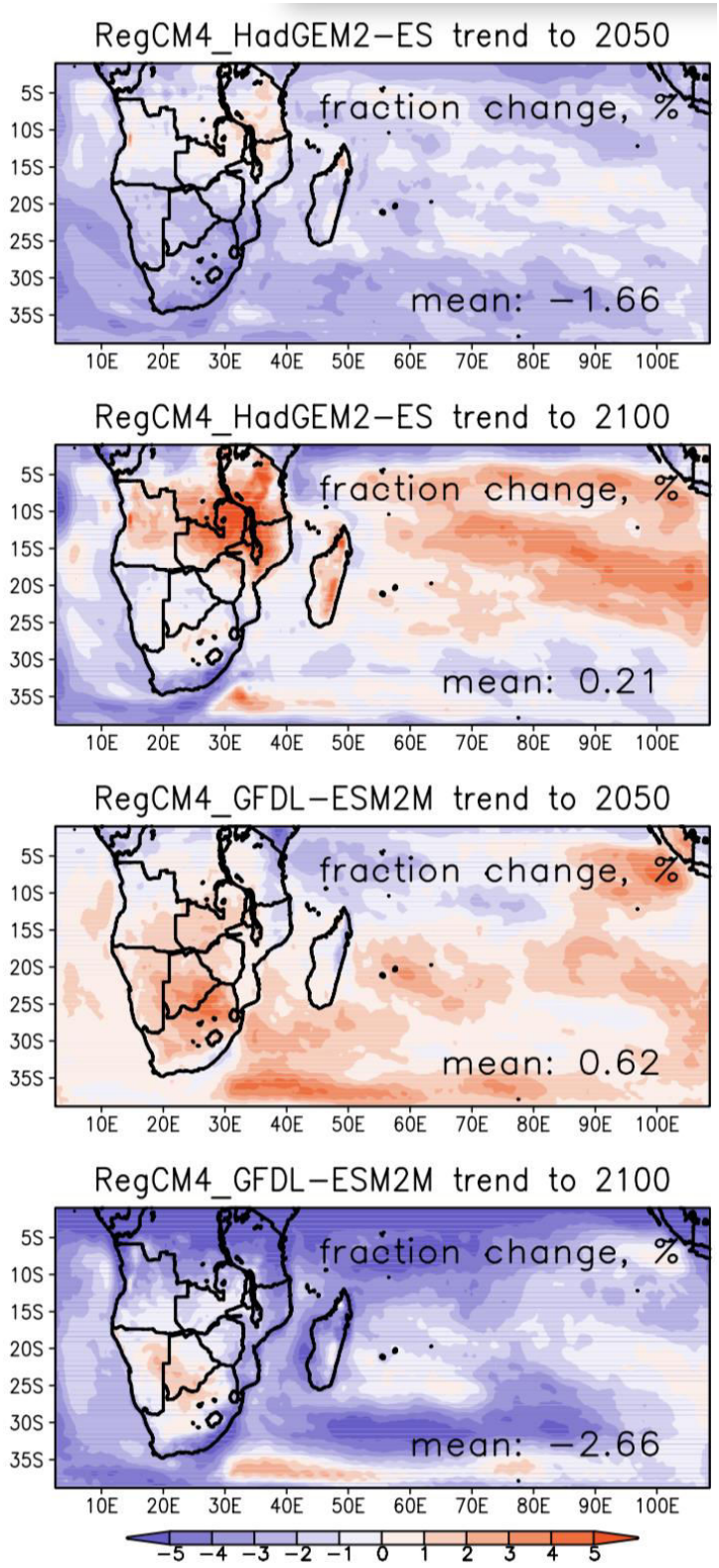

Fig. 4-16 Electricity Potential (EP) changes to 2050/2100 simulated by RegCM forced by HadGEM2-ES and GFDL-ESM2M.

4.5 Summary and conclusions of Chapter 4

In this chapter, a slice experiment conducted by RegCM4 driven by ERAINT and GCMs is discussed. This experiment consists of three temporal windows: a) the present 1996-2005; b) the future 2046-2055 and 2090-2099. Results indicate that:

1 RegCM4 simulates seasonal climatology quite well, however has a strong negative CLT bias when forced by ERAINT and GCMs.
2 To estimate internal variability of RegCM4, an ensemble experiment consisting of 20 simulations was forced by ERAINT during 1997-1998. Internal variability of simulated annual means (and winter means) is found to be of one order of magnitude smaller than the model bias. Thus, the possible dispersion of future projection is expected to be dominated by the model bias, and little imprinted by internal variability. However, in the case of simulated summer means, internal variability could play similar role as summer bias in contributing to the future projection dispersions.
3 RegCM4 simulations show different SSR changes signals when driven by different GCMs under RCP8.5 scenario, with an increase by 5 W/m^2 when driven by HadGEM2-ES and a decrease by -3 W/m^2 when driven by GFLD-ESM2M to the end of 21st century.
4 The bias pattern of CLT is correlated with that of SSR, which is physically reasonable because of the strong reflecting effect.
5 Electricity potential has been calculated using first order estimation. The trends indicate a change less then 2%.

The conducted slice simulation was taken mainly because of the limit of available computational resources for a requirement of long-term climate change impact study. Although there are several previous works using 10-year windows to estimate long-term climatology, e.g. Crook et al. (2011) and Gula and Peltier (2012), continuous simulations are the first choice because of better temporal coverage to capture inter-decadal variations. For solar energy application study, covering the near-term future is necessary when considering the life time of solar power equipment of 20-30 years. In this study, only two GCMs are downscaled to regional scale in a single RCP8.5 scenario. Understanding the role that boundary condition plays in downscaling process is a major concern for downscaling community. However, to isolate the impact of forcing data, a range of different boundary conditions has to be applied to particular RCMs, or one single forcing to drive several RCMs. In addition, at least another climate change scenario is needed to estimate the sensitivity to different forcings.

The study towards to a comprehensive knowledge of SSR changes in context of climate change is thus extended, using outputs from CORDEX-Africa program. As will be shown in Chapter 4, continuous outputs from 5 RCMs driven by 20 GCMs are analysed over southern Africa (SA)

domain under RCP4.5 and RCP8.5 based on the experience of modeling African climate in the climate modeling community.

5 Conclusion and Perspectives

OUTLINE:

5.1 Conclusion

Surface Solar Radiation (SSR) plays a prominent role in the climate system as it states a major energy exchange at the interface between the atmosphere, land, biosphere and ocean components. Changes in SSR have, therefore, the potential to significantly impact diverse aspects of the climate system, notably the socio-economic development of any nation (Wild, 2009). SSR changes over Southern Africa and the South West Indian Ocean (SA-SWIO) is currently not well documented.

The study analysised outputs from CORDEX-Africa. Over 100-year continuous outputs from 5 RCMs driven by 20 GCMs over southern Africa (SA) under RCP4.5 and RCP8.5 were analysed. Evaluation based on various references of this large ensemble has pointed out that:

- References from satellites retrievals and reanalyses compared well with ground-based measurements from Global Energy Balance Archive (GEBA), essentially located in the eastern part of SA (including Madagascar and Reunion Island). An overall overestimation of about 10 W/m^2 was found. The accuracy of these references is generally increasing with the latitude, with mean absolute bias from 30 W/m^2 near the equator to about 10 W/m^2 at about 30°S.

- GCMs generally overestimate SSR by about 1 W/m^2 (compensation of opposite biases over sub-regions of the domain) in austral summer and 7.5 W/m^2 in austral winter. RCMs ensemble mean shows underestimations of SSR in both seasons when driven by GCMs. This multi-model lower bias is dominated by the 4 simulations of CCLM4 and 10 of RCA4 models, where the negative biases are of up to -76 W/m^2 in summer and -32 W/m^2 in winter. RCMs ensemble has larger SSR uncertainty, because of large biases of particular RCM models (e.g. CCLM4 an RCA4) and not the internal variability as discussed above, compared with their driven GCMs ensemble.

- For individual RCM model, the SSR fields seem rather insensitive to the different forcings including ERA-Interim and GCMs, in line with previous finding over Europe (Bartók et al., 2016). One possible reason is that the GCMs' SSR is not directly introduced into the RCMs as forcing condition, leaving the latter to generate its own radiation budget with little limitation. Thus, the RCMs multi-model mean SSR bias shown in this study is probably due to the regional model itself and not due to the biases from their forcing GCMs. Since SSR, not like surface temperature or circulations, is not a direct forcing variable to the downscaling simulations, RCM has the potential to represent SSR in its own way.

- Simulated SSR change patterns are overall consistent with that in CLT as the finding from RegCM4 simulations.

- Multi-model mean projections of SSR change patterns by the GCMs and their embedded RCMs are fairly consistent. Also, an overall decrease in cloudiness over SA continent is consistently projected by both GCMs and RCMs under consideration, in contrast with previous findings in Europe (Bartók et al., 2016), where RCMs project cloudiness changes with different signs to their forcing GCMs.

- GCMs project, in their multimodel means, a statistically significant increase of SSR of about 8 W/m^2 in RCP4.5 and 12 W/m^2 in RCP8.5 by 2100 over Centre Southern Africa (SA-C) and a highly confident decreasing SSR over Eastern Equatorial Africa (EA-E) of about -5 W/m^2 in RCP4.5 and -10 W/m^2 in RCP8.5 during the DJF season. RCMs simulate SSR with statistical confidence over the similar area with a little spatial extension compared with GCMs, but the changes are in higher amplitude. The increase of SSR over SA-C is 18 W/m^2 in RCP8.5 by 2100, and the SSR decrease over EA-E is of about -10 W/m^2 in RCP4.5 and -20 W/m^2 in RCP8.5 by 2100. It resembles that RCMs are more sensitive to the forcing then their driven GCMs. However, in the JJA season an increase of SSR was found over EA-E of about 5 W/m^2 by 2100 under RCP4.5 and 10 W/m^2 under RCP8.5, the amplitudes are similar in GCMs and RCMs simulations.

- Significant cloudiness decrease was found over continent of SA for GCMs and consistently shown in RCMs.

- As expected in 2100, the larger SSR changes are found in the RCP8.5 than in the RCP4.5 scenario, with about 2.5 W/m^2 enhanced changes in GCMs and about 5 W/m^2 in RCMs.

- Total uncertainty of dynamical downscaling projection conducted by RCMs is dominated by the Internal Variability of climate system before 2050, and after that the scenario uncertainty and model uncertainty increase significantly and become comparable with or larger then that Internal Variability after about 2070.

To contribute to the proposed future project that aiming to further investigate SSR changes at local scale (~ 1km horizontal resolution) in Reunion Island and Mauritius Island, located in the South West Indian Ocean (SWIO), close to the broader of CORDEX-Africa domain, a slice downscaling experiment consisting of simulations covering three temporal windows: a) the present 1996-2005; b) the future 2046-2055 and 2090-2099 conducted with the Regional Climate Model (RCM) RegCM version 4, driven by 2 Global Climate Model (GCMs, HadGEM2-ES and GFDL-ESM2M) under the most pessimistic RCP8.5 scenario, over SA-SWIO were performed and evaluated as the first step of downscaling towards local scale. The model sensitivity to physical options and internal variability was notably assessed. It was found that:

- RegCM4 simulates seasonal climatology, surface air temperature and precipitation quite well, in spite of a strong negative CLT bias when forced by ERAINT and GCMs. Using an ensemble of RCMs (including RegCM3) from CORDEX-Africa, Kim et al. (2014) also found that the simulated cloudiness is not as reliable as precipitation or air temperature.

- Internal variability of RegCM4 simulated annual means and winter means (about 0.2 W/m^2) is of one order of magnitude smaller than the model bias compared with reference data (in range of 5-30 W/m^2). Thus, the dispersion of future projection is expected to be dominated by the model bias, and little impacted by internal variability. However, in the case of simulated summer means, internal variability could play similar role as summer bias in contributing to the future projection dispersions because they are in the same order.

- RegCM4 simulations show different SSR changes signals when driven by different GCMs under RCP8.5 scenario, with an increase by 5 W/m^2 when driven by HadGEM2-ES and a decrease by -3 W/m^2 when driven by GFLD-ESM2M to the end of 21st century.

- The bias pattern of CLT is correlated with that of SSR in line with previous works that highlighting the importance of CLT on SSR modeling (Bartók et al., 2016; Chiacchio et al., 2015; García-Díez et al., 2015; Jaeger et al., 2008; S Kothe & Ahrens, 2010; Steffen Kothe et al., 2011; Markovic et al., 2008; Zubler et al., 2011). It was also reported that the spread of SSR in GCM ensembles are likely related to the different way of handling clouds (Bartók et al., 2016).
- Electricity potential calculated using first order estimation indicates a change less then 2% to 2100 with respect to the present level.

The slice simulation was taken mainly because of the limit of available computational resources for a requirement of long-term climate change impact study. Although there are several previous

works using 10-year windows to estimate long-term climatology, e.g. Crook et al. (2011) and Gula and Peltier (2012), continuous simulations are the first choice because of better temporal coverage to capture inter-decadal variations.

5.2 Perspectives

The possible impact of climate change on Surface Solar Radiation is assessed based on a large ensemble from state-of-art regional and global models in the present study. Further research is still under perspective in the aspects relevant to SSR changes over Southern Africa and South West Indian Ocean (SA-SWIO).

First, the exact reason that explains SSR evolution is still not clear. The impact of cloudiness (not only cloud cover) and increased water vapor (atmosphere has enhanced water capacity with warmer air) on SSR changes has to be examined and predicted quantitatively. Second, the most RCMs use an aerosol climatology instead of interactive aerosols, mainly to reduce the calculation performance required. Implementation of more accurate aerosols would benefit in reducing simulated SSR bias and the multi-model dispersion. In addition, SSR is strongly correlated with local processes that change the convection and cloud characters, simulation at higher resolution, e.g. local scale (~ 1km) is necessary to detect SSR changes at finer spatial and temporal scales. At last, long-term trends of SSR are not clear over SA-SWIO because of lacking continuous robust observation with spatial coverage. And the ability of climate models to simulate these trends is the first to evaluate before investigating decadal variation of SSR over this particular region in future.

6 References

Adeniyi, M. O. (2014). Sensitivity of different convection schemes in RegCM4.0 for simulation of precipitation during the Septembers of 1989 and 1998 over West Africa. *Theoretical and Applied Climatology, 115*(1-2), 305-322. doi:Doi 10.1007/S00704-013-0881-5

Adler, R. F., Huffman, G. J., Chang, A., Ferraro, R., Xie, P.-P., Janowiak, J., Bolvin, D. (2003). The version-2 global precipitation climatology project (GPCP) monthly precipitation analysis (1979-present). *Journal of Hydrometeorology, 4*(6), 1147-1167.

Alexandri, G., Georgoulias, A., Zanis, P., Katragkou, E., Tsikerdekis, A., Kourtidis, K., & Meleti, C. (2015). On the ability of RegCM4 regional climate model to simulate surface solar radiation patterns over Europe: an assessment using satellite-based observations. *Atmospheric Chemistry and Physics, 15*(22), 13195-13216.

Allen, R., Norris, J., & Wild, M. (2013). Evaluation of multidecadal variability in CMIP5 surface solar radiation and inferred underestimation of aerosol direct effects over Europe, China, Japan, and India. *Journal of Geophysical Research: Atmospheres, 118*(12), 6311-6336.

Amiro, B., Stocks, B., Alexander, M., Flannigan, M., & Wotton, B. (2001). Fire, climate change, carbon and fuel management in the Canadian boreal forest. *International Journal of Wildland Fire, 10*(4), 405-413.

Anita, B. B. R., & Babypriya, B. (2009). Modelling, simulation and analysis of doubly fed induction generator for wind turbines. *Journal of Electrical Engineering, 60*(2), 79-85.

Attia, B., Heggarty, T., & Parikh, M. (2017). Global Solar Demand Monitor: Q2 2017. *Greentech Media*.

Bartók, B., Wild, M., Folini, D., Lüthi, D., Kotlarski, S., Schär, C., Imecs, Z. (2016). Projected changes in surface solar radiation in CMIP5 global climate models and in EURO-CORDEX regional climate models for Europe. *Climate Dynamics*, 1-19.

Boulard, D., Pohl, B., Crétat, J., Vigaud, N., & Pham-Xuan, T. (2013). Downscaling large-scale climate variability using a regional climate model: the case of ENSO over Southern Africa. *Climate Dynamics, 40*(5), 1141-1168. doi:10.1007/s00382-012-1400-6

Branker, K., Pathak, M., & Pearce, J. M. (2011). A review of solar photovoltaic levelized cost of electricity. *Renewable and Sustainable Energy Reviews, 15*(9), 4470-4482.

Brown, C., Greene, A., Block, P., & Giannini, A. (2008). Review of downscaling methodologies for Africa climate applications. *International Research Institute for Climate and Society Columbia University, 15*, 08-05.

Chiacchio, M., Solmon, F., Giorgi, F., Stackhouse, P., & Wild, M. (2015). Evaluation of the radiation budget with a regional climate model over Europe and inspection of dimming and brightening. *Journal of Geophysical Research: Atmospheres, 120*(5), 1951-1971.

Chou, M.-D., Suarez, M. J., Ho, C.-H., Yan, M. M., & Lee, K.-T. (1998). Parameterizations for cloud overlapping and shortwave single-scattering properties for use in general circulation and cloud ensemble models. *Journal of Climate, 11*(2), 202-214.

Christensen, J., Corti, S., Déqué, M., Heimann, D., Zemsch, M., Jones, R., Schär, C. (2004). *Prediction of regional scenarios and uncertainties for defining European climate change risks and effects (PRUDENCE)*. Retrieved from

Christensen OB, D. M., Christensen JH. (2006). The HIRHAM regional climate model version 5. . *DMI Tech, Rep 06–17:22*.

Church, J. A., & White, N. J. (2006). A 20th century acceleration in global sea-level rise. *Geophysical Research Letters, 33*(1).

Collins, W., Bellouin, N., Doutriaux-Boucher, M., Gedney, N., Hinton, T., Jones, C., Rae, J. (2008). Evaluation of the HadGEM2 model. *Hadley Cent. Tech. Note, 74*.

Conseil, C. (2010). Workshop to Compare Zooplankton Ecology and Methodologies between the Mediterranean and the North Atlantic (WKZEM).

Coppola, E., Giorgi, F., Mariotti, L., & Bi, X. (2012). RegT-Band: A tropical band version of RegCM4. *Climate Research, 2*, 115.

Crook, J. A., Jones, L. A., Forster, P. M., & Crook, R. (2011). Climate change impacts on future photovoltaic and concentrated solar power energy output. *Energy & Environmental Science, 4*(9), 3101-3109.

D'amato, G., & Cecchi, L. (2008). Effects of climate change on environmental factors in respiratory allergic diseases. *Clinical & Experimental Allergy, 38*(8), 1264-1274.

Dai, A. (2013). Increasing drought under global warming in observations and models. *Nature Climate Change, 3*(1), 52-58.

Davis, N., Bowden, J., Semazzi, F., Xie, L., & Onol, B. (2009). Customization of RegCM3 Regional Climate Model for Eastern Africa and a Tropical Indian Ocean Domain. *Journal of Climate, 22*(13), 3595-3616. doi:Doi 10.1175/2009jcli2388.1

Davy, R. J., & Troccoli, A. (2012). Interannual variability of solar energy generation in Australia. *Solar Energy, 86*(12), 3554-3560.

Demirbas, A. (2005). Potential applications of renewable energy sources, biomass combustion problems in boiler power systems and combustion related environmental issues. *Progress in energy and combustion science, 31*(2), 171-192.

Department of Energy. (2011). Department of Energy: Integrated Resource Plan for Electricity: 2010– 2030 (Revision 2 Final Report).

Dhainaut, J.-F., Claessens, Y.-E., Ginsburg, C., & Riou, B. (2003). Unprecedented heat-related deaths during the 2003 heat wave in Paris: consequences on emergency departments. *Critical Care, 8*(1), 1.

Dudley, B. (2004). BP World Energy Outlook 2004.

Dudley, B. (2016). BP Statistical Review of World Energy.

Dunne, J. P., John, J. G., Adcroft, A. J., Griffies, S. M., Hallberg, R. W., Shevliakova, E., Harrison, M. J. (2012). GFDL's ESM2 global coupled climate-carbon Earth System Models. Part I: Physical formulation and baseline simulation characteristics. *Journal of Climate, 25*(19), 6646-6665.

Eberhard, A., Rosnes, O., Shkaratan, M., & Vennemo, H. (2011). Africa's Power Infrastructure. *The World Bank*.

EIA. (2016). International Energy Outlook 2016.

El-Fadel, M., Chedid, R., Zeinati, M., & Hmaidan, W. (2003). Mitigating energy-related GHG emissions through renewable energy. *Renewable Energy, 28*(8), 1257-1276.

Ellabban, O., Abu-Rub, H., & Blaabjerg, F. (2014). Renewable energy resources: Current status, future prospects and their enabling technology. *Renewable and Sustainable Energy Reviews, 39*, 748-764.

Fant, C., Schlosser, C. A., & Strzepek, K. (2015). The impact of climate change on wind and solar resources in southern Africa. *Applied Energy*.
Farneti, R. (2017). Modelling interdecadal climate variability and the role of the ocean. *Wiley Interdisciplinary Reviews: Climate Change, 8*(1).
Feser, F., Rockel, B., von Storch, H., Winterfeldt, J., & Zahn, M. (2011). Regional climate models add value to global model data: a review and selected examples. *Bulletin of the American Meteorological Society, 92*(9), 1181.
Finger, D., Heinrich, G., Gobiet, A., & Bauder, A. (2012). Projections of future water resources and their uncertainty in a glacierized catchment in the Swiss Alps and the subsequent effects on hydropower production during the 21st century. *Water Resources Research, 48*(2).
FJ., L. (2010). EDF SEI et les systèmes énergétiques dans les îles.
Flannigan, M., Stocks, B., Turetsky, M., & Wotton, M. (2009). Impacts of climate change on fire activity and fire management in the circumboreal forest. *Global Change Biology, 15*(3), 549-560.
Flato, G., Marotzke, J., Abiodun, B., Braconnot, P., Chou, S. C., Collins, W. J., Eyring, V. (2013). Evaluation of Climate Models. In: Climate Change 2013: The Physical Science Basis. Contribution of Working Group I to the Fifth Assessment Report of the Intergovernmental Panel on Climate Change. *Climate Change 2013, 5*, 741-866.
Fotso-Nguemo, T. C., Vondou, D. A., Pokam, W. M., Djomou, Z. Y., Diallo, I., Haensler, A., Tchawoua, C. (2017). On the added value of the regional climate model REMO in the assessment of climate change signal over Central Africa. *Climate Dynamics, 49*(11-12), 3813-3838. doi:10.1007/s00382-017-3547-7
Fouillet, A., Rey, G., Laurent, F., Pavillon, G., Bellec, S., Guihenneuc-Jouyaux, C., Hémon, D. (2006). Excess mortality related to the August 2003 heat wave in France. *International archives of occupational and environmental health, 80*(1), 16-24.
Gaetani, M., Huld, T., Vignati, E., Monforti-Ferrario, F., Dosio, A., & Raes, F. (2014). The near future availability of photovoltaic energy in Europe and Africa in climate-aerosol modeling experiments. *Renewable and Sustainable Energy Reviews, 38*, 706-716.
Gaetani, M., Vignati, E., Monforti-Ferrario, F., Huld, T., Dosio, A., & Raes, F. (2015). Climate modelling and renewable energy resource assessment. *JRC Scientific and Policy Report EUR XXXXX EN*.
García-Díez, M., Fernández, J., & Vautard, R. (2015). An RCM multi-physics ensemble over Europe: multi-variable evaluation to avoid error compensation. *Climate Dynamics, 45*(11-12), 3141-3156.
Gilgen, H., Roesch, A., Wild, M., & Ohmura, A. (2009). Decadal changes in shortwave irradiance at the surface in the period from 1960 to 2000 estimated from Global Energy Balance Archive Data. *Journal of Geophysical Research: Atmospheres, 114*(D10).
Gilgen, H., Wild, M., & Ohmura, A. (1998). Means and trends of shortwave irradiance at the surface estimated from global energy balance archive data. *Journal of Climate, 11*(8), 2042.
Giorgi, F., Coppola, E., Solmon, F., Mariotti, L., Sylla, M. B., Bi, X., Brankovic, C. (2012). RegCM4: model description and preliminary tests over multiple CORDEX domains. *Climate Research, 52*(1), 7-29. doi:Doi 10.3354/Cr01018
Giorgi, F., Jones, C., & Asrar, G. R. (2009). Addressing climate information needs at the regional level: the CORDEX framework. *World Meteorological Organization (WMO) Bulletin, 58*(3), 175.

Giorgi, F., & Mearns, L. O. (2002). Calculation of average, uncertainty range, and reliability of regional climate changes from AOGCM simulations via the "reliability ensemble averaging"(REA) method. *Journal of Climate, 15*(10), 1141-1158.

Granovskii, M., Dincer, I., & Rosen, M. A. (2007). Greenhouse gas emissions reduction by use of wind and solar energies for hydrogen and electricity production: economic factors. *International Journal of Hydrogen Energy, 32*(8), 927-931.

Gula, J., & Peltier, W. R. (2012). Dynamical Downscaling over the Great Lakes Basin of North America Using the WRF Regional Climate Model: The Impact of the Great Lakes System on Regional Greenhouse Warming. *Journal of Climate, 25*(21), 7723-7742. doi:10.1175/jcli-d-11-00388.1

Gunderson, I., Goyette, S., Gago-Silva, A., Quiquerez, L., & Lehmann, A. (2015). Climate and land-use change impacts on potential solar photovoltaic power generation in the Black Sea region. *Environmental Science & Policy, 46*, 70-81.

Gupta, S., Stackhouse Jr, P., Cox, S., Mikovitz, J., & Zhang, T. (2006). Surface radiation budget project completes 22-year data set. *GEWEX News, 16*(4), 12-13.

Gupta, S. K., Ritchey, N. A., Wilber, A. C., Whitlock, C. H., Gibson, G. G., & Stackhouse Jr, P. W. (1999). A climatology of surface radiation budget derived from satellite data. *Journal of Climate, 12*(8), 2691-2710.

Guttler, I., Brankovic, C., O'Brien, T. A., Coppola, E., Grisogono, B., & Giorgi, F. (2014). Sensitivity of the regional climate model RegCM4.2 to planetary boundary layer parameterisation. *Climate Dynamics, 43*(7-8), 1753-1772. doi:Doi 10.1007/S00382-013-2003-6

Halder, S., Dirmeyer, P. A., & Saha, S. K. (2015). Sensitivity of the mean and variability of Indian summer monsoon to land surface schemes in RegCM4: Understanding coupled land - atmosphere feedbacks. *Journal of Geophysical Research: Atmospheres, 120*(18), 9437-9458.

Hansen, J., Nazarenko, L., Ruedy, R., Sato, M., Willis, J., Del Genio, A., Tausnev, N. (2005). Earth's energy imbalance: Confirmation and implications. *Science, 308*(5727), 1431-1435. doi:Doi 10.1126/Science.1110252

Harris, I., Jones, P., Osborn, T., & Lister, D. (2014). Updated high-resolution grids of monthly climatic observations–the CRU TS3. 10 Dataset. *International Journal of Climatology, 34*(3), 623-642.

Hawkins, E., & Sutton, R. (2009). The Potential to Narrow Uncertainty in Regional Climate Predictions. *Bulletin of the American Meteorological Society, 90*(8), 1095-1108. doi:10.1175/2009bams2607.1

Hawkins, E., & Sutton, R. (2011). The potential to narrow uncertainty in projections of regional precipitation change. *Climate Dynamics, 37*(1), 407-418. doi:10.1007/s00382-010-0810-6

Heidari, N., & Pearce, J. M. (2016). A review of greenhouse gas emission liabilities as the value of renewable energy for mitigating lawsuits for climate change related damages. *Renewable and Sustainable Energy Reviews, 55*, 899-908.

Hou, Y., Moorthi, S., & Campana, K. (2002). *Parameterization of solar radiation transfer in the NCEP models. NCEP Off*. Retrieved from

Huld, T., Šúri, M., & Dunlop, E. D. (2008). Geographical variation of the conversion efficiency of crystalline silicon photovoltaic modules in Europe. *Progress in photovoltaics: Research and applications, 16*(7), 595-607.

Hussain, M., Rahman, L., & Rahman, M. M. (1999). Technical note: techniques to obtain improved predictions of global radiation from sunshine duration. *Renewable Energy, 18*(2), 263-275.
IEA, O. (2008). Energy technology perspectives. In: Paris.
IPCC. (2007a). Climate change 2007: synthesis report. *IPCC, Geneva, Switzerland*.
IPCC. (2007b). Impacts, adaptation and vulnerability. Contribution of working group II to the fourth assessment report of the Intergovernmental Panel on Climate Change. 2007. *ML, Canziani, OF, Palutikof, JP, van der Linden, PJ, Hanson, CE (eds) Cambridge University Press, Cambridge*.
IPCC. (2013). The physical science basis. Contribution of working group I to the fifth assessment report of the intergovernmental panel on climate change. *K., Tignor, M., Allen, SK, Boschung, J., Nauels, A., Xia, Y., Bex, V., Midgley, PM, Eds*, 1535.
IRENA. (2016). IRENA Renewable Energy and Jobs – Annual Review 2016.
Jacob, D., Elizalde, A., Haensler, A., Hagemann, S., Kumar, P., Podzun, R., Sieck, K. (2012). Assessing the transferability of the regional climate model REMO to different coordinated regional climate downscaling experiment (CORDEX) regions. *Atmosphere, 3*(1), 181-199.
Jaeger, E. B., Anders, I., Luethi, D., Rockel, B., Schaer, C., & Seneviratne, S. I. (2008). Analysis of ERA40-driven CLM simulations for Europe. *Meteorologische Zeitschrift, 17*(4), 349-367.
Jerez, S., Tobin, I., Vautard, R., Montávez, J. P., López-Romero, J. M., Thais, F., Déqué, M. (2015). The impact of climate change on photovoltaic power generation in Europe. *Nature communications, 6*.
Jogleka, N. R., & Graber-Lopez, E. S. (2008). *A countdown towards solar power at grid parity: policy analysis based on the evolution of price-performance.* Paper presented at the Proceedings of 2008 ISDSI international conference.
Jones, C., Giorgi, F., & Asrar, G. (2011). The Coordinated Regional Downscaling Experiment: CORDEX, an international downscaling link to CMIP5. *Clivar Exchanges, 56*(16), 34-40.
Jordan, D. C., & Kurtz, S. R. (2013). Photovoltaic degradation rates—an analytical review. *Progress in photovoltaics: Research and applications, 21*(1), 12-29.
Journée, M., & Bertrand, C. (2010). Improving the spatio-temporal distribution of surface solar radiation data by merging ground and satellite measurements. *Remote Sensing of Environment, 114*(11), 2692-2704.
Junfeng, L., Lohani, B., Galàn, E. M., Monga, P., Mubiru, P., Nakicenovic, N., Pelosse, H. (2009). Renewable Energy Policy Network for the 21st Century.
Karlsson, K.-G., Anttila, K., Trentmann, J., Stengel, M., Meirink, J. F., Devasthale, A., Sedlar, J. (2017). CLARA-A2: the second edition of the CM SAF cloud and radiation data record from 34 years of global AVHRR data. *Atmospheric Chemistry and Physics, 17*(9), 5809.
Kay, J., Deser, C., Phillips, A., Mai, A., Hannay, C., Strand, G., Edwards, J. (2015). The Community Earth System Model (CESM) large ensemble project: A community resource for studying climate change in the presence of internal climate variability. *Bulletin of the American Meteorological Society, 96*(8), 1333-1349.
Kgatuke, M., Landman, W., Beraki, A., & Mbedzi, M. (2008). The internal variability of the RegCM3 over South Africa. *International Journal of Climatology, 28*(4), 505-520.

Kim, J., Waliser, D. E., Mattmann, C. A., Goodale, C. E., Hart, A. F., Zimdars, P. A., Hewitson, B. (2014). Evaluation of the CORDEX-Africa multi-RCM hindcast: systematic model errors. *Climate Dynamics, 42*(5-6), 1189-1202.

Kirkegaard, J. F., Hanemann, T., Weischer, L., & Miller, M. (2010). Toward a sunny future? Global integration in the solar PV industry. *Peterson institute for international economics working paper*(10-6).

Kishore, A., Prasad, R., & Karan, B. (2006). *Matlab simulink based DQ modeling and dynamic characteristics of three phase self excited induction generator.* Paper presented at the Progress in Electromagnetics Research Symposium, Cambridge, USA.

Kothe, S., & Ahrens, B. (2010). On the radiation budget in regional climate simulations for West Africa. *Journal of Geophysical Research: Atmospheres, 115*(D23).

Kothe, S., Dobler, A., Beck, A., & Ahrens, B. (2011). The radiation budget in a regional climate model. *Climate Dynamics, 36*(5-6), 1023-1036.

Li, P. (2015). Temporal and Spatial Variability of Surface Solar Radiation over the South-West Indian Ocean and Reunion Island : Regional Climate Modeling.

Li, P., Morel, B., Bessafi, M., Solmon, F., & Chiacchio, M. (2013). *The radiation budget in the regional climate model RegCM4: simulation results from two different radiative schemes over the south-western Indian Ocean.* Paper presented at the EGU General Assembly 2013.

Li, P., Morel, B., Solmon, F., Chiacchio, M., & Bessafi, M. (2014). Radiation Budget in the Regional Climate Model RegCM4: Simulation Results from Two Different Radiative Schemes over the South West Indian Ocean.

Liepert, B. G. (2002). Observed reductions of surface solar radiation at sites in the United States and worldwide from 1961 to 1990. *Geophysical Research Letters, 29*(10).

Liepert, B. G., Feichter, J., Lohmann, U., & Roeckner, E. (2004). Can aerosols spin down the water cycle in a warmer and moister world? *Geophysical Research Letters, 31*(6).

Lohmann, U., & Feichter, J. (2004). Global indirect aerosol effects: a review. *Atmospheric Chemistry and Physics Discussions, 4*(6), 7561-7614.

Longo, A., Markandya, A., & Petrucci, M. (2008). The internalization of externalities in the production of electricity: willingness to pay for the attributes of a policy for renewable energy. *Ecological Economics, 67*(1), 140-152.

Markovic, M., Jones, C. G., Vaillancourt, P. A., Paquin, D., Winger, K., & Paquin-Ricard, D. (2008). An evaluation of the surface radiation budget over North America for a suite of regional climate models against surface station observations. *Climate Dynamics, 31*(7-8), 779-794.

Martinot, E. (2005). Renewables 2005: Global status report. *REN21 Renewable Energy Policy Network/Worldwatch Institute*, 14.

Martinot, E. (2013). Renewables. Global futures report 2013.

McCormick, M. P., Thomason, L. W., & Trepte, C. R. (1995). Atmospheric effects of the Mt Pinatubo eruption. *Nature, 373*(6513), 399-404.

Menon, S., Hansen, J., Nazarenko, L., & Luo, Y. (2002). Climate effects of black carbon aerosols in China and India. *Science, 297*(5590), 2250-2253.

Mimura, N., Nurse, L., McLean, R., Agard, J., Briguglio, L., Lefale, P., Sem, G. (2007). Small islands. *Climate change, 16*, 687-716.

Ministry of Mines and Energy of Namibia. (2016). National Renewable Energy Policy for Namibia.

Ministry of Renewable Energy of Mauritius. (2009). Ministry of Renewable Energy, Republic of Mauritius Long-Term Energy Strategy 2009 – 2025.

Mlawer, E. J., Taubman, S. J., Brown, P. D., Iacono, M. J., & Clough, S. A. (1997). Radiative transfer for inhomogeneous atmospheres: RRTM, a validated correlated-k model for the longwave. *Journal of Geophysical Research: Atmospheres, 102*(D14), 16663-16682.

Monforti, F., Huld, T., Bódis, K., Vitali, L., D'isidoro, M., & Lacal-Arántegui, R. (2014). Assessing complementarity of wind and solar resources for energy production in Italy. A Monte Carlo approach. *Renewable Energy, 63*, 576-586.

Moss, R., Babiker, W., Brinkman, S., Calvo, E., Carter, T., Edmonds, J., Hibbard, K. (2008). Towards New Scenarios for the Analysis of Emissions: Climate Change, Impacts and Response Strategies. In: Intergovernmental Panel on Climate Change Secretariat (IPCC).

Moss, R. H., Edmonds, J. A., Hibbard, K. A., Manning, M. R., Rose, S. K., Van Vuuren, D. P., Kram, T. (2010). The next generation of scenarios for climate change research and assessment. *Nature, 463*(7282), 747-756.

Müller, B., Wild, M., Driesse, A., & Behrens, K. (2014). Rethinking solar resource assessments in the context of global dimming and brightening. *Solar Energy, 99*, 272-282.

Nicholls, R. J., Hoozemans, F. M., & Marchand, M. (1999). Increasing flood risk and wetland losses due to global sea-level rise: regional and global analyses. *Global Environmental Change, 9*, S69-S87.

Nogherotto, R., Tompkins, A. M., Giuliani, G., Coppola, E., & Giorgi, F. (2016). Numerical framework and performance of the new multiple-phase cloud microphysics scheme in RegCM4. 5: precipitation, cloud microphysics, and cloud radiative effects. *Geoscientific Model Development, 9*(7), 2533-2547.

O'Brien, T. A., Chuang, P. Y., Sloan, L. C., Faloona, I. C., & Rossiter, D. L. (2012). Coupling a new turbulence parametrization to RegCM adds realistic stratocumulus clouds. *Geoscientific Model Development, 5*(4), 989-1008. doi:Doi 10.5194/Gmd-5-989-2012

OER. (2010). Bilan Energétique de l'ile de la Réunion 2009 – version technique; 2010.

Ohmura, A. (2009). Observed decadal variations in surface solar radiation and their causes. *Journal of Geophysical Research: Atmospheres, 114*(D10).

Ohmura, A., Gilgen, H., Hegner, H., Müller, G., Wild, M., Dutton, E. G., Heimo, A. (1998). Baseline Surface Radiation Network (BSRN/WCRP): New precision radiometry for climate research. *Bulletin of the American Meteorological Society, 79*(10), 2115-2136.

Ohmura, A., Gilgen, H. J., & Wild, M. (1989). *Global Energy Balance Archive, GEBA*: Geographisches Institut, Eidgenössische Technische Hochschule Zürich.

Ohmura, A., & Wild, M. (2002). Is the hydrological cycle accelerating? *Science, 298*(5597), 1345-1346.

Panagea, I. S., Tsanis, I. K., Koutroulis, A. G., & Grillakis, M. G. (2014). Climate Change Impact on Photovoltaic Energy Output: The Case of Greece. *Advances in Meteorology, 2014*.

Panitz, H.-J., Berg, P., Schädler, G., & Fosser, G. (2012). *Modelling Near Future Regional Climate Change for Germany and Africa*, Berlin, Heidelberg.

Panitz, H.-J., Dosio, A., Büchner, M., Lüthi, D., & Keuler, K. (2014). COSMO-CLM (CCLM) climate simulations over CORDEX-Africa domain: analysis of the ERA-Interim driven simulations at 0.44 and 0.22 resolution. *Climate Dynamics, 42*(11-12), 3015-3038.

Parry, M., Rosenzweig, C., & Livermore, M. (2005). Climate change, global food supply and risk of hunger. *Philosophical Transactions of the Royal Society of London B: Biological Sciences, 360*(1463), 2125-2138.
Pasicko, R., Branković, Č., & Šimić, Z. (2012). Assessment of climate change impacts on energy generation from renewable sources in Croatia. *Renewable Energy, 46*, 224-231.
Pearce, J. M. (2002). Photovoltaics—a path to sustainable futures. *Futures, 34*(7), 663-674.
Perez, R., & Hoff, T. (2013). Solar resource variability. *Solar Energy Forecasting and Resource Assessment; Elsevier: Philadelphia, PA, USA*, 133-148.
Pessacg, N. L., Solman, S. A., Samuelsson, P., Sanchez, E., Marengo, J., Li, L., Jacob, D. (2014). The surface radiation budget over South America in a set of regional climate models from the CLARIS-LPB project. *Climate Dynamics, 43*(5-6), 1221-1239.
Peterson, T. (1995). Evaporation losing its strength. *Nature, 377*, 687-688.
Pfeifroth, U., Kothe, S., Müller, R., Trentmann, J., Hollmann, R., Fuchs, P., & Werscheck, M. (2017). Surface Radiation Data Set - Heliosat (SARAH) - Edition 2. Satellite Application Facility on Climate Monitoring. doi:10.5676/EUM_SAF_CM/SARAH/V002.
Pohl, B., Macron, C., & Monerie, P.-A. (2017). Fewer rainy days and more extreme rainfall by the end of the century in Southern Africa. *Scientific Reports, 7*.
Posselt, R., Mueller, R., Stöckli, R., & Trentmann, J. (2012). Remote sensing of solar surface radiation for climate monitoring—the CM-SAF retrieval in international comparison. *Remote Sensing of Environment, 118*, 186-198.
Poumadere, M., Mays, C., Le Mer, S., & Blong, R. (2005). The 2003 heat wave in France: dangerous climate change here and now. *Risk analysis, 25*(6), 1483-1494.
Power, H., & Mills, D. (2005). Solar radiation climate change over Southern Africa and an assessment of the radiative impact of volcanic eruptions. *International Journal of Climatology, 25*(3), 295-318.
Praene, J. P., David, M., Sinama, F., Morau, D., & Marc, O. (2012). Renewable energy: Progressing towards a net zero energy island, the case of Reunion Island. *Renewable and Sustainable Energy Reviews, 16*(1), 426-442.
Price, S., & Margolis, R. (2010). Solar technologies market report. *Energy Efficiency and Renewable Energy (NREL), Report No. DOE/GO-102010-2867*.
Primer, G. (2009). Renewable Energy Policy Network for the 21st Century.
Ramanathan, V., Chung, C., Kim, D., Bettge, T., Buja, L., Kiehl, J., Wild, M. (2005). Atmospheric brown clouds: Impacts on South Asian climate and hydrological cycle. *Proc Natl Acad Sci U S A, 102*(15), 5326-5333.
Ramanathan, V., Crutzen, P., Kiehl, J., & Rosenfeld, D. (2001). Aerosols, climate, and the hydrological cycle. *Science, 294*(5549), 2119-2124.
Reich, N. H., Mueller, B., Armbruster, A., Sark, W. G., Kiefer, K., & Reise, C. (2012). Performance ratio revisited: is PR> 90% realistic? *Progress in photovoltaics: Research and applications, 20*(6), 717-726.
Remund, J., & Müller, S. C. (2010). *Trends in global radiation between 1950 and 2100.* Paper presented at the 10th EMS Annual Meeting, 10th European Conference on Applications of Meteorology (ECAM) Abstracts, held Sept.
Robock, A. (2000). Volcanic eruptions and climate. *Reviews of Geophysics, 38*(2), 191-219.

Robock, A., Mu, M., Vinnikov, K., Trofimova, I. V., & Adamenko, T. I. (2005). Forty-five years of observed soil moisture in the Ukraine: No summer desiccation (yet). *Geophysical Research Letters, 32*(3).
Rockel, B., Will, A., & Hense, A. (2008). The regional climate model COSMO-CLM (CCLM). *Meteorologische Zeitschrift, 17*(4), 347-348.
Rossow, W. B., & Schiffer, R. A. (1999). Advances in understanding clouds from ISCCP. *Bulletin of the American Meteorological Society, 80*(11), 2261-2287.
Rotstayn, L. D., & Lohmann, U. (2002). Tropical rainfall trends and the indirect aerosol effect. *Journal of Climate, 15*(15), 2103-2116.
RSA. (2010). RSA (Republic of South Africa) Reducing Greenhouse Gas Emissions: The Carbon Tax Option.
Saha, S., Moorthi, S., Pan, H.-L., Wu, X., Wang, J., Nadiga, S., Behringer, D. (2010). The NCEP climate forecast system reanalysis. *Bulletin of the American Meteorological Society, 91*(8), 1015-1057.
Salby, M. L. (1996). *Fundamentals of atmospheric physics* (Vol. 61): Academic press.
Samuelsson, P., Jones, C. G., Willén, U., Ullerstig, A., Gollvik, S., Hansson, U., Wyser, K. (2011). The Rossby Centre Regional Climate model RCA3: model description and performance. *Tellus Series a-Dynamic Meteorology and Oceanography, 63*(1), 4-23.
Schmidhuber, J., & Tubiello, F. N. (2007). Global food security under climate change. *Proceedings of the National Academy of Sciences, 104*(50), 19703-19708.
Schneider, T., Bischoff, T., & Haug, G. H. (2014). Migrations and dynamics of the intertropical convergence zone. *Nature, 513*(7516), 45-54.
Shearer, C. (2011). *Kivalina: a climate change story*: Haymarket Books.
Sims, R. (2004). Renewable energy: a response to climate change. *Solar Energy, 76*(1), 9-17.
Sims, R. E., Rogner, H.-H., & Gregory, K. (2003). Carbon emission and mitigation cost comparisons between fossil fuel, nuclear and renewable energy resources for electricity generation. *Energy Policy, 31*(13), 1315-1326.
Skoczek, A., Sample, T., & Dunlop, E. D. (2009). The results of performance measurements of field-aged crystalline silicon photovoltaic modules. *Progress in photovoltaics: Research and applications, 17*(4), 227-240.
Solmon, F., Giorgi, F., & Liousse, C. (2006). Aerosol modelling for regional climate studies: application to anthropogenic particles and evaluation over a European/African domain. *Tellus B, 58*(1), 51-72.
Soni, V., Pandithurai, G., & Pai, D. (2012). Evaluation of long-term changes of solar radiation in India. *International Journal of Climatology, 32*(4), 540-551.
Southern African Power Pool. (2012). Southern African Power Pool Annual Report 2001/2. *Harare: Southern Africa Power Pool*.
Stern, N. H., Peters, S., Bakhshi, V., Bowen, A., Cameron, C., Catovsky, S., Edmonson, N. (2006). *Stern Review: The economics of climate change* (Vol. 30): Cambridge University Press Cambridge.
Streets, D. G., Yan, F., Chin, M., Diehl, T., Mahowald, N., Schultz, M., Yu, C. (2009). Anthropogenic and natural contributions to regional trends in aerosol optical depth, 1980–2006. *Journal of Geophysical Research: Atmospheres, 114*(D10).

Sylla, M., Diallo, I., & Pal, J. (2013). West African monsoon in state-of-the-science regional climate models. *Climate Variability—Regional and Thematic Patterns, 10*, 55140.
Sylla, M., Giorgi, F., Coppola, E., & Mariotti, L. (2013). Uncertainties in daily rainfall over Africa: assessment of gridded observation products and evaluation of a regional climate model simulation. *International Journal of Climatology, 33*(7), 1805-1817.
Sylla, M. B., Coppola, E., Mariotti, L., Giorgi, F., Ruti, P., Dell'Aquila, A., & Bi, X. (2010). Multiyear simulation of the African climate using a regional climate model (RegCM3) with the high resolution ERA-interim reanalysis. *Climate Dynamics, 35*(1), 231-247.
Tang, C., Morel, B., Wild, M., Pohl, B., Abiodun, B., & Bessafi, M. (2018). Numerical simulation of surface solar radiation over Southern Africa. Part 1: Evaluation of regional and global climate models. *Climate Dynamics*. doi:10.1007/s00382-018-4143-1
Tang, C., Morel, B., Wild, M., Pohl, B., Abiodun, B., Bessafi, M., & Lennard, C. (2018). Numerical simulation of surface solar radiation over Southern Africa. Part 2: Projections of regional and global climate models. *Climate Dynamics*.
Taylor, K. E., Stouffer, R. J., & Meehl, G. A. (2012). An Overview of Cmip5 and the Experiment Design. *Bulletin of the American Meteorological Society, 93*(4), 485-498. doi:Doi 10.1175/Bams-D-11-00094.1
Tegen, I., Hollrig, P., Chin, M., Fung, I., Jacob, D., & Penner, J. (1997). Contribution of different aerosol species to the global aerosol extinction optical thickness: Estimates from model results. *Journal of Geophysical Research: Atmospheres, 102*(D20), 23895-23915.
Thevenard, D., & Pelland, S. (2013). Estimating the uncertainty in long-term photovoltaic yield predictions. *Solar Energy, 91*, 432-445.
Tiedtke, M. (1989). A comprehensive mass flux scheme for cumulus parameterization in large-scale models. *Monthly Weather Review, 117*(8), 1779-1800.
Tsoutsos, T., Papadopoulou, E., Katsiri, A., & Papadopoulos, A. M. (2008). Supporting schemes for renewable energy sources and their impact on reducing the emissions of greenhouse gases in Greece. *Renewable and Sustainable Energy Reviews, 12*(7), 1767-1788.
Van Meijgaard, E., Van Ulft, L., Van de Berg, W., Bosveld, F., Van den Hurk, B., Lenderink, G., & Siebesma, A. (2008). The KNMI regional atmospheric climate model RACMO version 2.1. *Koninklijk Nederlands Meteorologisch Instituut*.
Van Vuuren, D. P., Edmonds, J., Kainuma, M., Riahi, K., Thomson, A., Hibbard, K., Lamarque, J.-F. (2011). The representative concentration pathways: an overview. *Climatic Change, 109*(1-2), 5.
Wang, K., Dickinson, R. E., & Liang, S. (2009). Clear sky visibility has decreased over land globally from 1973 to 2007. *Science, 323*(5920), 1468-1470.
Wild, M. (2005). Solar radiation budgets in atmospheric model intercomparisons from a surface perspective. *Geophysical Research Letters, 32*(7).
Wild, M. (2008). Short-wave and long-wave surface radiation budgets in GCMs: A review based on the IPCC-AR4/CMIP3 models. *Tellus Series a-Dynamic Meteorology and Oceanography, 60*(5), 932-945.
Wild, M. (2009). Global dimming and brightening: A review. *Journal of Geophysical Research-Atmospheres, 114*. doi:Artn D00d16
Doi 10.1029/2008jd011470

Wild, M. (2012). Enlightening global dimming and brightening. *Bulletin of the American Meteorological Society, 93*(1), 27.
Wild, M. (2016). Decadal changes in radiative fluxes at land and ocean surfaces and their relevance for global warming. *Wiley Interdisciplinary Reviews: Climate Change, 7*(1), 91-107.
Wild, M., Folini, D., Hakuba, M. Z., Schär, C., Seneviratne, S. I., Kato, S., König-Langlo, G. (2015). The energy balance over land and oceans: an assessment based on direct observations and CMIP5 climate models. *Climate Dynamics, 44*(11-12), 3393-3429.
Wild, M., Folini, D., & Henschel, F. (2017). *Impact of climate change on future concentrated solar power (CSP) production.* Paper presented at the AIP Conference Proceedings.
Wild, M., Folini, D., Henschel, F., Fischer, N., & Müller, B. (2015). Projections of long-term changes in solar radiation based on CMIP5 climate models and their influence on energy yields of photovoltaic systems. *Science Direct Solar Energy, 116*, 13. doi:10.1016/j.solener.2015.03.039
Wild, M., Grieser, J., & Schär, C. (2008). Combined surface solar brightening and increasing greenhouse effect support recent intensification of the global land-based hydrological cycle. *Geophysical Research Letters, 35*(17).
Wild, M., Ohmura, A., Gilgen, H., & Rosenfeld, D. (2004). On the consistency of trends in radiation and temperature records and implications for the global hydrological cycle. *Geophysical Research Letters, 31*(11). doi:Artn L11201
Doi 10.1029/2003gl019188
Wild, M., Ohmura, A., Schär, C., Müller, G., Folini, D., Schwarz, M., Sanchez-Lorenzo, A. (2017). The Global Energy Balance Archive (GEBA) version 2017: A database for worldwide measured surface energy fluxes 5.
Wild, M., & Schmucki, E. (2011). Assessment of global dimming and brightening in IPCC-AR4/CMIP3 models and ERA40. *Climate Dynamics, 37*(7-8), 1671-1688.
Willson, R. C., & Mordvinov, A. V. (2003). Secular total solar irradiance trend during solar cycles 21–23. *Geophysical Research Letters, 30*(5).
Wolter, K., & Timlin, M. S. (1998). Measuring the strength of ENSO events: How does 1997/98 rank? *Weather, 53*(9), 315-324.
Zhang, X., Liang, S., Wang, G., Yao, Y., Jiang, B., & Cheng, J. (2016). Evaluation of the Reanalysis Surface Incident Shortwave Radiation Products from NCEP, ECMWF, GSFC, and JMA Using Satellite and Surface Observations. *Remote Sensing, 8*(3), 225.
Zhang, Y., Rossow, W. B., & Stackhouse, P. W. (2007). Comparison of different global information sources used in surface radiative flux calculation: Radiative properties of the surface. *Journal of Geophysical Research: Atmospheres, 112*(D1).
Zubler, E., Folini, D., Lohmann, U., Lüthi, D., Schär, C., & Wild, M. (2011). Simulation of dimming and brightening in Europe from 1958 to 2001 using a regional climate model. *Journal of Geophysical Research: Atmospheres, 116*(D18).

POLE RECHERCHE
Ecoles **D**octorales

LETTRE D'ENGAGEMENT DE NON-PLAGIAT

Je, soussigné(e) Chao TANG,

en ma qualité de doctorant(e) de l'Université de La Réunion, déclare être conscient(e) que le plagiat est un acte délictueux passible de sanctions disciplinaires. Aussi, dans le respect de la propriété intellectuelle et du droit d'auteur, je m'engage à systématiquement citer mes sources, quelle qu'en soit la forme (textes, images, audiovisuel, internet), dans le cadre de la rédaction de ma thèse et de toute autre production scientifique, sachant que l'établissement est susceptible de soumettre le texte de ma thèse à un logiciel anti-plagiat.

Fait à ST-DENIS le : 12/12/2017

Signature : Chao Tang

Extrait du Règlement intérieur de l'Université de La Réunion
(validé par le Conseil d'Administration en date du 11 décembre 2014)

Article 9. Protection de la propriété intellectuelle – Faux et usage de faux, contrefaçon, plagiat

L'utilisation des ressources informatiques de l'Université implique le respect de ses droits de propriété intellectuelle ainsi que ceux de ses partenaires et plus généralement, de tous tiers titulaires de tels droits.
En conséquence, chaque utilisateur doit :
- utiliser les logiciels dans les conditions de licences souscrites ;
- ne pas reproduire, copier, diffuser, modifier ou utiliser des logiciels, bases de données, pages Web, textes, images, photographies ou autres créations protégées par le droit d'auteur ou un droit privatif, sans avoir obtenu préalablement l'autorisation des titulaires de ces droits.

La contrefaçon et le faux
Conformément aux dispositions du code de la propriété intellectuelle, toute représentation ou reproduction intégrale ou partielle d'une œuvre de l'esprit faite sans le consentement de son auteur est illicite et constitue un délit pénal.
L'article 444-1 du code pénal dispose : « Constitue un faux toute altération frauduleuse de la vérité, de nature à causer un préjudice et accomplie par quelque moyen que ce soit, dans un écrit ou tout autre support d'expression de la pensée qui a pour objet ou qui peut avoir pour effet d'établir la preuve d'un droit ou d'un fait ayant des conséquences juridiques ».
L'article L335_3 du code de la propriété intellectuelle précise que : « Est également un délit de contrefaçon toute reproduction, représentation ou diffusion, par quelque moyen que ce soit, d'une œuvre de l'esprit en violation des droits de l'auteur, tels qu'ils sont définis et réglementés par la loi. Est également un délit de contrefaçon la violation de l'un des droits de l'auteur d'un logiciel (…) ».

Le plagiat est constitué par la copie, totale ou partielle d'un travail réalisé par autrui, lorsque la source empruntée n'est pas citée, quel que soit le moyen utilisé. Le plagiat constitue une violation du droit d'auteur (au sens des articles L 335-2 et L 335-3 du code de la propriété intellectuelle). Il peut être assimilé à un délit de contrefaçon. C'est aussi une faute disciplinaire, susceptible d'entraîner une sanction.
Les sources et les références utilisées dans le cadre des travaux (préparations, devoirs, mémoires, thèses, rapports de stage…) doivent être clairement citées. Des citations intégrales peuvent figurer dans les documents rendus, si elles sont assorties de leur référence (nom d'auteur, publication, date, éditeur…) et identifiées comme telles par des guillemets ou des italiques.

Les délits de contrefaçon, de plagiat et d'usage de faux peuvent donner lieu à une sanction disciplinaire indépendante de la mise en œuvre de poursuites pénales.